PHOTOACTIVE MESOGENIC SUGARS: SYNTHESIS, LIQUID CRYSTALLINE AND PHOTOCHEMICAL PROPERTIES

THESIS SUBMITTED TO THE
UNIVERSITY OF KERALA
FOR THE DEGREE OF
DOCTOR OF PHILOSOPHY
IN CHEMISTRY
UNDER THE FACULTY OF SCIENCE

By

NARAYAN G.

PHOTOSCIENCES AND PHOTONICS
CHEMICAL SCIENCES AND TECHNOLOGY DIVISION
NATIONAL INSTITUTE FOR INTERDISCIPLINARY SCIENCE AND TECHNOLOGY
(*FORMERLY* REGIONAL RESEARCH LABORATORY), CSIR
TRIVANDRUM 695 019
KERALA, INDIA

AUGUST 2007

Statement

I hereby declare that the matter embodied in the thesis entitled: ***"Photoactive Mesogenic Sugars: Synthesis, Liquid Crystalline and Photochemical Properties"*** is the result of investigations carried out by me at the Photosciences and Photonics Section, Chemical Sciences and Technology Division, National Institute for Interdisciplinary Science and Technology, CSIR, Trivandrum under the supervision of Dr. Suresh Das and the same has not been submitted elsewhere for award of any degree, diploma, associateship or fellowship.

In keeping with the general practice of reporting scientific observations, due acknowledgement has been made wherever the work described is based on the findings of other investigators.

Narayan G.

National Institute for Interdisciplinary Science and Technology
(*formerly* Regional Research Laboratory, Trivandrum)

Council of Scientific and Industrial Research (CSIR)
Industrial Estate P.O.,Trivandrum 695 019
Kerala, INDIA
http://www.niist.res.in

ISO 9001 REGISTERED
DNV Certification B.V., The Netherlands

Dr. Suresh Das, F. A. Sc.
Head
Chemical Sciences and Technology Division

sureshdas55@gmail.com
Tel.: +91-471-2515318
Fax: +91-471-2490186

9th August 2007

Certificate

This is to certify that the work embodied in this thesis entitled, ***"Photoactive Mesogenic Sugars: Synthesis, Liquid Crystalline and Photochemical Properties"*** has been carried out by Mr. Narayan G. under my supervision and the same has not been submitted elsewhere for a degree.

Suresh Das
Research Supervisor

Contents

		Page
Preface		vi
Acknowledgements		ix
Chapter 1	**An overview of liquid crystalline and supramolecular self-assembling properties of amphiphilic sugars**	
	Abstract	1
1.	Introduction to liquid crystals	2
1.1.	Thermotropic liquid crystals	4
1.2.	Lyotropic liquid Crystals	9
1.3.	Amphotropic liquid crystals	12
1.4.	Chiral liquid crystals	12
1.4.1.	General aspects and significance of chirality	13
1.4.2.	From a chiral molecule to a chiral anisotropic phase: Some facts	15
1.4.3.	Properties of chiral liquid crystals	17
1.4.4.	Unique phases: Bent core mesogens	21
1.5.	Sugars / carbohydrates as candidates for chiral LCs	22
1.5.1.	Sugar based LCs	27
1.6.	Self-assembling properties of amphiphiles and bolaamphiphiles in solution	47
1.6.1.	Aggregate morphology	50
1.6.2.	An overview of sugar-based self-assembled systems	59

1.7.	Objectives of the present work	68
	References	70
Chapter 2	**Induction of chirality in amphiphilic sugars**	
	Abstract	78
2.1.	Introduction	79
2.2.	Results	83
2.2.1.	Synthesis of sugar-azobenzene derivatives	83
2.2.2.	Liquid crystalline properties and spectroscopic studies	86
2.2.2.1.	Monosugar derivatives	86
2.2.2.2.	Bolaamphiphiles	94
2.3.	Discussion	105
2.4.	Experimental section	108
2.5.	Conclusion	117
	References	117
Chapter 3	**Macroscopic chiral diphenylbutadiene cored bolaamphiphilic sugars**	
	Abstract	121
3.1.	Introduction	122
3.2.	Results	124
3.2.1.	Synthetic strategy	124
3.2.2.	Phase transition behavior	127
3.2.3.	X-ray diffraction studies	132
3.2.4.	Electro-optic measurements	138
3.2.5.	Absorption, fluorescence and circular dichroism spectra	140
3.3.	Discussion	145

3.4.	Experimental section	148
3.5.	Conclusion	157
	References	158
Chapter 4	**Aggregation of bolaamphiphiles in solution**	
	Abstract	162
4.1.	Introduction	163
4.2.	Results	166
4.2.1.	Synthesis	166
4.2.2.	Spectroscopic characterization of supramolecular aggregates in solution	166
4.2.2.1.	UV-vis and CD measurements	166
4.2.2.2.	Effect of temperature on the UV-vis and CD spectra	173
4.2.2.3.	Proton NMR characterization of the aggregates	179
4.2.3.	Aggregate morphology	181
4.2.4.	Photolysis of the aggregates	185
4.3.	Aggregation of CnGB bolaamphiphiles	190
4.3.1.	Aggregation behavior in acetonitrile	190
4.3.2.	Aggregation in DMSO/water mixed solvents	193
4.4.	Discussion	198
4.5.	Experimental section	201
4.6.	Conclusion	204
	References	204
	Annexure	209
	List of Publications	215

Preface

Liquid crystals (mesogens) belong to a class of materials, which have been extensively exploited for the past several decades for a variety of technological applications ranging from display devices to development of high strength polymers. When the mesogenic molecule is an achiral one doped with a chiral additive, or when it is inherently chiral, the directors of molecular layers adopt a helical arrangement resulting in macroscopically chiral LC phases. Two major classes of chiral liquid crystals (LCs) are the chiral nematic (cholesteric) and chiral smectic phases. Cholesteric LCs possess the inherent property of selective reflection of light due to a helical superstructure originating from their chirality. Smectic C LCs, due to their bistability, fast electro-optic switching and wide viewing angle find applications in commercial microdisplays, nonlinear optics and photonic applications. In view of these applications the design and development of chiral LCs are of technological importance. In order to synthesize LC molecules, which are inherently chiral, the chiral synthon used has to be selected based on ease of availability, structural diversity, mesogenic property and chemical stability. Sugars or carbohydrates in general possess all the ideal characteristics mentioned above. However, even though sugar molecules possess several chiral centres, the LC phases formed from them do not normally exhibit macroscopic chirality. The failure to express macroscopic chirality in the sugar LCs stems from the fact that their amphiphilic character is reinforced by the many –OH groups that readily enter into hydrogen bonding. This leads to rigidly packed layered structures that assemble into smectic, columnar or cubic phases. Therefore macroscopically chiral LC phases from sugars could hitherto be observed only by suppressing their amphiphilic character either by suitable derivatization or replacement of –OH groups by other functional groups. The major focus of the work described in this thesis is on design and synthesis of sugar-based chiral LCs possessing free hydroxyl groups. In addition to LC property in the bulk state, some of these molecules formed ordered aggregates such as vesicles and fibers in solution, which have been investigated in detail.*

These structures resemble biological self-organized systems (bio-membranes) and are therefore potential bio-mimetic materials.

The first chapter of this thesis provides an overview of the literature in this field and describes the objectives of the present work. Chapter 2 describes the design of sugar-based LCs starting from azobenzene linked sugar amphiphiles, which exhibited only macroscopically achiral smectic phases. These amphiphiles were then chemically modified to see whether macroscopic chirality would be expressed. However the products exhibited only achiral phases. When the bolaamphiphilic architecture was used wherein azobenzene moiety formed the core with sugar moieties attached as head groups through oligomethylene spacers, chiral thermotropic smectic C phases were observed. This was the first reported observation of macroscopically chiral smectic C* phase in sugar-based LCs containing free hydroxyl groups. The manifestation of the smectic C* phase in these bolaamphiphiles was observed to be critically dependant on the presence of the azobenzene moiety and suitable length of the oligomethylene spacer. The ability of the azobenzene group to induce chirality was attributed to its self-aggregation properties. In order to test this hypothesis we replaced the azobenzene moiety with diphenylbutadiene in the core of the above bolaamphiphiles, in view of the ability of the latter to form more stable aggregates. This also resulted in another series of very stable chiral smectic LCs confirming our hypothesis. The syntheses, liquid crystalline phase characterization and photochemical properties of the diphenylbutadiene-based derivatives are described in Chapter 3.*

The azobenzene-cored bolaamphiphiles underwent supramolecular self-assembly in water/DMSO solvent mixtures to form microstructures such as vesicles and fibers. Changes in the absorption spectra in these solvent mixtures indicated the formation of tightly packed H-aggregates. The absorption band attributable to the aggregates was CD active and the CD spectra of water rich solutions exhibited an unusual intensity increase on heating. The ease of formation and the stability of the aggregates were observed to increase with increase in the length of the oligomethylene spacers. These aspects as well as

the disruption of the aggregates induced by photoisomerization of the azobenzene unit followed by reformation via the subsequent thermal cis to trans isomerization are described in Chapter 4. In addition, preliminary aggregation studies of the diphenylbutadiene cored bolaamphiphiles in acetonitrile and water/DMSO were carried out. The thermal stability of the aggregates in water rich solutions was observed to be similar to that of the azo-bolas.

Acknowledgements

I have great pleasure in placing on record my deep sense of gratitude to Dr. Suresh Das, my research supervisor, for suggesting the research problem and for his guidance, support, constant encouragement and freedom to work which collectively lead to the successful completion of this work.

I would like to express my sincere thanks to Professor M. V. George for his constant encouragement and valuable discussions which have inspired and motivated me during this period.

I thank Professor T. K. Chandrasekhar, Director, NIST and former Directors Professor Javed Iqbal, Dr. G. Vijay Nair and acting directors Dr. B. C. Pai and Dr. G. D. Surender for providing necessary facilities for carrying out the work.

I am also grateful to:

- *Dr. A. Ajayaghosh, Dr. K. R. Gopidas, Dr. D. Ramaiah, Dr. K. George Thomas and Dr. A. Srinivasan, Scientists of the Photosciences and Photonics Section and Dr. K. V. Radhakrishnan of the Organic Chemistry Section for valuable suggestions and encouragement.*
- *Dr. N. Jayaraman, Department of Organic Chemistry, IISc, Bangalore and his group members Mr. Somak Paul and Dr. M. K. Singh for their help in the synthesis of some of the molecules described in this thesis.*
- *Dr. D. S. Shankar Rao, Dr. S. Krishna Prasad of CLCR, Bangalore for conducting X-ray and electro-optic measurements and Dr. Nigam P. Rath, University of Missouri-St. Louis, USA for single crystal X-ray analysis.*
- *Dr. Shibu Abraham, Dr. Riju Davis, Dr. Mahesh Hariharan former students and N. S. Saleesh Kumar, M. C. Basheer, Shinto Varghese, K. V. Ratheesh, Sajith Menon and Shafeekh K. M. of Photosciences and Photonics Section for their help and advice.*
- *Mr. Robert Philip, Mrs. Sarada Nair of Photosciences and Photonics Section, Dr. J. D. Sudha of Polymer Section and staff and students in all other sections of NIST for their whole hearted co-operation.*
- *Mrs. Saumini Mathew for recording FT-NMR, Mrs. S. Viji for Mass spectral and CHN analyses, Ms. Priya A. Nair for FT-IR and GC-MS analyses, Mr. M. R. Chandran for SEM and Mr. P. Guruswamy for powder XRD analysis.*
- *Dr. (Mrs.) M. Lalithambika, Scientist (retd.) and Dr. D. Bahulayan, former DST young scientist, NIST for their support and encouragement.*
- *DRDO, CSIR and DST, Government of India for funding.*
- *My parents, grand parents, sister, teachers and all other family members for their love and encouragement, which has been a great source of motivation.*

Narayan Gopinathan

Chapter 1

An Overview of Liquid Crystalline and Supramolecular Self-assembling Properties of Amphiphilic Sugars

Abstract

Liquid crystals (mesogens) belong to a class of materials with extensive technological applications. When the mesogenic molecule is an achiral one doped with a chiral additive or when it is inherently chiral, the directors of molecular layers adopt a helical arrangement resulting in macroscopically chiral LC phases. Two major classes of chiral liquid crystals (LCs) are the chiral nematic (cholesteric) and chiral smectic phases. Cholesteric LCs possess the inherent property of selective reflection of light due to a helical superstructure originating from their chirality. Smectic C LCs, due to their bistability, fast electro-optic switching and wide viewing angle find applications in commercial microdisplays, nonlinear optics and photonic applications. In view of these applications the design and development of chiral LCs are of technological importance. In order to synthesize LC molecules which are inherently chiral, the chiral synthon used has to be selected based on ease of availability, structural diversity, mesogenic property and chemical stability. Sugars or carbohydrates in general possess all the ideal characteristics mentioned above. However, even though sugar molecules possess several chiral centers, the LC phases formed from them do not exhibit macroscopic chirality. The failure to express*

macroscopic chirality in the sugar LCs stems from the fact that their amphiphilic character is reinforced by the many –OH groups that readily enter into hydrogen bonding resulting in double layers that assemble to smectic, columnar or cubic phases. Macroscopically chiral LC phases from sugars could hitherto be observed only by suppressing their amphiphilic character either by suitable derivatization or replacement of –OH groups by other functional groups. This Chapter provides an overview of the literature in this field and describes the objectives of the present work.

1. Introduction to Liquid Crystals

Liquid crystals (mesogens) are a class of substances, which have been extensively exploited for the past several decades for a variety of technological applications ranging from display devices[1,2] to development of high strength polymers.[3] The term liquid crystal (LC) signifies a state of aggregation that is intermediate between the solid state and the isotropic liquid.[4] Liquid crystals have been termed as Nature's delicate state of matter[5] which can be accessed by all types of materials and not just organic compounds. Thus inorganic, ionic, zwitterionic, elastomeric, dendrimeric and oligomeric systems as well as metal-organic complexes, organic complexes are some of the classes of molecules, which are known to exhibit mesomorphism.[6-9] Transitions to these intermediate mesomorphic states may be brought about by purely thermal processes (thermotropic mesomorphism) or by the influence of solvents (lyotropic

mesomorphism). A substance in the liquid crystalline state is strongly anisotropic in some of its properties and yet exhibits a certain degree of fluidity.[4] Depending on the detailed molecular structure and its mode of aggregation, the system may pass through one or more mesophases before it is transformed to the isotropic liquid.

In a classical approach, substances that can exhibit liquid crystalline phases are considered to belong to one of two distinct classes of molecules:[10] anisometric and amphiphilic (Figure 1.1).

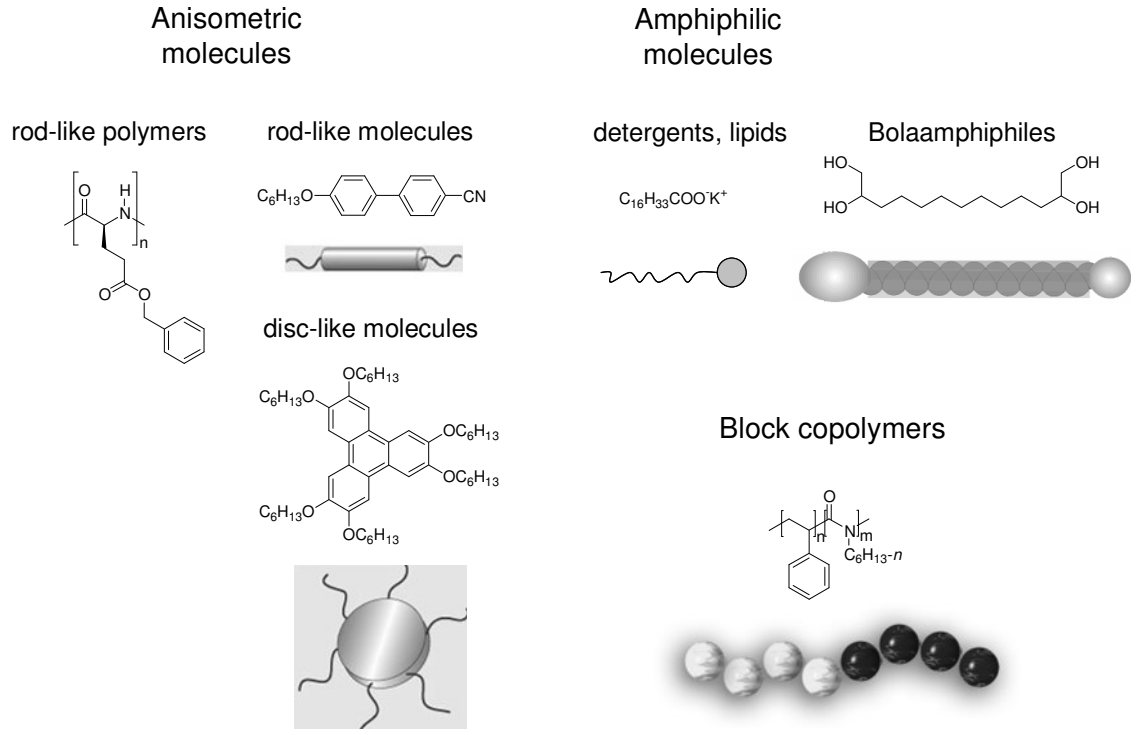

Figure 1.1. A few classes of molecules forming liquid crystalline phases.

Anisometric (non-amphiphilic) molecules include rod- or disc-like molecules or aggregates in most cases giving exclusively thermotropic liquid

crystals. LCs formed by anisometric molecules are also termed monophilic. The second class includes amphiphilic molecules such as detergents and lipids leading to lyotropic and also thermotropic mesophases. Both types of mesogenic molecules can be attached to a polymer backbone (LC-side-chain polymers) or can be incorporated in the polymer backbone (LC-main-chain polymers). More recently the interest in thermotropic and/or lyotropic mesophases of rod-like polymers (hairy rods, poly-peptides, poly-isocyanates, cellulose derivatives etc.) has grown significantly.

1.1. Thermotropic Liquid Crystals

Thermotropic liquid crystalline phases are observed between the solid and isotropic liquid state of neat substances by a change of temperature.[4,11] When the liquid crystalline state is thermodynamically stable and observed on heating the solid as well as on cooling the isotropic melt, it is termed *enantiotropic*, whereas when they are only formed on cooling from the isotropic liquid it is termed as *monotropic*. Monotropic compounds on heating transform directly to the isotropic phase.

Thermotropic liquid crystals are generally further distinguished with respect to the molecular shape of the constituent molecules,[10-12] being called calamitic for rod-like and discotic for disk-shaped. Liquid crystals can also be formed through noncovalent self-assembly of non-mesogenic components possessing the desired complimentary structural elements in fixed ratios.[13,14] These

basic molecular structures can be modified[10] in different ways giving rise to structural features of the mesophases (i.e., polycatenar liquid crystals[15] which are intermediate structures in which rod-like and disk-like molecular structures have been combined and sanidic liquid crystals formed from lath-shaped molecules[16]). The characteristic feature of thermotropic liquid crystals is the preferred orientation of molecules along a certain direction, which is described by a unit vector, the *director*, n.

The structure of the liquid crystalline phases is characterized by the arrangement and conformation of the molecules and the intermolecular interactions. Similar phase structures can be formed by molecules, which belong to completely different chemical classes. This shall be explained by looking at some of the most important phase structures.

The nematic phase is the one with the least order (Figure 1.2a).[17] It has a high degree of long-range orientational order of the molecules, but no long-range translational order. Thus it differs from the isotropic liquid in that the molecules are spontaneously oriented with their long axes approximately parallel. On surfaces, the nematic mesophase frequently adopts a characteristic 'threaded' texture, when viewed between crossed polarizers. The term 'nematic' is derived from the Greek word, 'nematos', meaning thread-like.

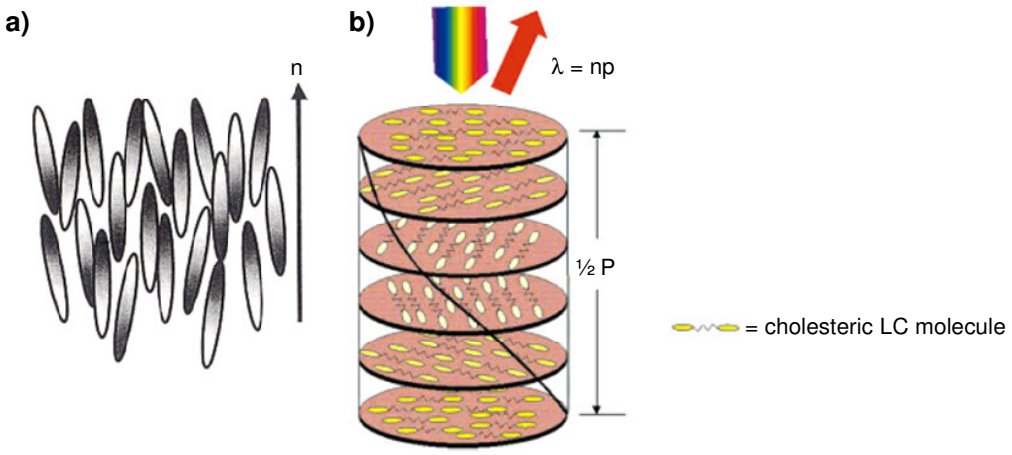

Figure 1.2. Arrangement of molecules in (a) nematic and (b) chiral nematic phase.

The chiral nematic mesophase is also a nematic type of liquid crystal except that it is composed of optically active molecules.[12,17] The phase consists of local nematic "layers" which are continuously twisted helically with respect to each other (Figure 1.2b). The first observation of the liquid crystalline phenomenon was of this chiral nematic phase by Reinitzer in cholesteryl benzoate (1888).[18] Since they were first observed in cholesterol derivatives, they are also called cholesterics. In spite of this historical name the structures of cholesteric molecules can considerably vary from cholesterol. The cholesteric phase is completely miscible with the achiral nematic phase occurring in the respective racemic mixture. The helical twist can be right- or left-handed depending on the molecular conformation, about an axis normal to the preferred molecular directions. The energy of twist forms only a minute part (~10^{-5}) of the total energy associated with the parallel alignment of molecules, so much so that when a small quantity of a

cholesteric substance, or even a non-mesogenic optically active substance is added to a nematic, the mixture adopts a helical configuration.[4] In the cholesteric phase, the helical pitch can be on the order of the wavelength of light. The optical properties of cholesterics have made them useful in display[12,19] and laser technologies[20] as well as in the visual arts.[12] Due to selective reflection of light of different wavelengths, cholesterics show intense iridescent colors with a metallic sheen. The periodically twisted helical structure can give rise to Bragg reflection. This occurs in a band of wavelengths $\lambda(\theta) = np \cos \theta$, where *n* is the mean refractive index of the liquid crystal, θ is the incident angle and $p = 2d$ is the pitch, d the spatial period.[19,20]

In smectic liquid crystalline phases the molecules are arranged into layers.[21,22] In addition to the orientational order found in the nematic state, *positional order* of the molecules centers of mass is the characteristic feature of the smectic phase. The molecules centers of mass arrange in layers. The term 'smectic' is itself derived from the Greek word, 'smectos' (soap like), because these phases were first discovered in soap solutions. There are several kinds of positional order within the layers, depending on which they are classified into different groups.[17,23]

In the smectic A phase, the molecules are upright (orthogonal) in each layer with their centers irregularly spaced in a 'liquid-like' fashion. The interlayer attractions are weak as compared with the lateral forces between molecules and

consequently the layers are able to slide over one another relatively easily. Thus this mesophase has fluid properties, though it is much more viscous than the nematic phase.

Smectic C is a tilted smectic phase. The molecules in this phase are inclined with respect to the layer normal. The smectic A and smectic C phases are the least-ordered smectic phases (Figure 1.3).

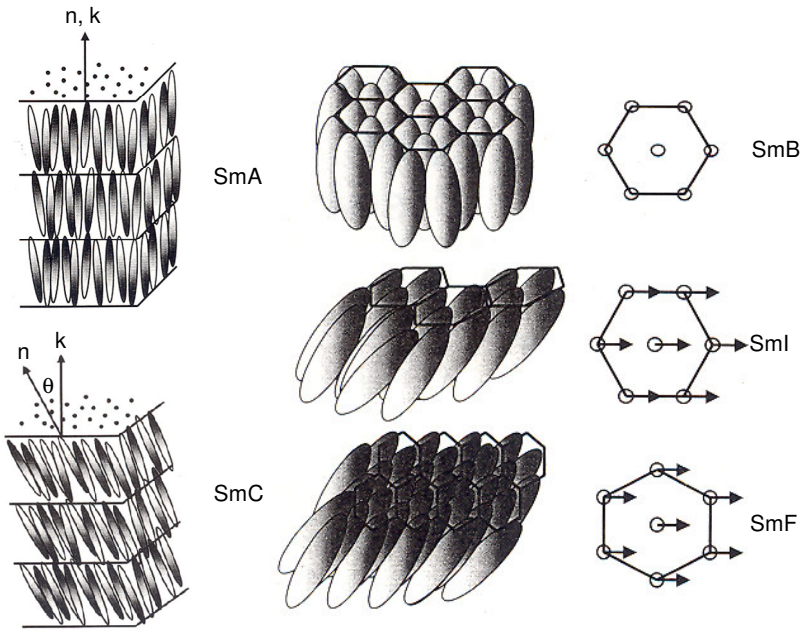

Figure 1.3. Molecular structure of the orthogonal smectic A (SmA) phase; tilted smectic C (SmC) phase; the orthogonal smectic B (SmB) phase; the smectic I (SmI) phase being tilted towards the apex of the hexagon and the smectic F (SmF) phase being tilted towards the side of the hexagon.

Phases possessing a so-called *bond orientational order* within their layers are smectic B_{hex} (orthogonal), I (tilted) and F (tilted). These phases are also designated as hexatic smectic phases. The molecules are locally ordered in

hexagons and the orientations of these hexagons possess long range order (Figure 1.3).

The columnar phase in its simplest form consists of disk-shaped molecules[4,24,25] stacked one on top of another to form columns, the different columns constituting a two-dimensional lattice (Figure 1.4). The structure is somewhat similar to the hexagonal phase of soap-water and lyotropic systems. Several variants of the structure have been identified: upright, tilted, hexagonal, rectangular columns, etc. In some cases, the columns are liquid like, i.e., the molecular centers are arranged aperiodically within each column while in others they are arranged in a regular, ordered fashion.

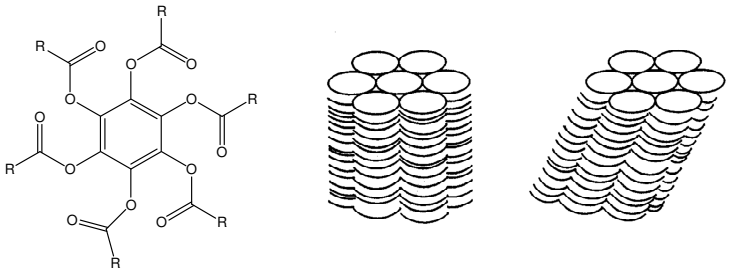

1, R = *n*-C_4H_9 to *n*-C_9H_{19}

Figure 1.4. Structure of benzene *hexa-n*-alkanoate. Schematic of arrangement of discotic molecules in columnar phases.

1.2. Lyotropic Liquid Crystals

Another way of creating this intermediate state of matter, than just by changing the temperature is by addition of solvents in appropriate amounts to suitable compounds. Thus lyotropic LCs are formed.[11,26,27] Typically lyotropic LCs are formed by amphiphilic molecules (amphiphilic molecules have a

hydrophilic head and a lipophilic tail bonded together in a molecule, i.e., they are naturally polarized[28]). Under suitable conditions, especially in well-defined concentration ranges, these molecules tend to organize themselves forming aggregates of various well-defined geometries such as micelles, vesicles, columns or lamellae. These supramolecular assemblies behave as mesogenic units forming lyotropic LC phases. In this type of LCs the *concentration range* in which the system is liquid crystalline can be compared with the *temperature range* between the melting and the clearing point of thermotropic LCs. However in the case of lyotropic LCs, the temperature is an additional degree of freedom. Thus lyotropic mesophases are always mixtures, whereas many of the reported thermotropic LCs are single compounds.

The most common lyotropic LC phase is the *lamellar* or L_α phase (Figure 1.5), which is formed by a stack of ordered bilayered aggregates separated by solvent layers. The head groups are in contact with the solvent (mostly water) and the alkyl chains (interdigitated) are located on the inside of the bilayer. Variations in temperature and structure can induce changes in packing. This lyotropic lamellar phase is the equivalent of the thermotropic smectic A phase. The *hexagonal* (H_I) phase consists of long cylindrically shaped micelles (Figure 1.5), which are packed into a hexagonal array with a diameter 1.5–2 times the molecular length and are surrounded by an aqueous phase. At low water content amphiphiles with a large hydrophobic section can form an inverted hexagonal (H_{II})

phase in which the head groups are arranged around cylinders of water and the alkyl chains fill the space between the hexagonally ordered water containing inner compartments.[29] This lyotropic phase is analogous to the thermotropic columnar phase formed by discotic molecules. Another lyotropic phase is the cubic phase (Figure 1.5). These lamellar, cubic and hexagonal lyotropic phases are observed for different concentrations of the amphiphiles in the solvent. Lyotropic LC phases and amphiphile self-assembly have immediate relevance in biology because of the prevalence of organized lipid structures in living systems.[30,31] However, one of the most promising new research directions for lyotropic LC assemblies is their use in the construction of non-biological, nanostructured organic materials.[30] Amphiphilic molecules have been combined with anisometric structural units to bridge the gap between thermotropic and lyotropic liquid crystals.[31]

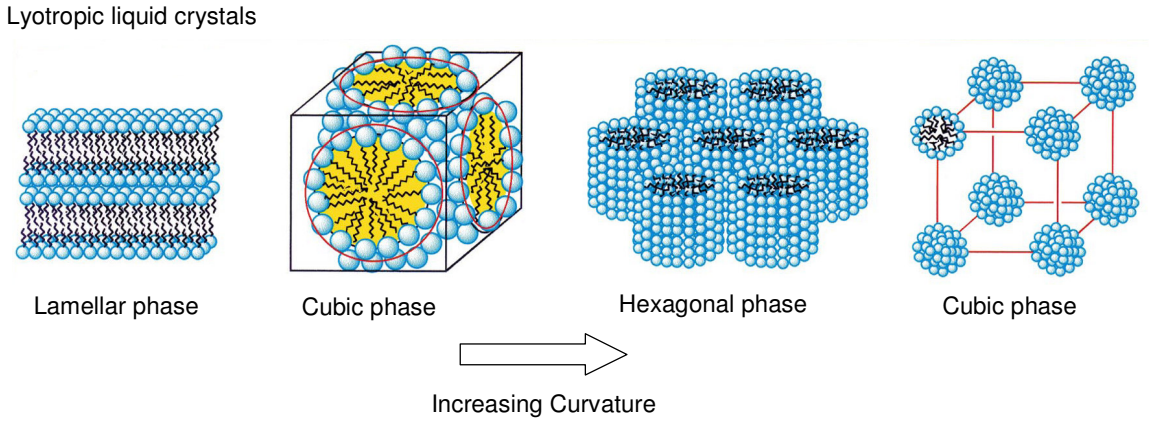

Figure 1.5. Arrangements of amphiphilic molecules in lyotropic phases.

1.3. Amphotropic Liquid Crystals

Molecules are said to act *amphotropically* if they give rise to both thermotropic and lyotropic liquid crystal formation.[26,31] Typical classes[26] of amphotropic materials are soaps, transition metal soaps (metallomesogens), viologens, quarternary amines and other ionic surfactants, block copolymers, cellulose derivatives, partially fluorinated *paraffins*, diols, peptide surfactants, lecithins, lipids, alkylated sugars and inositols, naturally occurring glycosides and silanols.

1.4. Chiral Liquid Crystals

When the mesogenic molecule is an achiral one doped with a chiral additive or inherently chiral, the directors of molecular layers adopt a helical arrangement resulting in a macroscopic chiral LC phase.[23] Two major classes of chiral liquid crystals are the chiral nematic[19] (cholesteric) and chiral smectic C phases.[32] Cholesteric LCs possesses the inherent property of selective reflection of light due to a helical superstructure originating from their chirality.[19] Chiral smectic C (SmC*) phases attract considerable attention, since their potential for application in display devices is next only to nematics, which are well known for their applications in flat panel LCDs.[2,32] The smectic C* LC state, due to its bistability, fast electro-optic switching (10^3 times faster than nematic LCs) and wide viewing angle finds application in commercial high-resolution reflective

microdisplays.[32] In addition, molecules possessing the smectic C* phase are potential candidates for nonlinear optics[33] and photonic applications.[34] In view of these applications the design and development of chiral LCs are of technological importance.

The main examples of chiral LC phases are:[23]

1. Chiral nematic phase
2. Blue phase
3. Twist Grain Boundary Phases (TGB)
4. Chiral smectic C phase
5. Chiral Columnar phase

When it comes to designing chiral LCs, it can be done in two ways,[23] with the technological application dictating how the chiral phase is obtained.

1. By doping of an achiral phase formed by achiral mesogens with a chiral dopant.

2. Design of mesogens with suitably located chiral centers in the same molecule, thus producing inherently chiral LCs.

1.4.1. General Aspects and Significance of Chirality

Since the birth of stereochemistry almost 160 years ago with Pasteur's discovery[35] of handedness in molecules interest in chiral molecules has greatly increased. The term 'chirality' was first coined by Lord Kelvin: "*I call any geometrical figure, or group of points, chiral and say it has chirality if its image in a plane mirror, ideally realized, cannot be brought to coincide with itself.*"[36]

Chirality permeates the entire fabric of the biological world. Indeed, life as we know it would not exist without chirality. The function of fundamental components of the cell such as actin, myosin, proteins and lipids relies upon their being chiral. The handedness of a molecule can affect its odour, potency and toxicity. Thus the synthesis of a single enantiomer of a compound is crucial for the delivery of safe and effective pharmaceuticals and food additives.[23]

Chiral objects are objects, which cannot be transformed into their mirror image by rotations or translations. Thus, a handedness can be defined for chiral objects, for example, a screw is said to be right-handed if its windings propagate clockwise along the screw axis and otherwise it is called left-handed. The name 'chirality' originates from the Greek vocabulary χείρ (hand), since a hand is a striking example of a chiral object. Other examples are snail's shells or creeping plants. However, the appearance of chirality is not restricted to macroscopic objects.[23] On the molecular level, many organic compounds are chiral because their molecules possess atom/s with four different groups bonded to it.[37]

Theoretically, one might expect that chiral objects of opposite handedness have the same energy and occur in nature with equal probability. However, it is known that many chiral structures occur either exclusively with one handedness or at least more often than the opposite handedness. This phenomenon is called homochirality. For example, all naturally occurring sugars are D-sugars. Likewise aminoacids are all L-aminoacids.

1.4.2. From a Chiral Molecule to a Chiral Anisotropic Phase: Some Facts

Transfer of chirality from the molecular level to the liquid crystal phase is a complex phenomenon, which is not well understood.[23] This was impeded by the absence of suitable and measurable structural quantities. It becomes apparent that no simple description for a structure/response relation can exist. Most studies on understanding the mechanism by which the chirality of the molecule is mapped onto the liquid crystalline phase deal with the mode of transfer of chirality from the chiral center of the molecule to the rest of the molecule (intramolecular transfer) and the subsequent transfer of chirality to the liquid crystalline phase (intermolecular transfer).[23] Several recent studies have addressed these issues for both host-guest systems[38] and in chiral molecules exhibiting liquid crystalline phases.[39]

Properties connected to the chirality of an object may have very different origins. A concept is thus introduced in which four levels of chirality exist. The first level of chirality is the chirality of the atoms caused by weak interactions. The second level is the chirality of molecules while the third level is derived from the ordering of atoms, ions or molecules in isotropic or anisotropic phases by long-range positional and long-range orientational order. The fourth level of chirality is the form of a macroscopic object which can be, e.g., an enantiomorphic crystalline form (habitus of the crystal).[23,40]

With a four-level concept of chirality, the question of how chirality can be transferred from one level to an adjacent level is of fundamental interest. The chirality of a molecule (second level) is mapped onto the liquid crystal phase (third level). Chirality is information which can be transferred from one level to the other without being lost in the level from which it originated. There are two possible statements:

1. The information about the absolute configuration in one level is transferred to and stored by the absolute configuration of the adjacent level.
2. The results of some of the chirality measurements of one level are correlated to the results of the chirality measurements of the adjacent level. The correlated chirality measurements do not have to be of the same type but not all possible chirality measurements can be taken for a correlation.

In the first case, a convention for the absolute configuration of each level is needed. For molecules (second level) the Cahn-Ingold-Prelog nomenclature R or S and P or M is available whereas, for example, in the case of the helicity of a cholesteric or a smectic C* phase (third level) can be given by P or M. Such a simple characterization is not possible for all chiral liquid crystal phases. If we consider that a chiral dopant (the second level), with a configuration R, for e.g., induces a cholesteric phase of helicity P, we can infer that the information "absolute configuration R" of the second level is transferred to the helicity P of the third level.

The mapping of the molecular chirality onto a liquid crystal phase has been wrongly interpreted as an effect of amplification of the chirality of a molecule under the consideration of the second statement. The chirality measurements for the adjacent levels can be of the same or of a different kind. The Cotton effect of the dopant (second level) can be compared to the Cotton effect of the induced cholestric phase (third level) which would be usually orders of mangnitude larger. The sign of the Cotton effects of the molecule belonging to different absorption bands depends on the nature of the transition and the chromophore environment. But the Cotton effects of the phase depend on the suprastructural chirality around the molecule. Thus only in special cases can these two be compared and correlated. The enhancement or amplification of the chirality of the molecule does not take place in all cases.[23]

1.4.3. Properties of Chiral Liquid Crystals

1.4.3.1. Induction of helical superstructures. The presence of chiral molecules in a liquid crystal can have various consequences. Chirality may cause an intrinsic helical structure of the director of the layers containing mesogens (Figure 1.6).

Instead of the uniform alignment of the director field occurring in the nematic phase, the corresponding chiral nematic phase exhibits a helical structure which shows a uniform helix axis. The director is perpendicular to this axis and its

azimuthal angle changes continuously. A helical director field also occurs in the chiral smectic C (SmC*) phase.

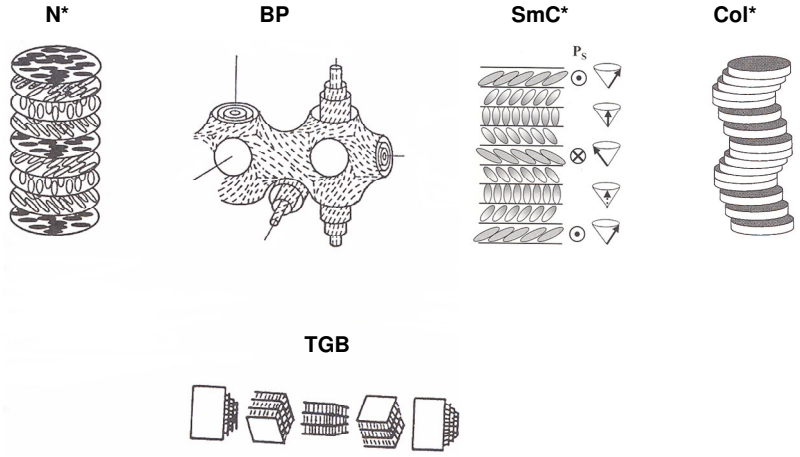

Figure 1.6. Helical structures formed in chiral liquid crystals. Cholesteric phase (N*), blue phase (BP), chiral smectic C phase (SmC*) chiral columnar (Col*) and twist grain boundary phase (TGB). Adapted from reference 23.

1.4.3.2. Electro-optic applications. The unique combination of high birefringence (typically $n_e - n_o \approx 0.2$) with the possibility to modulate either the direction of the optical axis or the optical retardation by an external electric field is the basis for the electro-optic application of LCs.[23] This application and the ferroelectric properties of chiral LCs is due to the spontaneous polarization *P*s. The spontaneous polarization is a chiral bulk property originating from a conformational preference of transverse molecular dipoles to orient in one direction along the polar axis because of steric coupling between polar functional groups and the stereogenic center(s) in the smectic C* mesogens (stereopolar coupling) (Figure 1.7).[39]

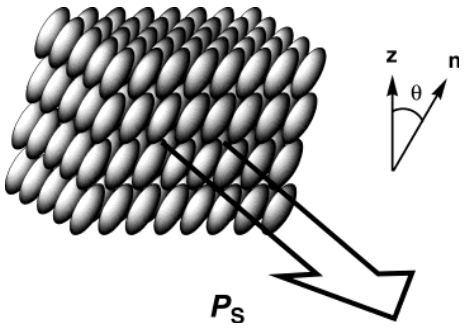

Figure 1.7. Schematic representation of the SmC* phase in a planar alignment. Adapted from reference 39.

For nonchiral liquid crystals, a spontaneous polarization can neither occur in the nematic phase, nor in the smectic A phase, nor in the smectic C phase. However, the presence of chiral molecules reduces the local symmetry of the respective phases, even when the helical director field is unwound, to the space groups D_∞ (chiral nematic and chiral smectic A phase) and C_2 (chiral smectic C) phase because of the lack of mirror symmetry. In a surface-stabilized planar alignment (Figure 1.8), the SmC* liquid crystals are ferroelectric; i.e., they possess a bulk electric polarization (spontaneous polarization, P_S) along a polar axis perpendicular to the plane defined by the molecular long axis *n* and the layer normal, *z* (tilt plane). This spontaneous polarization allows switching of the FLC between opposite tilt orientations by applying an electric field across the film.[4] They show bi- and multistable switching behavior and rather short switching times (down to 1 μs) and have memory as well. The principle of operation of this switch can be readily understood on the basis of the following simplified model. The ferroelectric LC is taken in a thin cell, usually about 2–3 μm thick. As long as the

cell thickness is less than the pitch of the helix, the strong surface forces align the molecules parallel to the substrate and the helix is unwound. The molecules are then arranged in the so-called 'bookshelf' geometry, all inclined one way at an angle of about 20° with respect to the layer normal as shown in Figure 1.8.[4]

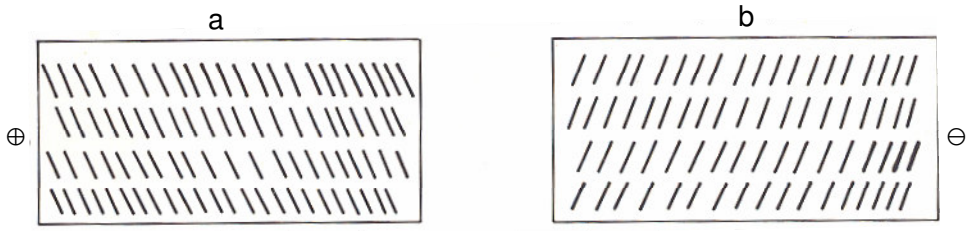

Figure 1.8. The SSFLC cell: The 'bookshelf' geometry of a thin film of smectic C* sandwiched between two glass plates (a) field 'up' (normal to the plane of the diagram) and (b) field 'down'. Adapted from reference 4.

The *P*s of every layer will therefore point in the same direction (say upwards). Now when a reverse electrical pulse is applied across the film, the polarizer will switch over to the opposite direction (downwards) and the molecular tilt will change by 2θ ~40°. By using a pair of polarizers and adjusting the cell thickness so that, in effect, the LC film becomes a half-wave plate, high optical contrast can be achieved. The remarkable feature of this device – which is known as the SSFLC (surface stabilized ferroelectric liquid crystal) device – is that the switch on and switch off times are just a few tens of microseconds, i.e., about 10^3 times faster than the twisted nematic device. For a given cell thickness, the material parameters that determine the switching speed are the polarization and viscosity.[4]

Other applications make use of the field-induced tilt or the electroclinic effect. Here again chiral molecules need to be present for a nonzero electroclinic coefficient. Unlike the SSFLC device, this effect does not possess bistability but it has faster (sub microsecond) response. By using the same bookshelf geometry and a suitable polarizer and retarder arrangement, the electroclinic effect can be used for modulating a light signal with a transmitted intensity linearly proportional to the applied voltage or as a tunable color filter.[4]

1.4.4. Unique phases: Bent core mesogens. Interestingly some types of nonchiral molecules are capable of forming chiral mesophases. This type of molecules, having a bent core ("banana-shaped" molecules) can build polar and even chiral liquid crystal structures.[41,42] The polar order of bent molecules in smectic layers can induce a chirality of the smectic layers although the individual molecules are achiral.[41,42] Bent-core molecules form a variety of new phases (B_1–B_7) which differ from the usual smectic and columnar phases. This nomenclature B_1–B_7 was suggested at the workshop Banana-Shaped Liquid Crystals: "Chirality by Achiral Molecules" held at Berlin in December 1997. According to this suggestion the smectic high-temperature phase of the pentyloxy and hexyloxy homologs of the parent series (Chart 1.1) is designated as B_1. The phase symbol B_2 is attributed to the switchable phase of longer-chained homologs whereas the low-temperature phases of the same compounds are designated as B_3 or B_4.

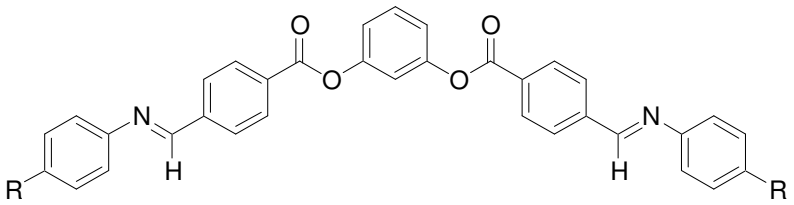

2a, R = -OC_5H_{11}; **2b**, R = -OC_6H_{13}

Chart 1.1

Further smectic phases formed by banana-shaped compounds get the code letters B_5–B_7 in the sequence of their discovery. None of the B phases are miscible with any smectic phase of calamitic compounds. Thus, a separate nomenclature is reasonable because the bent molecules obviously represent a new sub-field of liquid crystals.

1.5. Sugars / Carbohydrates as Candidates for Chiral LCs

Chiral liquid crystals are needed in gram scales for physical research and technical applications. Therefore they should be prepared by short synthetic pathways using easily available starting materials. Thus, synthetic strategies based on the chiral pool are more often used than asymmetric synthesis or chiral separation techniques.

A good chiral source for a chiral liquid crystal should have the following merits:[23]

1. Availability: The chiral raw material should be easily available.
2. Mesogenity: The moiety having the chiral centre should be able to induce liquid crystallinity by enhancing the anisotropic nature of the mesogen.

3. Diversity: The chiral source should have a wide structural diversity so as to be able to produce a library of LCs using it.
4. Polarity.
5. Stability: The chiral group introduced should be stable in the liquid crystal temperature range.
6. Effective mesogenic chirality.
7. Other material properties.

Sugars or carbohydrates possess most of the above characteristics necessary for a chiral liquid crystal. Sugars (carbohydrates) occur in every living organism. The sugar and starch in food, and the cellulose in wood, paper and cotton are nearly pure carbohydrates. Modified carbohydrates form part of the coatings around living cells,[43] other carbohydrates are part of DNA and RNA that carry our genetic information and some of them are used as medicines.[44] Carbohydrates are synthesized by green plants during photosynthesis, a complex process in which sunlight provides the energy to convert carbon dioxide and water into glucose plus oxygen. Many molecules of glucose are then chemically converted for storage by the plant in the form of either cellulose or starch. It has been estimated that more than 50% of the dry weight of the earth's biomass (all plants and animals) consists of glucose polymers.[44-46] When eaten and metabolized, carbohydrates provide the major source of energy required by organisms. The simplest carbohydrates are polyhydroxy carbonyl compounds with empirical formula of CH_2O, with

molecular formulae of $C_5H_{10}O_5$ and $C_6H_{12}O_6$ being most common. Carbohydrates are generally classed into two groups: simple and complex. Simple sugars or monosaccharides are carbohydrates like glucose and fructose that can't be converted into smaller sugars by hydrolysis. Complex carbohydrates are made of two or more simple sugars linked together. Sucrose (table sugar), for e.g., is a disaccharide made up of one glucose linked to one fructose. Similarly, cellulose is a polysaccharide made up of several thousand glucose units linked together. Hydrolysis of a polysaccharide breaks it down into its constituent monosaccharides. Monosaccharides are further classified as either aldoses or ketoses. The -ose suffix designates a carbohydrate and the aldo- and keto- prefixes identify the nature of the carbonyl group. The number of carbon atoms in the monosaccharide is indicated by using tri-, tetr-, pent-, hex- in the name. For example, glucose is an aldohexose (a six-carbon aldehydic sugar), fructose is a ketohexose (a six-carbon ketonic sugar) and ribose is an aldopentose (a five-carbon aldehydic sugar). Most of the commonly occurring sugars are either aldopentoses or aldohexoses. Each hexose e.g., D-Glucose (Chart 1.2, **3**) molecule in its cyclic hemiacetal form contains five chiral centers.[46]

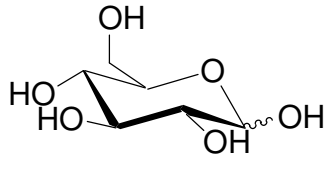

3

Chart 1.2

Thus being naturally abundant, inexpensive and a source of chiral centers[46] in addition to the merits listed above, sugars could be used as components for the design of chiral LCs. Interestingly in spite of all the favorable properties, none of the sugar-based mesogens so far reported in the literature have exhibited effective mesogenic chirality (macroscopic chirality), i.e., the liquid crystalline phases formed from sugars are achiral. The sugar molecules themselves are of course chiral and non-racemic. 'No mesogenic chirality' refers to the fact that the phases (as supramolecular aggregates) display no phase selective interactions with polarized light or a helical superstructure. Here the chirality of the bulk morphology is being probed, not that of the individual molecular components.[29] The carbohydrate mesogens form a class with high diversity. A large variety of compounds can be formed, e.g., by connecting alkyl chains of varying length with different monosaccharides which exist as different diastereomers (glucosides, mannosides, tallosides,…), constitutional isomers (pyranosides (6-membered rings), furanosides (5-membered rings), acyclic compounds), regioisomers (2-alkyl, 3-alkyl, 4,6-dialkyliden) and so on.[47]

Liquid crystalline organization of sugar amphiphiles are induced by 'intramolecular incompatibility'.[48] In other words, the liquid crystalline state can be described in terms of a microphase segregation.[10] This is a feature of amphiphilic molecules by which their hydrophilic and hydrophobic parts segregate in space into distinct microdomains. Due to the chemical bonding of the

amphiphilic parts, segregation does not lead to macroscopic phase separation. Instead, it results in the formation of different regions which are separated by interfaces at a molecular scale. These interfaces have characteristic mean interface curvatures, which are largely determined by the mean lateral areas of the competing parts of the amphiphilic molecules. Non-curved planar aggregates organize into lamellar (smectic) mesophases.[10] In the case of sugar amphiphiles, hydrophilic sugar head groups segregate by hydrogen bonding interactions and the hydrophobic alkyl (or fluoro alkyl) chains by van der Waals interactions. Goodby et al. developed the concept that amphiphilic mesophases (smectic) are basically held together by strong interactions of the hydroxyl groups, while aliphatic chains almost act as a liquid between the layers of the head groups.[48] The packing pattern obtained from the single crystal X-ray structures of these molecules revealed that the carbohydrate moieties were extensively hydrogen bonded with the alkyl chains intercalated (Figure 1.9).[49]

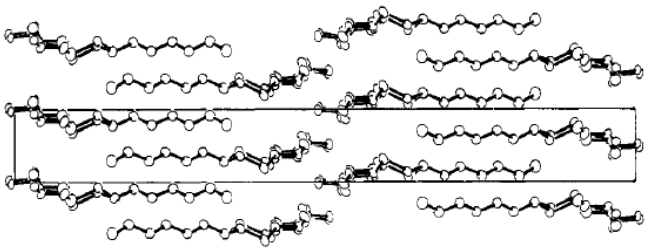

Figure 1.9. Head-to-head bilayer molecular packing in the crystal structure of heptyl 1-S-α-D-mannopyranoside. Adapted from reference 49.

The thermotropic phase transitions are believed to proceed in a stepwise process that begins with a partial breakdown of the three-dimensional network of

hydrogen bonds between the carbohydrate moieties (Cr–LC transition). The resultant LC state is mainly stabilized by the remaining hydrogen bonding between the sugar head groups in the hydrophilic part and additionally by van der Waals interactions. These interactions weaken at the clearing point (LC–I transition).[48]

1.5.1. Sugar based Liquid Crystals

Sugar LCs have been studied for almost a century. The first published work in the field was by Emil Fischer and Burckhardt Helferich who in 1911 reported[50] the double melting behavior of *n*-hexadecyl-β-D-glucopyranoside (Chart 1.3, **4**).

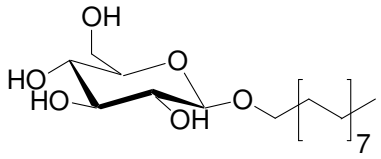

4

Chart 1.3

They recorded their observation as *'The cetyl glucoside is tasteless. It does not have a sharp melting point. Near 78 °C it starts to soften. At approximately 110 °C it melts to transparent droplets that flow together to form a colorless fluid with a clear meniscus near 145 °C. We have not been able to find the reason for this irregularity of the melting point'*.[50] Two years later Salway verified Fischers observations and extended the studies to steroidal glycosides.[26,51] In 1938, Noller and Rockwell recognized the phenomenon for what it was, namely that between

78 and 145 °C, cetylglucoside exists in a liquid crystalline state.[52] Mesogenic sugar containing compounds even exist in nature, e.g., tomatin (Chart 1.4, **5**). This compound in the pure state is a smectic A* liquid crystal.[23] It has been used as a highly efficient chiral dopant for lyotropic nematic phases.[53]

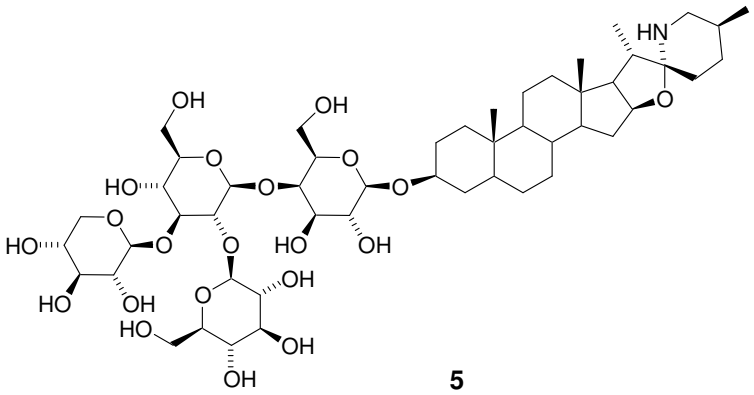

5

Chart 1.4

Another example is solanin (Chart 1.5, **6**), the poisonous compound in green potatoes, which for many years had been reported to possess two different melting points. Only recently was it shown that this compound is a smectic A* LC and two temperatures were its melting and clearing points.[26,54] This compound is amphotropic in nature, i.e., it forms both thermotropic and lyotropic liquid crystals.[26]

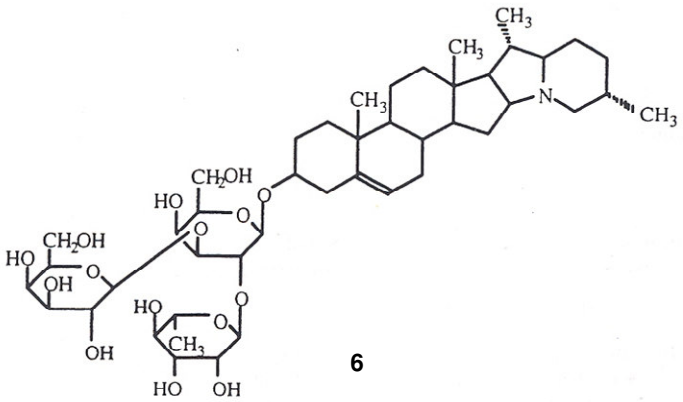

6

Chart 1.5

A large number of sugar-based LCs have also been synthesized and examined by many research groups. The *n*-alkyl-1-O-β-D-glucopyranosides, **7** and the *n*-alkyl-1-thio-α-D-mannopyranosides, **8** (Chart 1.6) were studied and shown by Jeffrey et al. to exhibit achiral liquid crystal phases by polarized light optical microscopy (POM), X-ray diffraction (XRD) and differential scanning calorimetric (DSC) investigations.[55] The *n*-alkyl-1-O-β-D-glucopyranosides possess a single LC mesophase which exhibited XRD patterns similar to that seen for smectic A* phases.

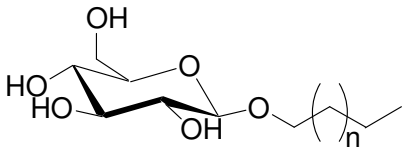

7

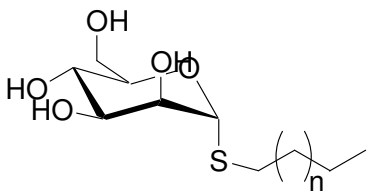

8

Chart 1.6

Even though these molecules were optically active, no macroscopic chiral textures could be seen by POM. XRD studies in the smectic phase agree with the calculated values for bilayer ordering in which the carbohydrate moieties overlap to produce an extensively hydrogen bonded structure (Figure 1.10).

This phase was classed as SmA_d*. The fact that the hydrogen bonding between neighboring sugar groups was very essential for showing liquid crystallinity could be understood from miscibility experiments with monophilic smectic A mesogens which showed that the phase formed by the carbohydrate derivatives were immiscible with these conventional smectogens. This was because the hydrogen bonding necessary for phase formation was disrupted in the binary mixtures which means that the phase is a separate subset of the smectic A* phase.[56]

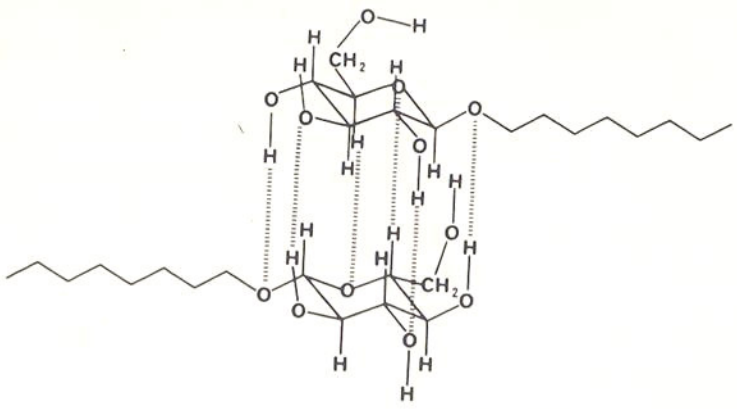

Figure 1.10. Stacking structures of the alkylated carbohydrates. Adapted from reference 56.

1.5.1.1. Why Macroscopic Chirality is not exhibited by Chiral Sugars?

The failure to express mesogenic chirality in the sugar derivatives has been attributed to sugars being too sugary (sticky)!.[29] The amphiphilic character is reinforced by the many hydroxyl groups that readily enter into hydrogen bonding. This leads to rigidly packed double layers that assemble into smectic phases.[29] Alkylated sugars are chiral compounds but not effective chiral LCs.[23] Lyotropic chiral phases based on asymmetric micelles were observed only in a few cases.[23]

Later diverse libraries of sugar amphiphiles were synthesized and their LC properties studied and reviewed. It has been found that the clearing and mesophase to mesophase transition temperatures are extremely sensitive to small structural changes at the molecular level. Many studies have been made in relation to the effects of substituent size and position on mesomorphic properties. One such comparison has been completed for the thermotropic properties of the *x*-O-dodecyl-α,β-D-glucopyranoses by Miethchen and other researchers.[57,58] Miethchen et al. demonstrated the effect on clearing point temperatures as a dodecyl chain is moved sequentially from one position to the next in substituted D-Glucopyranose systems (Chart 1.7). In this series, the dodecyl chain is moved from the 1- to the 6-position of the ring. The clearing points range from 140 to 167 °C, with the 2-substituted compound having the highest clearing temperature and the 4-substituted compound the lowest.

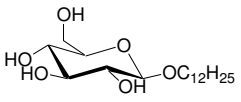

Cr 80.4 SmA* 143.4 I

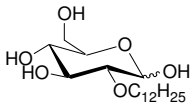

Cr 92.5 SmA* 167.2 I

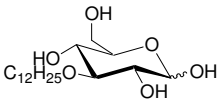

Cr 127.5 SmA* 141.8 I

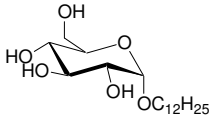

Cr 77 SmA* 151 I

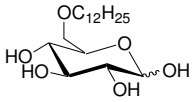

Cr 94 SmA* 163 I

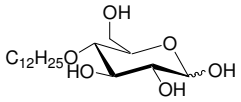

Cr 109 SmA* 140 I

Chart 1.7

Interestingly, the mesophase exhibited by all of the homologues is the same; i.e., a smectic A_d* phase. The fact that the mesophase type is lamellar suggests the shapes of the molecules for each of the members of the series, are rod-like, with the carbohydrate head group having a similar cross sectional area to the aliphatic chain. As a consequence, the sequential movement of the chain does not engender any curvature into the system which might lead to the formation of cubic or columnar phases.

Goodby et al. extended these studies further by examining the effect on mesomorphic properties of the position of substitution of an aliphatic chain in a disaccharide system. Thus a dodecyl aliphatic chain was moved sequentially from one position to the next in the mono-O-(2-hydroxydodecyl)sucrose family of

materials, and their the LC behavior examined. By introducing the disaccharide unit (sucrose in this case) it was expected that the relative cross-sectional area of the sugar head group would vary considerably as the aliphatic chain was moved sequentially from one position to the next (Chart 1.8).[58] These derivatives exhibited bilayer SmA_d*, Col_h or Cub phases depending on the position of attachment of the dodecyl aliphatic chain.[58]

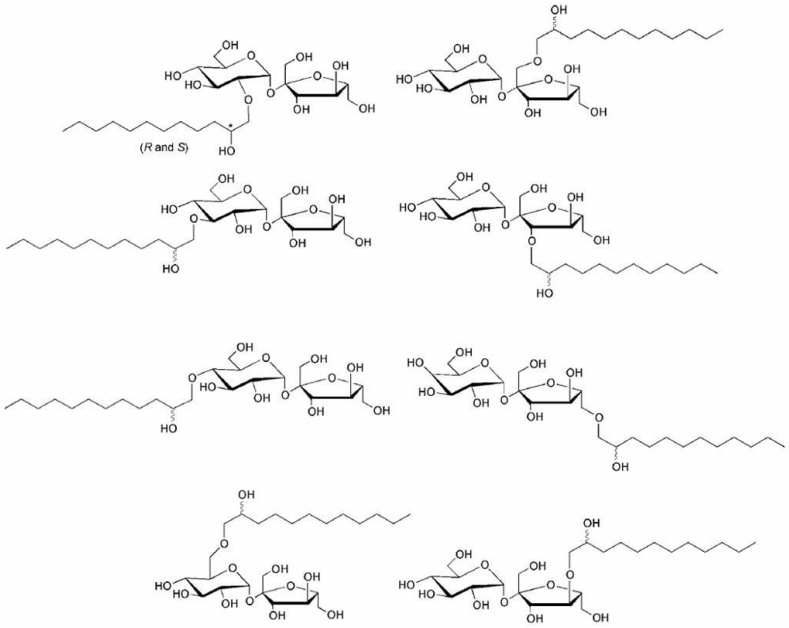

Chart 1.8

Another example of minor change in molecular geometry causing drastic change in phase behavior was reported by Weiss et al. They observed chiral columnar phases from the penta-O-*n*-alkanoylglucopyranoses (Chart 1.9).[59] This was in contrast to the report that tetraacetyl alkylglucopyranosides do not exhibit mesophases.[49,52,60]

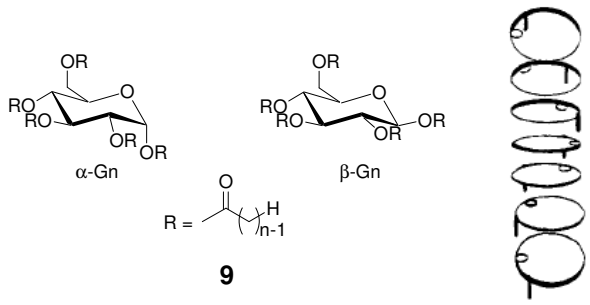

Chart 1.9

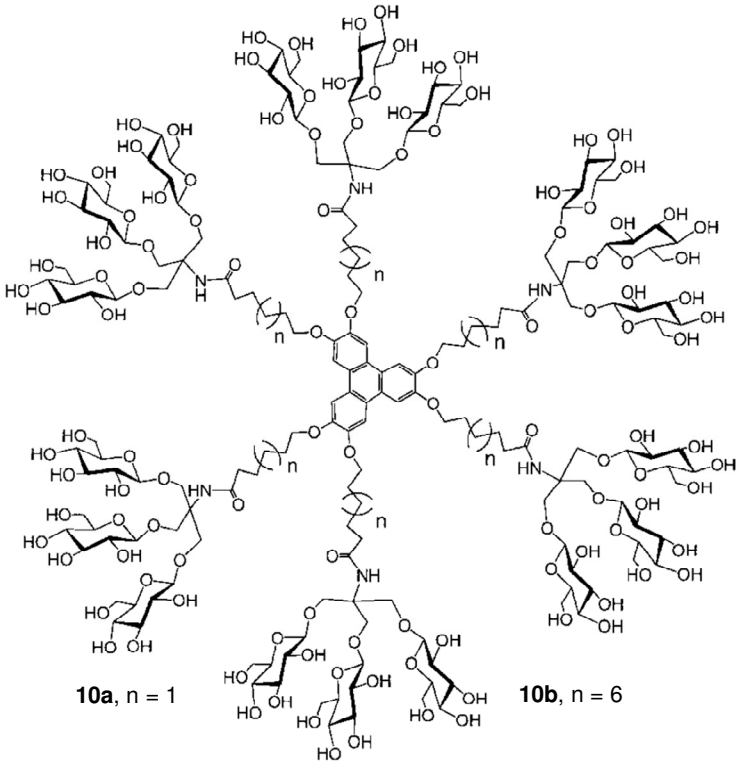

Chart 1.10

Stoddart et al. reported on the constitutional marriage between a classical thermotropic discotic molecule and a carbohydrate based amphiphile and studied the LC properties of the resulting compounds.[61] In these new hybrids, a

triphenylene unit served as the central core from which oligomethyleneoxy chains–either C_5 or C_{10}–radiate symmetrically through amide bonds to be terminated by β-D-glucopyranosyl residues either singly or as a cluster (**10a**,**b**) of three residues (Chart 1.10).

These compounds behave as unusual amphiphilic materials, showing two well defined molecular regions–the central hydrophobic part and the peripheral hydrophilic one. As a consequence, they exhibit amphotropic liquid crystalline properties, showing both thermotropic columnar phase and lyotropic behavior on contact preparation with pentaethylene glycol. The balance between the two different molecular regions controls the existence of mesomorphism and the type of columnar arrangement observed in the mesophase.[61]

1.5.1.2. Perfluoroalkylated Sugar based Liquid Crystals

Sugar amphiphiles that are linked to only one hydrophobic hydrocarbon chain form mostly smectic phases. When the hydrocarbon part of sugar amphiphiles is replaced with a perfluoroalkyl chain, also smectic phases are observed. These amphiphiles in general showed higher melting and clearing points than the fluorine-free alkyl-β-D-glucopyranosides with equal carbon chain length. The higher hydrophobicity of a fluorocarbon chain compared to alkyl chains enhances the amphiphilic character (intramolecular contrast) in these compounds. They are also more rigid than hydrocarbon chains because of a large energy

difference between their *gauche* and *trans* conformations. Fluorinated chains prefer the *trans* form with less conformational freedom and an essential helical conformation. Thus, replacement of an alkyl chain by a perfluorinated chain generally leads to a significant stabilization of the corresponding mesophases formed by an amphiphilic sugar. Even a perfluorobutyl chain linked to a sugar moiety was sufficient to make the molecule mesogenic. Alkylene (hydrocarbon) spacers such as in **11**, between the hydrophilic head group and the fluorocarbon tail enhance the flexibility of the chains (Chart 1.11). That may have the effect of lowering the clearing points in comparison to derivatives with the same perfluoroalkyl chain length, but without any spacer.

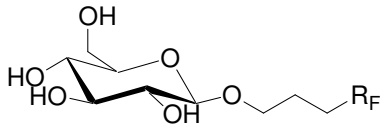

11, $R_F = C_4F_9, C_6F_{13}, C_8F_{17}, C_{10}F_{21}$

Chart 1.11

Mostly smectic A* phases were observed in these derivatives which aligned to form homeotropic layers after melting.[62] Only on preparing POM samples without a cover-slide could the characteristic textures of smectic A* phase such as stepped drops and fan-like textures be observed. No dechiralization lines characteristic of any helical phases were seen.

When an –OH group in the sugar moiety is replaced with a fluorine atom, significant destabilization of the LC phase occurs.[48] Whereas –OH groups contribute to the cooperative networks as H-bond donors and acceptors, C–F groups act exclusively as weak acceptors. Thus the amphiphiles which are monofluorinated within the hydrophilic head region show only narrow ranged mesophases compared to the analogous fluorine-free –OH compounds because replacement of C–OH by C–F reduces the hydrogen bonding between the head groups of the carbohydrate mesogens.[48]

Substitution of an –OH group by fluorine and hydrogen, respectively also brings about significant changes in thermal properties (Chart 1.12).[48]

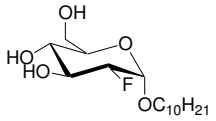

Cr 88 SmA* 110 I

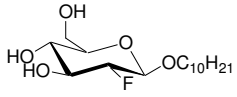

Cr 89 SmA* 127 I

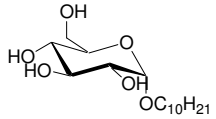

Cr 76 SmA* 138 I

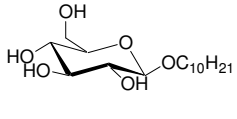

Cr 70.3 SmA* 135.5 I

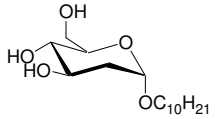

Isotropic at 73

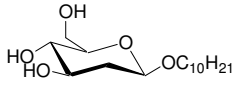

Isotropic at 91

Chart 1.12

Thus the two anomeric decyl D-*arabino*-hexopyranosides show, compared with the corresponding C–2 OH and C–2 F derivatives, the lowest clearing

temperatures, because the methylene moiety is not able to participate in the polar network in any way. The homologous alkyl-2-deoxy-2-fluoro-α-D-glucopyranosides form less stable mesophases (lower clearing temperatures) than alkyl-α-D-glucopyranosides. On the other hand, the mesophases of alkyl-2-deoxy-2-fluoro-α-D-glucopyranosides are less stable as compared to those of the corresponding alkyl-2-deoxy-2-fluoro-β-D-glucopyranosides as well as the corresponding alkyl-2-deoxy-2-fluoro-1-thio-α-D-glucopyranosides. The latter result correlates with the former observations that S-glucosides show higher clearing temperatures than the corresponding O-glucosides. Goodby et al. had earlier arrived at a general conclusion that the efficiency of the linking group in the formation of thermotropic phases follows the order –SR > OCOR > –OR.[48]

1.5.1.3. Liquid Crystals formed from Sugar based Bolaamphiphiles

Bolaamphiphilic molecules contain a hydrophobic skeleton (e.g., one, two, or three alkyl chains, a steroid, an aromatic moiety or a porphyrin) and two water-soluble groups on both ends (Figure 1.11a).[63] The name, bolaamphiphile derives from the resemblance of its general molecular architecture to the Argentine bola with leather balls which was a weapon used to fell animals (Figure 1.11b).

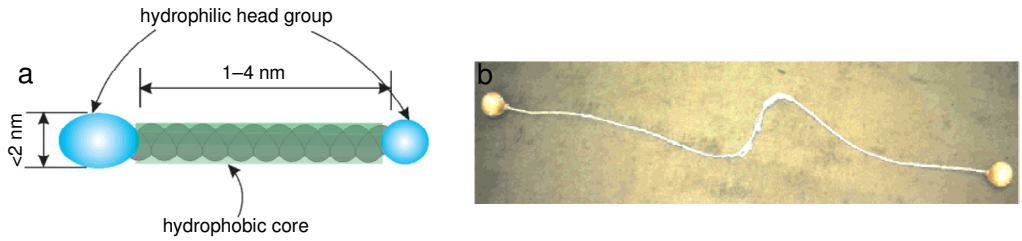

Figure 1.11. (a) Schematic drawing of the bolaamphiphile and (b) Photograph of an Argentine bola with leather balls. Adapted from reference 63.

Symmetrical and unsymmetrical bolaamphiphiles have been studied for their mesogenic properties. Macroscopic chiral mesophases were not observed in the bolaamphiphiles consisting of oligomethylene spacers constrained by glucopyranosyl head groups reported by Masuda et al. (**12**, Chart 1.13).[64] The self-assembly of these derivatives in solid-state were investigated using DSC, XRD, POM and FT-IR spectroscopy. Both the chain conformation and thermal behavior of the assemblies have been used to classify them into three categories, short ($6 \leq n \leq 8$, and $n = 10$), medium ($n = 9$, and $11 \leq n \leq 13$) and long chain ($14 \leq n \leq 20$). Thus, the bolaamphiphiles with a short-chain spacer self-assembled in water to form a *gauche*-including monolayered self-assembly, while the medium- and long-chain homologues formed monolayered assemblies with an all-*trans* oligomethylene conformation. The short- and long-chain bolaamphiphiles also exhibited a polymorphism on heating which proceeded with retention of the *gauche* chain conformation, with the long-chain homologues transforming from the Cr1 to Cr2 phase (keeping an all-*trans* conformation) and eventually into the

Cr3 phase with a *gauche*-including spacer. In addition, the long-chain derivatives showed a stable mesophase and that of medium-chain, n = 13, bolaamphiphiles were unstable. They all formed a thermotropic smectic A* mesophase. This smectic phase was the first example of a liquid crystalline phase for aldosamide bolaamphiphiles. Their melting and clearing temperatures were high when compared with those of other, structurally similar bolaamphiphilic tetraols or gemini-type sugar-based amphiphiles. The increased thermal stability of these derivatives stems from hydrogen-bond formation between amide groups as well as strong intermolecular interactions from double head groups since the amide hydrogen bond chain enhances the molecular ordering and enforces the formation of hydrogen bonding between the sugar hydroxyl groups.[64]

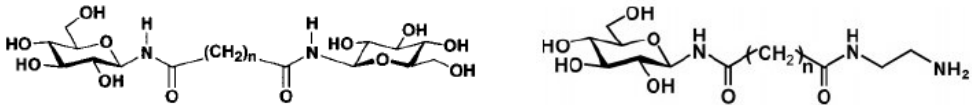

12, n = 6 – 14, 16, 18 and 20 **13**, n = 12, 14, 16, 17, 18 and 20

Chart 1.13

Recently the same group has reported the thermal phase transition behavior of unsymmetrical bolaamphiphiles having glucose- and amino-hydrophilic headgroups (**13**, Chart 1.13).[65] The DSC thermograms in the first heating run indicated that the long chain **13** (n = 18, 20) exhibits crystal polymorphism (Cr1 and Cr2) and a thermotropic LC phase before isotropic melting. POM studies

showed a fan-like birefringent texture for these derivatives and the phase was assigned as smectic. The short chain **13** (n = 12, 14, 16, 17) shows no such polymorphism, only Cr1 which transformed directly to the isotropic liquid. Thus the two examples[64,65] (Chart 1.13) showed that the sugar groups when present in the bolaamphiphilic structure did not exhibit macroscopic chiral phase but formed tightly packed hydrogen bonded layers resulting in achiral phases (smectic).

1.5.1.4. Thermotropic properties of non-amphiphilic (monophilic) derivatives: Chiral LCs from Chiral Sugars by Chemical Modification

It was thus firmly established in the literature that generation of macroscopic chiral LC phases from sugar derivatives containing free hydroxyl groups was not possible. It was felt that it could be only achieved by suppressing their amphiphilic character either by suitable derivatization or replacement of the hydroxyl groups by other functional groups.[29] When the –OH groups in sugar moieties are removed, the amphiphilic character is lost and the molecule becomes monophilic. These derivatives have prospect to exhibit chiral phases such as chiral nematic or smectic C*. Vill et al.[66] and Wong et al.[67] prepared non-amphiphilic sugar derivatives exhibiting chiral nematic liquid crystalline phases by removal of hydroxyl groups through chemical manipulation (Chart 1.14).

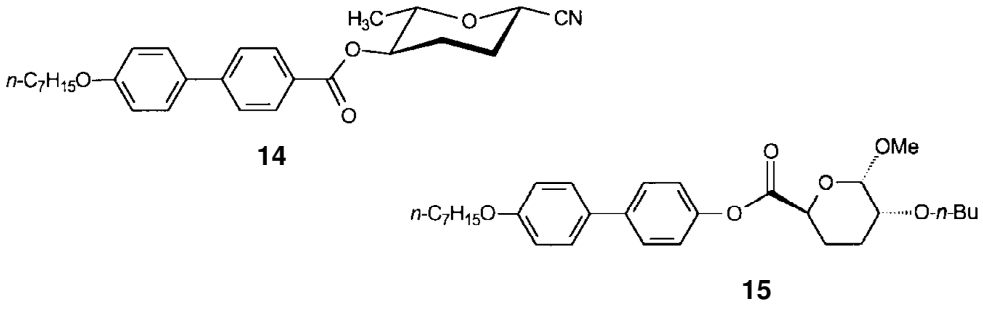

Chart 1.14

Kellogg et al. used another approach in which the –OH groups at the 4- and 6- positions of the glucoside were condensed with aromatic aldehydes to form the (*R*)-4,6-O-benzylideneacetal derivatives which embody the *trans*-decalin skeleton (Scheme 1.1).[29] Aliphatic and aromatic aldehydes with electron withdrawing (4–NO_2, 4–CHO) or electron donating (4–OCH_3, 4–CH_3) groups attached can be condensed across the 4,6-hydroxyl groups of the sugar tetraols. The 2- and 3-hydroxyl groups were left unchanged.

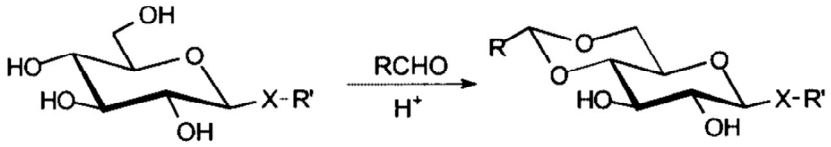

16, X = S; R = *n*-C_5H_{11}, *n*-$C_{10}H_{21}$, *n*-$C_{12}H_{25}$ **18**
17, X = 4-OC_6H_4; R = CH_3, *n*-$C_{10}H_{21}$, *n*-$C_{12}H_{25}$

Scheme 1.1

Schiff base derivatives which are extremely potent mesogens were coupled into this benzylidene acetal structure. By this way van Doren et al. prepared **20** as shown in Scheme 1.2 which exhibited an achiral smectic A liquid crystalline phase.[29,68]

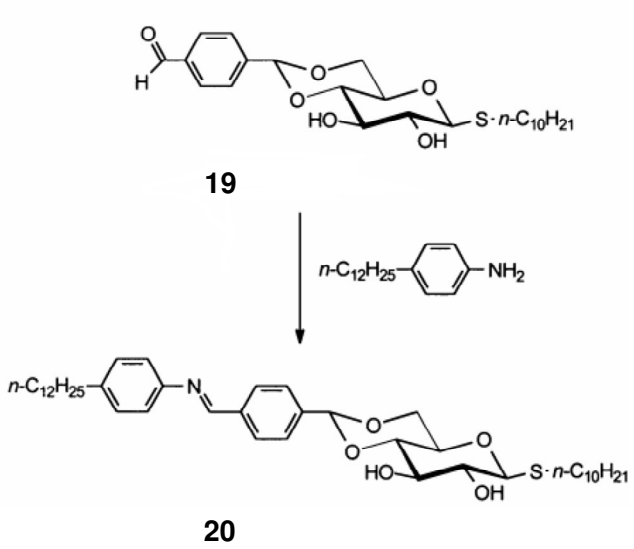

Scheme 1.2

This phase was also not miscible with the common smectic A phases, indicating that it organizes into a different arrangement in the thermotropic liquid crystalline state.

Subtle changes in structure can drastically influence the LC phase structure of mesogenic sugars.[29,69] An example has been demonstrated from the Kellogg group in which a minor operation of changing the direction in which the ester group runs, –C(O)O– compared to –OC(O)–, drastically affects the phase behavior as shown in Scheme 1.3. The overall dipole of the mesogenic unit is strongly affected by this 'minor' change.[29] Compounds **21** and **22** with XR' = S–alkyl or –OC_6H_4O–alkyl exhibit chiral nematic phases.[69] But surprisingly **23** and **24**, which have the ester group in the opposite direction, form achiral smectic phases.[29]

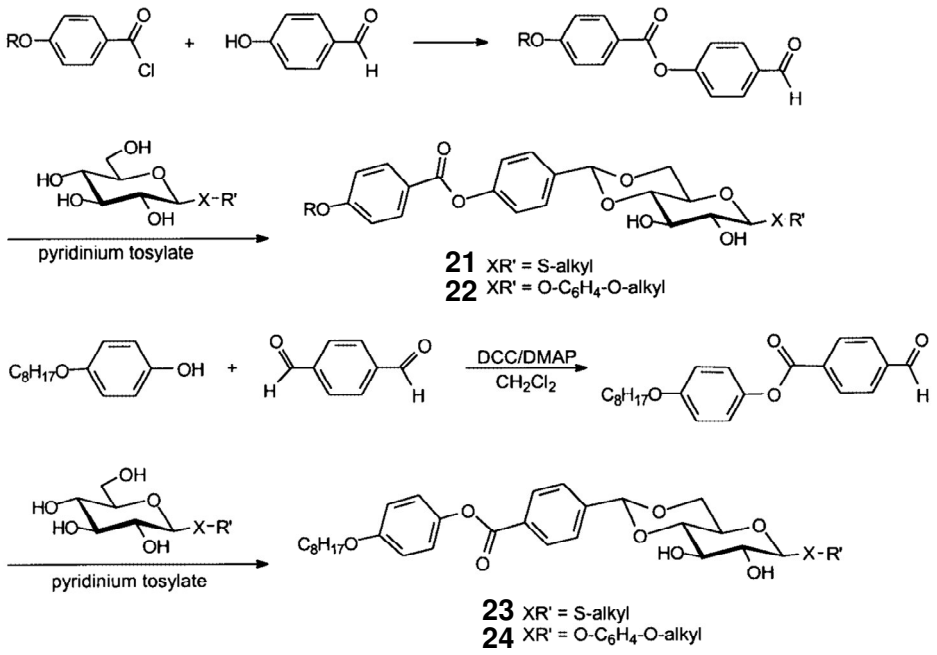

Scheme 1.3

The sequence of mesogenic group and hydrophobic chain may be reversed from the sense in compounds (**21**, **23**) wherein former was part of the aldehyde forming the *trans*-decalin structure and the latter attached to the anomeric centre. Some examples (**25**, **26**) with the reversed molecular design in which the mesogenic unit is attached to the anomeric carbon atom are shown in Scheme 1.4.[29] The sensitivity of liquid crystalline behavior to seemingly minor structural changes is illustrated in the case of **26** also. In **26**, if L = O, no liquid crystallinity is observed, whereas if L = OCH_2 (two atoms instead of one), smectic LC phase is observed. The difference mostly lies in the fact that with a one atom linker a bend is enforced on the molecule at the cost of the required calamitic character of the

molecule. With a two atom linker a more linear molecular geometry can be attained and as a consequence the molecules are liquid crystalline.

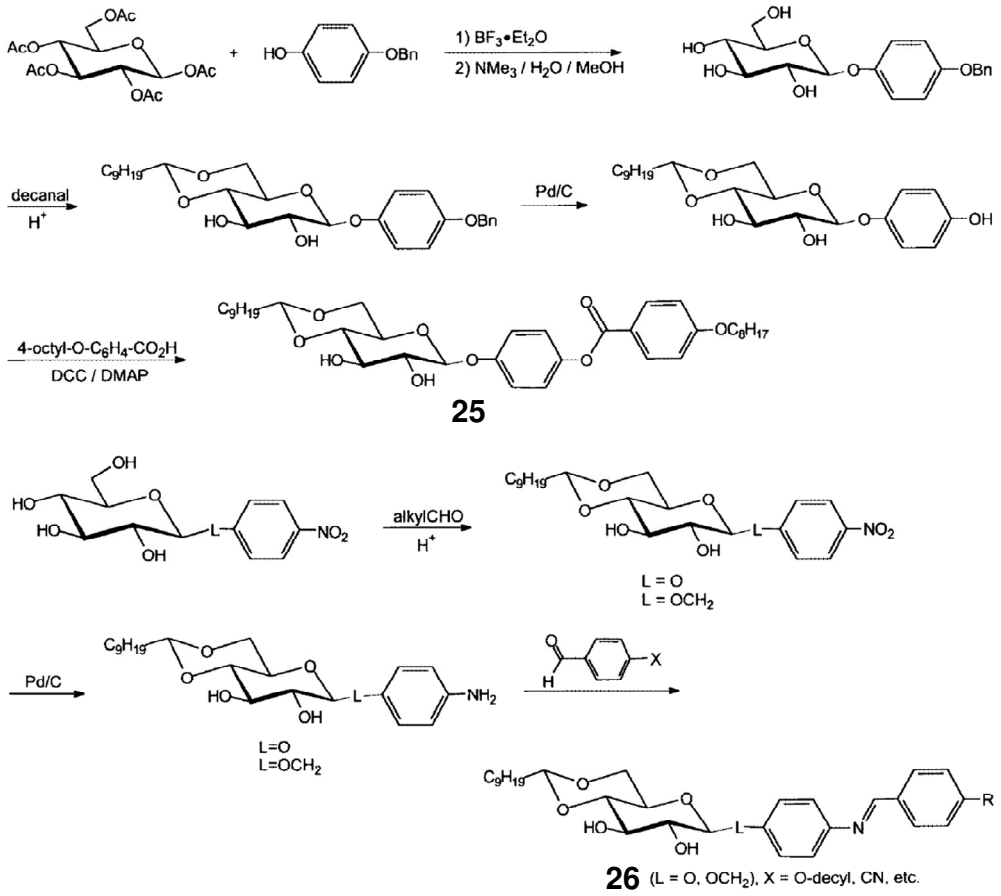

Scheme 1.4

The presence of fluorine containing sugar derivatives may improve the chemical stability and thermal properties of non-amphiphilic mesogens. The chiral fluorinated materials have even higher and broader temperature ferroelectric phases with larger *P*s. Thus from the point of view of preparing chiral LCs, fluorine containing sugar LCs should rather be non-amphiphilic because such

mesogens meet the requirements for the formation of chiral smectic C phases (Chart 1.15).[48]

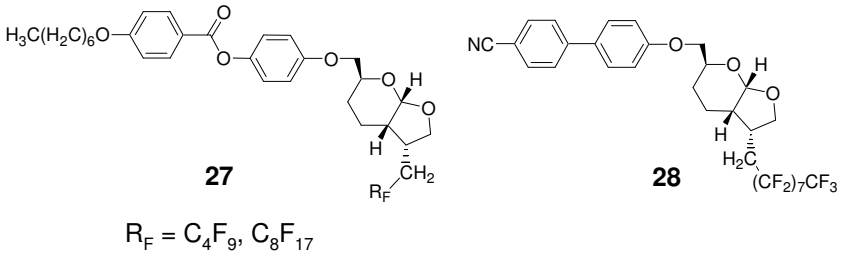

Chart 1.15

Dierking et al. developed the first bent-core mesogen with a chiral carbohydrate based central bent unit (**29**, Chart 1.16), which exhibited traditional calamitic phases along with banana phases.[70] From POM texture observations and electro-optic experiments it was concluded that the low temperature phase below the cholesteric phase of this compound is a fluid smectic, presumably a B_2 phase. Chart 1.16 shows the molecular structure of the mesogen along with its theoretically (AM1 and EF) calculated molecular geometry. The simulation of the molecular shapes was performed using the WinMOPAC V2.0 Molecular Orbital Program.

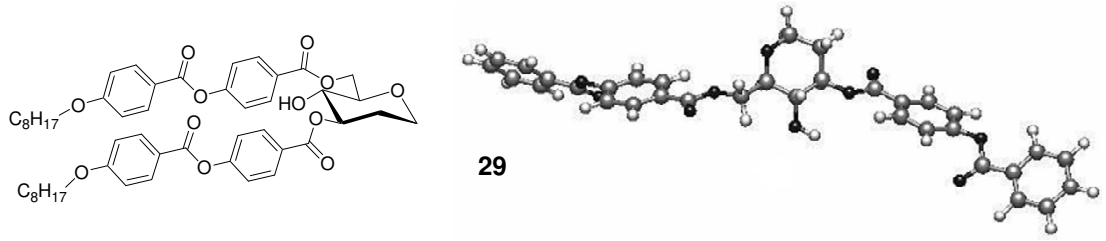

Chart 1.16

1.6. Self-assembling properties of Amphiphiles and Bolaamphiphiles in Solution

The amphiphiles and bolaamphiphiles which aggregate in the bulk to form liquid crystalline phases can also self-assemble in solvents above their critical aggregation concentration with the aid of noncovalent interactions to form a variety of supramolecular structures such as micelles, vesicles, planar lamellar structures, cones, fibers, nanotubes, etc. As mentioned earlier these lyotropic self-assembled structures have immediate relevance in biology because of the prevalence of organized lipid structures in living systems.[30] In particular, we will discuss glycolipids which are membrane components and occur in all kingdoms of organisms, i.e., bacteria, plants and animals including man.[71] Glycolipids comprise one of the three layers that constitute the biomembrane, the glycocalix, the other two namely: protein-lipid bilayer and the cytoskeleton (Figure 1.12).[72] Glycolipids, greatly contribute to the structural stability (cell surface rigidisation)[43] and the function of biomembranes in living systems.

The biological cell contains many kinds of organelles such as nucleus, mitochondria, ribosome and the Golgi apparatus. These organelles have characteristic morphologies that are directly related to their respective biological functions. The organelles are self-assembling systems which are composed mostly of proteins and biomembranes.

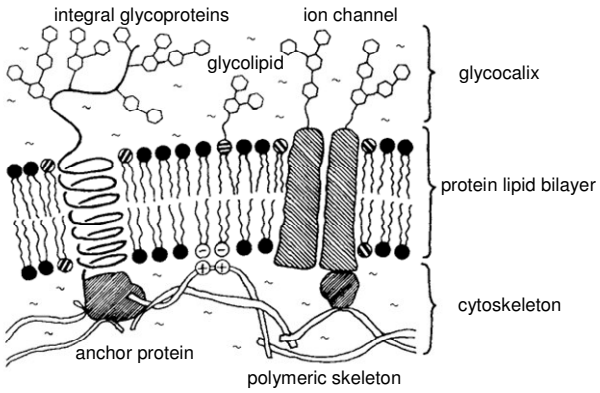

Figure 1.12. Schematic representation of a biomembrane. Adapted from reference 72.

Thus the importance of morphology in relation to the function is obvious in the biological world. However the morphology-related function is now being recognized in chemistry. To get a deeper insight into the structure-function relationships of biomembranes, a large number of bioorganic investigations are necessary. However, natural membranes show a high level of complexity. In order to study the properties of individual membrane components, it is necessary to concentrate at first on simple model membranes having a defined chemical composition.[72] In this regard various classes of synthetic self-assembling systems which possess designed morphologies have been developed.

The basic aggregate form: the micellar system is usually very fluid and dynamic and thus cannot have fixed morphologies. For formation of ordered structures by self-assembly using noncovalent interactions, amphiphiles should have the following basic structural features: hydrophilic head group, rigid segment and a flexible tail.[73]

Liquid crystalline property is an integral part of the bilayer formation. The molecular arrangement in the monolayer and bilayer of single-chain amphiphiles is fundamentally the same as that of the smectic mesophase.[73,74] G. W. Gray, the pioneer in the liquid crystal field has listed the structural requirements[75] for the mesomorphic behavior are: (i) elongated molecular geometry which is rod- or lath like in shape and (ii) appropriate intermolecular attractions for maintaining parallel molecular packing. It is expected that the amphiphilic molecules with these structural characteristics form stable membrane assemblies in water. Many of these self-assembling amphiphilic molecules are thermotropic liquid crystals in the bulk state.

The formation of the various self-assembled morphologies depends upon the molecular shapes of the constituent amphiphiles and their critical packing parameters (P) as illustrated in Figure 1.13.[76] Thus the self-assembled morphology can be predicted using the structural guide lines proposed by Israelachivili et al.[77] They put forward an optimal surface area per polar head group, which depends on the packing parameter, $P = v/(a_o \times l_c)$, where v is the volume of the hydrophobic chain, a_o is the polar head surface area at the critical micellar concentration (cmc) and l_c is the chain length (Figure 1.13). If $P < 1/3$, the amphiphile has a tendency to form spherical micelles; if $1/3 < P < ½$, cylindrical micelles will be favored; if $½ < P < 1$, bilayers with a spontaneous curvature (vesicles) are produced; if $P = 1$,

planar bilayers will be favored; and if $P > 1$, micellar aggregates with a reverse curvature will be formed.

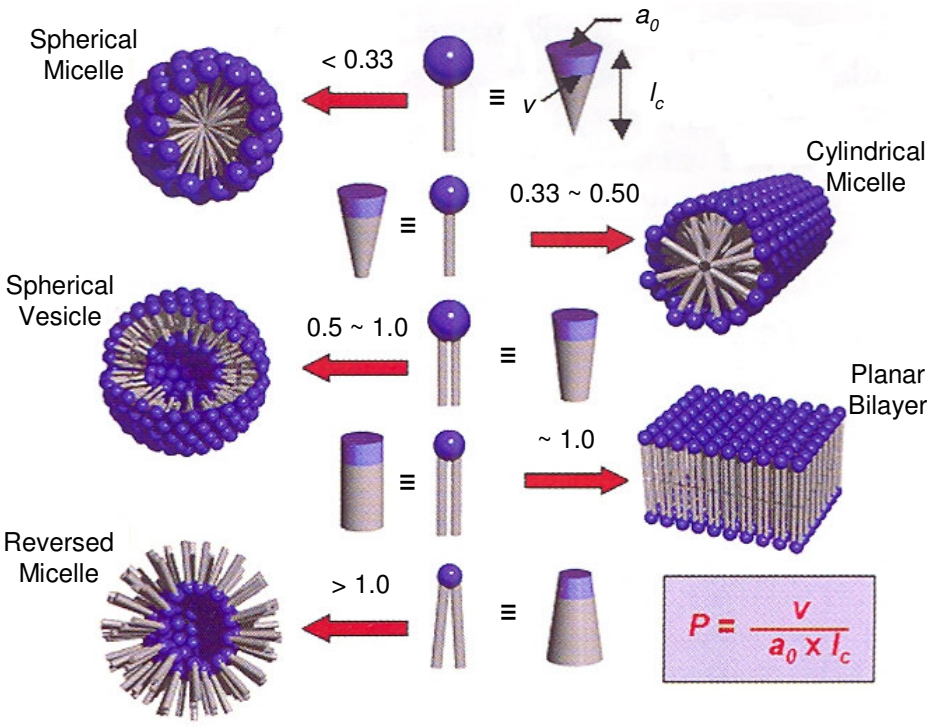

Figure 1.13. Various self-assembled morphologies depending on the critical packing parameter (*P*) of each amphiphile. Adapted from reference 76.

However, this prediction method becomes complicated if the packing of hydrophobic chains is crystalline. Only when the amphiphile possesses hydrophobic chains in a fluid state is the above prediction applicable.[76]

1.6.1. Aggregate Morphology

Typical morphologies adopted by amphiphiles include micelles, bilayers, vesicles, lamellae, rods, tubes and disks.[73,76] When added to water at certain concentrations, amphiphiles aggregate into micelles. Micelles have an external surface of hydrated head groups and an interior of interpenetrated hydrocarbon

chains. They are in the dynamic equilibrium with free surfactant amphiphilic molecules and the micellar core is known to have the liquid-like fluidity (Figure 1.14).

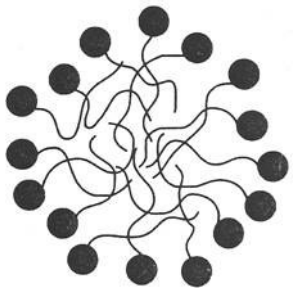

Figure 1.14. Schematic representation depicting the disordered and fluid nature of the micelle interior. Adapted from reference 78.

Thus they are difficult to characterize due to their dynamic nature and ill-defined structure. They do not usually give any definite morphology by microscopy techniques. They are commonly generalized as spheres formed from a few hundred amphiphilic monomeric units.[78]

Kunitake et al. have extensively studied synthetic amphiphile-based molecular membranes. Stable bilayer as well as monolayer membranes have been prepared in dilute aqueous solutions from a variety of totally synthetic amphiphiles which contain two higher alkyl chains as the hydrophobic moiety.[79] The hydrophilic group of these amphiphiles may be cationic, anionic, nonionic or zwitterionic. In very recent studies, it is shown that the hydrophobic portion of these bilayer-forming amphiphiles can be replaced by a single-chain unit which

contains a rigid segment such as diphenylazomethine, biphenyl group, etc. Figure 1.15 schematically illustrates these bilayer structures.

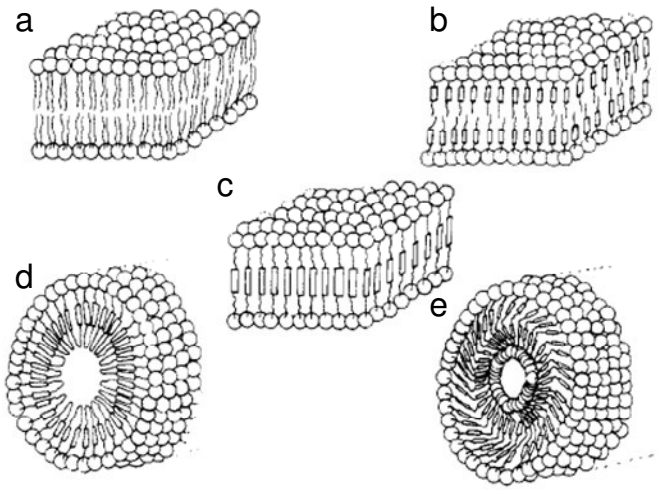

Figure 1.15. Schematic illustration of synthetic molecular membranes. Bilayer membrane formed from one-headed a) double-chain amphiphiles, b) single-chain amphiphiles, c) Monolayered membrane formed from two-headed single-chain amphiphiles, d) Rod-like structures and e) tubular structures. Adapted from reference 79.

The two-dimensional development of the bilayer assembly produces the typical bilayer membrane. The bilayers stack one over the other to form the lamellar structure. Bilayers can fold into various shapes forming supramolecular assemblies, the stability of which is governed by the thermodynamics of surfactant self-assembly.[80] This includes the membrane bending energy, the cohesive energy between molecules within the aggregates and the way by which the system closes the supramolecular structure to prevent the formation of edges. For instance, vesicles form to prevent the occurrence of such bilayer edges (Figure 1.16).[80,81]

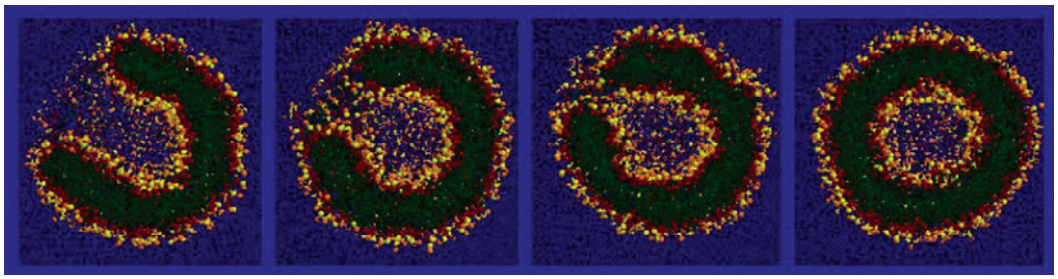

Figure 1.16. Spontaneous closing of the bilayer to the vesicle by molecular dynamics simulation. Snapshots are shown (from left to right) at t = 180, 200, 210 and 215 ns. Adapted from reference 81.

Vesicles (liposomes) are spherically closed lipid bilayers, which, in analogy to the cell membrane, enclose an aqueous compartment.[81-83] Vesicles can be prepared by numerous methods, which lead to the formation of completely different vesicle systems. They differ in diameter between 20 nm and 100 μm as well as in the number of bilayers. The ultrasonication of lipid suspensions in water for example, leads to small unilamellar vesicles (diameter ranging 20–100 nm). The swelling of lipid films, however, leads to uni- or multilamellar vesicles of the size of a cell. Bolaamphiphiles form monolayer membrane vesicles.[63] Liposomes are suitable for a large number of biophysical and biochemical investigations: e.g., for the measurement of membrane permeability for the reconstitution of active membrane proteins and for the study of surface recognition reactions or dynamic membrane processes.[72] More recently vesicles have been used as drug delivery carriers and controlled release agents.[82-84] Numerous papers in the literature have focused on the formation of vesicles from amphiphilic and bolaamphiphilic molecules.

Two-headed, single-chain ammonium amphiphiles in which the hydrophobic chain was made of the flexible decamethylene unit and the rigid diphenylazomethine or biphenyl unit were synthesized and studied by Kunitake et al.[79] These amphiphiles produced huge (10^6–10^7 daltons) aggregates in dilute aqueous solution. The basic structure of the aggregates was shown by electron microscopy to be the monolayer membrane. A rod-like structure resulted when the flexible moiety increased. Addition of second components drastically changed the aggregate structure. For instance, rigid lamellae were converted to large single-walled vesicles by incorporation of cholesterol. This was the first example of the formation of stable monolayer membranes (Figure 1.17).[79]

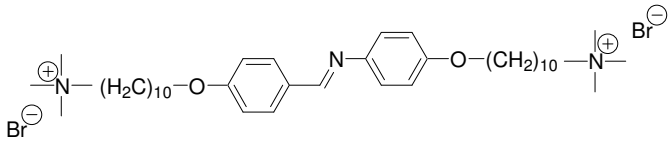

30

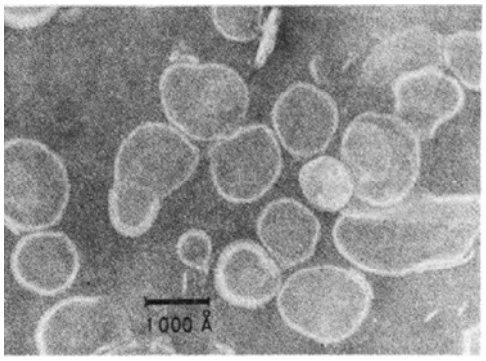

Figure 1.17. Molecular structure of the two-headed amphiphile (**30**) and TEM image (X 1,80,000) of the monolayered vesicles formed from **30** on addition of cholesterol. Adapted from reference 79.

Tew et al. recently reported vesicle formation from novel amphiphilic architecture namely discotic *ortho*-phenylene ethynylene cyclic trimer,[84] **31** as shown in Figure 1.18. This triethylene glycol (TEG) substituted triangle shaped macrocycle exhibited columnar hexagonal LC phase at room temperature.[85] In

addition to the bulk phase behavior, the rigid, hydrophobic core and polar, flexible side chains suggested that this molecule might self-assemble in aqueous solutions. The amphiphile self-assembles into vesicles with an average diameter of ~500 nm from 1:1 chloroform/water.[84] From TEM analysis (Figure 1.18) a wall thickness of ~3 nm was measured. Based on the this data and the molecular dimensions of the macrocycle, the authors postulate that the macrocycle packs into a bilayer structure with the phenylene ethynylene core toward the interior of the bilayer and the more polar TEG side chains exposed to solvent. This is illustrated schematically in Figure 1.18.

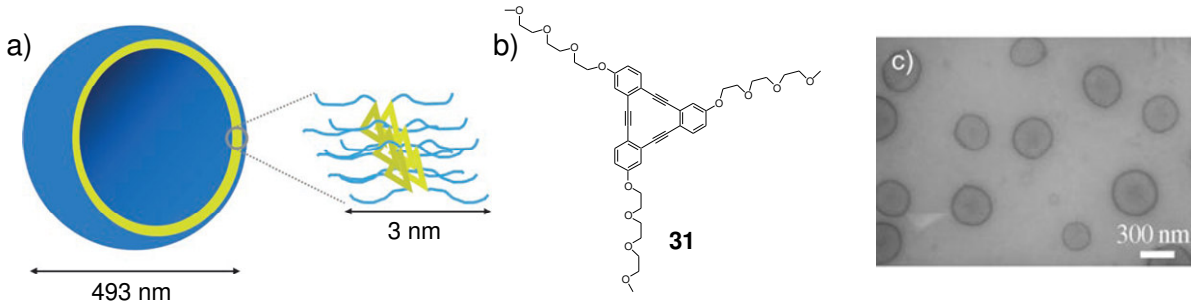

Figure 1.18. Schematic representation of bilayer vesicle formation (a) from *o*-phenylene ethynylene cyclic trimer (b) TEM image of the vesicles (c) Adapted from reference 84.

S. Das et al. have also recently observed, vesicle formation from amphiphilic butadiene derivative.[86] These derivatives undergo a hierarchical self-assembly from small sized vesicles at lower concentrations to larger vesicles at higher concentrations. The vesicles finally merge together to form a unique type of gel consisting of globular aggregates with solvents entrapped within them as

shown schematically (Figure 1.19). An aggregation-induced enhancement of fluorescence was also observed in this class of materials.

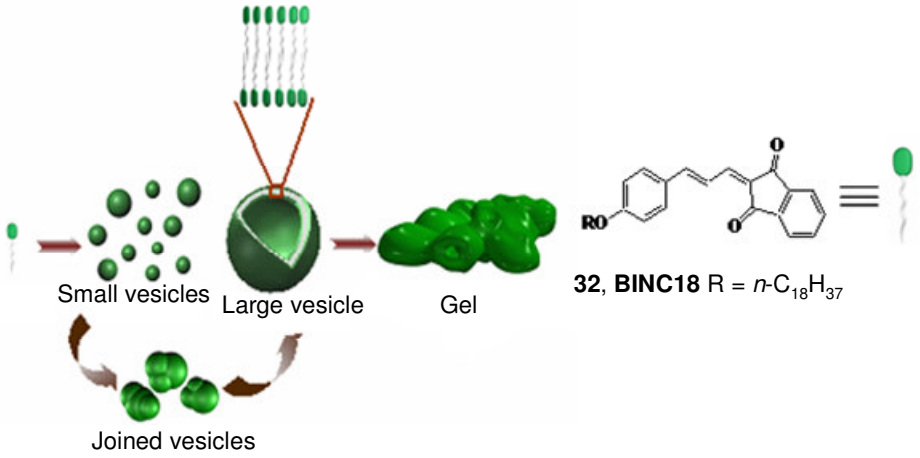

Figure 1.19. Schematic representation of the hierarchical organization from small to large vesicles and finally to gels from an amphiphilic butadiene, **BINC18**. Adapted from reference 86.

Both the vesicles and gels formed from these molecules were found to be photoresponsive due to light induced photoisomerization of the butadiene moiety. Figure 1.20 shows the effect of UV irradiation (445 nm) on the vesicles. Photo-irradiation of **BINC18** also resulted in disruption of its supramolecular aggregates. The AFM image of a film obtained from un-irradiated aged 5×10^{-6} M methanol solution of **BINC18** showed the existence of large joined vesicular aggregates. On irradiation, destruction of the larger vesicles and formation of small spherical aggregates was observed. AFM images obtained from the irradiated solutions kept in the dark for 24 h clearly indicated recovery of the large vesicular aggregates.[86]

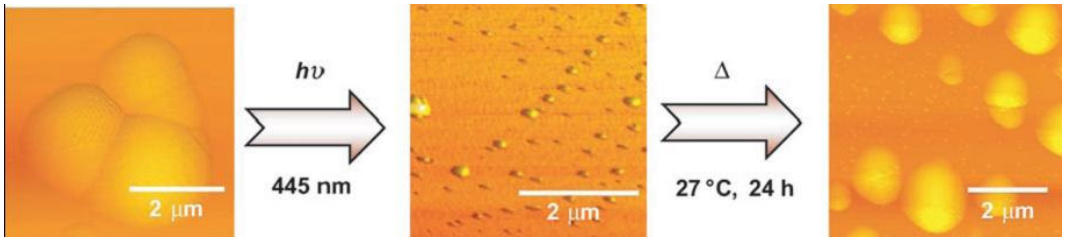

Figure 1.20. Photoinduced breaking and reformation of vesicles in an amphiphilic butadiene, **BINC18**. Adapted from reference 86.

Amphiphilic molecules having chiral centers also self-assemble in solution to form aggregates with high aspect ratios such as rods, tapes or tubes. Often, but not always, chirality is expressed in the morphology of these fibers at a supramolecular scale of nanometers to micrometers; the fibrous structures may be coiled, twisted or wound around one another and exist as a left-handed or a right-handed form. These intriguing shapes can be visualized by microscopic techniques and have fascinated both chemists and physicists.[87] On fundamental grounds, the relationship between molecular chirality (scale ~Å) and supramolecular chirality (scale ~μm) as expressed in these structures represents an excellent model for studying the emergence of specific shapes at a macroscopic scale through cooperative interactions between a large number of very small building blocks. In addition to this fundamental aspect, chiral fibrous objects possess a great potential for applications in the development of new functional supramolecular devices, taking advantage of the chirality of the molecular constituents organized in a hierarchical manner and/or of the supramolecular chirality of the fibers that can be generated. Among those applications are chiral recognition using chiral fibers,

using chiral fibers as templates for helical crystallization of proteins or the growth of inorganic replicas.[87] In a majority of cases, the handedness of a chiral self-assembled fiber is controlled by the stereochemistry of the molecule. One enantiomer gives a right-handed fiber and the other enantiomer a left-handed fiber. There are, however, some exceptions, as when a pure enantiomer gives a mixture of right- and left-handed helices or when the handedness depends on external parameters such as the cooling rate.[87]

Among a variety of chiral fibrillar structures encountered in the literature, probably the most commonly described are chiral ribbons of single or multiple bilayer membranes. Such ribbons can be classified into two different morphologies: helical and twisted shapes (Figure 1.21). Helical ribbons have a cylindrical curvature and can be precursors of tubules. For example, helical ribbons were obtained with diacetylenic lipids, *N*-octyl-l-galactonamide, cytidine myristoylphosphatidyl conjugates and some chiral single-chain ammonium amphiphiles. Tubules form using diacetylenic lipids, glycolipids and some steroids.

In contrast, twisted ribbons have Gaussian or saddle-like curvature. Typical examples of twisted morphologies are those of hydrostearic acid, of double-chain ammonium amphiphiles derived from glutamic acid or of diammonium cationic gemini surfactants.[87]

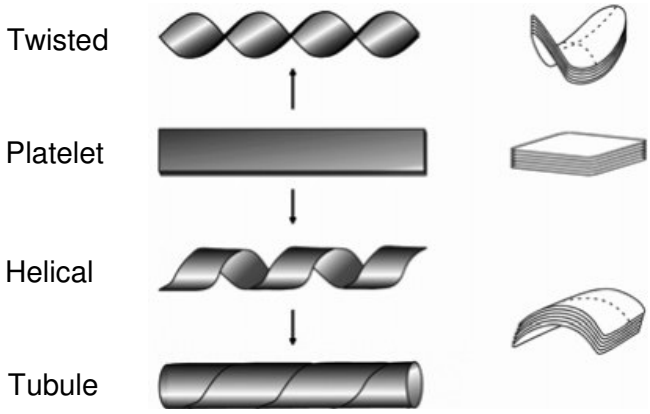

Figure 1.21. Schematic representation of twisted ribbons having saddle-like curvature versus helical ribbons and tubules with cylindrical curvature. Adapted from reference 87.

The above supramolecular assemblies are stable only at temperatures below the gel-to-liquid crystalline phase transition ($T_{g\text{-}l}$) of the amphiphiles ($T < T_{g\text{-}l}$). Heating the nanotube dispersion to temperatures above $T_{g\text{-}l}$ ($T > T_{g\text{-}l}$) induces instant morphological conversion from nanotubes into spheres.[76]

1.6.2. An overview of Sugar based self-assembled systems

Interesting self-assembled morphologies can be obtained from phospholipids, glycolipids and steroidal amphiphilic systems.[76] Which morphological structure is furnished by them, is influenced by its primary chemical structure and by extrinsic factors like temperature, pH and the concentration of bivalent ions. A major difference in properties of glycolipids and phospholipids results from the strong influence of hydrogen bonds on the phase behavior of the former (sugar head groups of glycolipids have a number of –OH groups), which leads to a relatively higher T_c and to metastable polymorphism.

The high T_c has the advantage of providing structural integrity in glycolipid-containing membranes.[71]

Here we will concentrate on sugar-based (glycolipids) amphiphilic and bolaamphiphilic molecules and their self-assembly to form a variety of supramolecular architectures. The name "glycolipid" usually refers to naturally occurring compounds, whereas more generally, the terms "amphiphilic carbohydrate", "neoglycolipid" or "hydrophobized carbohydrate" are used for synthetically prepared structures.[88] Octyl 1-O-β-D-glucopyranoside (**33**), methyl 6-O-heptylcarbamoyl β-D-glucopyranoside and alkanoyl-*N*-methylglucamide are the most widely used carbohydrate surfactants of biological interest.

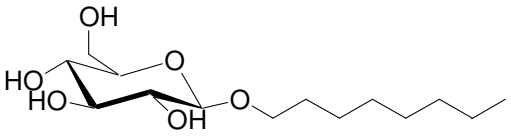

33

Chart 1.17

Sugars are often treated as classic hydrophilic nonelectrolytes.[89] Alkylated glycosides and alkylthioglycosides containing C8 to C12 *n*-alkyl chains have been commercially (Sigma) used as non-ionic detergents. The perfluoroalkylated sugar surfactants were shown to be highly effective as emulsifiers of fluorocarbons able to carry oxygen *in vivo*.[88]

Single short chain glycolipids (e.g., **33**) usually form micelles since their packing parameter, $P<1/3$.[76] A large variety of self-assembled morphologies generated from synthetic amphiphiles have been extensively studied from the viewpoint of how the introduction of various hydrophilic moieties, such as glucose, galactose, other aldopyranose-type sugars and noncyclic sugars affects self-assembled morphologies. The presence and local environment of diyne units in the hydrophobic chain of *N*-gluconamides has been shown to affect self-assembled morphologies; for example, among polymerizable gluconamides in Chart 1.18, amphiphiles having n = 1 and 5, in which 1,3-nonadiynyl units are combined with *N*-methyl- and *N*-pentylgluconamides formed nanotubes. The amphiphiles with n = 3 and 5 (**34**) self-assembled to form micellar rods.[76]

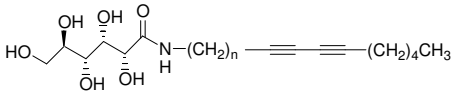

34, n = 1, 3, 5

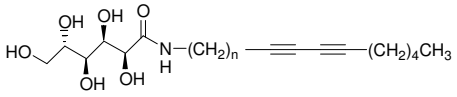

35, n = 5

Chart 1.18

A sugar-based (reduced glucose) gemini surfactant (Chart 1.19) formed vesicles in dilute aqueous solution near neutral pH.[90] At lower pH, there is a vesicle-to-micelle transition within a narrow pH region (pH 6.0–5.6). The vesicles

are transformed into large cylindrical micelles that in turn are transformed into small globular micelles at even lower pH. In the vesicular pH region, the vesicles are positively charged at pH < 7 and exhibit a good colloidal stability. However, close to pH 7, the vesicles become unstable and rapidly flocculate and eventually sediment out from the solution. Surprisingly, it was found that the vesicles are easily redispersed by increasing the pH to above 7.5.[90]

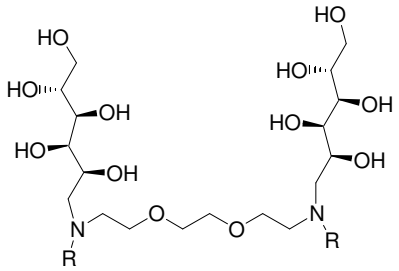

36, R = C18:1

Chart 1.19

When cyclic sugars were used as the hydrophilic moieties, these synthetic amphiphiles are known to produce chiral supramolecular fibers and ribbons by self-assembly in aqueous media.[91] Cardanol (a mixture of long chain phenol differing in the degree of unsaturation in the side chain), obtained from *Anacardium occidentale* L has been used as the starting material. This glycolipd is actually obtained as a mixture, the structure of the components are as shown in Figure 1.22. The type of fibrous self-assembled morphology obtained from them depends on whether the hydrophobic chains are saturated or include unsaturated units. The presence of unsaturation in the hydrophobic part led to helical (coiled)

fiber morphology whereas for the saturated component only all individual fibers show twisted morphology.

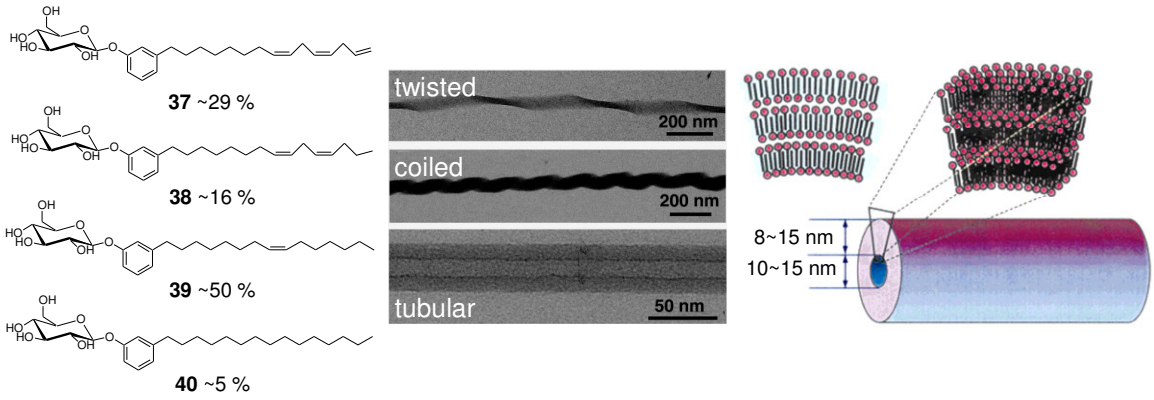

Figure 1.22. Components of cardanol and their percentages. EF-TEM showing morphologies (centre) formed from self-assembly. Schematic (right) of nanotube formation from the unsaturated components. Adapted from reference 91.

This was the first example of morphological control of helical architectures by unsaturation of the hydrophobic chains.[76,91] Interestingly, the helical nanofibers self-assembled from the unsaturated derivatives gradually converted to a tubular morphology. In contrast, the saturated homologue produced no tubular structures even after one year. In the phenolic glycoside, π-π interaction between the aromatic rings is indispensable for stabilizing nanotubes. In comparison, octadecyl-β-D-glucopyranoside (**41**), which lacks aromatic rings, forms no fibrous structures under these conditions.[76]

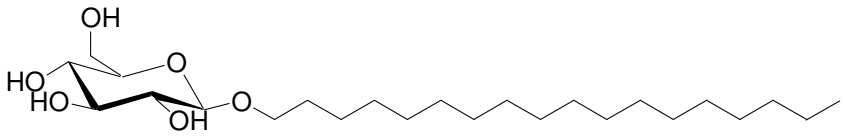

41

Chart 1.20

Kulkarni et al. reported that galactosylceramide (**42**) containing nervonoyl acyl chains self-assembles into nanotubular structures in excess water.[92]

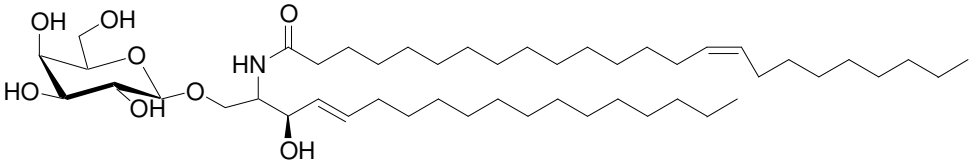

42

Chart 1.21

Blanzat et al. reported on a series of bolaamphiphilic systems forming vesicles (Figure 1.23).[93] The non-ionic bola derivative, **43** forms spherical aggregates in water upon ultrasonication. For catanionic associations the derivatives with dicarboxylate spacer chain length m = 3 and 5, did not form aggregates after dissolution in water, whereas association having spacer chain length m = 6 exhibited in DLS experiments a monodisperse distribution of objects, centered on a 100 nm diameter. Subsequently TEM studies indicated vesicles with a diameter of about 50–100 nm. The differences in the supramolecular behavior of these associations are due to the dicarboxylate spacer chain length and its possible arrangement inside the aggregate. The conformations of the bolaamphiphile and

their associations with the three alkanedioic acids in water have been evaluated by molecular modeling by the authors.[93]

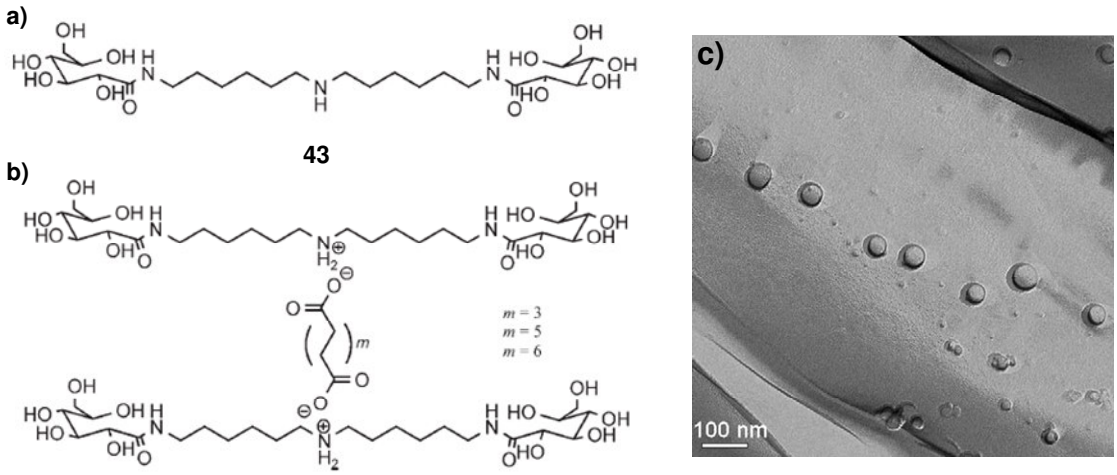

Figure 1.23. (a) Structure of bis(6-gluconamidohexyl)amine bolaamphiphile, **38**, (b) catanionic association of **38** with dicarboxylates and (c) FF-TEM image of vesicles formed from association of **38** with *m* = 6 dicarboxylate. Adapted from reference 93.

Bolaamphiphiles having sugar head groups separated by a long spacer could be possibly used for cross-linking cancer cells into a network. Having a "cancer net" around a solid tumor remains a viable approach to retarding growth and/or inhibiting metastasis of cancer cells.[94] Using this idea Menger et al. have designed and synthesized molecules with two galacto-calixarene macrocycles (**44**, Chart 1.22), covalently joined by a long spacer, which might "glycotarget" a group of cancer cells and thereby interconnect them and prevent the spreading of lethal cancerous cells to other organs.

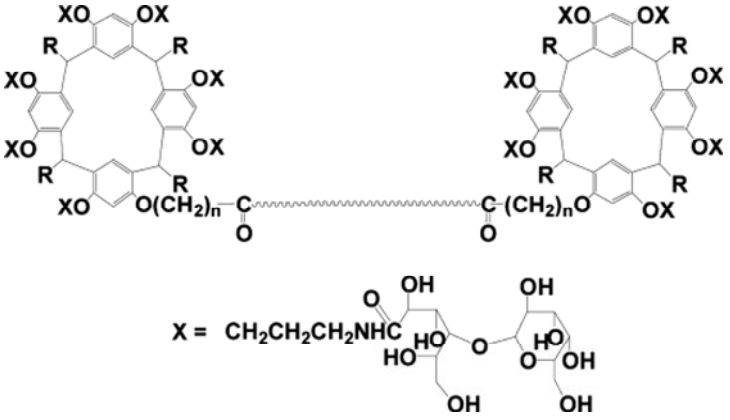

44

Chart 1.22

Galactose-based units were known to bind strongly to rat hepatoma cells, thus there existed the possibility of cross-linking the cancer cells into a network when these galactose moieties were present in the head group. These compounds prepared by Menger et al. however did not serve the required purpose; a fact which the authors claim could be potentially correctable by adjusting or rigidifying the spacer.[94]

Heteroditopic 1,ω-amphiphiles, which have headgroups that differ in size or properties tend to form nanotubular structures by self-assembly. Unsymmetrical bolaamphiphiles **45**(*n*), which have D-Glucose and carboxylic acid headgroups proved to produce nanotube structures exclusively.[76,95] TEM images of the nanotubes filled with a phosphotungstate staining reagent revealed 30–43 nm outer diameters, 14–29 nm inner diameters and lengths of several hundred micrometers. By comparing the membrane stacking periodicity obtained from powder XRD with the molecular packing within single crystals, Masuda et al. was able to give

strong evidence that these nanotubes consist of an unsymmetrical MLM, in which the molecules pack in parallel (Chart 1.23). The measured inner diameters were comparable with calculated values for the extended molecular lengths of bolaamphiphiles containing different oligomethylene spacer lengths.[76,95]

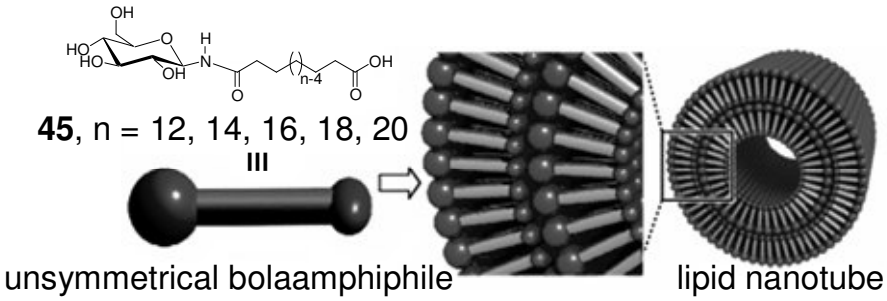

Chart 1.23

Recently Shimizu, Masuda and co-workers have shown that the morphology of the self-assembled structures of some bolaamphiphilic sugars (**13**, Chart 1.13) could be controlled by controlling the structure of the seed materials used.[96] Thus crystalline materials precipitated from methanol gave rise to tapes, whereas solid films of the same materials obtained by evaporating them from a DMF solution gave rise to nanotubes (Figure 1.24). In both cases the self-assembled materials were obtained by preparing hot aqueous dispersions (100 °C) of the two solids. These studies indicate that the supramolecular structural information stored in the seed materials are retained at least partially at the high temperatures allowing the materials to self-assemble into different structures on cooling. The innermost surfaces of the nanotube should be covered with amino head groups charged positively at neutral pH and the outermost surfaces should

have 1-glucosamide head groups. Such a nanotube with a positively charged inner surface is expected to encapsulate anionic molecular objects and biopolymers via electrostatic interactions. Successful encapsulation of sulfate-latex beads or ferritin in the hollow cylinders was achieved merely by mixing both aqueous dispersions (Figure 1.24).[96]

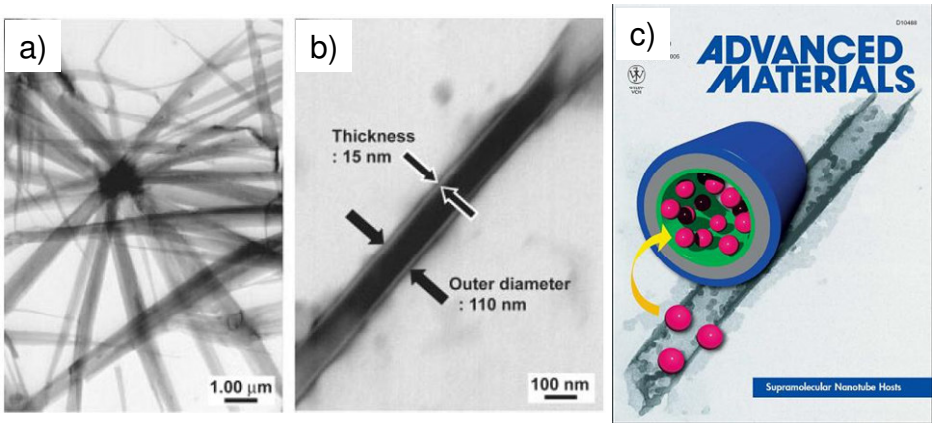

Figure 1.24. STEM images of (a) tapes formed from crystalline **13** precipitated from methanol and (b) nanotubes on evaporating a DMF solution of **13**. (c) TEM image of the lipid nanotubes seen encapsulating sulfate-latex beads. Adapted from reference 96.

1.7. Objectives of the Present Work

Macroscopic chiral liquid crystals such as the smectic C* LC phase finds application in displays, nonlinear optics and photonics. The chiral source for inducing macroscopic chirality should necessarily come from a chiral pool rather than by asymmetric synthesis because liquid crystals are needed in gram quantities for technical uses. Sugars fulfill most of the requirements for a chiral source, but most importantly do not exhibit macroscopic chirality in their LC phases. Strong intermolecular hydrogen bonding forces amphiphilic sugars to stack into achiral

smectic, columnar and cubic phases. Synthetic modification of the –OH groups are required for the expression of macroscopic chirality in the LC phases. The work described in this thesis deals with sugar-based amphiphiles and bolaamphiphiles containing azobenzene and diphenylbutadiene moieties. The advantage of having such chromophore in the molecule is that we can spectroscopically follow whether the molecule is in its monomeric or aggregated state. The sugar-azobenzene amphiphilic derivatives exhibited only achiral smectic phases. Interestingly in the sugar-azobenzene bolaamphiphiles, we observed macroscopic chiral smectic C phases. This was the first observation of macroscopic chirality in sugar-based LCs having free –OH groups. The manifestation of the smectic C* phase in these bolaamphiphiles was observed to be critically dependant on the presence of the azobenzene moiety and suitable length of the oligomethylene spacer. In order to confirm the role of a self-aggregating chromophore such as azobenzene in generating macroscopically chiral LCs, we replaced the azobenzene moiety with diphenylbutadiene in the core of the bolaamphiphilic structure. This resulted in another series of more stable chiral smectic LCs. In addition to thermotropic phases, the bolaamphiphilic sugars also aggregated in water/DMSO and *n*-hexane/THF solutions to form interesting structures such as vesicles and fibers. Their formation resulted in significant changes in the optical and chiroptical properties of these derivatives. The absorption band attributable to the aggregates was CD active and the CD spectra of water rich solutions exhibited an unusual

intensity increase on heating. The ease of formation and stability of the aggregates increased with increase in their hydrophobic chain length. Disruption of the aggregates induced by photoisomerization of the azobenzene unit and their reformation via the subsequent thermal *cis* to *trans* isomerization was also investigated.

References

(1) Kato, T. *Science (Washington, DC, U. S.)* **2002**, *295*, 2414–2418.

(2) Pauluth, D.; Tarumi, K. *J. Mater. Chem.* **2004**, *14*, 1219–1227.

(3) Chiellini, E.; Laus, M. Main Chain Liquid Crystalline Semiflexible Polymers, In *Handbook of Liquid Crystals (High Molecular weight liquid crystals)*; Demus, D., Goodby, J. W., Gray, G. W., Spiess, H.-W., Vill, V., Eds.; Wiley-VCH: Weinheim, 1998, Vol. 3, pp. 26–51.

(4) Chandrasekhar, S. *Liquid Crystals*; 2nd ed., Cambridge University Press: Cambridge, 1992.

(5) Collings, P. J. in *Liquid Crystals: Nature's delicate phase of matter*, 2nd Ed., Princeton University Press: Princeton, 2001.

(6) Praefcke, K., Singer, D., Charge Transfer Systems In *Handbook of Liquid Crystals (Low Molecular weight liquid crystals)*; Demus, D., Goodby, J. W., Gray, G. W., Spiess, H.-W., Vill, V., Eds.; Wiley-VCH: Weinheim, 1998, Ch. XVI, pp. 945–968.; Lydon, J. E., *Chromonics*, ibid., Ch. XVIII, pp. 981–1008; Kato, T. *Hydrogen Bonded Systems*, ibid., Ch. XVII, pp. 969–980.

(7) Deschenaux, R., Goodby, J. W. In *Ferrocenes*, Togni, A., Hayashi, T. Eds., VCH: New York, 1995, Ch. 9, pp. 471–495.

(8) Dessombz, A.; Chiche, D.; Davidson, P.; Panine, P.; Chanéac, C.; Jolivet, J. -P. *J. Am. Chem. Soc.* **2007**, *129*, 5904–5909 and references therein.

(9) Meier, H.; Lehmann, M.; Kolb, U. *Chem. –Eur. J.* **2000**, *6*, 2462–2469.

(10) Tschierske, C. *J. Mater. Chem.* **1998**, *8*, 1485–1508.

(11) Kelker, H.; Hatz, R. In *Handbook of Liquid Crystals*, Verlag Chemie: Weinheim, 1980.

(12) Bahadur, B., Ed., *Liquid Crystals: Applications and Uses*; World Scientific: Singapore, 1994; Vol. 1-3.

(13) Kato, T.; Mizoshita, N.; Kishimoto, K. *Angew. Chem., Int. Ed.* **2006**, *45*, 38–68.

(14) Mallia, V. A.; George, M.; Das, S. *Chem. Mater.* **1999**, *11*, 207–208.

(15) a) Nguyen, H. T.; Destrade, C.; Malthête, J. *Adv. Mater. (Weinheim, Ger.)* **1997**, *9*, 375–388. b) Gharbia, M.; Gharbi, A.; Nguyen, H. T.; Malthête, J. *Curr. Opin. Colloid Interface Sci.* **2002**, *7*, 312–325.

(16) Méry, S.; Haristoy, D.; Nicoud, J.-F.; Guillon, D.; Diele, S.; Monobe, H.; Shimizu, Y. *J. Mater. Chem.* **2002**, *12*, 37–41 and references therein.

(17) Dierking, I. *Textures of Liquid Crystals*, Wiley-VCH: Weinheim, 2003.

(18) Reinitzer, F. *Monatsh. Chem.* **1888**, *9*, 421–441.

(19) Tamaoki, N. *Adv. Mater. (Weinheim, Ger.)* **2001**, *13*, 1135–1147.

(20) Palffy-Muhoray, P. *Nature (London)* **1998**, *391*, 745–747.

(21) Gray, G. W.; Goodby, J. W. *Smectic Liquid Crystals: Textures and Structures*; Leonard Hill: Glasgow, 1984.

(22) Lagerwall, J. P. F.; Giesselmann, F. *ChemPhysChem* **2006**, *7*, 20–45.

(23) Kitzerow, H.-S., Bahr, C. Eds., *Chirality in Liquid Crystals,*Springer: New York, 2001.

(24) Chandrasekhar, S.; Sadashiva, B. K.; Suresh, K. A. *Pramana* **1977**, *9*, 471–480.

(25) Kumar, S. *Chem. Soc. Rev.* **2006**, *35*, 83–109.

(26) Blunk, D.; Praefcke, K.; Vill, V. In *Handbook of Liquid Crystals*; Demus, D., Goodby, J. W., Gray, G. W., Spiess, H.-W., Vill, V., Eds.; Wiley-VCH: Weinheim, 1998, Vol. 3, pp. 305–340.

(27) Friberg, S. Ed., *Lyotropic liquid crystals and the structure of biomembranes*, Advances in Chemistry Series; 152, American Chemical Society: Washington, D. C., 1976.

(28) G. W. Gokel, S. L. De Wall In *Advances in Supramolecular Chemistry*. Gokel, G. W. Ed., Jai Press Inc.: Stamford, Connecticut, 1999; Vol. 5, pp. 203–235.

(29) van Doren, H. A.; Smits, E.; Pestman, J. M.; Engberts, J. B. F. N.; Kellogg, R. M. *Chem. Soc. Rev.* **2000**, *29*, 183–199.

(30) Gin, D. L.; Gu, W.; Pindzola, B. A.; Zhou, W.–J. *Acc. Chem. Res.* **2001**, *34*, 973–980.

(31) Tschierske, C. *Prog. Polym. Sci.* **1996**, *21*, 775–852.

(32) Walba, D. M. *Science (Washington, DC, U. S.)* **1995**, *270*, 250–251.

(33) Walba, D. M.; Xiao, L.; Keller, P.; Shao, R.; Link, D.; Clark, N. A. *Pure Appl. Chem.* **1999**, *71*, 2117–2123.

(34) Ikeda, T.; Kanazawa, A. In *Molecular Switches*; Feringa, B. L., Ed.; Wiley-VCH: Weinheim, 2001; pp. 363–397.

(35) Pasteur, L. *Ann. Chim. Phys.* **1848**, *24*, 442.

(36) Thomson, W. *The Robert Boyle Lecture, Oxford University Junior Scientific Club, May 16, 1893*, reprinted in *Baltimore Lectures*, C. J. Clay & Sons: London, 1904.

(37) Eliel, E. L., Wilen, S. H., Mander, L. W. in *Stereochemistry of Organic compounds*; Wiley-Interscience: New York; 1994.

(38) Boulton, C. J.; Finden, J. G.; Yuh, E.; Sutherland, J. J.; Wand, M. D.; Wu, G.; Lemieux, R. P. *J. Am. Chem. Soc.* **2005**, *127*, 13656–13665.

(39) McCubbin, J. A.; Tong, X.; Wang, R.; Zhao, Y.; Snieckus, V.; Lemieux, R. P. *J. Am. Chem. Soc.* **2004**, *126*, 1161–1167.

(40) Jeong, K.-U.; Jin, S.; Ge, J. J.; Knapp, B. S.; Graham, M. J.; Ruan, J.; Guo, M.; Xiong, H.; Harris, F. W.; Cheng, S. Z. D. *Chem. Mater.* **2005**, *17*, 2852–2865.

(41) Niori, T.; Sekine, T.; Watanabe, J.; Furukawa, T.; Takezoe, H. *J. Mater. Chem.* **1996**, *6*, 1231–1233.

(42) Pelzl, G.; Diele, S.; Weissflog, W. *Adv. Mater. (Weinheim, Ger.)* **1999**, *11*, 707–724.

(43) Maeder, T. *Sci. Amer.* July **2002**, *287*, 24.; May, M. *Sci. Amer.* October **2002**, 18.

(44) McMurry, J. *Organic Chemistry*, 5th Ed., Brooks/Cole: Pacific Grove, CA, 2000, pp. 1030–1032.

(45) Lichtenthaler, F. W. Ed., *Carbohydrates as organic raw materials*; VCH: Weinheim; 1991.

(46) Collins, P. M.; Ferrier, R. J. in *Monosaccharides: Their Chemistry and their roles in Natural Products*, John Wiley & Sons: Chichester, 1995.

(47) Vill, V.; Hashim, R. *Curr. Opin. Colloid Interface Sci.* **2002**, *7*, 395–409.

(48) Miethchen, R.; Hein, M. *Carbohydr. Res.* **2000**, *327*, 169–183 and references therein.

(49) Jeffrey, G. A. *Acc. Chem. Res.* **1986**, *19*, 168–173.

(50) Fischer, E.; Helferich, B. *Justus Liebigs Ann. Chem.* **1911**, *383*, 68–91.

(51) Salway, A. H. *J. Chem. Soc.* **1913**, *103*, 1022.

(52) Noller, C. R.; Rockwell, W. C. *J. Am. Chem. Soc.* **1938**, *60*, 2076–2077.

(53) Pape, M.; Hiltrop, K. *Mol. Cryst. Liq. Cryst.* **1997**, *307*, 155–173.

(54) Grassert, V.; Vill, V. *Liq. Cryst. Today* **1994**, *4*, 4.

(55) Jeffrey, G. A.; Bhattacharjee, S. *Carbohydr. Res.* **1983**, *115*, 53–58.

(56) Goodby, J. W. *Mol. Cryst. Liq. Cryst.* **1984**, *110*, 205–219.

(57) Miethchen, R.; Holz, J.; Prade, H.; Liptak, A. *Tetrahedron* **1992**, *48*, 3061.

(58) Queneau, Y.; Gagnaire, J.; West, J. J.; Mackenzie, G.; Goodby, J. W. *J. Mater. Chem.* **2001**, *11*, 2839–2844.

(59) Morris, N. L.; Zimmermann, R. G.; Jameson, G. B.; Dalziel, A. W.; Reuss, P. M.; Weiss, R. G. *J. Am. Chem. Soc.* **1988**, *110*, 2177–2185.

(60) Kohne, B.; Praefcke, K. *Angew. Chem., Int. Ed.* **1984**, *23*, 82–83.

(61) Barberá, J.; Garcés, A. C.; Jayaraman, N.; Omenat, A.; Serrano, J. L.; Stoddart, J. F. *Adv. Mater. (Weinheim, Ger.)* **2001**, *13*, 175–180.

(62) Hein, M.; Miethchen, R. *Tetrahedron Lett.* **1998**, *39*, 6679–6682.

(63) Fuhrhop, J.-H.; Wang, T. *Chem. Rev. (Washington, DC, U. S.)* **2004**, *104*, 2901–2937.

(64) Masuda, M.; Vill, V.; Shimizu, T. *J. Am. Chem. Soc.* **2000**, *122*, 12327–12333.

(65) Kameta, N.; Masuda, M.; Minamikawa, H.; Shimizu, T. *Langmuir* **2007**, *23*, 4634–4641.

(66) Vill, V.; Bachmann, F.; Pelyvas, I.; Pudlo, P.; Thiem, J. *Mol. Cryst. Liq. Cryst.* **1992**, *213*, 57.

(67) Ho, W. M.; Wong, H. N. C.; Navailles, L.; Destrade, C.; Nguyen, H. T.; Isaert, N. *Tetrahedron* **1995**, *51*, 7373–7388.

(68) Smits, E.; Engberts, J. B. F. N.; Kellogg, R. M.; van Doren, H. A. *Mol. Cyst. Liq. Cryst.* **1995**, *260*, 185–199.

(69) Smits, E.; Engberts, J. B. F. N.; Kellogg, R. M.; van Doren, H. A. *Mol. Cryst. Liq. Cryst.* **1997**, *299*, 427–432.

(70) Gesekus, G.; Dierking, I.; Gerber, S.; Wulf, M.; Vill, V. *Liq. Cryst.* **2004**, *31*, 145–152.

(71) Fraser-Reid, B. O.; Tatsuta, K.; Thiem, J. Eds., *Glycoscience: Chemistry and Chemical Biology,* Springer-Verlag: Berlin, 2001; Vol. I–III.

(72) Ringsdorf, H.; Schlarb, B.; Venzmer, J. *Angew. Chem., Int. Ed.* **1988**, *27*, 113–158.

(73) Kunitake, T.; Okahata, Y.; Shimomura, M.; Yasunami, S.-I.; Takarabe, K. *J. Am. Chem. Soc.* **1981**, *103*, 5401–5413.

(74) Fendler, J. H. *Acc. Chem. Res.* **1980**, *13*, 7–13.

(75) Gray, G. W. *Molecular structure and the properties of liquid crystals*, Academic Press: New York, 1962.

(76) Shimizu, T.; Masuda, M.; Minamikawa, H. *Chem. Rev. (Washington, DC, U. S.)* **2005**, *105*, 1401–1443.

(77) Israelachvili, J. N.; Mitchell, D. J.; Ninham, B. W. *J. Chem. Soc., Faraday Trans. 2* **1976**, *72*, 1525–1568.

(78) Menger, F. M.; Zana, R; Lindman, B. *J. Chem. Educ.* **1998**, *75*, 115 and references therein.

(79) Okahata, Y.; Kunitake, T. *J. Am. Chem. Soc.* **1979**, *101,* 5231–5234.

(80) Douliez, J.-P. *J. Am. Chem. Soc.* **2005**, *127*, 15694–15695 and references therein.

(81) Marrink, S. J.; Mark, A. E. *J. Am. Chem. Soc.* **2003**, *125,* 15233–15242.

(82) Antonietti, M.; Förster, S. *Adv. Mater. (Weinheim, Ger.)* **2003**, *15*, 1323–1333.

(83) Discher, D. E.; Eisenberg, A. *Science (Washington, DC, U. S.)* **2002**, *297*, 967–973.

(84) Seo, S. H.; Chang, J. Y.; Tew, G. N. *Angew. Chem., Int. Ed.* **2006**, *45*, 7526–7530 and references therein.

(85) Seo, S. H.; Jones, T. V.; Seyler, H.; Peters, J. O.; Kim, T. H.; Chang, J. Y.; Tew, G. N. *J. Am. Chem. Soc.* **2006**, *128*, 9264–9265.

(86) Kumar, N. S. S.; Varghese, S.; Narayan, G.; Das, S. *Angew. Chem., Int. Ed.* **2006**, *45*, 6317–6321.

(87) Brizard, A.; Aimé, C.; Labrot, T.; Huc, I.; Berthier, D.; Artzner, F.; Desbat, B.; Oda, R. *J. Am. Chem. Soc.* **2007**, *129*, 3754–3762 and references therein.

(88) Boullanger, P., In *Topics in Current Chemistry*, Hugues, Driguez., Thiem, J. Eds., Springer-Verlag: Berlin, 1997; Vol. 187; pp. 275–311.

(89) Smith, B. D.; Gardiner, S. J. In *Advances in Supramolecular Chemistry*. Gokel, G. W. Ed., Jai Press Inc.: Stamford, Connecticut, 1999; Vol. 5, pp. 157–202.

(90) Johnsson, M.; Wagenaar, A.; Engberts, J. B. F. N. *J. Am. Chem. Soc.* **2003**, *125*, 757–760.

(91) John, G.; Masuda, M.; Okada, Y.; Yase, K.; Shimizu, T. *Adv. Mater. (Weinheim, Ger.)* **2001**, *13*, 715–718.

(92) Kulkarni, V. S.; Anderson, W. H.; Brown, R. E. *Biophys. J.* **1995**, *69*, 1976.

(93) Soussan, E.; Pasc-Banu, A.; Consola, S.; Labrot, T.; Perez, E.; Blanzat, M.; Oda, R.; Vidal, C.; Rico-Lattes, I. *ChemPhysChem* **2005**, *6*, 2492–2494.

(94) Menger, F. M.; Bian, J.; Sizova, E.; Martinson, D. E.; Seredyuk, V. A. *Org. Lett.* **2004**, *6*, 261–264 and references therein.

(95) Masuda, M.; Shimizu, T. *Langmuir* **2004**, *20*, 5969–5977.

(96) Kameta, N.; Masuda, M.; Minamikawa, H.; Goutev, N. V.; Rim, J. A.; Jung, J. H.; Shimizu, T. *Adv. Mater. (Weinheim, Ger.)* **2005**, *17*, 2732–2736.

Chapter 2

Induction of Chirality in Amphiphilic Sugars

Abstract

Amphiphilic sugars exhibit both lyotropic and thermotropic liquid crystalline behavior. Interestingly, in spite of the abundance of chiral centers in amphiphilic sugars, their liquid crystalline (LC) phases do not exhibit macroscopic chirality. This Chapter describes the design of sugar-based LCs containing an azobenzene unit. It was observed that the simple azobenzene linked sugar amphiphiles exhibited only macroscopic achiral smectic phases. Macroscopic chirality was not expressed even in derivatives of these molecules wherein the hydroxyl groups of the sugar moiety were protected. In bolaamphiphilic molecules with azobenzene in the core linked to sugar head groups through oligomethylene spacers, chiral thermotropic smectic C phases were however observed. This was the first observation of macroscopic chirality in sugar-based bolaamphiphiles containing free hydroxyl groups. The manifestation of the smectic C* phase in these bolaamphiphiles was observed to be critically dependant on the presence of the azobenzene moiety and suitable length of the methylene spacer. These results imply that by suitable selection of linker groups, mesogenic bolaamphiphiles exhibiting macroscopic chirality can be designed using a variety of naturally available sugar derivatives.*

2.1. Introduction

The liquid crystalline state has been known for more than a century.[1] This state is formed by basically two types of molecular structures viz., anisometric and amphiphilic molecules.[2] When the mesogenic molecule is an achiral one doped with a chiral additive, or when it is inherently chiral, the directors of molecular layers adopt a helical arrangement resulting in macroscopic chiral LC phases.[3] Among the macroscopic chiral LC phases, chiral nematic (N*)[4] and smectic C* (SmC*)[5] attract considerable attention, since their potential for application in display devices is next only to nematics, which are well known for their applications in flat panel LCDs.[6] The smectic C* LC state in particular, due to its bistability, fast electro-optic switching (10^3 times faster than nematic LCs) and wide viewing angle finds applications in commercial high-resolution reflective microdisplays.[1,5,7-9] In view of these applications the design and development of chiral LCs are of technological importance.

In order to synthesize LC molecules, which are inherently chiral, the chiral synthon used has to be selected based on ease of availability, structural diversity, mesogenic property and chemical stability.[3] Sugars or carbohydrates in general possess all the ideal characteristics mentioned above.[10,11] However, even though sugar molecules possess several chiral centers, the LC phases formed from them do not exhibit macroscopic chirality.[10,11] Thermotropic cholesteric phases were never observed and lyotropic cholesteric phases based on asymmetric micelles

were observed only in a few sugar-based derivatives.[3] The absence of macroscopic chirality in sugar LCs stems from the fact that their amphiphilic character is reinforced by the many –OH groups present which readily enter into hydrogen bonding. This leads to rigidly packed lamellar layers which assemble into smectic, columnar or cubic phases.[3,11] Macroscopic chiral LC phases from sugars could therefore only be observed by suppressing their amphiphilic character either by suitable derivatization or replacement of –OH groups by other functional groups. This involves drastic multiple step modifications of the sugar moieties.[11]

In view of the importance of liquid crystalline phases possessing macroscopic chirality in display and electro-optic switching devices[1,8] and the easy availability of a variety of sugar derivatives, observation of macroscopic chirality in amphiphilic sugars has been a long cherished goal. It was desirable to design macroscopic chiral amphiphilic sugars with free –OH groups.

In our interest to develop photoresponsive[12,13] as well as sugar-based liquid crystals, we have designed sugar-linked azobenzene derivatives (Chart 2.1). Moreover the incorporation of a rigid spacer unit linked to alkyl chains is known to stabilize amphiphilic mesophases.[11,14,15] During the course of our work, Goodby et al. reported[16] on the liquid crystalline properties of 4-(4′-*N*,*N*-didodecylamino-phenylazo)phenyl-1,2-*trans* glycosides (Figure 2.1). They linked a variety of sugar groups such as glucose, mannose, galactose, lactose and xylose to an azobenzene moiety possessing a didodecylamino alkyl chain at the *para*- position. The

glucoside derivative exhibited a rectangular columnar (Col_r) mesophase, whereas most others formed interdigitated smectic A_d* (SmA_d*) phases, while the xylose derivative was found to be non-mesomorphic. Subtle change of the stereochemistry of an –OH group from axial (C_4 –OH is axial in Galactose) to equatorial (all –OH groups are equatorial in Glucose) caused changes in the molecular arrangement in the mesophase from smectic to columnar (Figure 2.1).

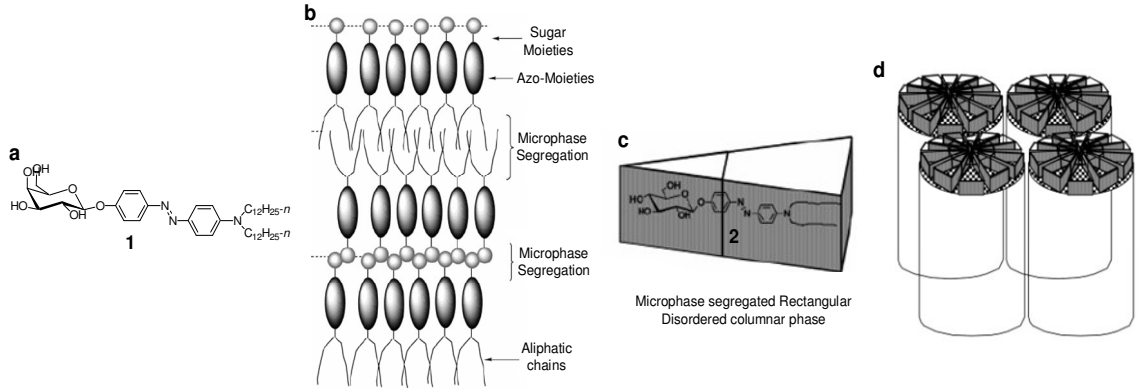

Figure 2.1. (a) Azobenzene connected galactoside, **1**; (b) Schematic representation of interdigitated smectic A_d* phase formed by **1**; (c) Azobenzene connected glucopyranoside, **2**; (d) Schematic representation of disordered rectangular columnar phase formed by **2**. Adapted from reference 16.

This difference in the mesophase formed was explained by differences in the curvature of the molecules when packed in the mesophase. As the molecules have two aliphatic chains it is likely that a curvature will be introduced into the system at the layer interfaces between the chains since the cross-sectional area of the two aliphatic chains is larger than the carbohydrate moiety. All of these liquid

crystalline phases were macroscopically achiral, similar to all the amphiphilic sugar mesogens previously reported in the literature.

This Chapter describes the synthesis and studies of chiral sugar-azobenzene based amphiphilic and bolaamphiphilic molecules (Chart 2.1).

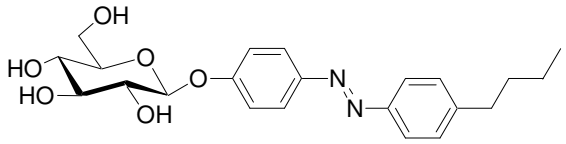

Glc-AB-Bu

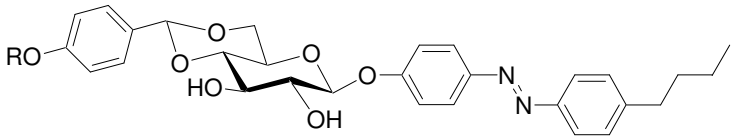

CnBA

n=1; R=CH_3 n=4; R=*n*-C_4H_9 n=8; R=*n*-C_8H_{17} n=12; R=*n*-$C_{12}H_{25}$

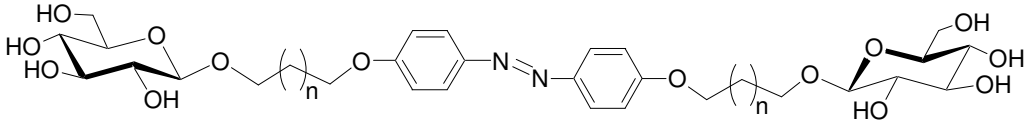

n = 3, **azo-bis 5**; n = 5, **azo-bis 7**; n = 6, **azo-bis 8**; n = 8, **azo-bis 10**; n = 10, **azo-bis 12**

Chart 2.1

2.2. Results

2.2.1. Synthesis of sugar-azobenzene derivatives

The synthesis of azobenzene-glycopyranoside derivatives involved the attachment of the sugar moiety i.e., monosaccharide such as D-Glucose either directly to the phenolic group of the azobenzene or with an oligomethylene spacer in between the azobenzene and sugar moiety. The synthesis of azobenzene moiety **1** was undertaken first. Diazotization of 4-*n*-Butyl aniline (Merck) followed by coupling with phenol furnished **1** in good yield (Scheme 2.1).

Commercially available D-Glucose was treated with benzoyl chloride in pyridine to give the perbenzoylated derivative **2**. This was then converted to the bromide, **3**. Glycosylation of **1** with α-D-Glucopyranosyl bromide tetrabenzoate, **3** using *tetra-n*-butylammonium bromide[17] and an aq NaOH solution under phase transfer conditions furnished the perbenzoylated glucopyranoside, **4**. Removal of the O-benzoyl protecting groups in **4** under *Zémplen* conditions (NaOMe/MeOH) afforded the fully deprotected phenolic glucoside, **Glc-AB-Bu** containing β-D-Glucopyranoside moiety (Scheme 2.1).

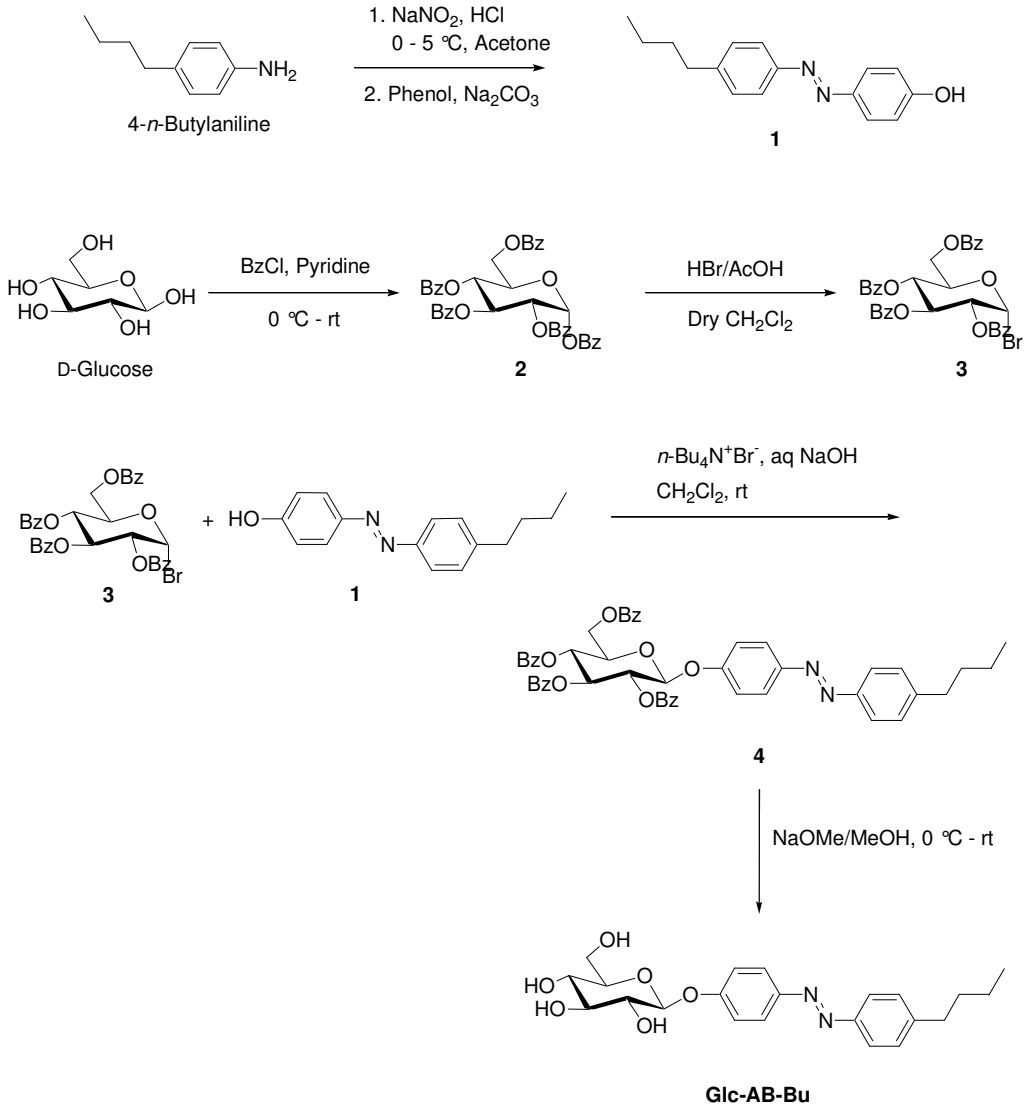

Scheme 2.1

The benzylidene acetal protected derivatives (**CnBA**, Chart 2.1) were prepared from **Glc-AB-Bu** as shown in Scheme 2.2.

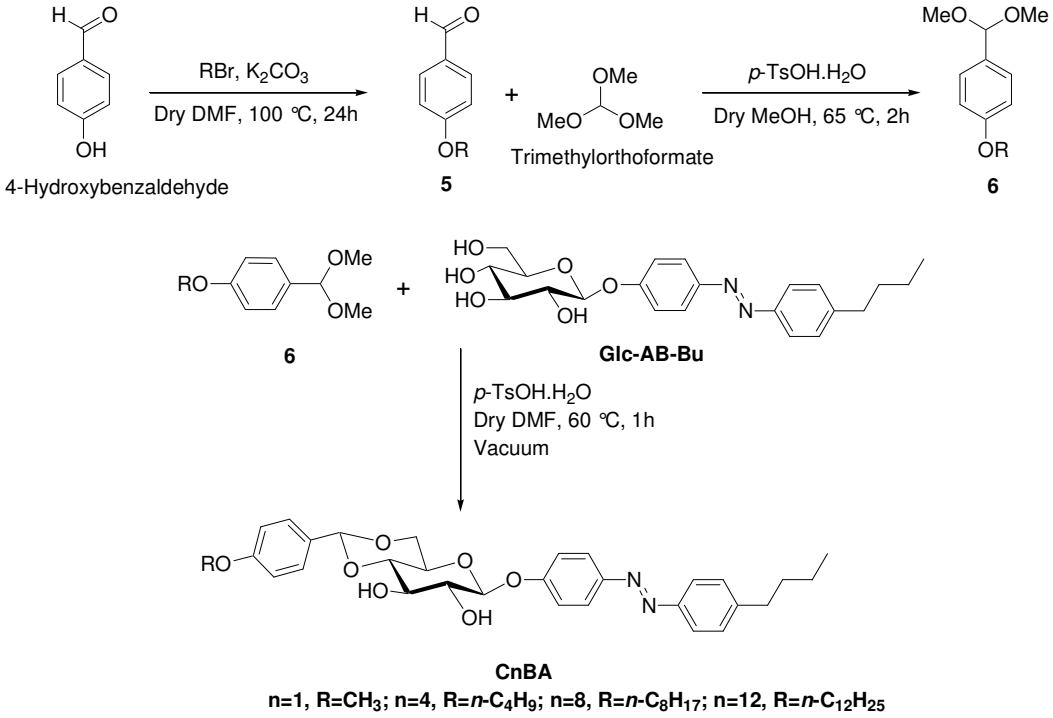

Scheme 2.2

4-Hydroxybenzaldehyde (Spectrochem) was O-alkylated with alkyl bromide (Williamson's synthesis) using activated potassium carbonate as base in DMF to give **5**. The aldehyde group in **5** was then converted to the dimethylacetal, **6** by reacting with Trimethylorthoformate, MeOH and *p*-Toluenesulfonic acid (cat).[18] **6** was then reacted by transacetalation with slight excess of **Glc-AB-Bu** in dry DMF using *p*-Toluenesulfonic acid as catalyst under vacuum.[19,20]

The structures of all these azobenzene-sugar derivatives were confirmed using spectroscopic methods. These details and preparation procedures are provided in the Experimental Section. The **Azo-bis** bolaamphiphiles (Chart 2.1)

were synthesized with the help of Jayaraman and co-workers and has been reported.[21]

2.2.2. Liquid crystalline properties and spectroscopic studies

2.2.2.1. Monosugar derivatives

The thermotropic liquid crystalline properties of azobenzene-sugar derivatives were investigated by polarized light optical microscopy (POM), differential scanning calorimetry (DSC) and X-ray diffractometry (XRD). POM studies of the azobenzene sugar derivative, **Glc-AB-Bu** indicated the presence of an enantiotropic smectic A* phase. On heating a pristine sample sandwiched between cover-slips, softening occurred at 133 °C and formation of a focal-conic texture[22,23] with homeotropic areas, typical of the smectic A* phase was clearly observable by 161 °C. On further heating, *bâtonnet* formation (Figure 2.2a) with homeotropic regions occurred above 200 °C and the material isotropized at 223 °C which could be seen as a broad shallow endotherm in the DSC (Figure 2.2b). Some amount of caramalization could be seen in the sample. On cooling, formation of bâtonnets was observed from 220 °C till 205 °C confirming the enantiotropic smectic phase. At 135–140 °C, the LC phase changed to a dark glass retaining the texture of the smectic A* mesophase. In the second heating cycle the glass–smectic A* transition was observed at 135 °C. Both the softening and melting described above were detectable as endotherms in the DSC scan. In addition to

these DSC transitions observed in accordance with POM, Cr–Cr transitions were also observed before melting occurred to the mesophase. The transitions in the cooling cycle could not be seen in the DSC trace due to the decomposition near to the isotropization temperature during heating.

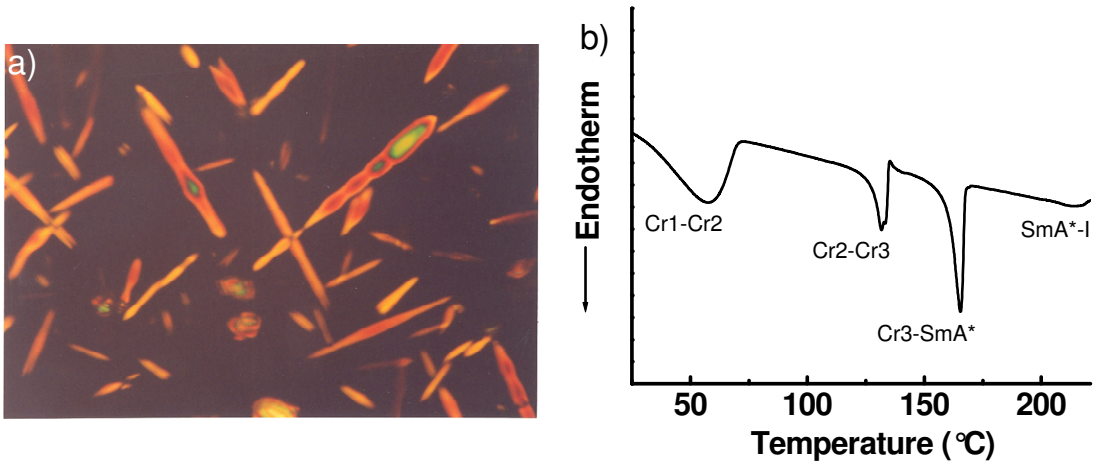

Figure 2.2. Polarized light optical micrograph of smectic A* phase observed for **GIc-AB-Bu** at 210 °C (× 100) (a) and its heating cycle DSC trace (b).

Note that the classification of the mesophase is smectic A*, because the materials are chiral.[24] However the material did not exhibit a macroscopic chiral LC phase.

The thermotropic properties of the benzylidene acetal protected derivatives (**CnBA**) were studied by POM and DSC. On heating, **C1BA** at 149 °C, we could observe a softening and a transition with focal-conic and oily streak textures characteristic of smectic A* phase.[22,23,25] On further heating, at above 200 °C signs of caramalization could be observed even though the mesophase had not become completely isotropic. On cooling from this state the smectic A* mesophase

nucleated from the previously isotropic regions in the form of *bâtonnets* which on further cooling coalesced to form focal-conic texture. **C1BA** solidified on cooling from the smectic A* phase maintaining the same texture, suggesting that the structure in the solid state closely matched that of the smectic A* phase. On heating the higher members i.e., **C4BA**, **C8BA** and **C12BA** transformed from solid to the isotropic state and a reduction in the melting point with increase in alkyl chain length was observed. None of these derivatives exhibited an LC phase. For example, **C4BA** melted to the isotropic liquid over a 10 °C range during which POM showed fibrous needle like birefringence but no characteristic LC textures (Figure 2.3a). The higher alkyl chain length derivatives showed reduced melting ranges.

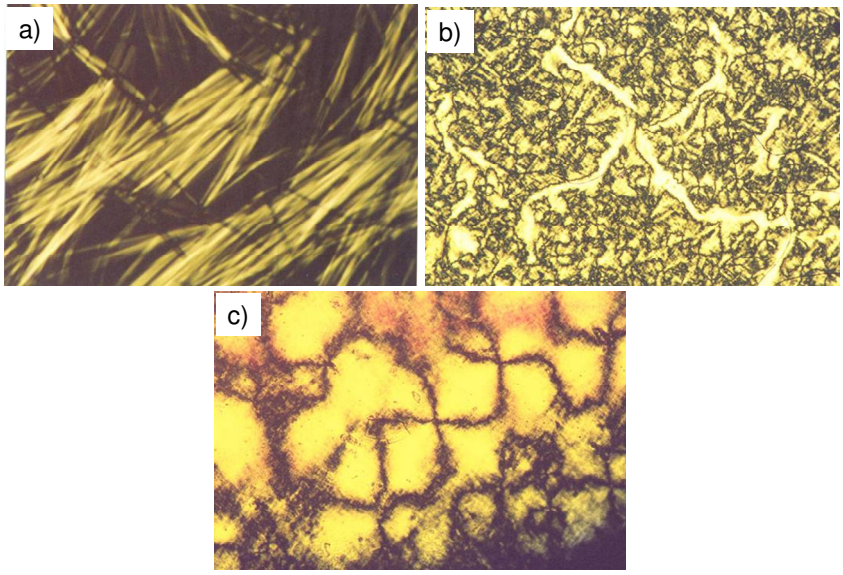

Figure 2.3. Polarized optical micrographs (× 100) of (a) **C4BA** crystals melting to isotropic state; (b) texture of the cooled glass of **C4BA** and (c) texture of the cooled glass of **C12BA**.

Figure 2.4a shows the DSC traces in the first heating cycle of the **CnBA** compounds. The transition from crystal to smectic A* phase at 149 °C in the heating cycle was indicated by an endothermic peak in the DSC (Figure 2.4a).

When cooled from their isotropic melt, **C4BA**, **C8BA** and **C12BA** solidified to form orange-red colored transparent glasses with the development of a texture close to the glassification temperature (Figure 2.3b,c). This texture disappeared on isotropization in the subsequent heating cycle but reappeared on cooling.

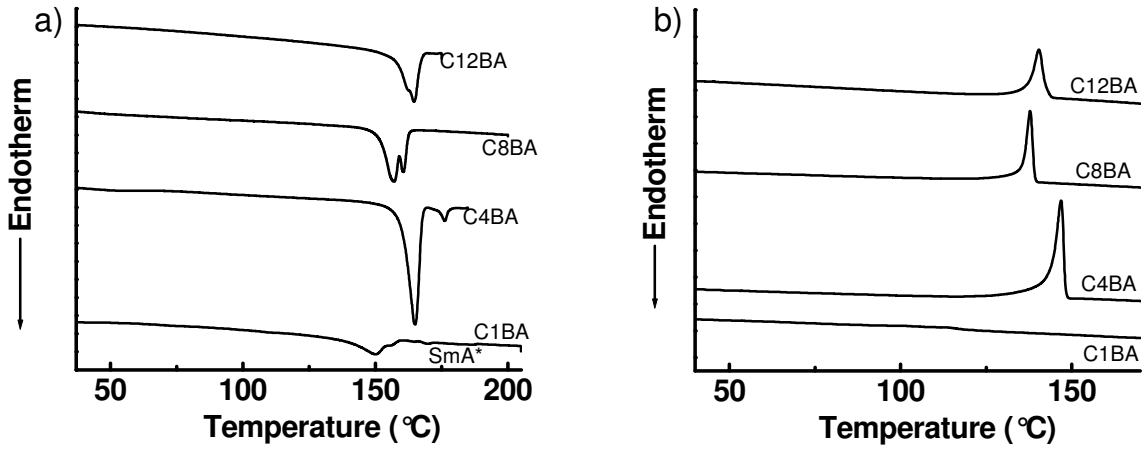

Figure 2.4. DSC traces of **CnBA** compounds in their first a) heating and b) cooling cycles (5 °C/min).

Due to the occurrence of decomposition close to isotropization, DSC of **C1BA** did not show any peaks in the cooling cycle. The DSC traces of all the higher members (**C4BA**, **C8BA** and **C12BA**) however exhibited a sharp exothermic peak in the cooling cycle on transition from isotropic to the glassy state (Figure 2.4b). Generally weak DSC peaks accompany transformation to the glassy

state. The intense peak in this case was unexpected. The formation of amorphous glassy phase on cooling were confirmed by recording XRD patterns of these cooled melts which showed no sharp peaks indicating absence of any crystallinity (Figure 2.5). It may be noted here that the XRD of unheated fresh **CnBA** powder samples also showed similar patterns indicating their amorphous nature.

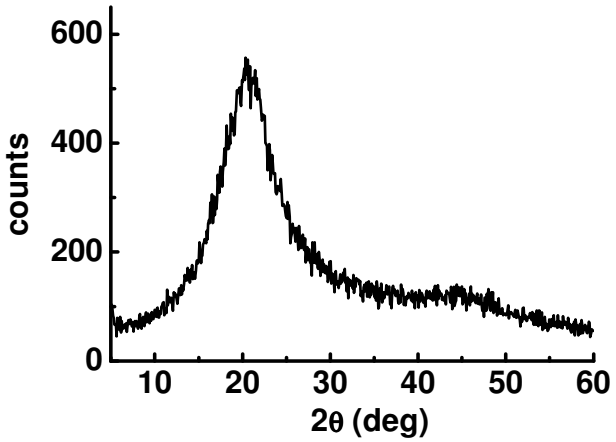

Figure 2.5. XRD of the cooled melt of **C4BA** recorded at room temperature showing its amorphous nature.

The thermal phase transition characteristics of **Glc-AB-Bu** and **CnBA** derivatives are given in Table 2.1. There was an appreciable reduction in the transition temperatures of **CnBA** derivatives when compared to the parent compound (**Glc-AB-Bu**) which had four free hydroxyl groups.

Table 2.1. Thermal phase transition characteristics of **Glc-AB-Bu** and the **CnBA** compounds

sample code	heating cycle, °C (ΔH, $kJmol^{-1}$)	cooling cycle, °C (ΔH, $kJmol^{-1}$)
Glc-AB-Bu	Cr_1 58 (44.1) Cr_2 132 (12.6) Cr_3 166 (19.1) SmA* 223 (0.9) I	I 220 SmA* 135–140 G
C1BA	Cr 131–160 (23.5) SmA* 200 I	I 185 SmA* 123 (5.1) G
C4BA	Cr 155–169 (25.7) × 173–179 (1.3) I	I 148 (22.4) G
C8BA	Cr 147–164 (29.3) I	I 140 (21.7) G
C12BA	Cr 151–169 (27.5) I	I 145 (23.3) G

Cr - Crystal; SmA* - smectic A*; I - Isotropic; G - Glass

The thermal behavior in the subsequent cycles was also examined. The **C1BA** acetal showed enantiotropic smectic A* phase although with some decomposition close to isotropization temperature. For the higher members, the transitions in the heating and cooling cycles was reproducible up to the investigated five cycles by DSC. This was in contrast with the parent compound for which considerable decomposition occurred after the second cycle. When the second DSC cycle of **C4BA** was performed the endothermic peak at 176 °C split into two peaks. In addition, an exothermic peak was seen in between (168 °C) the two endothermic peaks of the heating cycle (Figure 2.6a). The second heating run of **C8BA** also showed a re-entrant peak between the two previous peaks in the first heating cycle (Figure 2.6b). There was no corresponding POM observation for this re-entrant behavior seen for **C4BA** and **C8BA**. No such re-entrant phenomenon was seen for **C12BA** by DSC analysis.

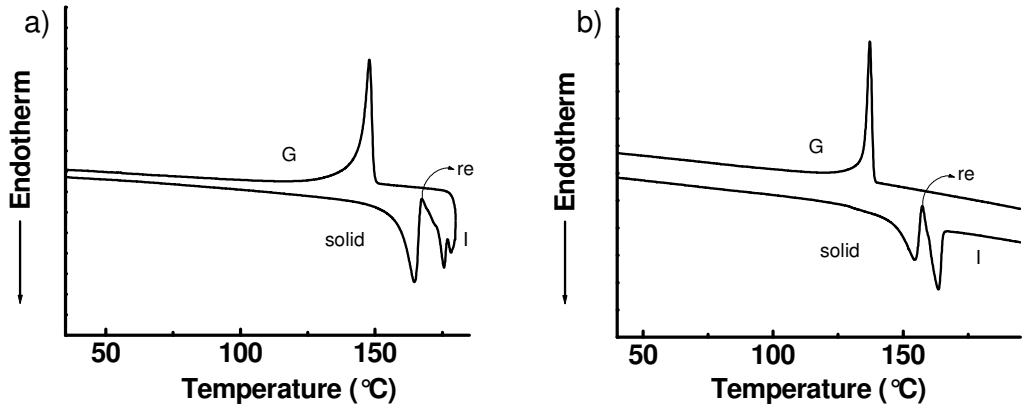

Figure 2.6. DSC traces of (a) **C4BA** and (b) **C8BA** in their second cycle (5 °C/min). The notation 're' denotes re-entrant.

The DSC analyses were also performed at a heating and cooling rate of 2 °C/min to investigate whether the merged transitions could be observed separately. No significant changes were seen for the benzylidene acetals, but in the case of **C12BA** a splitting in the endothermic peak was observed.

The UV-vis absorption properties of **Glc-AB-Bu** were investigated. In pure acetonitrile, **Glc-AB-Bu** exhibited a typical azobenzene monomer absorption spectrum with a weak n→π* transition in the 450 nm region and an intense π→π* transition moment along the long-axis (A band) at 345 nm.[26,27] On photolysis with 345 nm light, a decrease in intensity of the π→π* transitions and a small increase in intensity in the 450 nm region due formation of the *cis*-isomer was observed. A photostationary state was reached with 6 min of irradiation. The kinetics of thermal *cis* to *trans* isomerization at room temperature was investigated by monitoring the recovery of the optical density at the wavelength corresponding to the maximum of

$\pi \rightarrow \pi^*$ transition. The *cis*-isomer was observed to be fairly stable and the rate constant for the recovery of *trans* form was calculated as 4.4×10^6 s^{-1}.

Photolysis of **C8BA** with 360 nm light resulted in a decrease in intensity of the peak centered at 345 nm and a slight increase in intensity of absorbance in the 450 nm region indicating formation of the *cis*-isomer. A photostationary state was reached in 11 min (Figure 2.7a). The kinetics of *cis* to *trans* isomerization was studied by following the increase in absorbance at 345 nm as a function of time and a lifetime of 1.8×10^5 s was determined (Figure 2.7b).

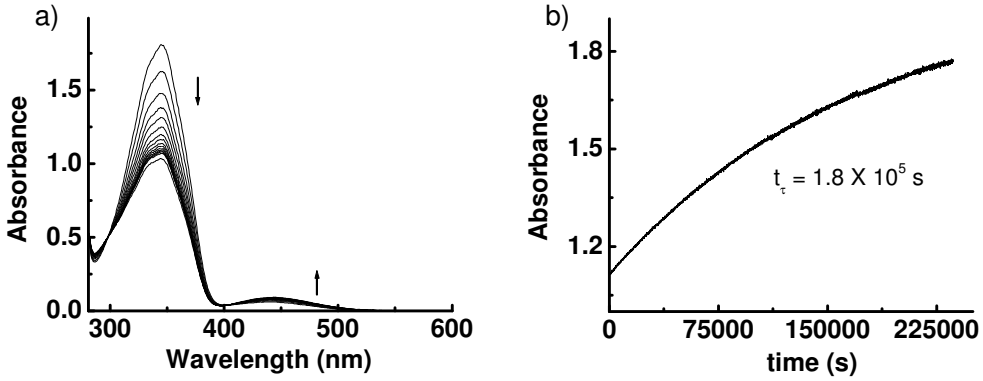

Figure 2.7. UV-vis spectra of **C8BA** in toluene showing a) *trans* to *cis* photoisomerization change from the all *trans* to photostationary state over a period of 11 min on irradiation with 360 nm band-pass; b) thermal *cis* to *trans* isomerization monitored by a time-course spectrum.

The colored glasses formed by the benzylidene acetal derivatives were investigated UV-vis spectroscopy. The absorption spectra were recorded in the glassy state by heating **C12BA** to isotropization and cooling to room temperature between two quartz plates. The absorption spectra showed peaks at 234, 343 and

~465 nm (Figure 2.8). Similar spectral characteristics were observed for the other acetal compounds.

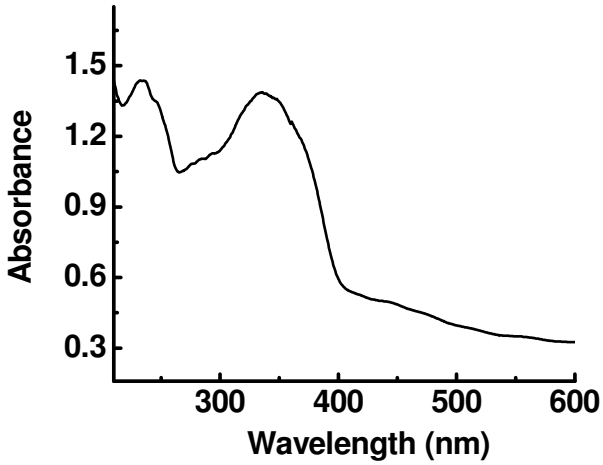

Figure 2.8. UV-vis spectra of cooled melt thin film of **C12BA**.

2.2.2.2. Bolaamphiphiles

The liquid crystalline properties of **Azo-bis** bolaamphiphiles (Chart 2.1) were studied by POM, DSC and XRD. On heating, **azo-bis 5** melted above 220 °C and a focal-conic texture characteristic of a smectic A* (SmA*) phase was formed on further heating (Figure 2.9a). The compound however started to decompose at 241 °C, making further characterization difficult. When **azo-bis 8** was heated, it exhibited a liquid crystalline behavior at 137 °C and fingerprint-type texture characteristic of chiral phases started to appear close to isotropization at 215 °C (Figure 2.9b). On cooling from the isotropic state, formation of *bâtonnets* were initially observed, followed by an equidistant line pattern superimposed on the fan texture which indicated the smectic C* phase.[22,23]

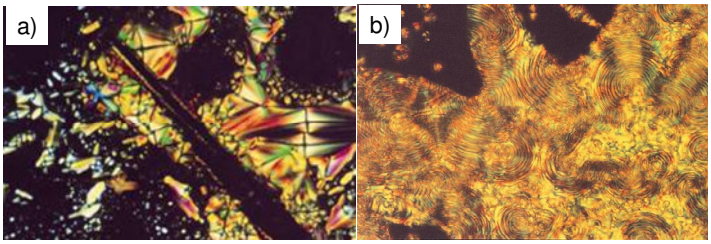

Figure 2.9. Polarized optical photomicrograph of (a) smectic A* phase observed for **azo-bis 5** at 179 °C (× 100) and (b) smectic C* phase observed for **azo-bis 8** at 205 °C (× 100).

DSC of **azo-bis 8** confirmed the results obtained from POM, but in addition showed a transition at 173 °C for which a corresponding textural change was not observed by POM (Figure 2.10).

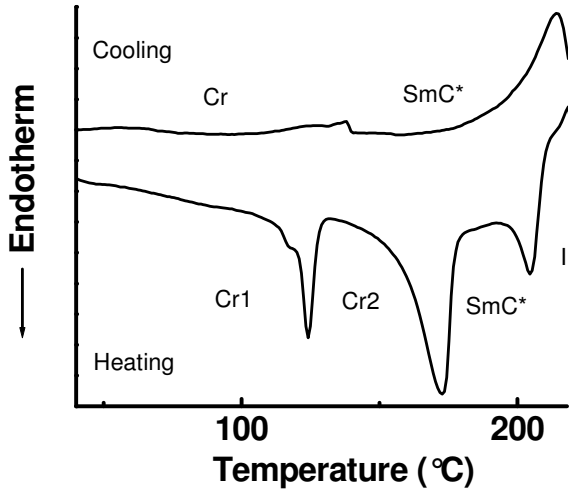

Figure 2.10. The DSC thermograms of **azo-bis 8** in the first heating/cooling cycles (scan rate 5 °C/min).

Similarly, **azo-bis 7** (Figure 2.11a,b), **azo-bis 10** (Figure 2.11c) and **azo-bis 12** exhibited chiral smectic phases in the heating and cooling cycles, i.e., enantiotropic (thermodynamically stable) LC phase.

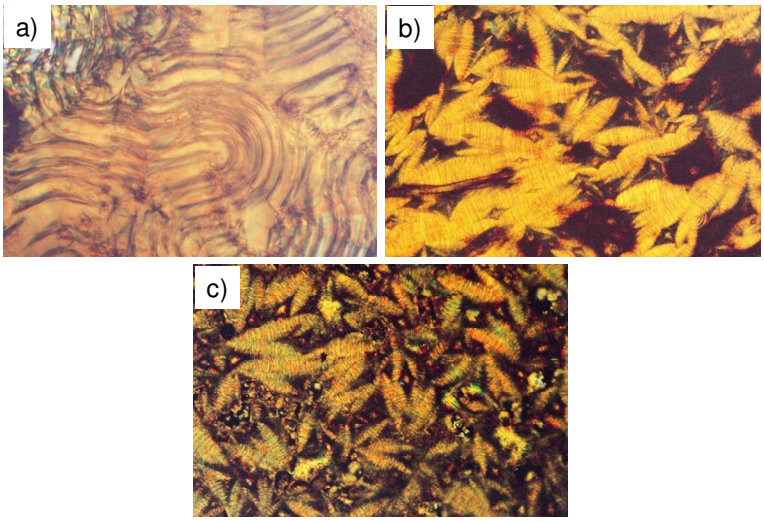

Figure 2.11. Polarized optical photomicrograph of smectic C* phase observed for (a) **azo-bis 7** at 169 ℃ (× 400); solidified (b) **azo-bis 7** (× 100) and (c) **azo-bis 10** (× 100) at room temperature obtained by slow cooling.

Clear peaks were not observed in the cooling cycle of the DSC of **azo-bis 8** (Figure 2.10) while that of **azo-bis 10** showed three clear peaks in both the heating and cooling cycles (Figure 2.12).

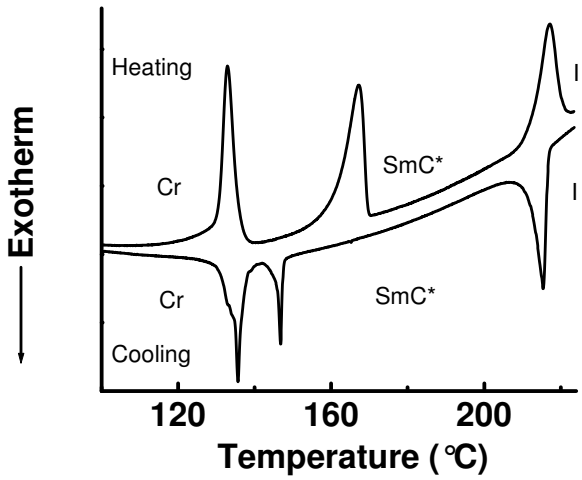

Figure 2.12. DSC thermograms of **azo-bis 10** in first heating/cooling cycles (scan rate 5 ℃/min).

The peaks observed at 167 °C in the heating cycle and at 146 °C in the cooling cycle were not accompanied by any textural change in the POM (Table 2.2).

Table 2.2. Phase transition characteristics of **Azo-bis** bolaamphiphiles in their first heating cycle

Sample code	heating cycle, °C (ΔH, $kJmol^{-1}$)
azo-bis 5	Cr 220 SmA* 241 dec.
azo-bis 7	Cr 164[a] (27.61) SmC* 205[a] (17.40) I
azo-bis 8	Cr_1 124[a] (10.41) Cr_2 173[a] (30.84) SmC* 205[a] (3.11) I
azo-bis 10	Cr_1 133[a] (22.64) Cr_2 167[a] (28.46) SmC* 217[a] (20.63) I
azo-bis 12	Cr 118 SmC* 218 I

[a]As observed by DSC; Cr - Crystal; SmA* - smectic A*; SmC* - smectic C*; I - Isotropic

The striated textures with stripes characteristic of smectic C* phase observed at high temperatures remained on cooling to room temperature, by which time the sample had crystallized (Figure 2.11b,c; 2.13a).

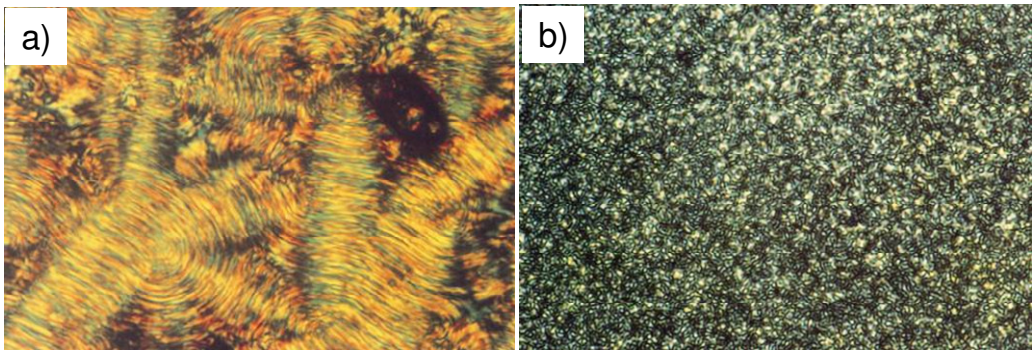

Figure 2.13. Polarized photomicrographs of solidified **azo-bis 8** at room temperature obtained by (a) slow cooling and (b) rapid cooling from the isotropic state.

The texture of the solidified crystalline phase as observed using POM was identical to that observed for the high temperature smectic C* phase suggesting

that the two phases possess sufficiently similar lattice parameters. Thus the smectic C* structure was well maintained in the crystal and no significant reorientation or formation of grain boundaries took place on crystallization.

The nature of the solid film formed from these compounds was observed to be highly sensitive to the manner in which it was prepared.[28,29] Whereas slow cooling resulted in the formation of solid phase in which the smectic C* texture was maintained (Figure 2.13a), a sample cooled rapidly from its isotropic state to ~0 °C resulted in the formation of a glassy state with a grainy texture (Figure 2.13b).[28] The crystalline smectic C* phase scattered light, while the glassy state was transparent with selective reflection of green light. XRD measurements on the former phase showed sharp peaks indicative of crystalline arrangement.

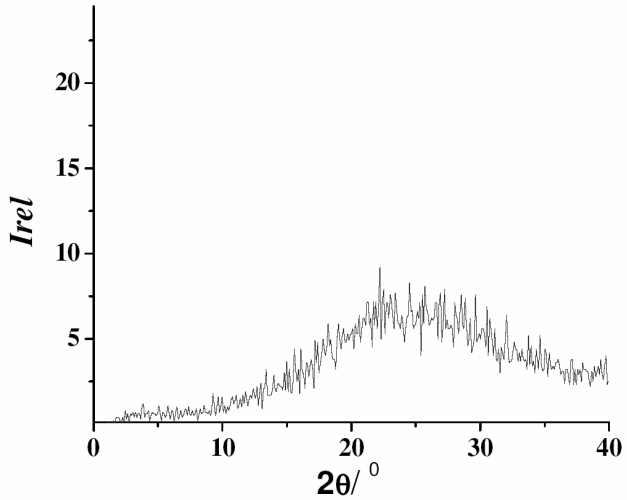

Figure 2.14. X-ray diffraction pattern of **azo-bis 10** in the glassy state recorded at room temperature.

The glassy nature of the sample formed by quick quenching from isotropic state to ~0 °C was confirmed by its XRD pattern which did not possess any sharp peaks and showed only a diffuse halo in the wide angle region (Figure 2.14).

Figure 2.15 shows the X-ray diffraction pattern, as well as the intensity versus diffraction angle (2θ) profile extracted from the pattern, for the mesophase of **azo-bis 10** at 155 °C.

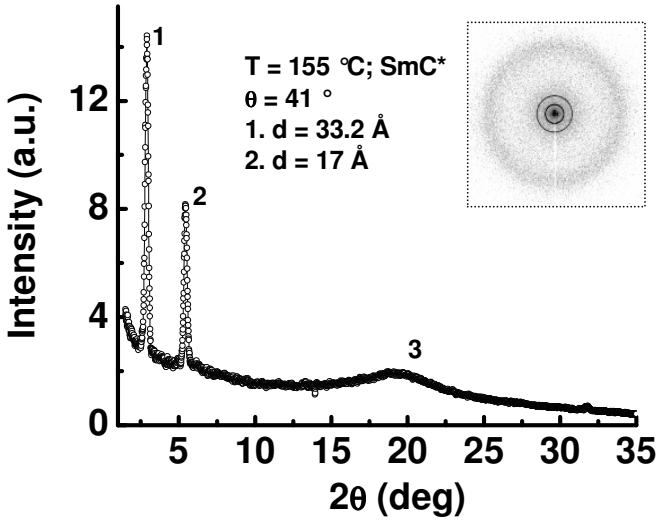

Figure 2.15. One-dimensional intensity vs. 2θ profile for **azo-bis 10** in the smectic C* phase at 155 °C. Inset shows the diffraction pattern of **azo-bis 10**.

Similar diffraction patterns were obtained from 190 °C to 155 °C in the cooling cycle. Whereas two sharp and intense peaks (at $2\theta_1$ and $2\theta_2$) were seen at low angles, a weak and diffuse peak (marked as **3**) was observed at wider angles. The sharp lower angle peak (at $2\theta_1$) accompanied by a diffuse peak at higher

angles is characteristic of a smectic phase in which the molecules are stacked into layers with short-range, liquid-like positional order within the layers.

The molecular length of the bolaamphiphile (**azo-bis 10**) determined from molecular models calculated using Insight II software gave an average molecular length (*l*) of 44 Å (Figure 2.16).

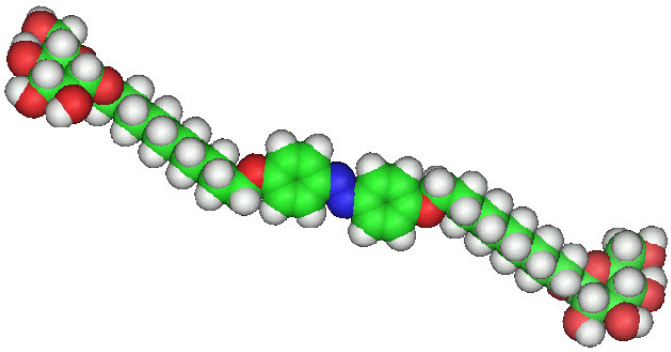

Figure 2.16. The Corey–Pauling–Koltun (CPK) model of the energy minimized conformation of **azo-bis 10** obtained using Insight II software.

The spacing corresponding to $2\theta_1$ is 33.2 Å which is much smaller than 44 Å, the length of the all-*trans* isomer estimated from its energy minimized conformation. Lower *d*-spacing values are indicative of either a tilted arrangement of molecules in the smectic phase or interdigitation of the smectic layers. This result in conjunction with characteristic striped focal-conic textures observed in the POM, confirms the smectic C* phase in these molecules. A significant point to be noticed in the X-ray pattern is the presence of a sharp and intense peak at low angles (at $2\theta_2$), a feature not commonly observed for the smectic phases. The ratio of the spacing corresponding to $2\theta_1$ and $2\theta_2$ is almost exactly 2, suggesting that the

latter is the second harmonic of the fundamental peak at $2\theta_1$. The ratio of the intensities of the second order and the principal peaks, I_2/I_1 was 0.51 for **azo-bis 10**. The presence of a strong second harmonic suggests that the layering is much better defined in this system, probably due to intermolecular hydrogen bonding as well as the nanoscale hydrophilic and hydrophobic separation that takes place owing to the rigid parts being separated by flexible alkyl chains. With a very few exceptions,[30] higher order peaks in liquid crystal diffraction pattern are generally not observed. Normally, the tendency for layering in smectic phases is rather weak, with the density distribution along the layer normal being close to a cosine wave. Consequently, in the X-ray diffraction pattern, the higher order diffraction maxima are either absent, or when present are extremely weak. For example the ratio of I_2/I_1 in most smectogens are generally as low as 2×10^{-7}.[31,32]

2.2.2.2.1. Electro-optic measurements

In 1975, Meyer et al. showed that tilted smectic LC phases (e.g., smectic C* phase) in materials composed of chiral molecules exhibit a spontaneous polarization.[7-9,33-35] In bulk samples the chiral nature of the molecules leads to the appearance of helix, which imposes a precession in the direction of the in-layer spontaneous polarization. Consequently the net polarization is zero. To realize a non-zero value for the polarization an electric field of a magnitude sufficient to unwind the helix has to be applied to the sample. Thus the phase is helielectric and not truly ferroelectric. In the smectic C* phase, the direction of spontaneous

polarization is coupled to the direction of tilt (azimuthal angle) of the molecules. By reversing the sign of an applied electric field the molecules can be made to switch between two bistable tilting directions, resulting in an electro-optical effect that is the essence of display devices based on these materials. The magnitude of the tilt angle, θ can be directly determined using the electro-optic effect.[34,35] Consider the texture observed in the SmC* phase (shown in Figure 2.17) with a certain sign of the field, through a polarizing microscope set for crossed polarizer configuration.

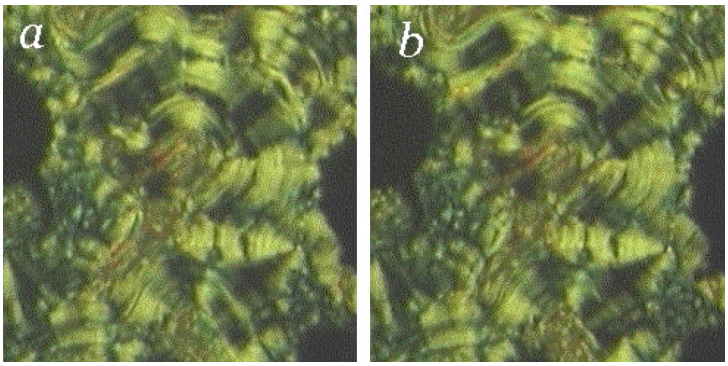

Figure 2.17. Polarizing microscope photographs of textures obtained in the smectic C* phase of the sample **azo-bis 10** on application of (a) +9V and (b) –9V electric field.

The dark bands in this photograph occur wherever the director (the average orientation direction of the molecules) is orthogonal to either the polarizer or the analyzer and serves to indicate the director orientation on a local scale. Now a reversal in the sign of the field will make the dark band rotate by an amount equal to twice the tilt angle (2θ) of the molecules. For the **azo-bis 10** compound studied here, we observed that the textural patterns seen in the equilibrium states show

hardly any difference (Figure 2.17) when the sign of the field is changed. A transient change in the birefringence of the system was however clearly noticeable.

This is possible only if the director rotates by 90 ° upon sign reversal of the field, suggesting that the tilt angle is 45 °. This value is in close agreement with that obtained (41 °) from XRD measurements and further in corroboration with the general observation that very large tilt angle values are seen when there is a direct transition from the isotropic to the smectic C* phase.[21]

In the smectic C* phase, the application of an electric field with a triangular wave-form results in a current peak, the area under which is a direct measure of the spontaneous polarization.[34] Figure 2.18 shows a typical current peak profile in the smectic C* phase of **azo-bis 10**. In fact, the electrical purity of the sample had to be improved substantially by repeated crystallization from MeOH/water before the electrical switching studies could be undertaken. The polarization value determined from the area under the peak was 850 nC/cm^2 (at 155 °C), a value much higher than that normally obtained for the smectic C* phase. This may be attributed to the appreciable hindrance to the rotation of the molecule caused by the strong hydrogen bonding present in the system. The polarization current profiles were obtained using an experimental setup similar to that reported earlier[36] and based on a method first developed by Miyasato et al.[35]

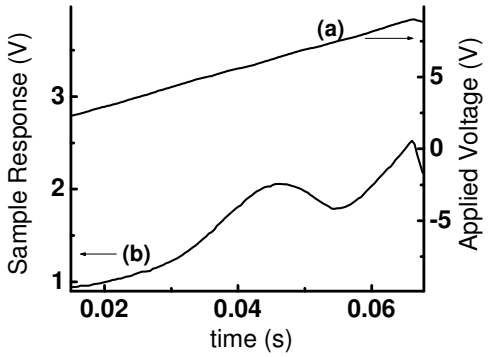

Figure 2.18. Oscilloscope traces of the (a) applied triangular wave field and (b) the sample current response in the smectic C* phase of **azo-bis 10**.

2.2.2.2.2. Absorption and CD spectral studies

The absorption spectra of all the five bolaamphiphiles studied in a solvent such as DMSO exhibited a typical azobenzene monomer absorption spectrum with a weak n→π* transition at 454 nm and an intense π→π* transition along the long-axis (A band) at 364 nm.[26,27] The solution state spectra (in pure DMSO) were CD silent indicating absence of aggregation and macroscopic chiral ordering. Thin films of **azo-bis 10** were prepared by drop-casting its solution on quartz plates, followed by heating and slow cooling to room temperature, to obtain films in which the smectic C* texture was maintained. The broad (λ_{max} = 344 nm) (Figure 2.19) nature of the absorption spectrum of the film was indicative of the formation of aggregates.[37-39] The existence of macroscopic chiral ordering in the films was confirmed by circular dichroism (CD) studies. Coupled CD bands centered at 390 nm and a weaker negative band around 300 nm were observed (Figure 2.19). The fact that the solution state (in pure DMSO) spectra are CD silent and the thin films

show strong CD signals, indicate that the CD spectra of the films do not arise from chirality in the monomeric species but from intermolecular dipole–dipole interactions in the aggregate species in a macroscopically chiral environment.

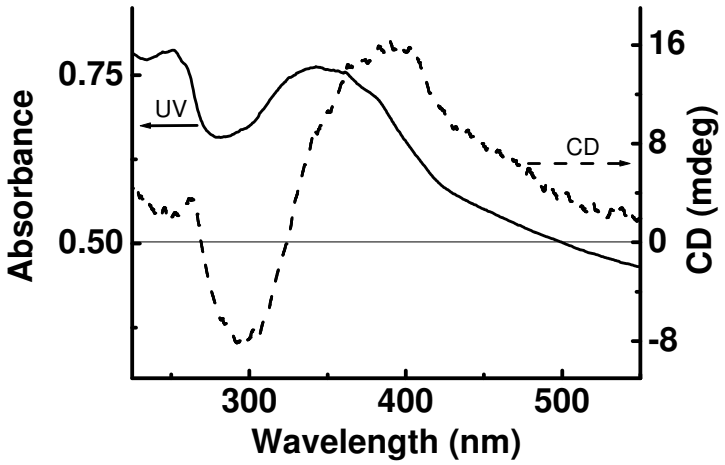

Figure 2.19. UV-vis (solid line) and CD (dashed line) spectra of cooled melt thin film of **azo-bis 10** possessing smectic C* texture.

2.3. Discussion

The azobenzene containing sugar amphiphile, **Glc-AB-Bu** was observed to form an achiral phase. This is in agreement with the phase behavior reported for sugar-based liquid crystals. Since the cause attributed to absence of macroscopic chirality in sugar-based liquid crystals is the formation of extensive hydrogen bond networks resulting in layered smectic like structures, we chemically modified these molecules by condensing the hydroxyl groups at 4- and 6- positions of the sugar group with aromatic aldehydes possessing different alkyl chain lengths (**CnBA** series). We expected that this modification would reduce the hydrogen bonding interactions of the amphiphiles and that this would result in expression of

macroscopic chirality in the mesophase. The stability of liquid crystalline phases of these modified amphiphiles was drastically reduced as a result of reduction of its amphiphilic nature. Whereas the derivative with methyl group on the aldehyde (**C1BA**) retained the mesogenic properties of the parent compound, **Glc-AB-Bu**, i.e., smectic A* phase, the longer chain derivatives were non-mesogenic. This could be explained as follows: As the hydrophobic alkyl chain part attached to the sugar –OH groups increases, the structure becomes more and more non-amphiphilic. This could be seen in the melting ranges of the DSC heating traces (Figure 2.4a).

When the bolaamphiphilic architecture was used, chiral thermotropic smectic C* phases were observed. This was the first reported observation of macroscopic chiral smectic C* phase in sugar-based LCs containing free hydroxyl groups.[21] The role of the length of oligomethylene chains on the solid-state self-assembly behavior of carbohydrate based bolaamphiphiles has recently been investigated by Masuda and co-workers.[40] Mainly smectic A* liquid crystalline phases were exhibited by these materials.[40]

Based on the chain conformation and thermal behavior, Masuda et al. observed that the short chain spacer ($6 \leq n \leq 8$) self-assembled to form a monolayer with *gauche* orientation of the methylene chain, whereas medium- and long-chain homologues formed monolayered assemblies with an all-*trans* oligomethylene conformation. This has been attributed to the dominant packing

interactions arising from the sugar head groups involving hydrogen bonding and electrostatic interactions in the lower homologues. In contrast, hydrophobic interactions of the long-chain oligomethylene spacers balances the head group packing interactions and this hydrophobic–hydrophilic balance resulted in retaining the all-*trans* conformation in the crystalline phase. The observation of smectic C* phase in **azo-bis 7**, **azo-bis 8**, **azo-bis 10** and **azo-bis 12** in the present study can be similarly attributed to a combination of hydrophobic interactions between the oligomethylene chains and aromatic interactions of the azobenzene moiety. Azobenzene chromophores are known to possess strong intermolecular interactions leading to the formation of both H-[37,38] and J-[39] type aggregates. It is interesting to note that only achiral mesophases are observed in both the azobenzene-linked sugar amphiphiles reported by Goodby et al.[16] and the oligomethylene linked bolaamphiphiles reported by Masuda et al.[40] In the present study an achiral smectic phase was observed in the C5 derivative, i.e., **azo-bis 5**, whereas the higher homologues exhibited smectic C* phases.

Based on the above mentioned observations it can be proposed that the lengthening of the methylene spacers together with the self-interaction of the azobenzene chromophores may be responsible in shifting the fine balance between competing electrostatic interactions and van der Waals forces resulting in favoring of the tilted smectic C* structure over the orthogonal smectic A* structure.

2.4. Experimental Section

2.4.1. Methods

Solvents and reagents for synthesis were purified prior to their use by reported methods.[41] Melting points were determined in a Mel-Temp II (Laboratory Devices, USA) melting point apparatus using open capillary tubes and are uncorrected. FT-IR spectra were recorded in a Shimadzu IR Prestige 21 spectrophotometer. NMR spectra were recorded in a Bruker Avance DPX 300 spectrometer. Mass spectral analysis was carried out either in a Shimadzu GC-MS QP 2010 analyzer (EI mode) or using a Jeol JMS600 instrument in FAB+ ionization mode. UV-vis spectra were recorded on a Shimadzu UV-2401 PC UV-vis scanning double-beam spectrophotometer. CD Measurements were carried out using Jasco J-810 spectropolarimeter. Phase transitions were observed using a Nikon HFX 35A Optiphot 2-Pol polarized light optical microscope, equipped with a Linkam THMS 600 heating and freezing stage connected to a Linkam TMS 93 temperature programmer. DSC analyses were carried out using a Perkin Elmer DSC7. The X-ray measurements were done using Cu K_α radiation (λ = 1.5418 Å) from a fine focus sealed-tube generator (Enraf-Nonius FR590), in conjunction with double mirror focusing optics. For polarization measurements the sample was subjected to a triangular wave profile of 4 Hz frequency through a function generator (HP 33120A) and a high voltage amplifier (Trek 50/750). The sample response current was measured as a voltage generated across a standard resistor in

series with the sample. The profiles were acquired using a digital oscilloscope (Tektronix TDS 420 A) and transferred to a PC for further analysis.

2.4.2. General procedures and Characterization data

4-Hydroxy-4'-*n*-butyl azobenzene (**1**): 4-*n*-Butyl aniline was dissolved in 1:1 HCl:water and 5 mL acetone. The solution was cooled and maintained at 0–5 °C. Aqueous sodiumnitrite was added drop-wise to this cooled mixture. Phenol was dissolved in aq sodium carbonate, cooled well and was added to this mixture. The resulting yellow-orange colored reaction mixture was stirred overnight at room temperature. The alkaline reaction mixture was neutralized with ice-cold dil HCl and partitioned between CH_2Cl_2 and water, extracted, dried (Na_2SO_4) and concentrated. The crude **1** was crystallized from cyclohexane to yield orange-red flakes. Yield: 80%. mp 83–84 °C. ^{1}H NMR ($CDCl_3$, 300 MHz) δ (ppm): 7.85 (d, *J* = 8.8 Hz, 2H, Ar), 7.78 (d, *J* = 8.3 Hz, 2H, Ar), 7.30 (d, *J* = 8.3 Hz, 2H, Ar), 6.92 (d, *J* = 8.9 Hz, 2H, Ar), 5.3 (brs, Ar–OH), 2.67 (t, 2H, Ar–C$\underline{H_2}$), 1.64 (m, 2H), 1.37 (m, 2H), 0.94 (t, 3H), D_2O exchange 4.7 (HOD signal). ^{13}C NMR ($CDCl_3$, 75.4 MHz) δ (ppm): 158.3, 150.9, 147.0, 146.0, 129.1, 124.8, 122.5, 115.8, 35.5, 33.4, 22.3, 13.9.

α-D-Glucopyranose pentabenzoate (**2**): 10 g (1 equiv) of D-Glucose was dissolved in 225 mL pyridine and the solution was cooled to 0 °C. 52 mL (~8 equiv) of benzoyl chloride was added to this mixture slowly while maintaining the

flask at 0 °C. On completion of the addition the reaction mixture turned rose-red in color. Stirring was continued for 24 h during which the mixture was allowed to attain room temperature. The reaction was quenched by adding it to ice-cold water in a 500 mL beaker. The resulting solution was extracted with CH_2Cl_2 and the organic layer was washed repeatedly with ice-cold dil HCl to remove pyridine. The organic layer was then washed with saturated aq $NaHCO_3$ in order to neutralize the excess acid. After washing with brine, the solution was dried (Na_2SO_4) and concentrated. The residue was dissolved in minimum quantity of $CHCl_3$ and petroleum ether was added resulting in an off-white colored precipitate of **2**, which was collected by filtration and dried. Yield: 70%. mp 185–188 °C. ^{1}H NMR ($CDCl_3$, 300 MHz) δ (ppm): 8.16 (d, *J* = 8.4 Hz, 2H, *o*-Benzoyl), 8.0 (d, *J* = 8.4 Hz, 2H, *o*-Benzoyl), 7.94 (d, *J* = 8.5 Hz, 2H, *o*-Benzoyl), 7.88 (d, *J* = 7.5 Hz, 4H, *o*-Benzoyl), 7.6–7.25 (m, 15H), 6.85 (d, *J* = 3.6 Hz, 1H), 6.32 (t, *J* = 10 Hz, 1H), 5.83 (t, *J* = 9.8 Hz, 1H), 5.68 (dd, 1H), 4.61 (d, 2H), 4.48 (dd, 1H).

α-D-Glucopyranosyl bromide tetrabenzoate (**3**): **2** (1 equiv) was dissolved in dry CH_2Cl_2 and the flask was ice-cooled to 0 °C. 33% HBr/Glacial AcOH (7.75 equiv) was added dropwise. After the initial evolution of gas ceased, the flask was stoppered and stored in a refrigerator overnight. The reaction mixture was then diluted with CH_2Cl_2 and washed with saturated aq sodium bicarbonate, washed with water and dried using Na_2SO_4. The solution on concentration gave the bromide. Yield: 65%. mp 128–131 °C. ^{1}H NMR ($CDCl_3$, 300 MHz) δ (ppm): 8.1

(d, *J* = 8.3 Hz, 2H, *o*-Benzoyl), 8.0 (d, *J* = 8.3 Hz, 2H, *o*-Benzoyl), 7.9 (d, *J* = 8.4 Hz, 2H, *o*-Benzoyl), 7.8 (d, *J* = 8.3 Hz, 2H, *o*-Benzoyl), 7.53–7.3 (m, 12H, Ar), 6.9 (d, *J* = 4.0 Hz, 1H), 6.3 (t, 1H), 5.85 (t, 1H), 5.35 (dd, 1H), 4.7 (m, 2H), 4.5 (dd, 1H).

4-[(4-Butylphenyl)azo]phenyl-2,3,4,6-tetra-O-benzoyl-β-D-glucopyranoside (**4**): 0.64 g (**1**) was dissolved in 1 M aq NaOH solution. **3**, *tetra-n*-butylammoniumbromide[17] was dissolved in $CHCl_3$ and added drop wise from a pressure equalizing funnel into the stirred alkaline solution of **1** and stirred at room temperature overnight. The reaction mixture was diluted with $CHCl_3$, washed with dil NaOH solution followed by washing with water and dried over Na_2SO_4. The solution was concentrated and column chromatographed over silica gel (100–200 mesh) with 15% Ethyl acetate/petroleum ether to obtain **4** as a red solid. ^{1}H NMR ($CDCl_3$, 300 MHz) δ (ppm): 8.09 (d, *J* = 8.3 Hz, 2H), 8.03–7.7 (m, 10H), 7.5–7.29 (m, 14H), 7.17 (d, *J* = 8.9 Hz, 2H), 6.09 (t, *J* = 9.4 Hz, 1H), 5.91 (t, *J* = 9.4 Hz, 1H), 5.79 (t, *J* = 9.6 Hz, 1H), 5.56 (d, *J* = 7.6 Hz, 1H), 4.75 (d, *J* = 12 Hz, 1H), 4.6 (m, 1H), 4.4 (m, 1H), 2.72 (t, 2H), 1.6 (m, 2H), 1.4 (m, 2H), 0.98 (t, 3H).

4-[(4-Butylphenyl)azo]phenyl-β-D-glucopyranoside (**Glc-AB-Bu**): **4** was dissolved in MeOH/THF and the solution was ice-cooled. To this was carefully added a few cut pieces of sodium metal. The reaction mixture was maintained at 0°C and stirred overnight after which MeOH/THF was evaporated under reduced pressure and the residue was diluted with ice-cold water, extracted with EtOAc,

dried over Na_2SO_4, concentrated and column chromatographed over silica gel (100–200 mesh) with 10% MeOH/$CHCl_3$ to obtain **Glc-AB-Bu** as an orange solid in 69% yield. mp 133–223 °C. ^{1}H NMR (300 MHz, Acetone-d_6) δ (ppm): 7.89 (d, J = 6.9 Hz, 2H), 7.82 (d, J = 8.4 Hz, 2H), 7.39 (d, J = 8.4 Hz, 2H), 7.24 (d, J = 8.4 Hz, 2H), 5.11 (d, J = 7.2 Hz, 1H), 4.7 (app d, 1H), 4.46 (br s, 1H), 4.37 (d, J = 3.9 Hz, 1H), 3.93–3.43 (band, 7H), 2.72 (t, 2H, J = 7.5 Hz), 1.64 (m, 2 H), 1.41 (m, 2H), 0.98 (t, J = 6.9 Hz, 3H). ^{13}C NMR (75 MHz, DMSO-d_6) δ (ppm): 161.1, 151.8, 148.6, 147.0, 125.1, 123.4, 117.6, 101.6, 77.9, 74.7, 73.1, 71.7, 62.6, 36.0, 34.3, 22.9, 14.2. ESI-MS (HRMS): calcd for $C_{22}H_{28}N_2O_6$: *m/z*: 439.1845 [M + Na]$^+$; found : 439.1862 [M + Na]$^+$. Also GC-MS (EI) Mass *m/z* 416.

4-*n*-Butyloxybezaldehyde (**5**): 4-Hydroxybenzaldehyde and activated anhyd K_2CO_3, were mixed in dry DMF and maintained under stirring at 60 °C for 15 min. To this *n*-butylbromide was added dropwise. After completion of addition, the reaction mixture was maintained at 100 °C for 16 h. The cooled reaction mixture was quenched by pouring it into ice-cold 1:1 HCl. The organic layer was extracted with CH_2Cl_2, dried (Na_2SO_4), concentrated under reduced pressure and column chromatographed through silica gel (100–200 Mesh) to afford **5**. Yield: 70%. Pale yellow liquid. FT-IR (ν/cm^{-1}): 2960, 2934, 2872, 2738, 1693, 1600, 1507, 1253. ^{1}H NMR ($CDCl_3$, 300 MHz) δ (ppm): 9.7 (s, 1H), 7.7 (d, J = 7.0 Hz, 2H), 6.8 (d, J = 7.2 Hz, 2H), 3.9 (t, 2H), 1.65 (m, 2H), 1.36 (m, 2H), 0.8 (m, 3H).

4-*n*-Butyloxybezaldehyde dimethylacetal (**6**): A mixture of **5** (1 equiv), trimethylorthoformate (1.1 equiv), methanol and *p*-Toluenesulphonic acid (cat) was gently heated while the Methyl formate formed in the reaction was distilled out through a short *vigreux* column.[18] The cooled reaction mixture was made basic by addition of a few drops of sodium methoxide solution and partitioned between ether and water. The organic phase was washed with brine and dried with potassium carbonate. Evaporation of the solvent afforded a good yield of dimethylacetal (**6**) as a colorless to yellow liquid. Yield: 75%. Pale yellow liquid. FT-IR (ν/cm^{-1}): 2970, 2826, 1594, 1615, 1512, 1470, 1186, 1057. ^{1}H NMR ($CDCl_3$, 300 MHz) δ (ppm): 7.61 (d, J = 8.4 Hz, 2H), 6.9 (d, J = 8.7 Hz, 2H), 5.35 (s, 1H), 3.9 (t, 2H), 3.3 (s, 6H), 1.7 (m, 2 H), 1.5 (m, 2 H), 0.9 (t, 3H). ^{13}C NMR (75 MHz, DMSO-d_6) δ (ppm): 159.2, 129.6, 127.5, 113.3, 102.3, 54.4, 51.6.

4-[(4-butylphenyl)azo]phenyl-4,6-O-[[4-(butyloxy)phenyl]methylene]-β-D-glucopyranoside (**C4BA**): **Glc-AB-Bu** and **6** were taken in a 10 mL RBF and catalytic amount of *p*-Toluenesulphonic acid was added. The mixture was evacuated under high vacuum and purged with N_2. To this ~4 mL of dry DMF was added and the flask was attached to a rotavapor, evacuated and heated in a water bath at 60 ± 5 °C. After 1 h, the reaction was quenched by addition of a few mL of triethylamine, and the flask was again attached to the rotavapor as above and heated in the water bath above 80 °C and the DMF and triethylamine were distilled off. The flask was then cooled and removed from the evaporator.[19,20] TLC

indicated formation of the product. To this residue was added a solution of sodium hydrogen carbonate in water, and the solution was extracted with chloroform, dried using Na_2SO_4, concentrated under reduced pressure and column chromatographed through silica gel (100–200 Mesh) (Before loading crude product, the silica column was eluted with 5 mL of triethylamine in 100 mL hexane in order to reduce the acidity of silica and thereby prevent hydrolysis of the benzylidene acetal) to obtain **C4BA** on elution with 40–50% Ethyl acetate/Hexane as an orange-red solid.

C4BA was also synthesized using another method in which **5** was reacted with **Glc-AB-Bu** in the presence of anhyd $ZnCl_2$ as catalyst. Anhyd $ZnCl_2$ was prepared as follows: Commercial $ZnCl_2$ was taken in a RBF, closed with a pressure adapter and evacuated through the pressure adapter using a vacuum pump and heated simultaneously in a heating mantle. This was continued until the $ZnCl_2$ which was sticky in nature became a free flowing solid. The $ZnCl_2$ purified in this way was immediately used for the reaction.

To the RBF containing dried anhydrous $ZnCl_2$ was added **5**, **Glc-AB-Bu** and the mixture was stirred in a water bath at 50 °C for 20 h. TLC indicated that the reaction occurred. The reaction mixture was poured into ice-cold water, extracted with ethyl acetate, dried (Na_2SO_4) and concentrated under reduced pressure to yield the crude product which was then purified by column chromatography.

4-[(4-butylphenyl)azo]phenyl-4,6-O-[[4-(methoxy)phenyl]methylene]-β-D-glucopyranoside (**C1BA**): Yield: 61%. mp (POM) 149–200 °C. ^{1}H NMR ($CDCl_3$, 300 MHz) δ (ppm): 7.8 (d, *J* = 7.7 Hz, 2H), 7.71 (d, *J* = 7.2 Hz, 2H), 7.32 (d, *J* = 7.8 Hz, 2H), 7.20 (d, *J* = 7.7 Hz, 2H), 7.0 (d, *J* = 7.7 Hz, 2H), 6.8 (d, *J* = 7.6 Hz, 2H), 5.4 (s, 1H), 5.0 (d, *J* = 7.4 Hz, 1H), 4.3 (m, 1H), 3.8 (s, 1H), 3.7 (t, 2H), 3.5 (q, 2H), 2.6 (t, 2H), 1.58 (t, 2H), 1.3 (m, 2H), 0.9 (t, 3H). ^{13}C NMR ($CDCl_3$, 75 MHz) δ (ppm): 160.0, 158.6, 151.0, 148.6, 146.3, 139.3, 129.2, 127.6, 124.4, 122.7, 117.0, 116.0, 114.3, 114.0, 102.0, 101.0, 80.1, 74.2, 73.2, 69.0, 68.0, 67.0, 49.4, 34.0, 33.4, 32.0, 31.2, 30.0, 29.5, 29.1, 28.9, 26.7, 22.7, 22.3, 19.2, 14.1, 13.9, 13.8. FAB+ Mass *m/z* calcd for $C_{30}H_{34}N_2O_7$: 534.6, found: 535.21.

4-[(4-butylphenyl)azo]phenyl-4,6-O-[[4-(butyloxy)phenyl]methylene]-β-D-glucopyranoside (**C4BA**): Yield: 70%. mp (POM) 171–181 °C. UV-vis (MeCN) λ_{max} = 343 nm (ε_{343} 27300) ^{1}H NMR ($CDCl_3$, 300 MHz) δ (ppm): 7.9 (d, *J* = 8.9 Hz, 2H), 7.8 (d, *J* = 8.2 Hz, 2H), 7.41 (d, *J* = 8.6 Hz, 2H), 7.3 (d, *J* = 8.3 Hz, 2H), 7.14 (d, *J* = 8.9 Hz, 2H), 6.89 (d, *J* = 8.6 Hz, 2H), 5.5 (s, 1H), 5.1 (d, *J* = 7.5 Hz, 1H), 4.4 (m, 1H), 3.94 (t, 2H), 3.8 (q, 2H), 3.6 (m, 2H), 2.9 (br, 2 –OH), 2.68 (t, *J* = 7.6 Hz, 2H), 1.77–1.64 (m, 4H), 1.48–1.36 (m, 5H), 0.98–0.85 (m, 9H). ^{13}C NMR ($CDCl_3$, 75 MHz) δ (ppm): 160.0, 158.6, 151.0, 148.6, 146.3, 139.3, 129.2, 127.6, 124.4, 122.7, 117.0, 116.0, 114.3, 114.0, 102.0, 101.0, 80.1, 74.2, 73.2, 69.0, 68.0, 67.0, 49.4, 34.0, 33.4, 32.0, 31.2, 30.0, 29.5, 29.1, 28.9, 26.7, 22.7,

22.3, 19.2, 14.1, 13.9, 13.8. GC-MS (EI) Mass *m/z* calcd for $C_{33}H_{40}N_2O_7$: 576.68, found: 576.

4-[(4-butylphenyl)azo]phenyl-4,6-O-[[4-(octyloxy)phenyl]methylene]-β-D-glucopyranoside (**C8BA**): Yield: 75%. mp (POM) 162–168 °C. UV-vis (MeCN) λ_{max} = 343 nm (ε_{343} 24769) FT-IR (KBr, ν / cm^{-1}): 3406, 3310, 2926, 2854, 1606, 1593, 1496, 1466, 1427 (–N=N–), 1384, 1305, 1242, 1170, 1091, 1016, 978, 841, 725. ^{1}H NMR ($CDCl_3$, 300 MHz) δ (ppm): 7.9 (d, *J* = 8.7 Hz, 2H), 7.8 (d, *J* = 8.1 Hz, 2H), 7.41 (d, *J* = 8.4 Hz, 2H), 7.31 (d, *J* = 8.1 Hz, 2H), 7.16 (d, *J* = 8.7 Hz, 2H), 6.89 (d, *J* = 8.4 Hz, 2H), 5.52 (s, 1H), 5.13 (d, *J* = 7.5 Hz, 1H), 4.4 (d, 1H), 3.94 (t, 2H), 3.83 (q, 2H), 3.64 (t, 2H), 2.9 (br, 2 –OH), 2.68 (t, *J* = 7.6 Hz, 2H), 1.79–1.62 (m, 8H), 1.44–1.34 (m, 15H), 0.96–0.86 (m, 6H). ^{13}C NMR ($CDCl_3$, 75 MHz) δ (ppm): 160.1, 158.8, 151.0, 148.8, 146.5, 129.3, 127.8, 124.7, 123.0, 117.2, 114.6, 102.2, 101.0, 97.4, 80.4, 74.4, 73.4, 68.7, 68.3, 49.2, 66.8, 35.8, 33.7, 32.0, 29.6, 29.4, 26.2, 22.9, 22.5, 14.3, 14.1. FAB+ Mass *m/z* calcd for $C_{37}H_{48}N_2O_7$: 632.79, found: 633.78 also GC-MS (EI) Mass *m/z* found: 632. Elemental analysis calcd (%) for $C_{37}H_{48}N_2O_7$: C 70.23; H 7.65; N 4.43. Found: C 70.43; H 8.11; N 4.65.

4-[(4-butylphenyl)azo]phenyl-4,6-O-[[4-(dodecyloxy)phenyl]methylene]-β-D-glucopyranoside (**C12BA**): Yield: 75%. mp (POM) 167–171 °C. UV-vis (MeCN) λ_{max} = 343 nm (ε_{343} 29406) ^{1}H NMR ($CDCl_3$, 300 MHz) δ (ppm): 7.9 (d, *J* = 7.7 Hz, 2H), 7.8 (d, *J* = 7.2 Hz, 2H), 7.41 (d, *J* = 7.8 Hz, 2H), 7.31 (d, *J* = 7.7 Hz, 2H),

7.16 (d, *J* = 7.7 Hz, 2H), 6.9 (d, *J* = 7.6 Hz, 2H), 5.53 (s, 1H), 5.13 (d, *J* = 7.4 Hz, 1H), 4.4 (d, 1H), 3.94 (t, 2H), 3.83 (q, 2H), 3.64 (t, 2H), 3.0 (br, 2 –OH), 2.68 (t, *J* = 7.6 Hz, 2H), 1.78–1.62 (m, 11H), 1.41–1.26 (m, 22H), 0.97–0.86 (m, 6H). ^{13}C NMR ($CDCl_3$, 75 MHz) δ (ppm): 159.9, 158.7, 150.8, 148.5, 146.2, 129.0, 127.6, 124.4, 122.7, 117.0, 114.3, 102.0, 101.0, 80.1, 74.2, 73.2, 68.5, 68.1, 66.6, 35.6, 33.4, 32.0, 29.6, 29.4, 29.3, 29.2, 26.0, 22.7, 22.3, 14.0.

2.5. Conclusion

We describe for the first time, the observation of macroscopic chirality in the liquid crystalline phases of sugars containing free hydroxyl groups. Our results indicate that the manifestation of smectic C* phases in sugar-based bolaamphiphiles are dependent critically on the length of the oligomethylene spacers and the presence of the azobenzene chromophore. These results imply that mesogenic bolaamphiphiles possessing macroscopic chirality can be designed by suitable selection of other aromatic linker groups capable of intermolecular noncovalent interactions and variety of naturally occurring sugar derivatives.

References

(1) Demus, D., Goodby, J. W., Gray, G. W., Spiess, H.-W., Vill, V., Eds. *Handbook of Liquid Crystals*; Wiley-VCH: Weinheim, 1998; Vol. 1,2A,2B.

(2) Tschierske, C. *J. Mater. Chem.* **1998**, *8*, 1485–1508.

(3) Kitzerow, H.-S.; Bahr, C., Eds., *Chirality in Liquid Crystals*, Springer-Verlag: New York, 2001.

(4) Tamaoki, N. *Adv. Mater. (Weinheim, Ger.)* **2001**, *13*, 1135–1147.

(5) Walba, D. M.; Eshdat, L.; Korblova, E.; Shao, R.; Clark, N. A. *Angew. Chem., Int. Ed.* **2007**, *46*, 1473–1475 and references therein.

(6) Pauluth, D.; Tarumi, K. *J. Mater. Chem.* **2004**, *14*, 1219–1227.

(7) Clark, N. A.; Lagerwall, S. T. *Appl. Phys. Lett.* **1980**, *36*, 899–901.

(8) McCubbin, J. A.; Tong, X.; Wang, R.; Zhao, Y.; Snieckus, V.; Lemieux, R. P. *J. Am. Chem. Soc.* **2004**, *126*, 1161–1167.

(9) Lagerwall, J. P. F.; Giesselmann, F. *ChemPhysChem* **2006**, *7*, 20–45.

(10) Vill, V.; Hashim, R. *Curr. Opin. Colloid Interface Sci.* **2002**, *7*, 395–409.

(11) van Doren, H. A.; Smits, E.; Pestman, J. M.; Engberts, J. B. F. N.; Kellogg, R. M. *Chem. Soc. Rev.* **2000**, *29*, 183–199.

(12) Davis, R.; Mallia, V. A.; Das, S. *Chem. Mater.* **2003**, *15*, 1057–1063.

(13) Abraham, S.; Mallia, V. A.; Ratheesh, K. V.; Tamaoki, N.; Das, S. *J. Am. Chem. Soc.* **2006**, *128*, 7692–7698.

(14) Loos, M.; Baeyens-Volant, D.; David, C.; Sigaud, G.; Achard, M. F. *J. Colloid Interface Sci.* **1990**, *138*, 128–133.

(15) Tschierske, C.; Lunow, A.; Zaschke, H. *Liq. Cryst.* **1990**, *8*, 885.

(16) Laurent, N.; Lafont, D.; Dumoulin, F.; Boullanger, P.; Mackenzie, G.; Kouwer, P. H. J.; Goodby, J. W. *J. Am. Chem. Soc.* **2003**, *125*, 15499–15506.

(17) Allcock, H. R.; Kim, C. *Macromolecules* **1989**, *22*, 2596–2602.

(18) a) Napolitano, E.; Fiaschi, R.; Mastrorilli, E. *Synthesis* **1986**, 122–125. b) Johansson, R.; Samuelsson, B. *J. Chem. Soc., Perkin Trans 1* **1984**, 2371.

(19) Calinaud, P.; Gelas, J. In Hanessian, S. *Preparative Carbohydrate Chemistry*, Marcel Dekker, Inc.: New York; 1997; p. 3–33.

(20) Roën, A.; Padrón, J. I.; Vázquez, J. T. *J. Org. Chem.* **2003**, *68*, 4615–4630.

(21) Abraham, S.; Paul, S.; Narayan, G.; Prasad, S. K.; Rao, D. S. S.; Jayaraman, N.; Das, S. *Adv. Funct. Mater.* **2005**, *15*, 1579–1584.

(22) Gray, G. W.; Goodby, J. W. *Smectic liquid crystals: Textures and structures*; Leonard Hill: Glasgow, 1984.

(23) Dierking, I. *Textures of liquid crystals*, Wiley-VCH: Weinheim, 2003.

(24) Molinier, V.; Kouwer, P. J. J.; Fitremann, J.; Bouchu, A.; Mackenzie, G.; Queneau, Y.; Goodby, J. W. *Chem. –Eur. J.* **2006**, *12*, 3547–3557.

(25) Gray, G. W. *Molecular structure and the properties of liquid crystals*, Academic Press: New York, 1962.

(26) Kawasaki, T.; Tokuhiro, M.; Kimizuka, N.; Kunitake, T. *J. Am. Chem. Soc.* **2001**, *123*, 6792–6800.

(27) Anzai, J.-I.; Osa, T. *Tetrahedron* **1994**, *50*, 4039–4070.

(28) Chen, S. H.; Chen, H. M. P.; Geng, Y.; Jacobs, S. D.; Marshall, K. L.; Blanton, T. N. *Adv. Mater. (Weinheim, Ger.)* **2003**, *15*, 1061–1065.

(29) Hassheider, T.; Benning, S. A.; Kitzerow, H.-S.; Achard, M.-F.; Bock, H. *Angew. Chem., Int. Ed.* **2001**, *40*, 2060–2063.

(30) Lobo, C. V.; Prasad, S. K.; Rao, D. S. S. *Phys. Rev. E: Stat., Nonlinear, Soft Matter Phys.* **2004**, *69*, 051706 1–8.

(31) Ocko, B. M.; Kortan, A. R.; Birgeneau, R. J.; Goodby, J. W. *J. Phys. (Paris)* **1984**, *45*, 113.

(32) Seddon, J. M. In *Handbook of Liquid Crystals: Fundamentals* Demus, D., Goodby, J. W., Gray, G. W., Spiess, H.-W., Vill, V., Eds.; Wiley-VCH: Weinheim, 1998, Vol. 1; pp. 635–679.

(33) Meyer, R. B.; Liébert, L.; Strzelecki, L.; Keller, P. *J. de Phys. Lett.* **1975**, *36*, L69.

(34) Lagerwall, S. T. *Ferroelectric and Antiferroelectric Liquid Crystals*, Wiley-VCH: Weinheim, 1999.

(35) Miyasato, K.; Abe, S.; Takezoe, H.; Fukuda, A.; Kuze, E. *Jpn. J. Appl. Phys.* **1983**, *22*, L661–L663.

(36) Prasad, S. K.; Nair, G. G.; Chandrasekhar, S. *J. Mater. Chem.* **1995**, *5*, 2253–2256.

(37) Caculitan, N. G.; Scudder, P. H.; Rodriguez, A.; Casson, J. L.; Wang, H.-L.; Robinson, J. M.; Johal, M. S. *Langmuir* **2004**, *20*, 8735–8739.

(38) Narayan, G.; Kumar, N. S. S.; Paul, S.; Srinivas, O.; Jayaraman, N.; Das, S. *J. Photochem. Photobiol., A* **2007**, *189*, 405–413.

(39) Dante, S.; Advincula, R.; Frank, C. W.; Stroeve, P. *Langmuir* **1999**, *15*, 193–201.

(40) Masuda, M.; Vill, V.; Shimizu, T. *J. Am. Chem. Soc.* **2000**, *122*, 12327–12333.

(41) Armarego, W. L. F.; Chai, C. L. L., In *Purification of Laboratory Chemicals* 5th Edn., Butterworth-Heinemann: Amsterdam, 2003.

Chapter 3

Macroscopic Chiral Diphenylbutadiene Cored Bolaamphiphilic Sugars

Abstract

A series of symmetrical bolaamphiphiles possessing a diphenylbutadiene core and glucopyranoside head groups linked together by oligomethylene spacers, were synthesized and their thermotropic liquid crystalline properties were investigated by polarized light optical microscopy, differential scanning calorimetry, X-ray diffraction and electro-optic switching. In spite of the presence of chiral centers, amphiphilic sugars in general do not exhibit macroscopic chirality and this phenomenon is attributed to strong hydrogen bonding between sugar head groups resulting in microphase-segregated layer like arrangements. In the present study, all the molecules investigated exhibited the smectic C phase i.e., tilted lamellar phase with macroscopic chiral ordering of the molecules. The stability of this phase increased with increase in the length of the oligomethylene spacers. Whereas for derivatives with spacers containing ≤ 4 methylene groups, the smectic C* phase was observed only in the cooling phase, for those containing spacers with ≥ 5 methylene groups this phase was observed both in the heating and cooling cycles. The absorption and fluorescence spectra of these materials suggest that the unusual observation of*

macroscopic chirality in these bolaamphiphiles containing free hydroxyl groups could be attributed to self-aggregating behavior of the diphenylbutadiene core.

3.1. Introduction

Liquid crystals (LCs) belong to a class of materials, which have been extensively exploited for the past several decades for a variety of technological applications ranging from display devices[1-4] to the development of high strength polymers.[5] From a fundamental point of view, large gaps exist in the understanding of structure-property relationships, especially with respect to molecules containing more than one mesogenic unit.[6] Among the various liquid crystalline phases, macroscopic chiral LCs such as chiral nematic (N*)[7] and chiral smectic C (SmC*)[8] attract considerable attention, since their potential for application in display devices is next only to nematics, which are well known for their applications in flat panel LCDs.[4] The smectic C* LC state in particular, due to its bistability, fast electro-optic switching (10^3 times faster than nematic LCs), and wide viewing angle finds applications in commercial high-resolution reflective microdisplays.[1,9-11] In addition, molecules possessing the smectic C* phase are potential candidates for nonlinear optics[12] and photonic applications.[13]

It is well recognized that induction of macroscopic chirality in LCs can be achieved either by introduction of a chiral dopant into a non-chiral LC host[14-16] or by designing inherently chiral liquid crystalline molecules.[14,17,18] However, the

mechanism by which molecular chirality is transferred to macroscopic chirality of the LC phases still remains an intriguing subject.[14]

Sugar-based amphiphiles and bolaamphiphiles have been well studied for their thermotropic liquid crystalline properties.[19-21] Though these compounds were molecularly chiral, they were not effective chiral LCs.[14] In Chapter 2 we have described our studies related to the observation of a macroscopic chiral smectic C phase in azobenzene linked bolaamphiphiles containing sugar moieties.[22] This was the first report of a macroscopic chiral thermotropic mesophase among sugar mesogens possessing free hydroxyl groups. Our studies indicated that the manifestation of smectic C* phases in these sugar-based bolaamphiphiles was dependent critically on the presence of the azobenzene moiety and suitable length of the intervening oligomethylene spacers. The appearance of macroscopic chirality in these derivatives was attributed to noncovalent aromatic interactions of the azobenzene moiety[22] in view of its known ability to undergo intermolecular interactions leading to the formation of both H-type[23] and J-type[24,25] aggregates. We hypothesized that the replacement of the azobenzene core by moieties with enhanced ability to form aggregates would result in the formation of a highly stabilized smectic C* phase. In order to test this we have synthesized a series of diphenylbutadiene cored sugar bolaamphiphiles (Scheme 3.1, 3.2) since earlier studies in our group had shown the diphenylbutadiene chromophore to be a versatile photoresponsive moiety,[26] with a strong tendency to form aggregates in

the bulk phase.[27,28] A useful aspect of this chromophore is that its absorption and emission spectra are very sensitive to the state of its aggregation, providing distinct signatures for the presence of the monomer and the aggregated forms.[27-29] In this Chapter we describe the synthesis, liquid crystalline and optical properties of this class of bolaamphiphiles. As anticipated the formation of highly stabilized smectic C* phase was observed for these molecules and rationalization of these results based on the aggregation behavior of the diphenylbutadiene chromophore is provided.

3.2. Results

3.2.1. Synthetic strategy

For the preparation of the diphenylbutadiene core of the bolaamphiphiles, 4-Methoxybenzaldehyde (Sisco) was first reduced to the carbinol (**1**) using sodium borohydride in methanol. Treatment of **1** with phosphorus tribromide gave 4-Methoxybenzyl bromide (**2**), which due to its tendency to hydrolyze quickly was immediately treated with triethyl phosphite and converted to Diethyl-4-methoxybenzylphosphonate (**3**). On treatment of **3** with 4-Methoxycinnamaldehyde (Lancaster) using Potassium *tert*-butoxide as base in DMF (Wittig-Horner reaction), 4,4'-Dimethoxydiphenylbuta-1*E*,3*E*-diene (**DBC1**) was obtained as a crystalline solid. X-ray quality single crystals of this derivative were obtained by slow evaporation of its benzene/chloroform solution. The crystals were analyzed by single crystal XRD and its structure and packing mode

confirmed. The **DBC1** molecules packed in a herringbone fashion in the orthorhombic unit cell. Figure 3.1 shows the packing pattern obtained for **DBC1** in the crystalline state.

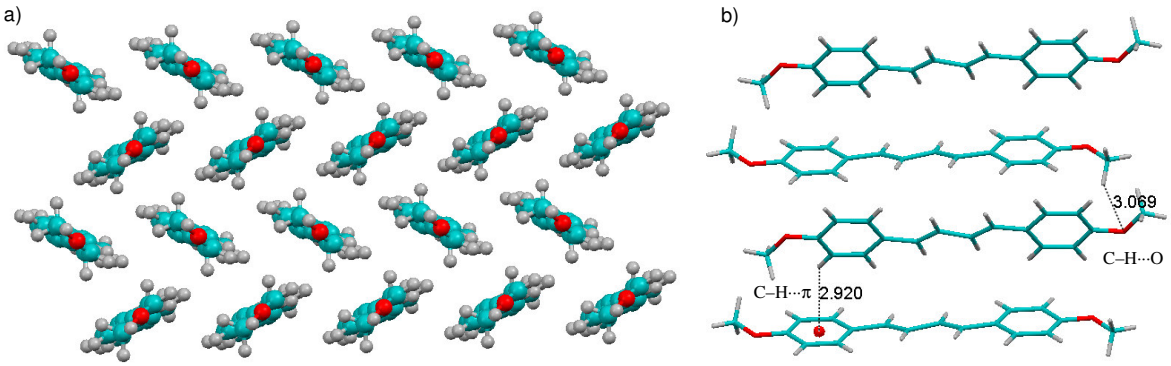

Figure 3.1. The packing diagram of **DBC1** in crystalline state showing a) herringbone packing and b) intermolecular interactions (numbers are distances in Å unit). This packing diagram was obtained from the CIF file using Mercury 1.4.1 software.

4,4'-Dihydroxydiphenylbuta-1*E*,3*E*-diene (**DBCOH**) was obtained by the deprotection[30] of **DBC1**. The conditions are as shown in the Scheme 3.1. Glycosylation of bromoalcohols with glucopyranose peracetate in the presence of $BF_3.Et_2O$ afforded bromoalkyl group containing glucopyranosides (**GlcCnBr**).[31] O-Alkylation of **DBCOH** with **GlcCnBr**, followed by a de-O-acetylation, using NaOMe/MeOH, afforded bolaamphiphiles **CnGB** (Scheme 3.2). The structures of all compounds were confirmed by spectroscopic methods (see Experimental Section for details).

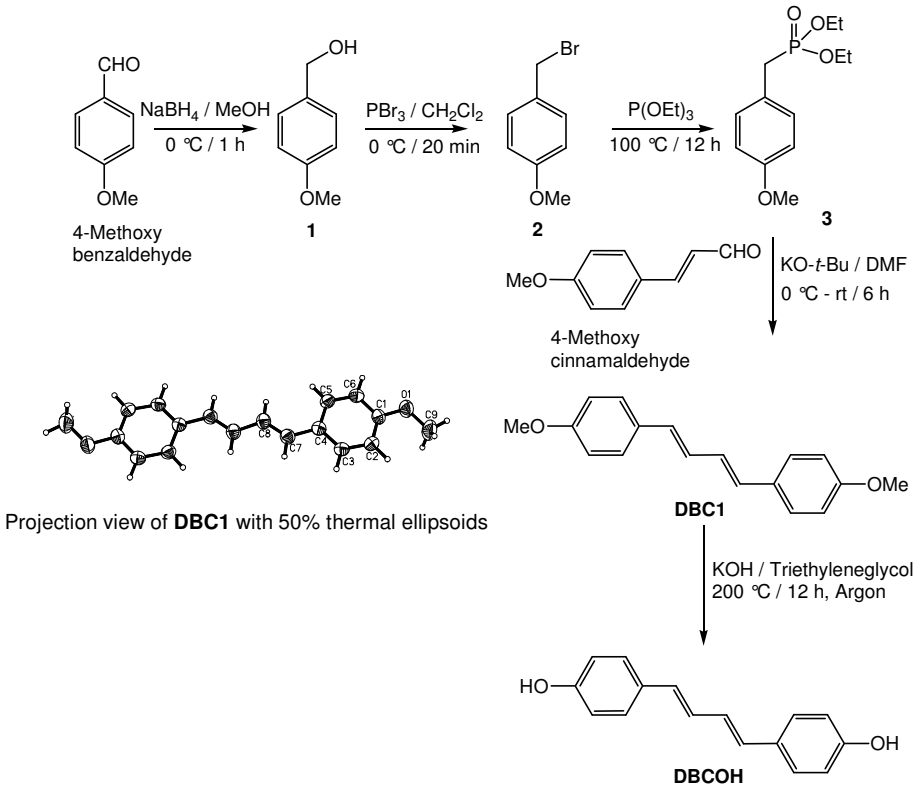

Projection view of **DBC1** with 50% thermal ellipsoids

Scheme 3.1

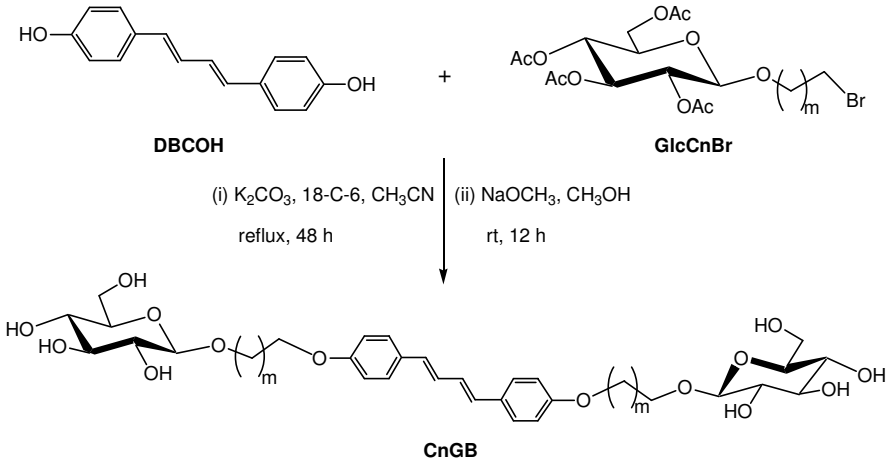

m = 1: **C2GB**, 2: **C3GB**, 3: **C4GB**, 4: **C5GB**, 6: **C7GB**, 7: **C8GB**, 9: **C10GB**, 11: **C12GB**

Scheme 3.2

3.2.2. Phase transition behavior

There are very few reports on the thermotropic LC properties of substituted diphenylbutadiene containing mesogens.[26,29,32-34] The thermotropic LC properties of **DBC1** has been reported.[32,33] The phase behavior of **DBC1** was observed by polarized light optical microscopy (POM) and differential scanning calorimetry (DSC). **DBC1** transformed from crystalline state to a nematic phase at 237 °C which on further heating above 250 °C sublimed without becoming isotropic. The transition from crystal to nematic phase was accompanied by an endothermic peak in the DSC trace. Figure 3.2 shows the POM texture in the nematic phase and the DSC trace in the heating cycle observed for **DBC1**.

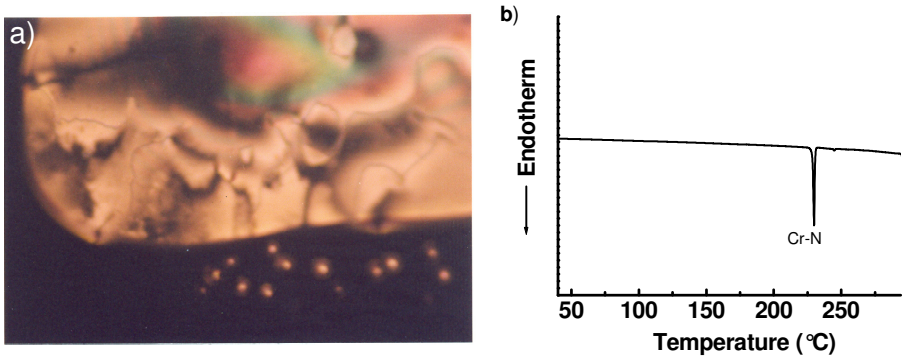

Figure 3.2. (a) Polarized light optical micrograph of nematic phase observed for **DBC1** at 248 °C in the heating cycle (× 100) and (b) the heating cycle DSC trace.

The mesomorphic properties of the **CnGB** bolaamphiphiles were then investigated using POM, DSC and X-ray diffraction (XRD). All the derivatives showed enantiotropic (thermodynamically stable) LC phases. The transition temperatures and corresponding enthalpy values are summarized in Table 3.1.

Table 3.1. Phase transition temperatures of the **CnGB** compounds in their first heating/cooling cycles

Sample code	heating cycle, °C (ΔH, kJmol^{-1})	cooling cycle, °C (ΔH, kJmol^{-1})
C2GB	Cr 201 (26.6) SmA* 261 (11.07) I	I 260[a] SmA* 212[a] SmC* 150[a] Plastic
C3GB	Cr_1 97 (7.7) Cr_2 140 (1.8) Cr_3 189 (8.2) SmA* 268 (5.1) I	I 266[a] SmA* 229[a] SmC* 194 (1.3) Cr
C4GB	Cr_1 187 (5.6) Cr_2 198 (7.8) SmA* 258 (12.5) I	I 257 (3.3) SmA* 222 (0.8) SmC* 198 (4.2) Cr
C5GB	Cr_1 167 (13.4) Cr_2 183 (8.2) SmC* 259 (16) I	I 257 (0.6) SmC* 199 (5.1) Cr
C7GB	Cr_1 168 (19.1) Cr_2 191 (6.0) SmC* 262 (15.7) I	I 261 (0.5) SmC* 203 (4.6) Cr
C8GB	Cr_1 145 (23.05) Cr_2 173 (18.8) Cr_3 194 (7.8) SmC* 265[a] I	I 258[a] SmC* 166 (1.3) Cr
C10GB	Cr_1 164.3 (19.2) Cr_2 203 (6.5) SmC* 260 (18.8) I	I 255[a] SmC* 205 (2.3) Cr
C12GB	Cr_1 109 (5.3) Cr_2 203 (8.8) SmC* 256 (29.5) I	I 251[a] SmC* 206 (5.9) Cr

[a]ΔH value not given due to absence of clear DSC signal; Cr - Crystal; SmA* - smectic A*; SmC* - smectic C*; I - Isotropic

POM studies indicated that in the heating cycle the bolaamphiphiles with ≤ C4 oligomethylene spacers underwent a crystal to smectic A* phase transition characterized by their typical focal-conic texture (Figure 3.3a).[35,36] Cooling of the isotropic phase of these derivatives, resulted initially in the formation of the smectic A*, which on subsequent cooling transformed to the smectic C* state, i.e., tilted lamellar phase with macroscopic chiral ordering of the molecules (Figure 3.3b). For example on cooling the isotropic phase of **C2GB**, transition to the smectic A* phase was indicated by the formation of *bâtonnets* at 260 °C, which coalesced to form focal-conic domains. At 212 °C, a change in texture with appearance of equidistant stripes across the fans was observed which indicated a transition to the smectic C* phase.[35,36]

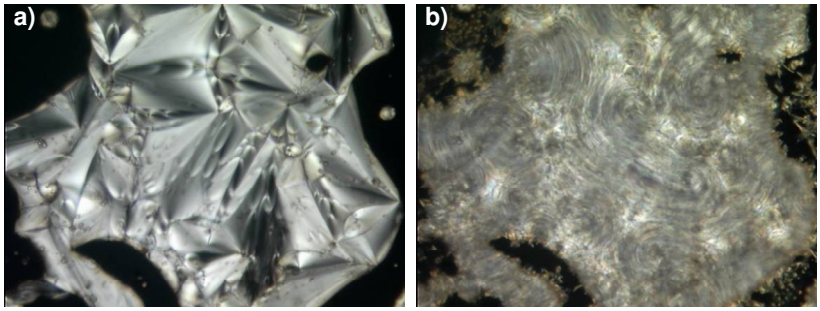

Figure 3.3. Polarized light optical micrographs of (a) smectic A* and (b) smectic C* phases observed for **C2GB** at 220 °C and 203 °C respectively in the cooling cycle (×32).

The transition from smectic A* to the smectic C* phase at 222 °C could be clearly seen in the cooling DSC trace of **C4GB** (Figure 3.4).

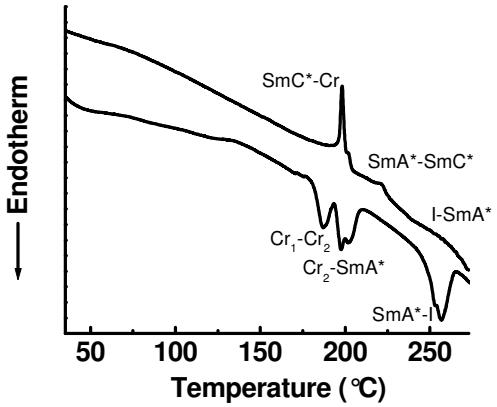

Figure 3.4. DSC trace showing the thermal transitions observed for **C4GB** in the first cycle at 5 °C/min.

For the derivatives with ≥ C5 oligomethylene spacers however, the smectic C* phase was observed in the heating cycle itself. Thus the compounds melted to yield a striated fan-shaped texture (Figure 3.5) clearly indicating the formation of the smectic C* phase.

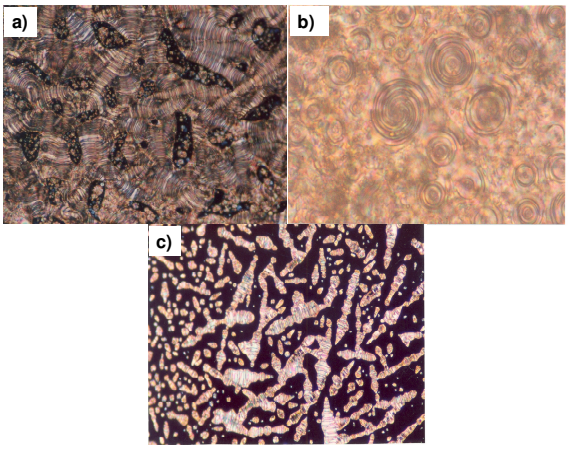

Figure 3.5. Polarized light optical micrographs of smectic C* phase observed for (a) **C5GB** at 252 °C in the cooling cycle (× 100), (b) **C10GB** at 205 °C in the heating cycle (× 100) and (c) **C12GB** at 245 °C in the cooling cycle (× 100).

In the cooling cycle an isotropic to smectic C* phase transition was observed for the derivatives with ≥ C5 oligomethylene spacers. All the derivatives, except **C2GB**, solidified on cooling from the smectic C* phase maintaining the same texture, suggesting that the structure in the solid state closely matched that of the smectic C* phase.

In accordance with our previous observations in the case of the azo-bolas,[22] the nature of the solid film formed from these compounds was observed to be highly sensitive to the manner in which it was prepared. Whereas slow cooling resulted in the formation of crystalline phase in which the smectic C* texture was maintained (Figure 3.6a), a sample cooled rapidly from its isotropic state to ~0 ^{o}C resulted in the formation of a transparent glassy state with a grainy texture (Figure 3.6b).[22] XRD measurements of the slowly cooled phase showed well resolved peaks in the wide angle region indicative of crystalline arrangement.

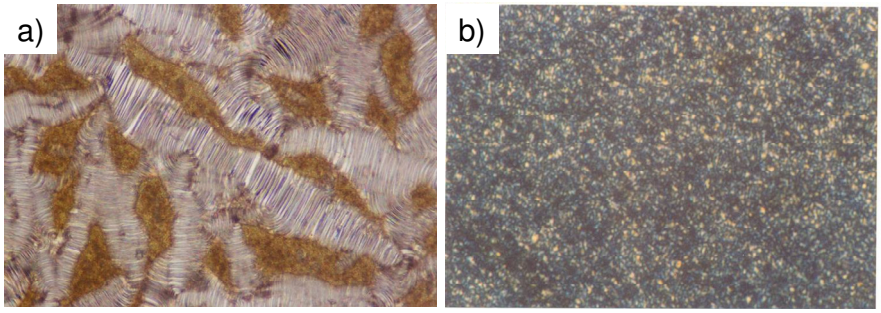

Figure 3.6. Polarized light optical micrographs (× 100) of solidified **C10GB** at room temperature obtained by (a) slow cooling and (b) rapid cooling from isotropic state.

The phase transitions were also confirmed using DSC. In addition, the DSC traces exhibited a crystal–crystal transition (Cr–Cr) in the first heating cycle for all the derivatives, for which a corresponding change was not observed in the POM study. The Cr–Cr transitions were not observed in the subsequent heating cycles. The DSC trace of **C10GB** in the first cycle is shown in Figure 3.7a. Thermogravimetric analysis (TGA) of these samples indicated that no substantial weight loss occurred up to ~300 °C. Figure 3.7b shows the TGA curve for **C10GB**.

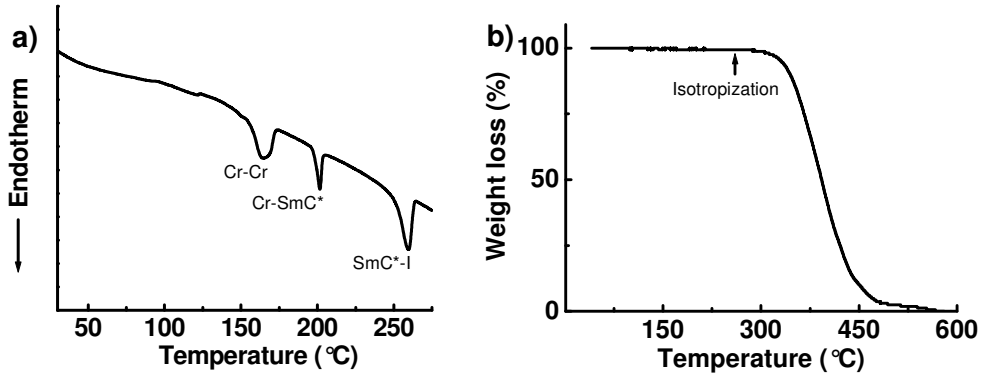

Figure 3.7. Thermal phase transitions and thermal stability of **C10GB** analyzed by (a) differential scanning calorimetry and (b) thermogravimetric analysis respectively.

The stability of the compounds was also indicated by the similarity of the FT-IR spectra and the molecular ion (*m/z* value) obtained by mass spectral analysis of samples heated to above their isotropic temperatures and cooled to room temperature to that of the unheated fresh samples (Figures 3.8).

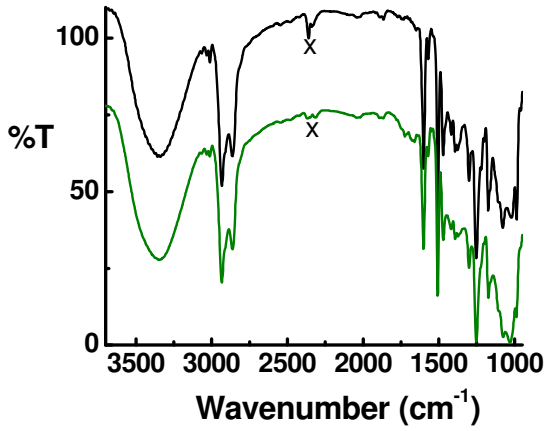

Figure 3.8. FT-IR (KBr) spectra of a fresh sample (black trace) and one heated to 280 ℃ (above isotropization temp) and cooled (green trace) of **C7GB**. The peaks marked '×' are due to atmospheric CO_2 in the sample chamber.

Thus the bolaamphiphilic molecules used in the present study possessed unusually high thermo-chemical stability. During microscopic studies, however a slight tendency for caramalization was observed close to isotropization temperatures, especially for the derivatives with shorter oligomethylene spacers.

3.2.3. X-ray diffraction studies

X-ray diffraction analysis of these compounds confirmed the LC phase assignments observed by POM. It may be noted that the samples generally

exhibited a spontaneous orientation in the Lindemann capillaries, with the quality of alignment being as good as for monodomain samples.

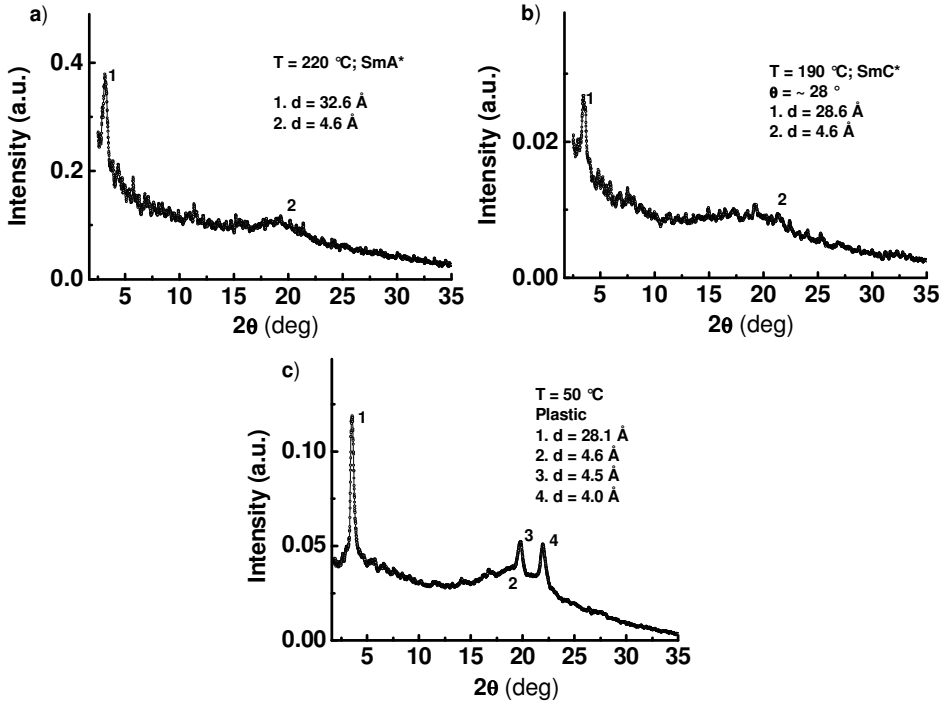

Figure 3.9. One-dimensional intensity vs. 2θ profile for **C2GB** in the (a) smectic A*, (b) smectic C* and (c) plastic phase.

The X-ray pattern of **C2GB** obtained at 220 °C (Figure 3.9a) is characteristic of the smectic A* mesophase, exhibiting a strong low angle reflection corresponding to the smectic layer spacing of d = 32.6 Å and a broad and diffuse peak at 4.6 Å corresponding to the lateral spacing of the mesogenic side groups. The layer spacing was higher than the length (l) of the **C2GB** molecule (l = 26.2 Å) as calculated using ChemDraw 3D, suggesting interdigitation of the molecules. The XRD pattern recorded for **C2GB** at 190 °C in the cooling cycle (Figure 3.9b), showed the principal reflection at 28.6 Å, which is

less than that in the smectic A* phase, a feature typical of a tilted smectic phase, and in conjunction with the characteristic POM texture observed at this temperature, confirmed the phase to be smectic C*. On further cooling a transition from the smectic C* to another phase was observed at 150 °C. The X-ray pattern obtained in this phase (Figure 3.9c) at 50 °C exhibited two sharp peaks overriding the usual diffuse peak at wide angles. Such a feature is generally seen for a plastic crystal phase.[37-39] Similarly, the layer spacing was higher than the length *l* of **C3GB** (*l* = 29.2 Å) also, suggesting interdigitation of the molecules in the smectic A* phase (Figure 3.10).

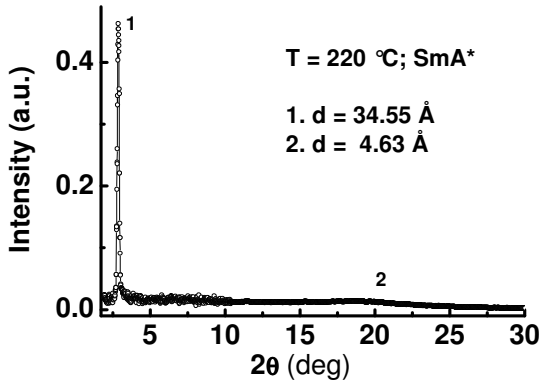

Figure 3.10. One-dimensional intensity vs. 2θ profile for **C3GB** in smectic A* phase.

The smectic C* phase of **C8GB** was confirmed in a similar fashion with the X-ray pattern being very similar to that of **C2GB**, except for the presence of a second reflection at small angles (see Figure 3.11a). The *d*-spacings of the two reflections were in the ratio 1:2, as expected for a lamellar phase. More interesting features were seen for the higher homologues, **C10GB** and **C12GB**. The diffraction pattern shown in Figure 3.11c (as inset) for **C12GB** and the I–2θ

profiles for the two homologues (Figure 3.11b and c) exhibited up to five sharp peaks in the small angle region although with diminishing peak intensity with increase in 2θ.

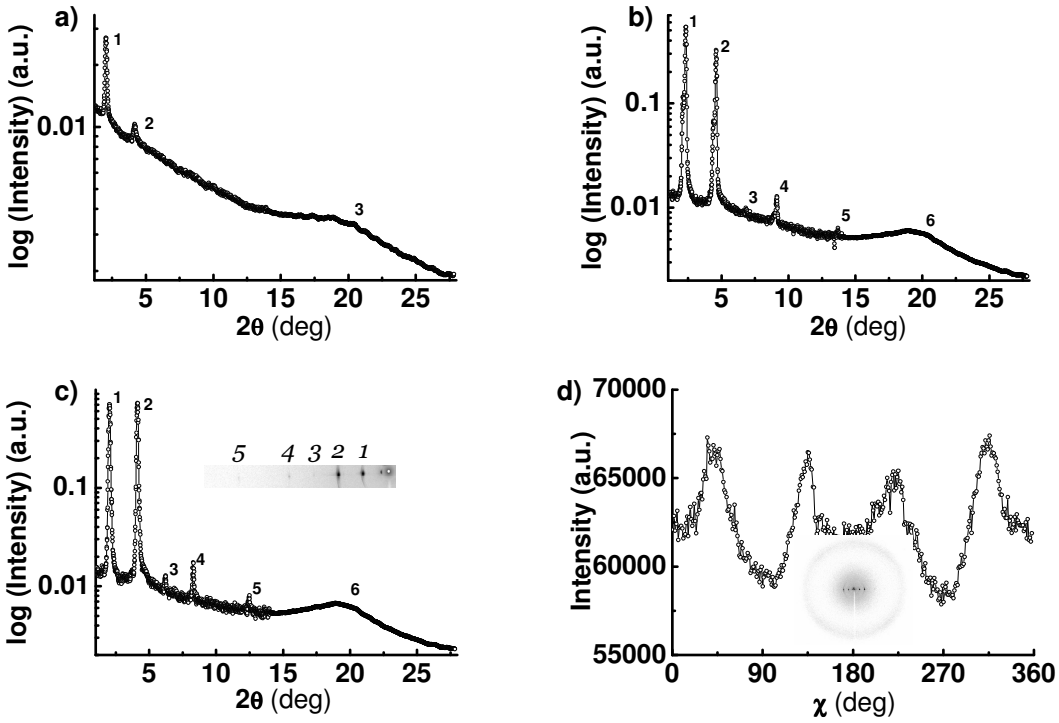

Figure 3.11. One-dimensional intensity vs. 2θ profile for (a) **C8GB**, (b) **C10GB**, (c) **C12GB** in the smectic C* phase at 210 °C. Inset in (c) shows the diffraction pattern of **C12GB** indicating the aligned nature of sample; and (d) two-dimensional XRD pattern and its azimuthal profile (at a 2θ value of ~19.3°) for **C12GB** at 210 °C.

What is more important is that the ratio of the *d*-spacings for the successive peaks was 1:2:3:4:6, which is again in conformity with the lamellar nature of the phase. It must be pointed out that observation of such sub-harmonic peaks is extremely rare, especially in thermotropic systems. Three interesting features associated with these X-ray patterns to be noted are described below.

Firstly the smectic phase of all the homologues studied here, exhibit a diffuse peak in the wide angle (θ ~10°) region confirming the fluid nature of the phase, despite the presence of multiple harmonic peaks in the low angle region. Secondly, the intensity of the second harmonic is exceptionally high, with I_2/I_1, the ratio of the intensities between the second harmonic (peak # 2 in the Figures 3.11a–c) and the fundamental (peak # 1) being 0.19, 0.70 and 1.00 for **C8GB**, **C10GB** and **C12GB** respectively. This may be compared with the ratio of I_2/I_1 as low as[40,41] 10^{-4} or even[42,43] 2×10^{-7} for the archetypal smectic phase. It must be recalled that smectic layering occurs due to a nanophase separation of the aromatic core regions and the aliphatic tail portions. In the usual thermotropic smectic phases, it has been shown that the layering or more precisely the mass density distribution along the layer normal direction is described by a cosine wave as against a square wave suggested by simple ideas of layering. Obviously a pure cosine wave would mean the absence of higher harmonics as is indeed reflected in the X-ray diffraction patterns observed for typical smectic phases, although exceptions have been recently reported.[22,44] However in situations which are congenial for a very effective separation of the two portions of the molecules, as for example in the case of certain side chain polymers[45] and lipid systems[46,47] in which the separation is made effective by the presence of the backbone in the former case and sheet of water in the latter, strong harmonics do appear suggesting a mass density wave significantly distorted from the pure sinusoidal form. Thus the

observation of intense and multiple harmonics in the present systems indicate that the sugar units provide an effective method to augment the layering property of the medium. This conclusion is strengthened by the fact that an intense XRD higher order peak (I_2/I_1 = 0.51) was also observed for the similar azobenzene cored bolaamphiphile system reported earlier by us (see Chapter 2).[22] Finally, an alternation in the peak intensity values is observed for the harmonic peaks (see Table 3.2), instead of a monotonic decrease: $I_2>I_3$, but $I_3<I_4$. Currently we do not have a clear understanding of this anomalous feature.

Table 3.2. Ratios of the X-ray peak intensity (after background subtraction) of the harmonic peaks to that of the fundamental in the smectic C* phase of the three sugar derivatives.

sample code temp	I_2/I_1	I_3/I_1	I_4/I_1	I_5/I_1
C8GB 210 °C	0.19	–	–	–
C10GB 210 °C	0.7	0.013	0.014	0.005
C12GB 210 °C	1.0	0.005	0.011	0.003

The spontaneous alignment of the molecules mentioned earlier proved to be quite useful in providing a clear proof of the tilted smectic C* phase as shown in Figure 3.11d. It may be noted that the sharp low angle reflections are lined up as spots in the equatorial direction indicating the direction of the layer normals. In contrast, the intensity maximum of the wide angle diffuse reflection occurs at four

azimuthal angles inclined with respect to the equatorial direction as is indeed expected for a tilted layer structure. This is evident from the 'χ scan' profile shown in Figure 3.11d, obtained by plotting the intensity variation as a function of the azimuthal angle χ, at a fixed 2θ value (at ~19.3°). The four intensity maxima, arising from the four-arc pattern serves two purposes: (i) the maxima occurring at an angle equal to the equatorial direction (χ = 0° or 180°) or orthogonal to it (χ = 90° or 270°) gives a qualitative indication of the molecules tilted with respect to the layer normal. (ii) The difference in χ between the two successive maxima is twice the tilt angle and thus can be quantitatively used to determine the tilt angle (θ). The tilt angle calculated in this fashion is 45° for **C10GB** and **C12GB** samples (for which clear four-arc pattern could be obtained), which is not unusual considering the fact that these materials undergo a direct transition from the isotropic to the smectic C* phase. Combining this independently determined tilt angle value and the *d*-spacing value and assuming a rigid-rod model, we estimate the extent of interdigitation to be ~16% which suggests a slight overlapping of the sugar units in the smectic C* phase. Also the tilt angle of the mesogens in the smectic C* state was found to increase with temperature.

3.2.4. Electro-optic measurements

The tilted smectic LC phases (e.g., smectic C* phase) in materials composed of chiral molecules exhibit spontaneous polarization.[2,9-11,48-50] In the smectic C* phase, the direction of spontaneous polarization is coupled to the

direction of tilt (azimuthal angle) of the molecules. By reversing the sign of an applied electric field, the molecules can be made to switch between two bistable tilting directions, resulting in an electro-optical effect that is the essence of display devices based on similar organic materials. The magnitude of the tilt angle, θ could be conveniently determined using the electro-optic effect.[49,50] Upon application of electric field the helix is unwound and the sample is poled.[2] This could be seen as a fan-shaped texture with absence of superimposed equidistant line pattern. At 0 V the natural texture of smectic C* phase was observed which indicated the reformation of the helical superstructure (Figure 3.12).

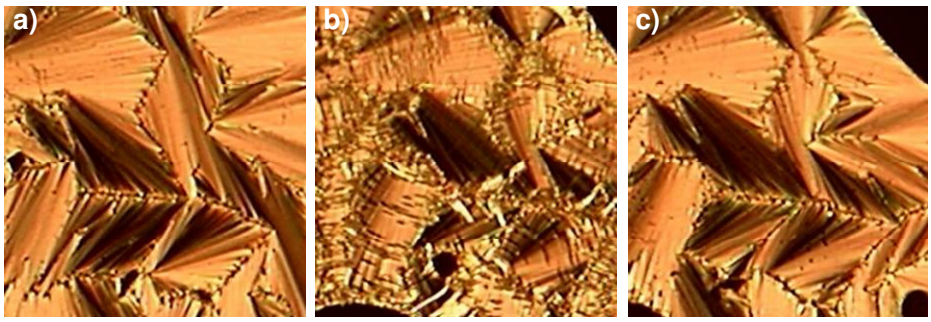

Figure 3.12. Polarized light optical micrographs obtained in the smectic C* phase of **C10GB** at 207 °C on application of (a) –85 V; (b) 0 V and (c) +85 V electric field.

We could not get a polarization current peak (as would be expected for the smectic C* phase) even after application of very high field (~10 V/μm) perhaps due to a very weak transverse dipole moment. Notice that there is no birefringence change between the positive and negative voltage states. This indicates a tilt angle of 45°, in confirmation with the value measured from XRD. Therefore the angle

between the + and − states will be 90°, thus causing no change in the birefringence.

3.2.5. Absorption, fluorescence and circular dichroism spectra

The absorption and fluorescence spectra of **C10GB** in THF solutions and in the solidified phase possessing the smectic C* texture are shown in Figure 3.13.

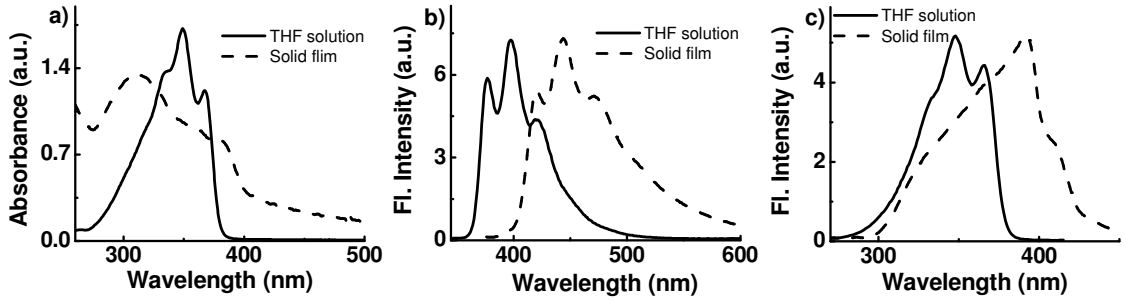

Figure 3.13. Optical spectra of **C10GB** in THF solution and in the solid film obtained by cooling the smectic C* phase between quartz plates: (a) UV–vis absorption spectra, (b) fluorescence emission spectra (λ_{ex} was 330 nm for solution and 360 nm for film) and (c) fluorescence excitation spectra (λ_{em} was 420 nm for solution and 475 nm for film). All spectra were recorded at room temperature.

The absorption spectrum of **C10GB** in THF solution exhibited a structured narrow band characteristic of solvated molecules, with a maximum at 349 nm. In the solid state the absorption was much broader indicating aggregation of the chromophore. The higher baseline in the spectrum of the solid sample can be attributed to increased light scattering in the solid samples. The changes in the absorption spectra brought about by interaction of chromophores in their ground state has been explained by McRae and Kasha[51] in terms of exciton coupling

theory, in which the excited state of aggregates splits into two energy levels (Davydov splitting). The transition to the upper state is allowed in the case of H-type aggregates, characterized by a hypsochromically shifted absorption band and that to the lower state for J-type aggregates marked by a bathochromically shifted absorption band compared to the isolated monomer. The presence of two additional bands in the spectrum of the solid film (Figure 3.13a), bands that are blue- (312 nm) and red-shifted (381 nm) compared to that of the monomer peak indicates the presence of both H- and J-type aggregates.

Figure 3.13b shows the fluorescence emission spectrum of **C10GB** in THF and in the solid films obtained by cooling the smectic C* phase. The fluorescence quantum yield of **C10GB** in THF solution was estimated as 0.2 and the emission spectrum was relatively narrow with a major peak at 398 nm and minor peaks at 377 and 420 nm. The spectrum was nearly a mirror image of the ground state absorption indicating that the ground and excited state geometry were relatively similar. In contrast, the fluorescence spectrum of the solid film was much broader and clearly red-shifted. Figure 3.13c shows the excitation spectrum of **C10GB** in solution and in the solid film. The main peak in the excitation spectrum of the solid film was significantly red-shifted to 392 nm, which is close to the red-shifted band maximum at 381 nm observed in its absorption spectrum. The red-shift in the emission and excitation spectra is suggestive of a J-type emission from the aggregated species. A shoulder in the 350 nm region in the excitation spectrum of

the solid film indicates that some emission also arises from the monomer. The H-aggregated species is known to be non-fluorescent.[52]

Figure 3.14 shows the circular dichroism spectra of a solid film of **C10GB**, which shows a strong negative peak at 395 nm, which is again close to the red-shifted absorption and excitation peaks observed in the film state. The CD activity of the band attributable to the butadiene moiety is clearly indicative of the chiral ordering of the chromophore transition moment. The fact that the solution state spectra (molecularly dissolved state in DMSO and THF) was CD silent and the thin films show strong CD signals indicate that the CD spectra of the film do not arise from chirality in the monomeric species, but from intermolecular dipole-dipole interactions in the aggregated species existing in a macroscopic chiral environment. Similar results were obtained for all the other derivatives.

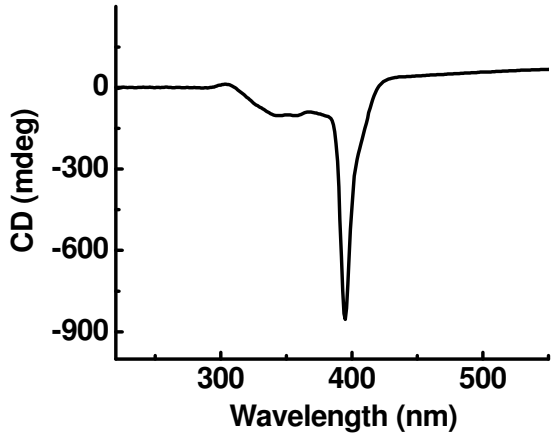

Figure 3.14. Circular Dichroism spectra of **C10GB** in the solid film obtained by cooling its smectic C* phase between quartz plates. Spectra were recorded at room temperature.

The fluorescence lifetime (τ) decay profile of **C10GB** is shown in Figure 3.15. In general, the **CnGB** bolas showed slightly longer fluorescence life-times in THF solutions (~0.6 ns) when compared to that in DMSO (~0.4 ns).

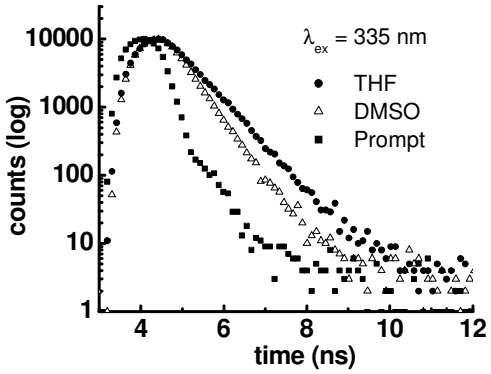

Figure 3.15. Fluorescence decay profiles of **C10GB** in THF and DMSO solutions. Excitation source (LED): 335 nm. Emission collected at 398 nm for THF solution and 404 nm for solution in DMSO.

The powder form of **DBC1** on excitation at 365 nm emitted light in the blue region (Figure 3.16a). The main peak in the excitation spectra at 395 nm was accompanied by another peak at 419 nm (Figure 3.16b). The thin film formed on condensing the sublimed vapor showed the same blue emission as the powder.

The absorption and emission maxima (λ_{max}), fluorescence quantum yields (ϕ_f) and fluorescence lifetime (τ) data of **DBC1** and the **CnGB** derivatives in molecularly dissolved solutions are shown in Table 3.3.

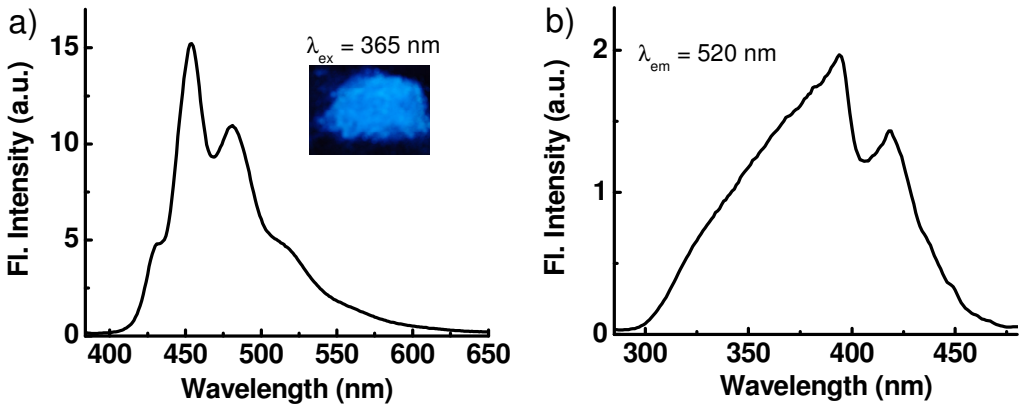

Figure 3.16. Fluorescence (a) emission and (b) excitation spectra of **DBC1** in powder form. Inset in (a) shows the emission of **DBC1** powder on shining a 365 nm UV lamp. Spectra were recorded at room temperature.

Table 3.3. UV-vis absorption, fluorescence emission λ_{max}, ϕ_f and τ values of **DBC1** and **CnGB** compounds in solution state

Sample code	Solvent	Absorption λ_{max} (nm)	Emission λ_{max} (nm)	ϕ_f	τ (ns) λ_{ex} = 335 nm
	DCM	334, **347**, 365	379, **398**, 419	0.139	
DBC1	MeCN	330, **343**, 361	375, **394**, 417	0.08	
	DMSO	337, **351**, 370	382, **403**, 422	0.09	
	THF	335, **347**, 365	375, **395**, 418	0.26	
C2GB	DMSO	339, **353**, 371	384, **405**, 427	0.1	0.42
	THF	335, **349**, 368	377, **398**, 420		
C3GB	DMSO	339, **353**, 371	384, **405**, 427	0.1	0.43
	THF	335, **349**, 368	377, **398**, 420		
C4GB	DMSO	339, **353**, 371	384, **405**, 427	0.13	0.43
	THF	335, **349**, 368	377, **398**, 420	0.23	0.60
C5GB	DMSO	339, **353**, 371	384, **405**, 427	0.16	0.43
	THF	335, **349**, 368	377, **398**, 420	0.24	0.62
C7GB	DMSO	339, **353**, 371	384, **405**, 427	0.15	0.42
	THF	335, **349**, 368	377, **398**, 420	0.21	0.62
C8GB	DMSO	339, **353**, 371	384, **405**, 427	0.11	0.43
	THF	335, **349**, 368	377, **398**, 420	0.21	0.62
C10GB	DMSO	339, **353**, 371	384, **405**, 427	0.09	0.42
	THF	335, **349**, 368	377, **398**, 420	0.24	0.61
C12GB	DMSO	339, **353**, 371	384, **405**, 427	0.1	0.41
	THF	335, **349**, 368	377, **398**, 420	0.21	0.60

3.3. Discussion

Transfer of chirality from the molecular level to the liquid crystal phase is a complex phenomenon, which is not well understood.[14] Most studies on understanding the mechanism by which the chirality of the molecule is mapped onto the liquid crystalline phase, deal with the mode of transfer of chirality from the chiral center of the molecule to the rest of the molecule (intramolecular transfer) and the subsequent transfer of chirality to the liquid crystalline phase (intermolecular transfer).[53] Several recent studies have addressed these issues for both host-guest systems and in chiral molecules exhibiting liquid crystalline phases.[10,14-18] The butadiene cored sugar bolaamphiphiles investigated in the present study however, provide a unique example of liquid crystals in which the self-interaction of a non-chiral core enables transfer of chiral information in the sugar moieties to the liquid crystalline phase.

The absence of macroscopic chirality in most of the sugar-based liquid crystals has largely been attributed to strong hydrogen bonding networks, which give rise to rigidly packed double layers resulting mostly in the formation of smectic phases. In earlier studies, expression of macroscopic chirality in sugar-based liquid crystals were achieved only by suppression of its amphiphillic character, i.e., by suitable derivatization of the sugar head groups. In the present study, POM, XRD and electro-optic switching experiments clearly confirm the formation of the smectic C* phase in the butadiene cored sugar bolaamphiphiles.

In our earlier study on azobenzene cored sugar bolaamphiphiles[22] the chiral smectic C phase was observed only in the derivatives wherein the azobenzene core was separated from the sugar head groups by greater than five methylene groups. In the present study, evidence for the smectic C* phase was observed even in the lowest homologue studied where the sugar head groups are separated from the butadiene core by only two methylene units, albeit in the cooling phase. This suggests that the butadiene core is capable of inducing macroscopic chirality more effectively than azobenzene. Earlier studies in our group[26-29] have also shown that the tendency of the diphenylbutadiene chromophore to form aggregates is much higher than that of the azobenzene chromophore. Evidence for the formation of J-type aggregates in the butadiene-cored bolaamphiphiles was obtained from the absorption and emission spectra. Figure 3.17 shows the proposed arrangement of the molecules.

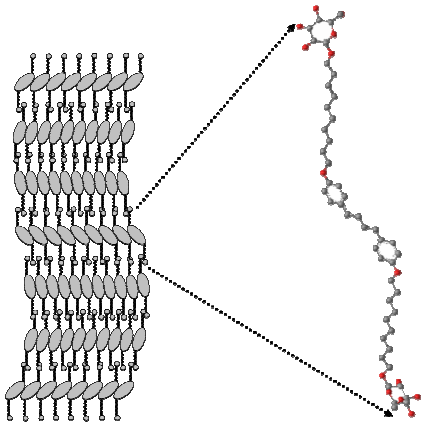

Figure 3.17. Schematic representation of the molecular layers in the smectic C* phase shown along with the minimum energy conformation of **C10GB**.

The slipped-stack organization of J-type aggregates could result in an arrangement of the molecules as depicted in Figure 3.17, which could favor formation of the smectic C* phase.

In the lower homologues the sugar character dominates resulting predominantly in the formation of an LC phase which does not possess macroscopic chirality, namely the smectic A* phase. With increasing length of the oligomethylene spacers, the butadiene core is able to self-organize more effectively and as a result induces macroscopic chirality more efficiently. It may be argued that the effect of the butadiene core would be to reduce the microphase segregation in the bolaamphiphiles. The presence of the higher order peaks in the XRD pattern however contradicts this, as it indicates that the microphase segregation in this class of molecules is more pronounced especially in the higher homologues, with the additional self-assembling property of the butadiene chromophore resulting in a better definition of the layered structure of the smectic C* phase. Thus the mechanism of chirality transfer in this class of molecules could initially involve transfer of chiral information from the sugar moiety intramolecularly to the butadiene core, which can subsequently transfer this information into the macroscopic domain via intermolecular interactions with the core units of other molecules. The CD activity of the butadiene absorption band in thin solid films in which the smectic C* arrangement is retained is clearly indicative of a chiral arrangement of the butadiene chromophore.

3.4. Experimental Section

3.4.1. Synthesis

Solvents were dried and distilled according to literature procedures.[54] All chemicals were purchased from commercial sources and were used without further purifications. Silica gel (230–400 mesh) was used for column chromatography and TLC analysis was performed on commercial plates coated with silica gel 60 F_{254}. High-resolution mass spectra were obtained from Q-TOF instrument by electro spray ionization (ESI). ^{1}H and ^{13}C NMR spectral analyses were performed on a spectrometer operating at 300 MHz, 400 MHz, 500 MHz and 75 MHz, 100 MHz, 125 MHz, respectively. The coupling constants (*J*) of ~15 Hz for the vinylic protons in ^{1}H NMR spectra of all diphenylbutadiene derivatives confirmed their *E* stereochemistry.[26] Microanalyses were performed on an automated C, H and N analyzer.

3.4.2. Single Crystal X-ray analysis

Single crystal XRD analyses were carried out on a Siemens SMART-1K CCD diffractometer using graphite monochromated Mo K_α radiation (λ = 0.71073 Å). For crystal packing visualization, the Crystallographic Information File (CIF) was opened using the Mercury 1.4.1 (http://www.ccdc.cam.ac.uk/mercury) software. For detailed crystal data and structure refinement see the Annexure.

3.4.3. Synthesis Procedures and Characterization data

4-Methoxybenzyl alcohol (**1**): 4-Methoxy benzaldehyde (1 equiv) dissolved in methanol was cooled to 0 °C and kept stirring. Sodium borohydride (5 equiv) was added slowly and continued stirring for 20 min. Excess sodium borohydride was quenched by adding water and the product was extracted using dichloromethane, dried (Na_2SO_4) and concentrated.

Yield: 91%. mp 22–25 °C.[55] IR ν_{max} (smear on NaCl): 1248, 1510, 2401, 3367. ^{1}H NMR ($CDCl_3$, 300 MHz) δ (ppm): 3.7 (s, 3H, –OC$\underline{H_3}$), 4.47 (s, 2H, ArC$\underline{H_2}$), 6.78 (d, J = 6.8 Hz, 2H, Ar), 7.17 (d, J = 7.2 Hz, 2H, Ar).

4-Methoxybenzyl bromide (**2**): 4-Methoxybenzyl alcohol (1 equiv) was dissolved in dry dichloromethane and kept stirring. The solution was cooled to 0 °C and PBr_3 (1/3 equiv) solution in dichloromethane was added slowly and the mixture was stirred for 20 min. A saturated solution of sodium bicarbonate was added to quench the excess PBr_3. The organic layer was extracted with dichloromethane, dried (Na_2SO_4), concentrated and immediately converted to the phosphonate ester as described below.

Diethyl-4-methoxybenzylphosphonate (**3**): **2** (1 equiv) and triethyl phosphite (1.5 equiv) were heated at 100 °C for 12 h and the excess triethyl phosphite was distilled out under reduced pressure or removed by purging air. The residue was purified by column chromatography through silica gel (100–200 mesh) using 50 % ethyl acetate/hexane as the mobile phase.

Yield: 92%. IR ν_{max} (KBr): 837, 750, 964 and 1058 (P–O–C)[56,57], 3018, 3684 cm^{-1}; ^1H NMR ($CDCl_3$, 300 MHz) δ (ppm): 1.23 (t, 6H, –$OCH_2C\underline{H_3}$), 3.04–3.11 (d, *J* = 21 Hz, 2H, Ar–$C\underline{H_2}$–P–), 4.0 (q, 4H, –$OC\underline{H_2}CH_3$), 6.83 (d, *J* = 8.7 Hz, 2H, Ar), 7.2 (d, *J* = 8.4 Hz, 2H, Ar). ^{13}C NMR ($CDCl_3$, 75 MHz) δ (ppm): 16.2, 32.0, 34.0, 53.6, 62, 121.6, 128.4, 130.0, 150.0. FAB+ Mass (*m/z*) calcd for $C_{12}H_{19}O_4P$: 258.25; found 259.29.

4,4'-Dimethoxydiphenylbuta-1*E*,3*E*-diene (**DBC1**): A mixture of Diethyl-4-methoxybenzylphosphonate (1 equiv) and Potassium *tert*-butoxide (6 equiv) was stirred in dry DMF at room temperature and cooled to 0 °C. 4-Methoxycinnamaldehyde (1 equiv) dissolved in dry DMF was slowly added into the solution. The reaction mixture was stirred for 12 h, cooled to room temperature, poured into ice water, extracted with $CHCl_3$, dried (Na_2SO_4) and concentrated under reduced pressure. The residue was washed with ethyl acetate and filtered. **DBC1** being insoluble in ethyl acetate remained in the residue. This was repeatedly washed with ethyl acetate (small quantities) to obtain pure **DBC1**. The small amount of **DBC1** which remained in the filtrate was recovered by column chromatography through silica gel (100–200 mesh), using 5–10% ethyl acetate/hexane as the mobile phase.

Yield: 73%. mp < 250 °C (sublimes). FT-IR ν_{max} (KBr): 959 (wagging vib mode of *trans* C=C)[58], 1219, 1601 (C=C asym str), 3013 cm^{-1}; H NMR ($CDCl_3$, 300 MHz) δ (ppm): 3.82 (s, 6H, –$OC\underline{H_3}$), 6.57 (d, *J* = 14.8 Hz, 2H, *trans* C=C), 6.78–6.88

(m, 6H, Ar, C=C), 7.37 (d, *J* = 8.7 Hz, 4H, Ar). ^{13}C NMR ($CDCl_3$, 75 MHz), δ (ppm): 53.6, 94.5, 108.7, 112.7, 126.0, 129.8. FAB+ Mass (*m/z*) calcd for $C_{18}H_{18}O_2$: 266.33; found 266.07.

4,4'-Dihydroxydiphenylbuta-1*E*,3*E*-diene (**DBCOH**): A mixture of **DBC1** (1 equiv) and KOH (~27 equiv) in triethyleneglycol (10 mL) was treated at 210 °C for 12 h in inert atmosphere.[30] The reaction mixture was then poured in to ice water and neutralized using 6N HCl. The precipitated product was filtered and purified by column chromatography over silica gel (100–200 mesh), using 40% ethyl acetate/hexane as the mobile phase. Yield: 89%. mp 304–305 °C. FT-IR ν_{max} (KBr): 1253, 1601, 3015, 3415 cm^{-1}; ^{1}H NMR (DMSO-d_6, 300MHz) δ (ppm): 6.51–6.56 (d, *J* = 14.2 Hz, 2H, *trans* C=C) 6.71–6.74 (d, *J* = 8.4 Hz, 4H, Ar), 6.78–6.83 (d, *J* = 14.7 Hz, 2H, *trans* C=C), 7.28–7.31 (d, *J* = 8.4 Hz, 4H, Ar), 9.55 (s, 2H, –O<u>H</u>); ^{13}C NMR (DMSO-d_6, 75 MHz), δ (ppm): 115.5, 126.6, 127.4, 128.4, 131.0, 157.0. FAB+ Mass (*m/z*) calcd for $C_{16}H_{14}O_2$: 238.28; found 238.44.

General procedure for CnGB bolaamphiphiles: To a solution of ω-bromoalkyl-2,3,4,6-tetra-O-acetyl-D-glucopyranoside (2.2 equiv) and 4,4'-Dihydroxydiphenylbuta-1*E*,3*E*-diene (1 equiv) in MeCN (20 mL), K_2CO_3 (6 equiv) and 18-C-6 (cat) were added and the reaction mixture refluxed for 48 h. The reaction mixture was filtered, the filtrate was evaporated *in vacuuo* and the resulting residue in MeOH (10 mL) was admixed with NaOMe (2 mL) and stirred for 12 h. The solution was neutralized with aqueous acetic acid, filtered, washed

with water, MeOH and $CHCl_3$ and recrystallized from MeOH-$CHCl_3$ (1:1, v/v) to afford the bolaamphiphiles, as light yellow solids.

[(1*E*,3*E*)-1,3-Butadiene-1,4-diyl]bis(4,1-phenyleneoxy-2,1-ethanediyl)bis-β-D-glucopyranoside (**C2GB**): Yield: 53%. ^{1}H NMR (300 MHz, DMSO-d_6) δ (ppm): 7.42 (d, 4 H, *J* = 8.4 Hz), 6.93-6.87 (m, 6 H), 6.63 (d, 2 H, *J* = 14.7 Hz), 5.06 (d, 2 H, *J* = 5.2 Hz), 4.96 (m, 4 H), 4.53 (t, 2 H, *J* = 5.4 Hz), 4.23 (d, 2 H, *J* = 7.8 Hz), 4.06 (br s, 4 H), 3.88-3.43 (m, 12 H). ^{13}C NMR (75 MHz, DMSO-d_6) δ (ppm): 158.0, 131.2, 130.0, 127.6, 114.8, 103.1, 77.0, 76.8, 73.4, 67.3, 67.1, 61.1. ESI-MS: *m/z* calcd for $C_{32}H_{42}O_{14}Na$: 673.2472; found: 673.2450. Elemental analysis: calcd for $C_{32}H_{42}O_{14}$: C 59.07, H 6.51; found: C 59.33, H 6.71.

[(1*E*,3*E*)-1,3-Butadiene-1,4-diyl]bis(4,1-phenyleneoxy-3,1-propanediyl)bis-β-D-glucopyranoside (**C3GB**): Yield: 48%. ^{1}H NMR (300 MHz, DMSO-d_6) δ (ppm): 7.41 (d, 4 H, *J* = 8.4 Hz), 6.92-6.86 (m, 6 H), 6.63 (d, 2 H, *J* = 14.4 Hz), 5.03 (br, 6 H), 4.50 (br, 2 H), 4.14 (d, 2 H, *J* = 7.5 Hz), 4.07 (t, 4 H, *J* = 6.3 Hz), 3.88 – 3.43 (m, 12 H), 1.96 (m, 4 H). ^{13}C NMR (75 MHz, DMSO-d_6) δ (ppm): 158.1, 131.2, 129.9, 127.5, 114.8, 103.0, 76.9, 76.7, 73.5, 70.1, 65.4, 64.7, 61.1, 29.2. ESI-MS: *m/z* calcd for $C_{34}H_{46}O_{14}Na$: 701.2785; found: 701.2781. Elemental analysis: calcd for $C_{34}H_{46}O_{14}$: C 60.17, H 6.83; found: C 60.04, H 7.09.

[(1*E*,3*E*)-1,3-Butadiene-1,4-diyl]bis(4,1-phenyleneoxy-4,1-butanediyl)bis-β-D-glucopyranoside (**C4GB**): Yield: 39%. ^{1}H NMR (400 MHz, DMSO-d_6) δ (ppm): 7.39 (d, 4 H, *J* = 8.5 Hz), 6.88-6.81 (m, 6 H), 6.60 (d, 2 H, *J* = 14.33 Hz), 5.11 (d,

2 H, *J* = 5.2 Hz), 5.03 (m, 4 H) 4.68 (t, 2 H, *J* = 5.6 Hz), 4.13 (d, 2 H, *J* = 7.8 Hz), 3.95 (t, 4 H, *J* = 5.6 Hz,), 3.88 3.50 (m, 12 H), 1.72-1.63 (m, 8 H). ^{13}C NMR (100 MHz, DMSO-d_6) δ (ppm): 158.5, 131.5, 130.2, 127.9, 115.1, 103.0, 77.0, 76.9, 73.8, 70.5, 68.7, 67.7, 61.4. 26.1, 25.7. ESI-MS: *m/z* calcd for $C_{36}H_{50}O_{14}Na$: 729.3098; found: 729.3096. Elemental Analysis: calcd. for $C_{36}H_{50}O_{14}$: C 61.18, H 7.13; found: C 61.24, H 7.25.

[(1*E*,3*E*)-1,3-Butadiene-1,4-diyl]bis(4,1-phenyleneoxy-5,1-pentanediyl)bis-β-D-glucopyranoside (**C5GB**): Yield: 53%. ^{1}H NMR (300 MHz, DMSO-d_6) δ (ppm): 7.40 (d, 4 H, *J* = 8.4 Hz), 6.90-6.83 (m, 6 H), 6.62 (d, 2 H, *J* = 15.3 Hz), 4.97 (d, 2 H, *J* = 5.0), 4.90 (b, 4 H), 4.48 (t, 2 H, *J* = 5.3 Hz), 4.11 (d, 2 H, *J* = 7.8 Hz), 3.97 (t, 4 H, *J* = 5.3 Hz), 3.79-3.50 (m, 12 H), 1.70 – 1.46 (m, 12 H). ^{13}C NMR (75 MHz, DMSO-d_6) δ (ppm): 158.3, 131.3, 129.9, 127.6, 114.8, 102.9, 76.9, 73.6, 70.2, 68.6, 67.5, 61.2, 29.1, 28.6. ESI–MS: *m/z* calcd for $C_{38}H_{54}O_{14}Na$: 757.3411; found: 757.3471. Elemental analysis: calcd for $C_{38}H_{54}O_{14}$: C 62.11; H 7.41; found C 61.90, H 7.67.

[(1*E*,3*E*)-1,3-Butadiene-1,4-diyl]bis(4,1-phenyleneoxy-7,1-heptanediyl)bis-β-D-glucopyranoside (**C7GB**)**:** Yield: 37%. ^{1}H NMR (300 MHz, DMSO-d_6) δ (ppm): 7.40 (d, 4 H, *J* = 9.0 Hz), 6.89-6.85 (m, 6 H), 6.61 (d, 2 H, *J* = 14.7 Hz), 4.97 (d, 2 H, *J* = 5.5 Hz), 4.91 (m, 4 H), 4.50 (t, 2 H, *J* = 5.8 Hz), 4.09 (d, 2 H, *J* = 7.8 Hz), 3.94 (t, 4 H, *J* = 5.8 Hz), 3.78-3.50 (m, 12 H), 1.72 – 1.31 (m, 20 H). ^{13}C NMR (75 MHz, DMSO-d_6) δ (ppm): 158.4, 131.3, 129.9, 127.6, 114.8, 102.9,

76.8, 73.6, 70.2, 68.6, 67.5, 61.2, 29.1, 28.6. ESI–MS: *m/z* calcd for $C_{42}H_{62}O_{14}Na$: 813.4037; found: 813.3974. Elemental analysis: calcd for $C_{42}H_{62}O_{14}.2H_2O$: C 61.00, H 8.04; found: C 61.14, H 7.71.

[(1*E*,3*E*)-1,3-Butadiene-1,4-diyl]bis(4,1-phenyleneoxy-8,1-octanediyl)bis-β-D-glucopyranoside (**C8GB**): Yield: 63%. ^{1}H NMR (400 MHz, DMSO-d_6) δ (ppm): 7.41 (d, 4 H, *J* = 8.8 Hz), 6.91-6.87 (m, 6 H), 6.63 (d, 2 H, *J* = 14.7 Hz), 4.95 (b, 6 H), 4.52 (t, 2 H, *J* = 5.8 Hz), 4.10 (d, 2 H, *J* = 7.8 Hz), 3.96 (t, 4 H, *J* = 5.8 Hz), 3.78-3.40 (m, 12 H), 1.70–1.31 (m, 24 H). ^{13}C NMR (100 MHz, DMSO-d_6) δ (ppm): 158.7, 131.6, 130.2, 127.9, 115.0, 103.3, 77.2, 73.9, 70.2, 69.0, 67.9, 61.6, 29.7, 29.3, 29.2, 29.1, 26.1, 25.9. ESI–MS: *m/z* calcd for $C_{44}H_{66}O_{14}Na$: 841.4350; found: 841.4296. Elemental analysis: calcd for $C_{44}H_{66}O_{14}.5H_2O$: C 58.14; H 8.42; found: C 58.49; H 8.22.

[(1*E*,3*E*)-1,3-Butadiene-1,4-diyl]bis(4,1-phenyleneoxy-10,1-decanediyl)bis-β-D-glucopyranoside (**C10GB**): Yield: 61%. ^{1}H NMR (300 MHz, DMSO-d_6) δ (ppm): 7.40 (d, 4 H, *J* = 8.4 Hz), 6.89-6.83 (m, 6 H), 6.61 (d, 2 H, *J* = 14.4 Hz), 4.90 (m, 6 H), 4.45 (t, 2 H, *J* = 5.8 Hz), 4.10 (d, 2 H, *J* = 7.5 Hz), 3.94 (t, 4 H, *J* = 5.8 Hz), 3.78-3.50 (m, 12 H), 1.68-1.26 (m, 32 H). ^{13}C NMR (75 MHz, DMSO-d_6) δ (ppm): 158.2, 131.1, 129.8, 127.4, 114.7, 102.8, 76.8, 73.4, 70.1, 68.6, 67.5, 61.1, 29.3, 29.0, 28.9, 28.8, 28.7, 25.5. ESI–MS: *m/z* calcd for $C_{48}H_{74}O_{14}Na$: 897.4976; found: 897.5210. Elemental analysis: calcd for $C_{48}H_{74}O_{14}.3H_2O$ C: 62.05; H: 8.67; found: C: 62.47; H: 8.25.

[(1*E*,3*E*)-1,3-Butadiene-1,4-diyl]bis(4,1-phenyleneoxy-12,1-dodecanediyl)bis-β-D-glucopyranoside (**C12GB**): Yield: 63%. ^{1}H NMR (300 MHz, DMSO-d_6) δ (ppm): 7.40 (d, 4 H, *J* = 8.4 Hz), 6.89-6.83 (m, 6 H), 6.61 (d, 2 H, *J* = 15.3 Hz), 4.90 (m, 6 H), 4.44 (t, 2 H, *J* = 6.0 Hz), 4.09 (d, 2 H, *J* = 7.8 Hz), 3.94 (t, 4 H, *J* = 6.0 Hz), 3.75-3.40 (m, 12 H), 1.68-1.24 (m, 40 H). ^{13}C NMR (75 MHz, DMSO-d_6) δ (ppm): 158.2, 131.1, 129.8, 127.4, 114.7, 102.8, 76.8, 73.4, 70.1, 68.6, 67.5, 61.1, 29.3, 29.0, 28.8, 28.7, 25.5. ESI–MS: *m/z* calcd for $C_{52}H_{82}O_{14}Na$: m/z 953.5602; found: 953.5948. Elemental analysis: calcd for $C_{52}H_{82}O_{14}.2H_2O$ C: 64.57; H: 8.96; found: C: 64.99; H: 8.49.

3.4.4. Liquid crystalline and optical studies

Phase transitions were observed using a Leitz DMRXP polarized light optical microscope with crossed polarizer configuration, equipped with a Mettler FP82HT heating and freezing stage connected to a Mettler FP90 temperature programmer. The POM textures were observed on untreated glass or quartz slides. The characteristic chiral textures could be observed even in preparations without a cover slide and on sodium chloride disks. Differential scanning calorimetry was performed using a Perkin-Elmer Pyris 6 DSC instrument in sealed aluminum pans under nitrogen flow at a rate of 5 °C/min. Thermo gravimetric analysis was carried out on a Shimadzu DTG-60 apparatus under nitrogen flow at a rate of 10 °C/min. The residues were analyzed using a mass spectrometer in FAB+ ionization mode using 1-Thioglycerol as matrix. FT-IR analysis of the heat, cooled **CnGB**

compounds were done in a Shimadzu Prestige-21 spectrophotometer using KBr. X-Ray diffraction studies were carried out on samples contained in Lindemann capillaries with Cu K_α radiation (λ = 1.5418 Å). The sample capillaries were held at required temperatures using a Mettler hot stage. To determine the structural parameters, one-dimensional intensity vs. the diffraction angle (I–2θ) profiles were extracted from the two-dimensional diffraction pattern and the peak analysis carried out by fitting the data to a sum of Lorentzian expressions while floating the three-parameter (peak position, peak intensity and the full-width-at-half-maximum) set for each peak in the profile. Electro-optic measurements were carried out in cells of ~8 μm thickness with substrates treated for planar alignment of the sample. An AC electric field having frequency of 100 mHz was used for electro-optic switching. UV-vis spectra were recorded on a Shimadzu UV-2401 PC UV-vis scanning double-beam spectrophotometer. Fluorescence excitation and emission spectra in solution and solid state were recorded on a SPEX Fluorolog-2 spectrofluorometer. Relative fluorescence quantum yields (ϕ_f), were determined by comparison with anthracene (purified by sublimation) in ethanol (ϕ_f = 0.27), which was used as the fluorescence standard. The fluorescence life times were measured by time-correlated single photon counting, TCSPC (IBH, UK). The solutions were excited at a wavelength of λ_{ex} = 335 nm using a NanoLED source having 1 MHz repetition rate and fitted in the single exponential mode using DAS6 fluorescence decay analysis software. The χ^2 values of the fit result were in the 0.99–1.04 range.

Ultrasonication of solutions was carried out in a Julabo USR 3 bath sonicator. Measurements of solid state fluorescence were carried out using the front face emission scan mode. CD spectral measurements were carried out in Jasco J-810 spectropolarimeter. Contribution from linear dichroism (LD) was negligible as turning of the sample had no effect on the type of spectra observed.

3.5. Conclusion

The present study on the liquid crystalline properties of symmetrical bolaamphiphiles possessing a diphenylbutadiene core and glucopyranoside head groups linked together by oligomethylene spacers using POM and XRD clearly indicate the manifestation of smectic C* phases in this class of molecules. It is generally known in the literature that sugar-based amphiphiles and bolaamphiphiles do not exhibit macroscopic chirality and this has been attributed to strong intermolecular hydrogen bonding resulting in highly microphase segregated lamellar structures. Liquid crystalline phase transition behavior and comparison of the spectroscopic properties of solutions and thin films of the bolaamphiphiles investigated in the present study clearly indicate that the manifestation of macroscopic chirality in their LC phase may be attributed to the self-aggregating behavior of the diphenybutadiene core, in agreement with our earlier report on azobenzene cored sugar bolaamphiphiles described in Chapter 2.

References

(1) Demus, D., Goodby, J. W., Gray, G. W., Spiess, H.-W., Vill, V., Eds. *Handbook of Liquid Crystals*; Wiley-VCH: Weinheim, 1998; Vol. 1,2A,2B.

(2) Chandrasekhar, S. In *Liquid Crystals*; 2nd Ed., Cambridge University Press: Cambridge, 1992.

(3) Kato, T. *Science (Washington, DC, U. S.)* **2002**, *295*, 2414–2418.

(4) Pauluth, D.; Tarumi, K. *J. Mater. Chem.* **2004**, *14*, 1219–1227.

(5) Finkelmann, H.; Meier, W.; Scheuermann, H. in *Liquid Crystals: Applications and Uses*, Vol. 3 (B. Bahadur Ed.), World Scientific: Singapore, 1994, Ch. 22.

(6) Imrie, C. T.; Henderson, P. A.; Seddon, J. M. *J. Mater. Chem.* **2004**, *14*, 2486–2488.

(7) Tamaoki, N. *Adv. Mater. (Weinheim, Ger.)* **2001**, *13*, 1135–1147.

(8) Walba, D. M.; Eshdat, L.; Korblova, E.; Shao, R.; Clark, N. A. *Angew. Chem., Int. Ed.* **2007**, *46*, 1473–1475 and references therein.

(9) Clark, N. A.; Lagerwall, S. T. *Appl. Phys. Lett.* **1980**, *36*, 899–901.

(10) McCubbin, J. A.; Tong, X.; Wang, R.; Zhao, Y.; Snieckus, V.; Lemieux, R. P. *J. Am. Chem. Soc.* **2004**, *126*, 1161–1167.

(11) Lagerwall, J. P. F.; Giesselmann, F. *ChemPhysChem* **2006**, *7*, 20–45.

(12) Walba, D. M.; Xiao, L.; Keller, P.; Shao, R.; Link, D.; Clark, N. A. *Pure Appl. Chem.* **1999**, *71*, 2117–2123.

(13) Ikeda, T.; Kanazawa, A. In *Molecular Switches*; Feringa, B. L., Ed.; Wiley-VCH: Weinheim, 2001; pp. 363–397.

(14) Kitzerow, H.-S.; Bahr, C., Eds., *Chirality in Liquid Crystals*, Springer: New York, 2001.

(15) di Matteo, A.; Todd, S. M.; Gottarelli, G.; Solladié, G.; Williams, V. E.; Lemieux, R. P.; Ferrarini, A.; Spada, G. P. *J. Am. Chem. Soc.* **2001**, *123*, 7842–7851.

(16) Eelkema, R.; Pollard, M. M.; Katsonis, N.; Vicario, J.; Broer, D. J.; Feringa, B. L. *J. Am. Chem. Soc.* **2006**, *128*, 14397–14407.

(17) Kato, T.; Matsuoka, T.; Nishii, M.; Kamikawa, Y.; Kanie, K.; Nishimura, T.; Yashima, E.; Ujiie, S. *Angew. Chem., Int. Ed.* **2004**, *43*, 1969–1972.

(18) Solladié, G.; Hugelé, P.; Bartsch, R. *J. Org. Chem.* **1998**, *63*, 3895–3898.

(19) Vill, V.; Hashim, R. *Curr. Opin. Colloid Interface Sci.* **2002**, *7*, 395–409.

(20) van Doren, H. A.; Smits, E.; Pestman, J. M.; Engberts, J. B. F. N.; Kellogg, R. M. *Chem. Soc. Rev.* **2000**, *29*, 183–199.

(21) Masuda, M.; Vill, V.; Shimizu, T. *J. Am. Chem. Soc.* **2000**, *122*, 12327–12333.

(22) Abraham, S.; Paul, S.; Narayan, G.; Prasad, S. K.; Rao, D. S. S.; Jayaraman, N.; Das, S. *Adv. Funct. Mater.* **2005**, *15*, 1579–1584 and references therein.

(23) Caculitan, N. G.; Scudder, P. H.; Rodriguez, A.; Casson, J. L.; Wang, H.-L.; Robinson, J. M.; Johal, M. S. *Langmuir* **2004**, *20*, 8735–8739.

(24) Dante, S.; Advincula, R.; Frank, C. W.; Stroeve, P. *Langmuir* **1999**, *15*, 193–201.

(25) Nithyanandhan, J.; Jayaraman, N.; Davis, R.; Das, S. *Chem. –Eur. J.* **2004**, *10*, 689–698.

(26) Davis, R.; Mallia, V. A.; Das, S. *Chem. Mater.* **2003**, *15*, 1057–1063 and references therein.

(27) Davis, R.; Rath, N. P.; Das, S. *Chem. Commun. (Cambridge, U. K.)* **2004**, 74–75.

(28) Davis, R.; Abraham, S.; Rath, N. P.; Das, S. *New J. Chem.* **2004**, *28*, 1368–1372.

(29) Abraham, S.; Mallia, V. A.; Ratheesh, K. V.; Tamaoki, N.; Das, S. *J. Am. Chem. Soc.* **2006**, *128*, 7692–7698.

(30) Wang, S. J.; Tjong, S. C.; Meng, Y. Z.; Fung, M. K.; Lee, S. T.; Hay, A. S. *J. Appl. Polym. Sci.* **2003**, *89*, 1645–1651.

(31) Takano, T.; Nakatsubo, F.; Murakami, K. *Carbohydr. Res*. **1990**, *203*, 341–342.

(32) Mates, T. E.; Ober, C. K. *J. Polym. Sci., A* **1992**, *30*, 2541–2547.

(33) Rotarski, Th. *Chem. Ber.* **1908**, *41*, 1994–1998.

(34) Brettle, R.; Dunmur, D. A.; Hindley, N. J.; Marson, C. M. *J. Chem. Soc., Perkin Trans. 1* **1993**, 775–781.

(35) Gray, G. W.; Goodby, J. W. *Smectic liquid crystals: Textures and structures*; Leonard Hill: Glasgow, 1984.

(36) Dierking, I. *Textures of liquid crystals*; Wiley-VCH: Weinheim, 2003.

(37) Sherwood, J. N., Ed. *The plastically crystalline state: Orientationally-disordered crystals*; John Wiley & Sons: Chichester, 1979.

(38) Prasad, S. K.; Rao, D. S. S.; Chandrasekhar, S.; Kumar, S. *Mol. Cryst. Liq. Cryst.* **2003**, *396*, 121–139 and references therein.

(39) Bayer, A.; Zimmermann, S.; Wendorff, J. H. *Mol. Cryst. Liq. Cryst.***2003**, *396*, 1–22.

(40) Als-Nielsen, J.; Birgeneau, R. J.; Kaplan, M.; Litster, J. D.; Safinya, C. R. *Phys. Rev. Lett.* **1977**, *39*, 1668–1671.

(41) Cladis, P. E.; Stamatoff, J.; Guillon, D.; Cross, M. C.; Bilash, T.; Finn, P. In *Advances in Liquid Crystal Research and Applications*, Bata, L., Ed., Pergamon: Oxford, 1981.

(42) Ocko, B. M.; Kortan, A. R.; Birgeneau, R. J.; Goodby, J. W. *J. Phys. (Paris)* **1984**, *45*, 113.

(43) Seddon, J. M. In *Handbook of Liquid Crystals: Fundamentals* Demus, D., Goodby, J. W., Gray, G. W., Spiess, H.-W., Vill, V., Eds.; Wiley-VCH: Weinheim, 1998, Vol. 1; pp. 635–679.

(44) Lobo, C. V.; Prasad, S. K.; Rao, D. S. S. *Phys. Rev. E: Stat., Nonlinear, Soft Matter Phys.* **2004**, *69*, 051706 1–8.

(45) Davidson, P.; Levelut, A. M. *Liq. Cryst.* **1992**, *11*, 469–517.

(46) Tristram-Nagle, S.; Nagle, J. F. *Chem. Phys. Lipids* **2004**, *127*, 3–14.

(47) Smith, G. S.; Safinya, C. R.; Roux, D.; Clark, N. A. *Mol. Cryst. Liq. Cryst.* **1987**, *144*, 235–255.

(48) Meyer, R. B.; Liébert, L.; Strzelecki, L.; Keller, P. *J. de Phys. Lett.* **1975**, *36*, L69.

(49) Lagerwall, S. T. *Ferroelectric and Antiferroelectric Liquid Crystals*, Wiley-VCH: Weinheim, 1999.

(50) Miyasato, K.; Abe, S.; Takezoe, H.; Fukuda, A.; Kuze, E. *Jpn. J. Appl. Phys.* **1983**, *22*, L661–L663.

(51) McRae, E. G.; Kasha, M. In *Physical Processes in Radiation Biology*, Augenstein, L., Mason, R., Rosenberg, B. Eds., Academic Press: New York, 1964; pp. 23–42.

(52) Rösch, U.; Yao, S.; Wortmann, R.; Würthner, F. *Angew. Chem., Int. Ed.* **2006**, *45*, 7026–7030 and references therein.

(53) Kuball, H.-G.; Höfer, T. In *Chirality in Liquid Crystals*; Kitzerow, H.-S., Bahr, Ch. Eds., Springer-Verlag: New York, 2001, pp. 67–100.

(54) Armarego, W. L. F.; Chai, C. L. L., In *Purification of Laboratory Chemicals* 5th Edn., Butterworth-Heinemann: Amsterdam, 2003.

(55) Aldrich handbook of fine chemicals, Sigma-Aldrich: 2007–2008.

(56) Silverstein, R. M.; Webster, F. X. In *Spectrometric identification of organic compounds*; 6th Ed., John Wiley & Sons: New York, 2004.

(57) Ayyappan, P.; Evans, O. R.; Cui, Y.; Wheeler, K. A.; Lin, W. *Inorg. Chem.* **2002**, *41*, 4978–4980.

(58) Meier, H.; Lehmann, M.; Kolb, U. *Chem. –Eur. J.* **2000**, *6*, 2462–2469.

Chapter 4

Aggregation of Bolaamphiphiles in Solution

Abstract

Azobenzene cored bolaamphiphiles (Chapter 2) were found to undergo supramolecular self-assembly in water/DMSO solvent mixtures to form microstructures such as vesicles and fibers. Changes in the absorption spectra in these solvent mixtures indicated the formation of tightly packed H-aggregates. Aggregates were also formed by these molecules in n-hexane/THF solvent mixtures. The absorption band attributable to the aggregates was CD active and the CD spectra of water rich solutions exhibited an unusual intensity increase on heating. A model explaining this unusual phenomenon has been proposed. The ease of formation and the stability of the aggregates were observed to increase with increase in the length of the oligomethylene spacers. Disruption of the aggregates induced by photoisomerization of the azobenzene unit and their reformation via the subsequent thermal cis to trans isomerization was also investigated. Preliminary studies on the aggregation of diphenylbutadiene cored bolaamphiphiles (Chapter 3) were carried out in acetonitrile and water/DMSO solvent mixtures. Changes in absorption spectra and onset of CD activity indicated the formation of H-type aggregates as in the case of the azo-bolas. The effect of aggregation on the fluorescence spectra was also investigated.

4.1. Introduction

Self-assembly of bolaamphiphiles (bolas) have been receiving increasing attention in recent years in view of their potential to form a variety of supramolecular architectures and biomimetic materials.[1,2] Interest in the self-assembly of bolaamphiphiles arises mainly from the fact that the macrostructures formed can simulate the architecture of monolayered membranes of Archaebacteria in the manner of placement of their hydrophobic and hydrophilic parts.[1,2] Archaebacteria are microorganisms which have been found in "extreme" environments such as hot geysers, Antarctic ice-fields, undersea hydrothermal vents, sulfurous lakes and highly saline areas like salt-lakes and seas.[3] Their unique sturdiness is attributed to the fact that in the lipid molecules which make up their cell membrane, the saturated hydrocarbon chains are linked to the hydrophilic groups by ether bonds, which provides hydrolytic stability under such conditions.[4,5] An interesting feature of naturally occurring lipids found in Archaebacteria is the high proportion of glycosylated structures.[6] This aspect as well as the ability of sugars present in the glycocalix of biomembranes to participate in intracellular recognition processes and thus induce affinity for target cells,[7] has motivated several groups to synthesize and study supramolecular assemblies of sugar containing bolas.[8-10]

The strength of supramolecular assemblies of amphiphilic molecules can be enhanced by introducing various assembling units, which can self-aggregate via

different noncovalent interactions.[11,12] Introduction of mesogenic units into amphiphiles is known to substantially stabilize nanostructures obtained from them.[11,13]

In this regard, Shinkai et al. studied a series of bolaamphiphiles with an azobenzene containing arylamide moiety forming the mesogenic hydrophobic part and sugar units as hydrophilic end groups.[14] These bolas exhibited H-type aggregation in mixed solvents which resulted in helical fibrous morphology (Figure 4.1).

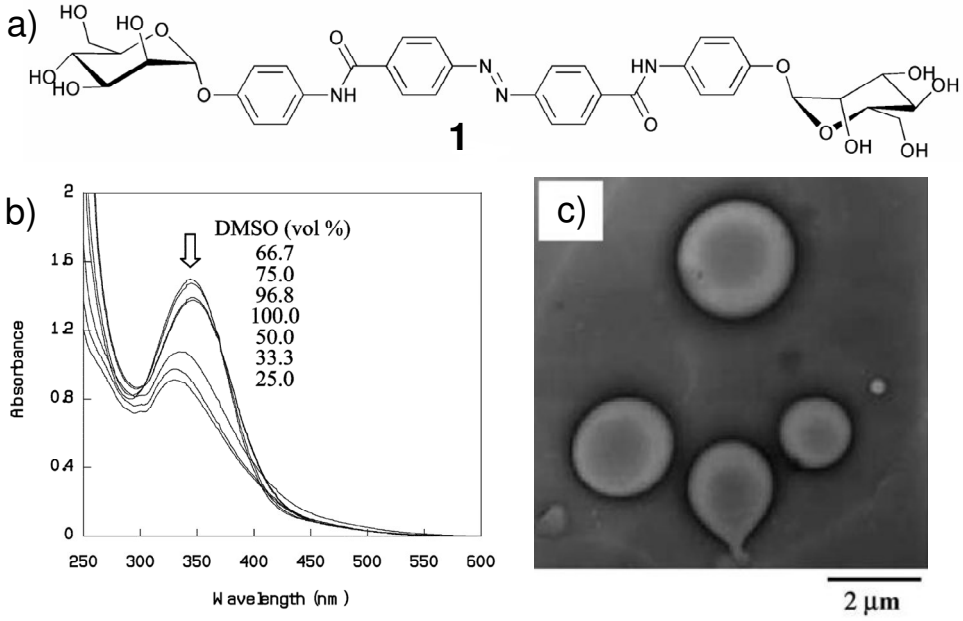

Figure 4.1. a) Structure of one of the sugar-based bolaamphiphiles **1**. b) UV-vis spectra of **1** showing the hypochromicity on increasing water concentration in its DMSO solution and c) TEM image of vesicles formed from **1**. Adapted from reference 14.

When boronic acid-appended Poly(L-lysine) was added, the fibrous aggregates (gel) changed into vesicular aggregates (sol) at the microscopic level. These changes, which are usually induced by a change in temperature, were attributed to the specific boronic acid–sugar interactions occurring at constant temperature. Interestingly, when D-Fructose which shows high affinity for the boronic acid group was added, the sol phase and the vesicular aggregate were changed back to the gel phase and the fibrous aggregate respectively. Thus the phase and morphological changes in the sugar-integrated bolaamphiphiles could be controlled reversibly.

As a part of our ongoing studies on investigating the correlations between molecular structure and self-assembly of molecules containing photoresponsive mesogenic units,[15] this Chapter describes the study on self-aggregating properties of a series of sugar-based bolaamphiphiles (Chart 4.1), in which the sugar moieties are linked to an azobenzene chromophore via oligomethylene spacers.[16] These molecules were the first examples of carbohydrate-based thermotropic liquid crystals possessing free hydroxyl groups, which exhibited a macroscopic chiral mesophase (smectic C*).[17] Based on the thermotropic liquid crystalline property of these molecules, we expected them to aggregate into lamellar structures in solution.[11,18,19] Aggregation of bolas is known to result in the formation of a variety of supramolecular structures such as planar molecular monolayers, monolayer vesicles, fibers and tubes.[1,2]

The role of chain-length in controlling supramolecular organization of molecules in solution has been increasingly recognized in recent years.[20] The oligomethylene chains also form a major component of various naturally occurring membrane lipids, including those of Archaebacteria.[8] In the present study, the role of the oligomethylene spacers and π-stacking ability of the azobenzene chromophore, as well as the effect of the *trans* to *cis* photoisomerization and the subsequent thermal *cis* to *trans* isomerization of the azobenzene chromophore in controlling the nature of the supramolecular aggregates formed in solutions have been investigated.[16]

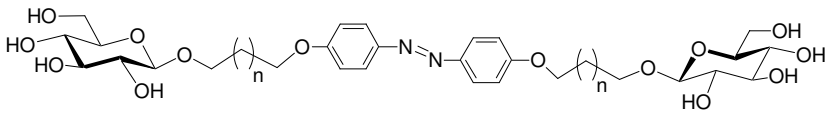

azo-bis 5: n = 3 **azo-bis 8**: n = 6
azo-bis 10: n = 8 **azo-bis 12**: n = 10

Chart 4.1

4.2. Results

4.2.1. Synthesis

The azo-bolas[17] and model compound[16], **2** were synthesized by Jayaraman and co-workers and have been reported.

4.2.2. Spectroscopic Characterization of Supramolecular Aggregates in Solution

4.2.2.1. UV-vis and CD Measurements

The azo-bolas were highly soluble in DMSO and insoluble in water except for **azo-bis 5** which dissolved in water on mild ultrasonication. Figure 4.2a and

4.2b show the absorption spectra of 2.5×10^{-5} M solutions of **azo-bis 12** and **azo-bis 10** respectively in water/DMSO solvent mixtures with varying water content. In pure DMSO, **azo-bis 10** exhibited a typical azobenzene monomer absorption spectrum[14,21] with a weak n→π* transition at 454 nm and an intense π→π* transition along the long-axis (A band) at 364 nm. Progressive increase of the water volume fraction in these solutions resulted initially in a steady decrease in the main absorption band centered at 364 nm (hypochromicity of 10%), indicating aggregation of the chromophore.[21,22]

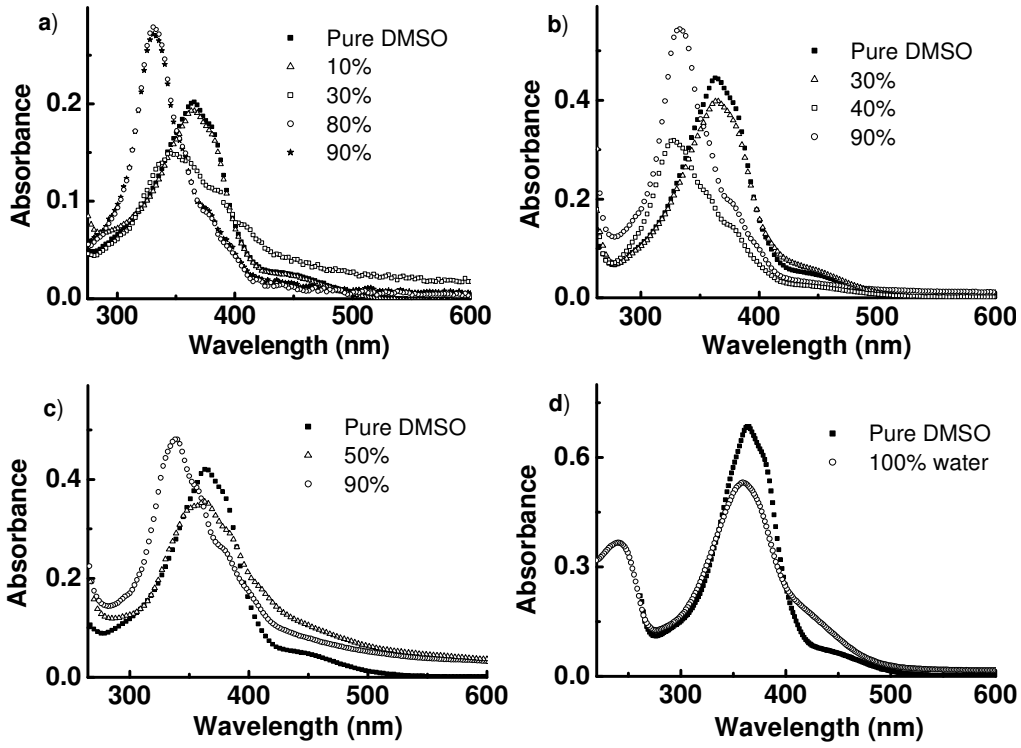

Figure 4.2. Effect of varying water content on the UV-visible spectra of a) **azo-bis 12** (2.6×10^{-5} м), b) **azo-bis 10** (2.5×10^{-5} м), c) **azo-bis 8** (2.7×10^{-5} м), d) **azo-bis 5** (1.6×10^{-5} м) in water/DMSO solvent mixtures.

All the aggregate solutions were slightly turbid, resulting in scattered light as indicated by the asymptotic nature of the absorption spectra in the non-absorbing, long wavelength region. A similar hypochromic effect on aggregation was also reported earlier for bolas consisting of rigid aryl amide linkers connecting azobenzene with sugar headgroups (Figure 4.1).[14] In the present study, when the water content of the solvent mixture reached 40%, a significant blue-shift ($\Delta\lambda_{max}$ = 31 nm) in the absorption band was observed (Figure 4.2b).

With subsequent increase in water content, the blue-shift was accompanied by an increase in intensity (hyperchromicity of 75%) and narrowing of the band. In solvent mixtures containing 90% water, the full width at half-maximum was narrower than that of the corresponding monomer band by 658 cm^{-1}. Similar results were observed for **azo-bis 8** and **azo-bis 12**. The UV-vis spectrum of **azo-bis 12** in 80% water/DMSO was more intense than that in 90% water/DMSO which was in contrast to the other derivatives for which the 90% water/DMSO solutions were the most hyperchromic. This was perhaps due to solubility reason, since **azo-bis 12** had the longest hydrophobic spacers giving rise to enhanced aggregate stability in 80% water/DMSO.

For **azo-bis 5** however, only a slight decrease in intensity of absorption and a small blue-shift of 4 nm was observed in the water rich solvent mixtures (Figure 4.2d). A hump was observed in the 400–450 nm region in the **azo-bis 5** aggregate spectrum, which was absent in the monomer spectrum. This effect on the UV-

visible spectra of **azo-bis 5** on aggregation (Figure 4.2d) was similar to the spectral change (Figure 4.1b) observed by Shinkai et al. in the aggregation of bolas consisting of rigid aryl amide linkers connecting azobenzene with sugar end groups.[14]

Formation of a blue-shifted band by amphiphilic azobenzene derivatives in aqueous or water rich media has been attributed to the formation of H-aggregates, which essentially consist of a "card pack" array of transition moments of the individual molecules.[23,24] The blue-shifted band of H-aggregated species is normally wider and less intense than the monomer band, as is indeed observed in most of the azobenzene derivatives hitherto investigated.[24-28] When the excitons are strongly coupled however, due to a high degree of ordering of the constituent molecules, a large hypsochromic shift of the band accompanied by an increase in intensity and narrowing of the band are observed.[29] Such an effect is clearly indicative of the formation of closely packed three-dimensional H* aggregate of which only limited examples are reported.[22,30] The formation of H* aggregate by the bolas reported in the present study and its absence in the similar bolas reported earlier[14] may be attributed to the additional hydrophobic nature (intramolecular contrast) imparted to the molecule by the oligomethylene linker groups as well as the relatively non-polar nature of the ether linkage. The intense nature of H-type aggregate peak over monomer was not due to light scattering effect since its auto-zeroed UV-vis spectrum also was more intense than the monomer. A blue-shifted

absorption spectrum indicative of H-type aggregate formation was also obtained in thin films of **azo-bis 10** drop-cast on quartz plates from an acetone/methanol mixture (See Figure 2.19 in Chapter 2).[17]

The aggregation behavior of the azo-bolas was also studied in *n*-hexane/THF solvent mixtures. It should be noted that the azo-bolas are insoluble in *n*-hexane and could be molecularly dissolved in THF. Figure 4.3 shows the UV-vis spectral changes on addition of *n*-hexane to a solution of **azo-bis 10** in THF. Only a decrease in absorption intensity and a blue-shift of 15 nm was observed, indicating formation of loosely packed aggregates in contrast to what was observed in water/DMSO solvent mixtures.

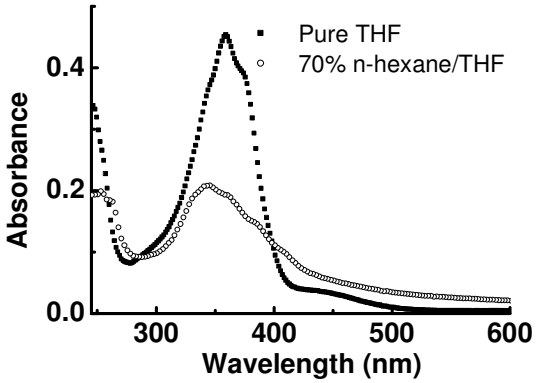

Figure 4.3. Effect of *n*-hexane addition on UV-visible spectra of **azo-bis 10** (2.5×10^{-5} M) in *n*-hexane/THF solvent mixtures.

The absorption band attributable to the aggregates was CD active indicating a chiral arrangement of the transition moments of the azobenzene segment within the aggregates (Figure 4.4). Figure 4.4b shows the CD spectra of **azo-bis 10** aggregates in the water/DMSO solvent mixtures. Whereas solutions of **azo-bis 10**

in pure DMSO were CD silent, a positive first Cotton effect and negative second Cotton effect was observed for solutions containing water, indicating a right-handed chiral arrangement of the transition moments of the azobenzene chromophores within the aggregates.

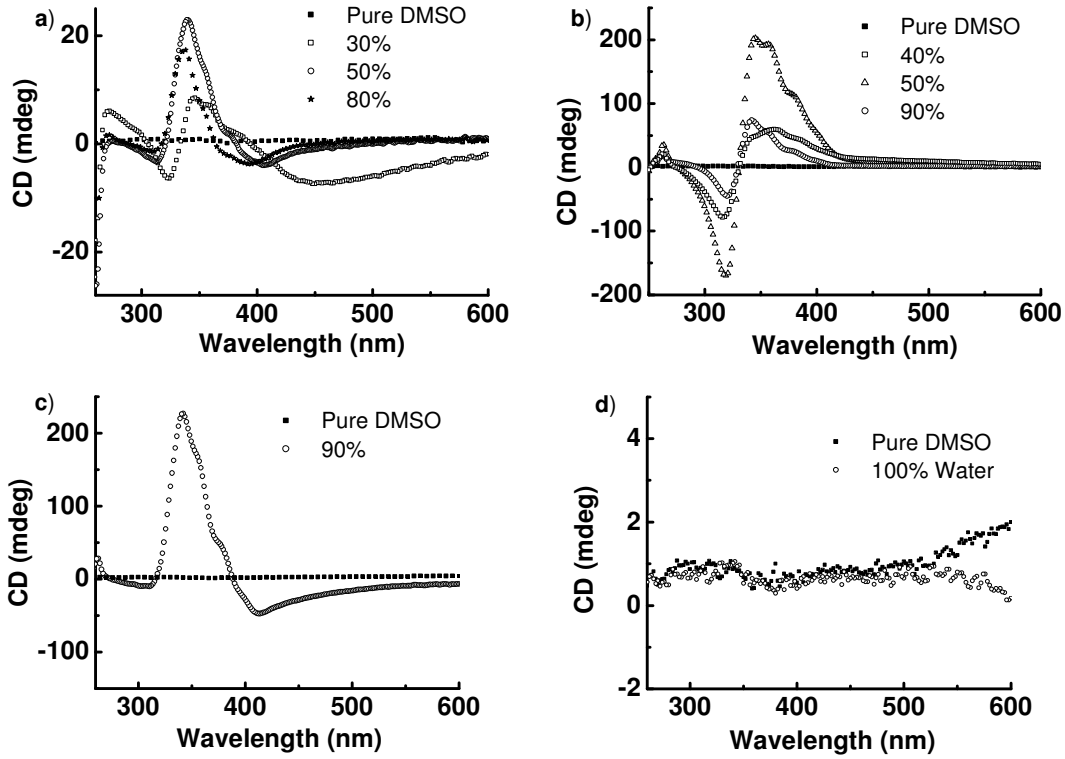

Figure 4.4. Effect of varying water content on the CD spectra of a) **azo-bis 12** (2.6×10^{-5} м), b) **azo-bis 10** (2.5×10^{-5} м), c) **azo-bis 8** (2.7×10^{-5} м), d) **azo-bis 5** (1.6×10^{-5} м) in water/DMSO solvent mixtures.

The CD spectra were observed only when the blue-shifted absorption spectrum attributable to the aggregate was present. The zero-crossing point was close to the absorption maximum of the aggregated chromophore, indicating the CD spectra to be due to the exciton coupling bands of the aggregate. The CD

intensity did not vary linearly on increasing water concentration but fluctuated. In solvent mixtures with high water content, UV-vis and CD spectra indicated formation of aggregates of the azo-bolas over a wide concentration range (2×10^{-6} – 7.5×10^{-3} M).

CD spectra could also be observed for the aggregate formed in THF on addition of *n*-hexane (Figure 4.5).

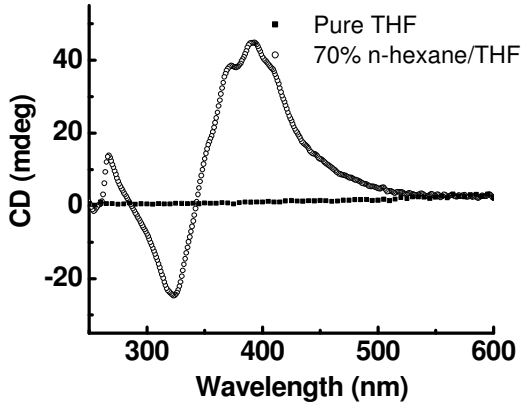

Figure 4.5. Effect of *n*-hexane on the CD spectra of **azo-bis 10** (2.5×10^{-5} M) in *n*-hexane/THF solvent mixtures.

The tendency for aggregation of the azo-bolas was chain-length dependent. Whereas **azo-bis 5** solutions were CD silent (Figure 4.4d), indicating a much lesser tendency to form strongly coupled H* aggregates, onset of CD activity for **azo-bis 8** occurred in 50% water/DMSO solutions. The onset of aggregation in **azo-bis 10** and **azo-bis 12** started form solvents containing 40 and 30% water respectively. In this context it is interesting to note that in bolaamphiphilic systems, where the terminal sugar moieties were linked to a central azobenzene via arylamide units,[14] aggregation only resulted in a 15 nm blue-shifted band of lower intensity. Thus the

presence of the oligomethylene linker units of a suitable length was observed to be essential for the formation of the H* aggregates.

4.2.2.2. Effect of temperature on the UV-vis and CD spectra

The effect of temperature on the aggregate solutions was studied by variable temperature UV-vis and CD spectroscopy. The aggregate of **azo-bis 5** showed a hyperchromic effect on heating with a slight reduction in the intensity of the hump in the 400–450 nm region (Figure 4.6). The hyperchromic effect on heating indicated conversion from the aggregated state to a molecularly dissolved form.

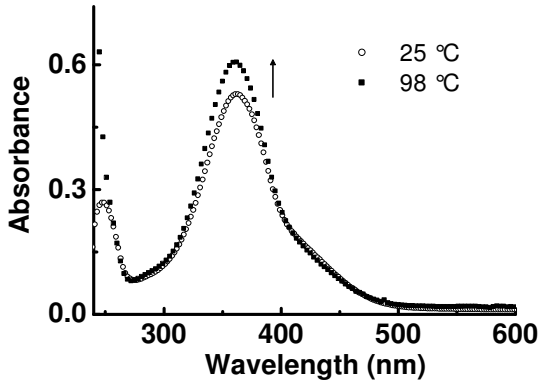

Figure 4.6. Changes in the UV-vis spectrum of **azo-bis 5** aggregate (1.6×10^{-5} M) on heating.

The formation of strongly coupled aggregates in **azo-bis 8**, **azo-bis 10** and **azo-bis 12** was indicated by the persistence of the aggregate band and CD acitivity at high temperatures. In the case of **azo-bis 10** the blue-shifted band exhibited a slight decrease in intensity and considerable broadening (Figure 4.7a), indicating a weakening of the interaction among the azobenzene transition moments in the

aggregate.[21] Above 90 °C, however a considerable decrease in intensity and red-shift in the band indicated break-up of the aggregate to the monomer form (Figure 4.7a). Interestingly the CD amplitude (A_{CD}) increased by ~4.3 times on heating until the temperature reached 80 °C, after which a decrease was observed (Figure 4.7b). To the best of our knowledge, such an effect, namely increase in the CD intensity accompanied by broadening of the absorption band of the aggregate on heating, is unprecedented. In general, for chiral supramolecular assemblies, the CD intensity decreases on heating.[31,32]

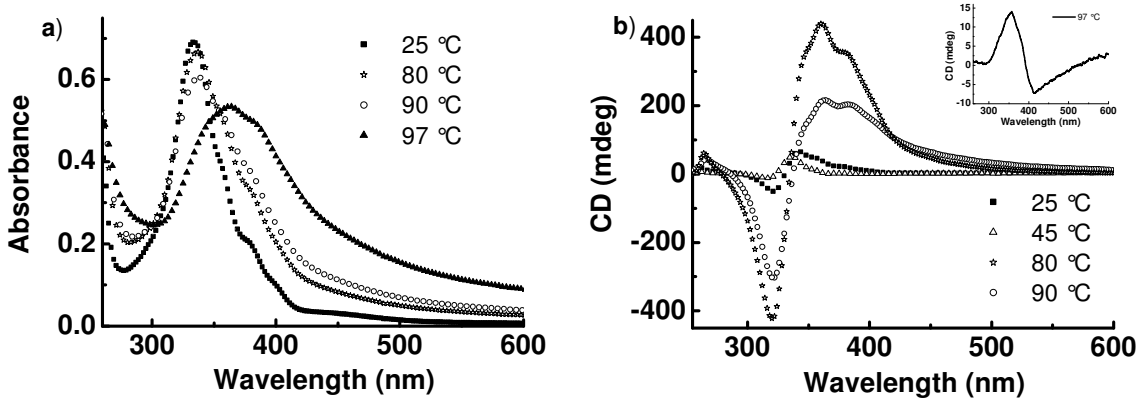

Figure 4.7. Effect of temperature on a) UV-vis and b) CD spectra of **azo-bis 10** in 80% water/DMSO (2.5×10^{-5} M). Inset in b) shows the CD spectra at 97 °C. UV-vis spectra at 45 °C was almost same as that at 25 °C, so not shown in a).

A possible explanation for the observed results is schematically shown in Figure 4.8. At room temperature, a near parallel face-to-face stacking of the transition moments of the H* aggregates would be stabilized by intermolecular hydrogen bonding between the sugar groups. With increasing temperature, weakening of the intermolecular hydrogen bonding between the sugar moieties could result in a shift

of the transition moments from a near parallel face-to-face stacking to a chiral arrangement (Figure 4.8), resulting in broadening of the absorption band and enhancement in the CD intensity. It is known that the A_{CD} value is maximal when the angle of interacting moments is ~70 °.[33] Further increase in temperature could result in the gradual break-up of the aggregates leading to reduction in A_{CD} due to formation of the monomer.

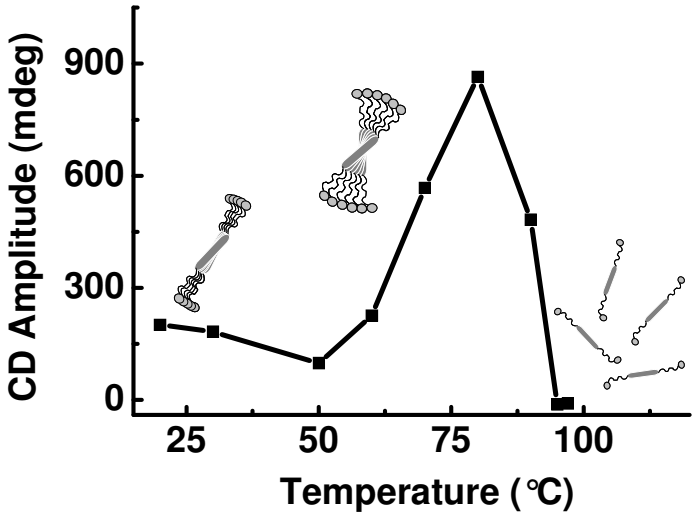

Figure 4.8. Changes in CD amplitude with temperature of the **azo-bis 10** aggregate in 80% water/DMSO (For CD spectrum, see Figure 4.7b). Also shown is a schematic representation of the probable arrangements of the molecules at various temperatures.

The persistence of CD activity at 97 °C (Figure 4.7b inset) in these solutions was indicative of the unusually high thermal stability of the aggregates. On cooling, the UV-vis absorption spectrum underwent a blue-shift along with a hyperchromic effect typical of reformation of the H-aggregate (Figure 4.9a). The corresponding CD signals reached a bisignate couplet of different shape at ambient temperature (Figure 4.9b).

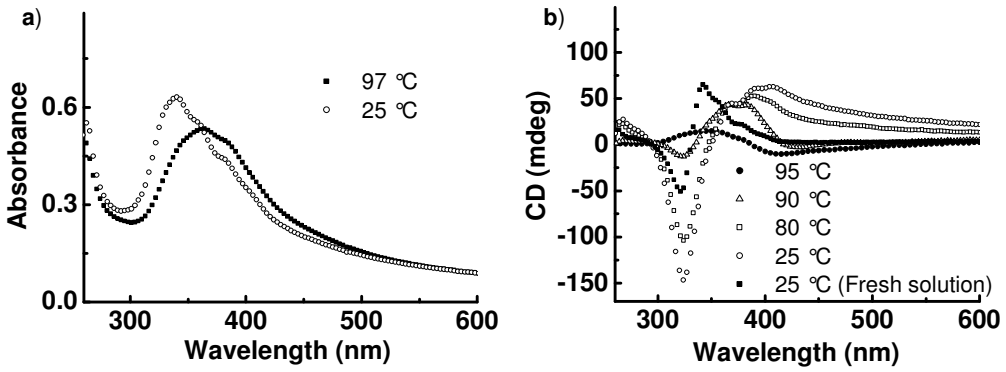

Figure 4.9. Changes in UV-vis and CD spectra of **azo-bis 10** in 80% water/DMSO (2.5×10^{-5} M) on cooling (For heating cycle spectra, see Figure 4.7).

In the second heating cycle, the CD enhancement was not observed which indicated that after the first heating and cooling cycle, the system could have reached a thermodynamically stable state.

The unusual CD effect discussed above could have been due to some macroscopically anisotropic structure in the sample solution at the temperatures where the CD signal enhancement was observed. In order to rule out these effects, variable temperature dynamic light scattering (VT-DLS) study was carried out on a freshly prepared, equilibrated solution. Figure 4.10 shows the changes in aggregate size (Z-average diameter) monitored as a function of temperature. During the heating cycle (where the unusual CD signal enhancement was seen), we could not detect any aggregate with size ranging above 800 nm (Figure 4.10a). This indicated that the enhancement in CD signal was due to a real effect involving intermolecular interactions.

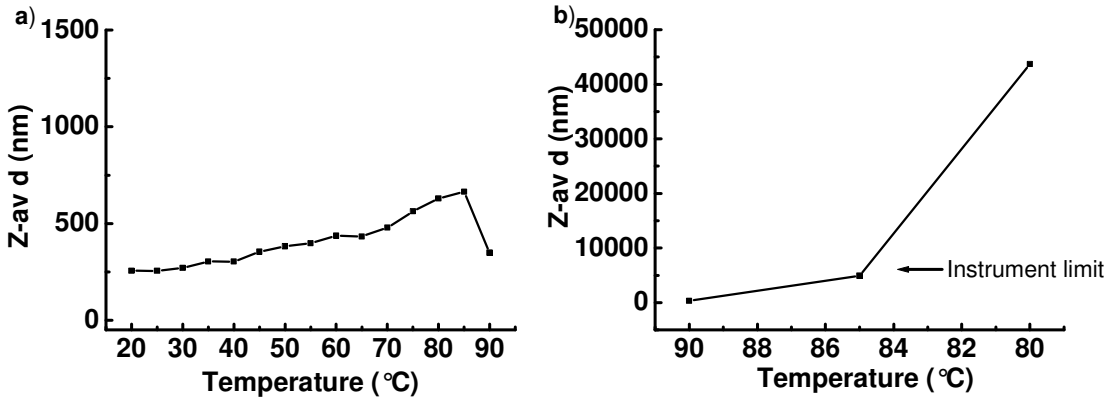

Figure 4.10. Variable temperature DLS intensity profile showing changes in aggregate size for **azo-bis 10** in 80% water/DMSO during a) heating and b) cooling.

Interestingly on cooling, the aggregate size increased rapidly and went beyond the detection limits of the instrument as shown in Figure 4.10b. Visual examination of the solution at various stages during heating also showed that it was optically clear, whereas during cooling the solution had become very cloudy (turbid). These observations matched that of the VT-DLS experiment.

This unusual CD intensity increase was less pronounced in the case of **azo-bis 8** with the CD intensity only slightly increasing on heating up to 60 °C and thereafter decreasing to become CD silent above 80 °C (Figure 4.11a). However, on cooling this solution to room temperature it was seen that the CD couplets recovered and was even more intense than in the freshly prepared solutions (Figure 4.11b).

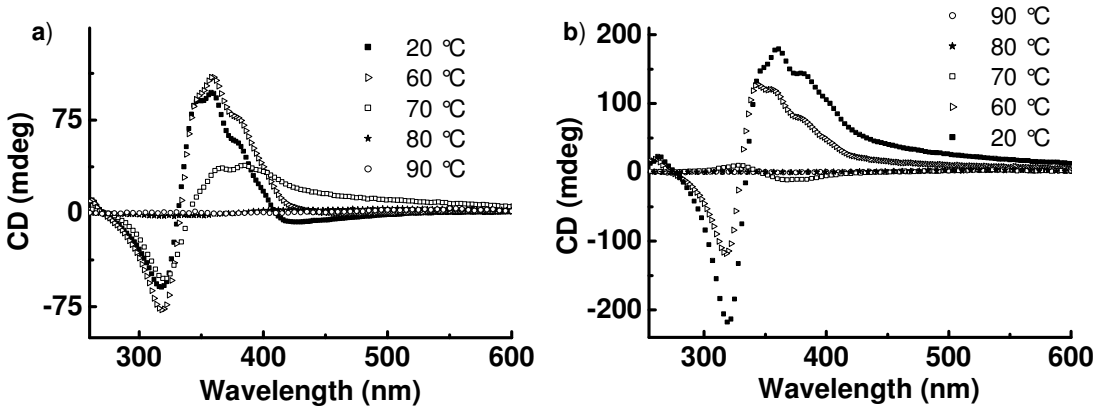

***Figure 4.*11.** CD spectral changes of **azo-bis 8** (2.7 × 10^{-5} м) aggregate in 80% water/DMSO on a) heating; b) cooling.

The aggregate of **azo-bis 12** however showed a higher degree of enhancement of the CD signal than that in **azo-bis 10** on heating and was intense even at 99 °C (Figure 4.12a).

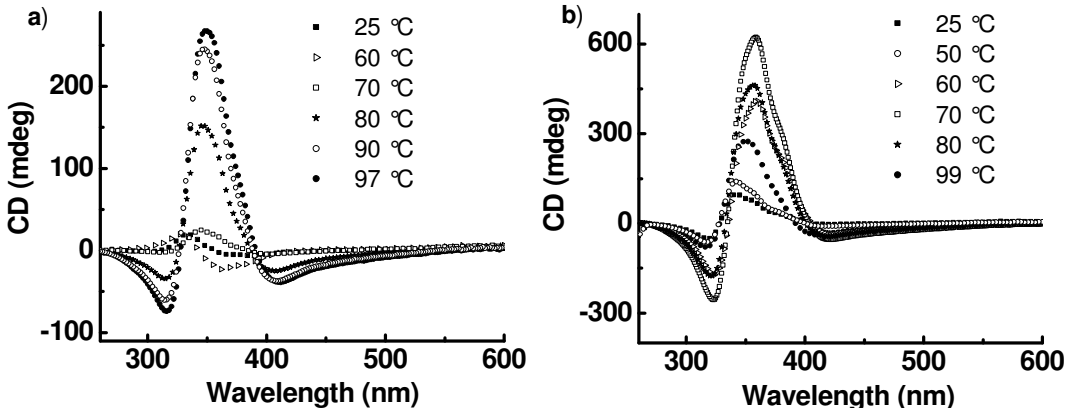

Figure 4.12. CD spectral changes of **azo-bis 12** (2.6 × 10^{-5} м) aggregate in 80% water/DMSO on a) heating; b) cooling.

Interestingly, in the cooling cycle, the CD intensity increased even more than in the heating phase (Figure 4.12b). In solvent compositions (e.g., 50%

water/DMSO) where the CD became silent at high temperatures, reappearance of the couplets on cooling was observed indicating reformation of the aggregates.

4.2.2.3. Proton NMR characterization of the aggregates

^{1}H NMR spectra of the aggregates were examined to gain further insight into the mode of molecular packing within the aggregates. Aggregation of molecules can make their motion anisotropic and reduced rate of motion of molecular parts in solution can lead to long correlation times.[34,35] For the NMR studies, aggregation was induced by adding D_2O to a DMSO-d_6 solution of the azo-bolas. The spectrum of **azo-bis 8** in pure DMSO-d_6 displayed the expected resonances (Figure 4.13a).[17,36] On addition of D_2O, a slight resonance broadening occurred in the aromatic (δ = 7.10 and 7.82 ppm) and oligomethylene (δ = 1.21–1.83 ppm) peaks. Further addition of D_2O, resulted in a coalescence of the aromatic doublets until finally the aromatic peaks collapsed and the region became featureless, indicating total loss of freedom of movement in the aromatic segment as a result of strong aggregation. The line broadening and decrease in intensity was lesser for the oligomethylene peaks, indicating that this part of the molecule was less tightly packed within the aggregates, and retained considerable amount of their flexibility.

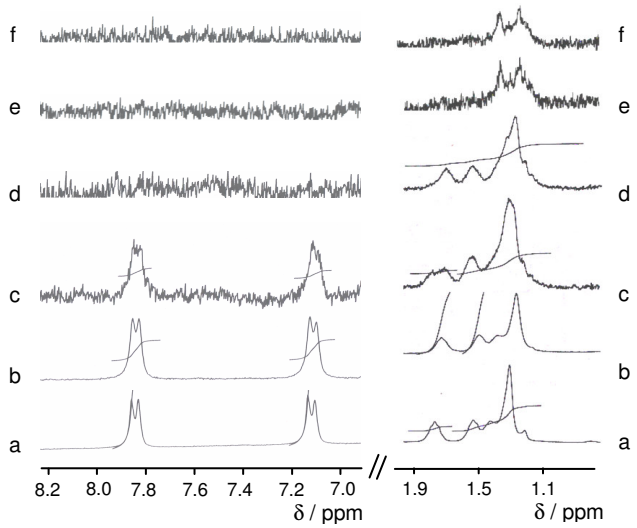

Figure 4.13. ^{1}H NMR spectra of **azo-bis 8** showing aromatic and oligomethylene protons: a) in pure DMSO-d_6 (16 mM); b)–f) changes upon adding D_2O in 100 µL increments (T=27 °C).

The onset of the collapse of the aromatic peaks in the NMR spectra on addition of D_2O was chain-length dependent. For a 16 mM solution of **azo-bis 8** in DMSO-d_6, the aromatic peaks collapsed (molecules aggregated) when the D_2O concentration reached 40%, whereas for an **azo-bis 10** solution of the same concentration, the collapse occurred at a concentration of 30% D_2O.

The ^{1}H NMR of this aggregate was recorded (500 MHz) at various temperatures (Figure 4.14). In the spectrum at 27 and 47 °C, poorly resolved, low intensity, broad peaks could be seen in the aromatic region, which could be attributed to irregular coupling environments in the densely packed aggregate. With increasing temperature (>70 °C), the resonances of molecularly dissolved **azo-bis 8** progressively appeared. Similar behavior on heating was observed for the **azo-bis 10** aggregate.

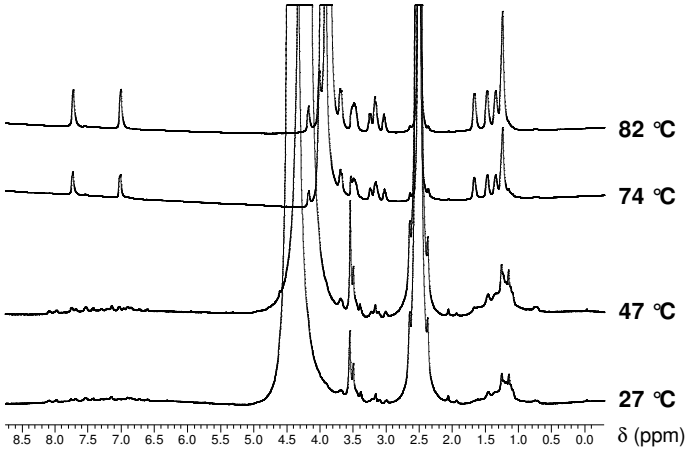

Figure 4.14. Thermal evolution of molecular **azo-bis 8** from its aggregate (7.5 mM) as shown by temperature dependent ^{1}H NMR.

4.2.3. Aggregate morphology

DLS studies on solutions of **azo-bis 8** in water/DMSO indicated the presence of polydisperse aggregates ranging from 200 nm to 1.5 μm (Figure 4.15).

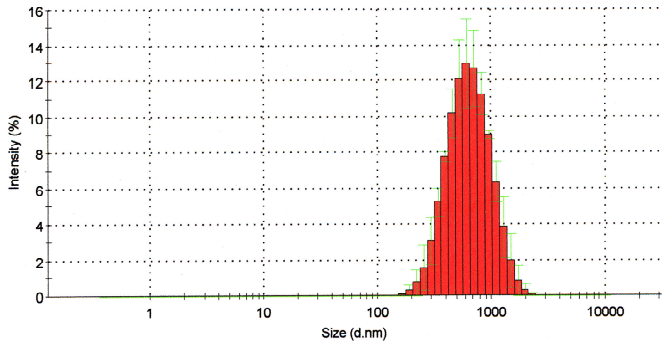

Figure 4.15. DLS intensity profile for **azo-bis 8** in 90% water/DMSO (2.7×10^{-5} M; T=20 °C).

Microscopic (AFM, SEM and TEM) investigations of the solutions were carried out in order to visualise the morphology of the aggregates. AFM images of films deposited on mica by drop-casting 10^{-5} M solutions of **azo-bis 8** in 90%

water/DMSO indicated the presence of spherical aggregates existing singly as well as in the clustered state (Figure 4.16).

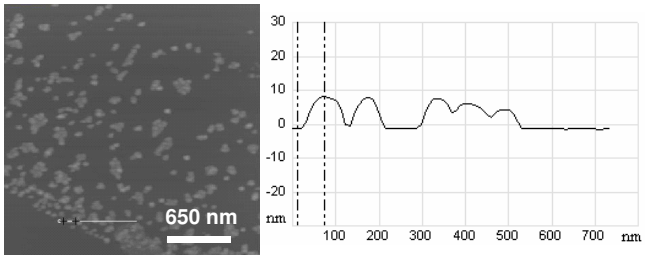

Figure 4.16. Vesicles of **azo-bis 8** (2.7×10^{-5} M) imaged by contact mode AFM and their cross-section analysis.

The spherical particles were also observed in the SEM images (Figure 4.17a). Several collapsed vesicles were also observed, which could be attributed to the presence of vacuum and dehydrating environment during electron microscopy.[37] The spherical particles were confirmed to be vesicles by TEM analysis which showed a clear electron contrast between the membrane and centre of the vesicles (Figure 4.17b).[38,39]

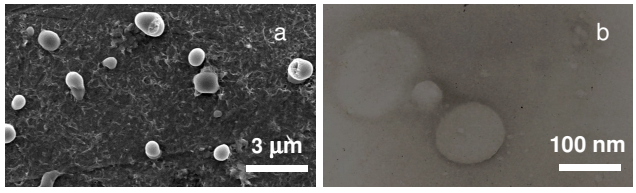

Figure 4.17. Vesicles of **azo-bis 8** (2.7×10^{-5} M) viewed by a) SEM; b) TEM.

The heights of the spheres estimated by cross-section analysis of the AFM images were in the range of 8.2–9.4 nm which was equal to or little more than twice the length of the all *trans*-form of **azo-bis 8** (l = 3.8 nm). This is indicative

of a bilayer stacking, which can occur in collapsed vesicles possessing a monolayer membrane structure. In samples deposited from concentrated solutions (1×10^{-4} M) of **azo-bis 8** in 90% water/DMSO, plate like structures could be seen in addition to the vesicles. These structures when examined by TEM in the SAED mode (selected area electron diffraction) showed characteristic *diffuse* haloes confirming their amorphous nature (Figure 4.18b).[40] When viewed between crossed polarizers, concentrated solutions of **azo-bis 8** in water/DMSO showed maltese cross extinction which was characteristic of spherical lamellar structures.[41,42]

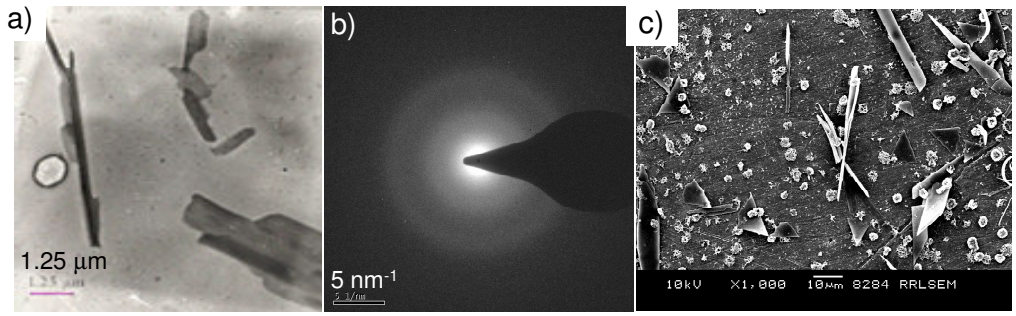

Figure 4.18. Morphology observed for **azo-bis 8** (1×10^{-4} M) viewed by a) TEM; b) SAED of the plate like structures; c) SEM.

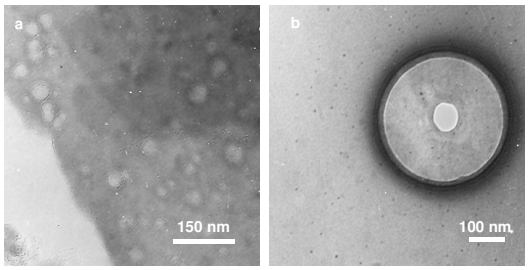

Figure 4.19. TEM images showing vesicles formed by **azo-bis 5** (1.6×10^{-5} M).

Formation of vesicles was also observed in water/DMSO solutions of **azo-bis 5** (Figure 4.19).

For **azo-bis 10** the morphology of the aggregates was found to be dependent on the method of preparation of the solution. Films deposited from solutions of **azo-bis 10** in water/DMSO prepared under identical conditions, viz., by adding water to DMSO solutions of the azo-bola, indicated the presence of fibers consisting of 200–300 nm wide fibrils (Figures 4.20a and 4.21a) instead of vesicles. Formation of fibers and tubular structures have been reported for a large number of sugar based amphiphiles and bolaamphiphiles.[2,12,43] However, films deposited from the same solutions which had been heated to 97 °C and cooled to room temperature did not contain fibers, with only vesicles being observed (Figures 4.20b and 4.21b).

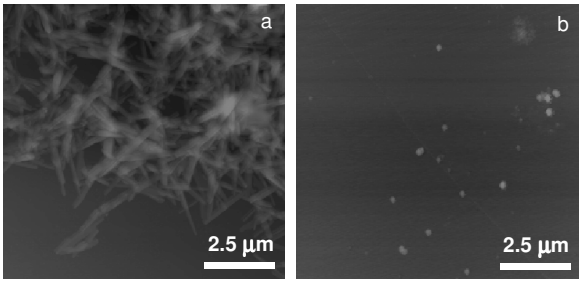

Figure 4.20. Tapping mode AFM images of aggregates formed by **azo-bis 10** (2.5×10^{-5} м): a) fiber morphology when drop-cast in freshly prepared state; b) vesicular morphology when drop-cast after heating to 97 °C and cooling.

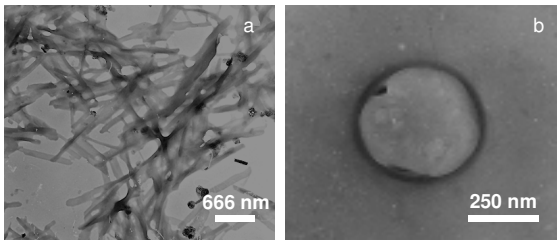

Figure 4.21. TEM images of aggregates formed by **azo-bis 10** (2.5×10^{-5} M): a) fiber morphology in films cast from a freshly prepared solution; b) vesicular morphology observed in a film deposited from solutions heated to 97 °C and cooled to ambient temperature.

4.2.4. Photolysis of the aggregates

In pure DMSO solutions, the azo-bolas underwent *trans* to *cis* photoisomerization when irradiated with 364 nm light isolated from a 450 W Xe lamp (Figure 4.22a). The reverse isomerization (*cis* to *trans*) occurred in the dark over a period of 24 h (Figure 4.22b). The time-course spectrum of the reverse isomerization is shown in Figure 4.22c.

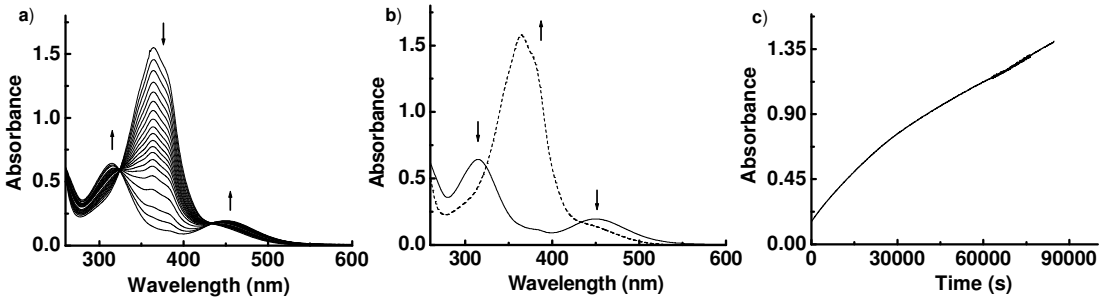

Figure 4.22. UV-vis spectra of **azo-bis 10** in DMSO showing a) *trans* to *cis* photoisomerization change from all *trans* to photostationary state over a period of 14 min on irradiation with 364 nm monochromatic light; b) *cis* to *trans* thermal isomerization; photostationary state (solid line), spectra obtained after 24 h (dashed line) and c) thermal isomerization monitored by a time-course.

In the H-aggregated state, the azobenzene chromophore is known to be resistant to photoisomerization.[26] Thus photoisomerization was not observed on

irradiation with the UV light output of the Xe lamp. On exposure of a solution of **azo-bis 8** in water/DMSO, to 355 nm laser pulses (~50 mJ/pulse), however, a decrease in intensity of the 339 nm band and appearance of a broad band centered at 450 nm attributable to the n→π* transition of the *cis*-isomer was observed (Figure 4.23a). Changes in the UV-vis spectrum were accompanied by a significant reduction in the scattering nature of the solution. The CD spectrum of the irradiated solution showed reduced intensity with the zero-crossing points remaining unchanged (Figure 4.23b), indicating disruption of the aggregate due to *trans* to *cis* photoisomerization of the azobenzene moiety.

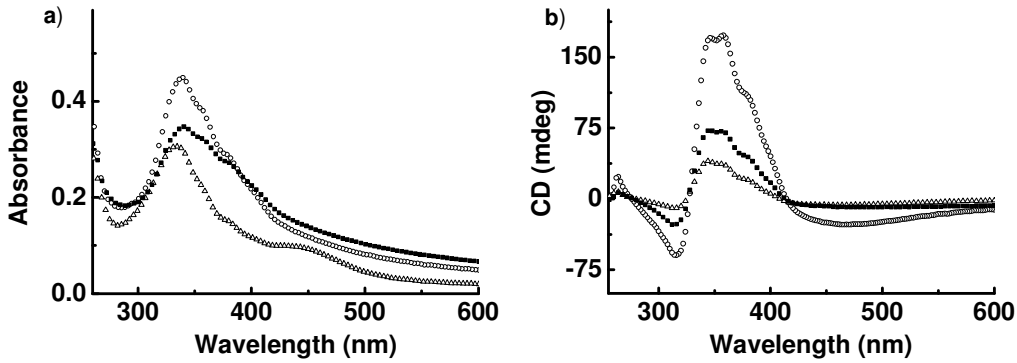

Figure 4.23. Effect of irradiation on the UV-vis spectra (a) and CD spectra (b) of the aggregate of **azo-bis 8** (2.7×10^{-5} м) in 90% water/DMSO: (O) Before irradiation; (Δ) after irradiation; (■) Irradiated solution kept in dark for 24 h.

Recovery of the blue-shifted aggregate band was observed when the irradiated solutions were kept in the dark for 24 h (Figure 4.23a). However the final spectra were less intense and also slightly broader, suggesting a difference in the nature of the aggregated species formed.

Disruption of the aggregates due to photolysis was also indicated by changes in the ^{1}H NMR spectrum (Figure 4.24). A new peak centered at δ = 6.79 ppm appeared in the aromatic region on exposure of the solution containing aggregates to 355 nm laser pulses (~70 mJ/pulse) and peaks attributable to oligomethylene linkers and glucoside moieties became fairly well resolved following irradiation.

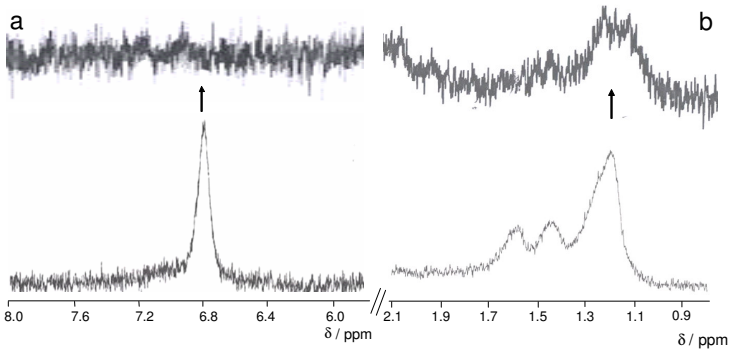

Figure 4.24. Changes in ^{1}H NMR a) aromatic protons; b) oligomethylene protons of **azo-bis 8** aggregate upon irradiation with 355 nm laser pulses (bottom) and recorded after keeping irradiated solution in the dark for 24 h (top; 7.5 mM, T=27 ℃).

The peak centered at δ = 6.79 ppm could be attributed to multiplet of the *cis*-isomer by comparison with the NMR spectra of irradiated solutions of a model compound (**2**, Chart 4.2), 10,10'-[(1*E*)-Azobis(4,1-phenyleneoxy)]bis[1-decanol].

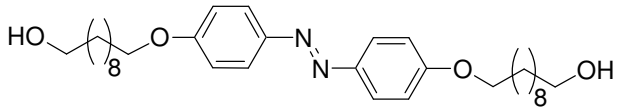

2

Chart 4.2

Irradiated solutions of **2** also showed doublets at δ = 7.10 and 7.82 ppm attributable to the residual *trans*-isomer (Figure 4.25).

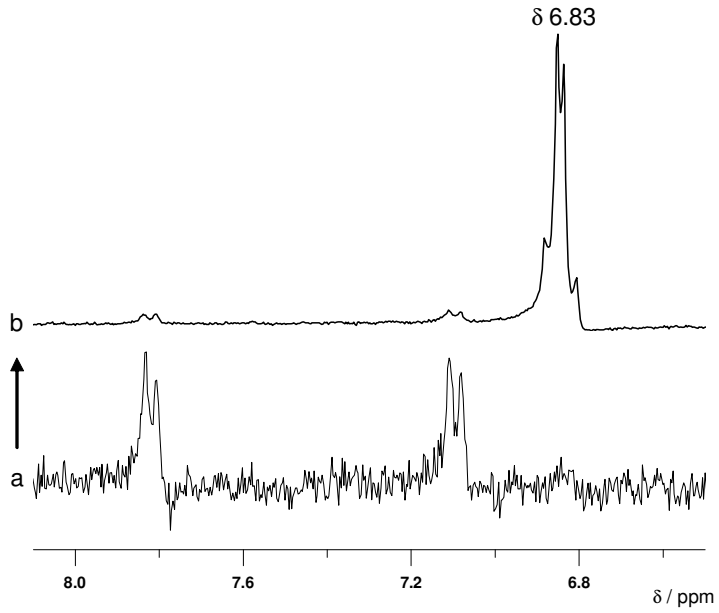

Figure 4.25. Partial ^{1}H NMR spectra of model compound, **2** in pure DMSO-d_6 (12 mM, T=27 °C) showing a) aromatic doublets of a fresh sample; b) appearance of *cis*-isomer on irradiation at 355 nm. The un-isomerized *trans*-form is seen as less intense doublets in (b).

Peaks attributable to the *trans*-isomer were however not observed in irradiated solutions of the aggregated **azo-bis 8**, indicating the strong tendency of the residual *trans*-isomer to remain in the aggregated state. On keeping the irradiated solution at room temperature for 24 h, the peak due to the *cis*-isomer disappeared, implying thermal isomerization to the *trans*-isomer and subsequent aggregation (Figure 4.24). At high temperatures (>70 °C) appearance of the peaks attributable to the *trans*-isomer indicated that no permanent chemical transformation had occurred on laser irradiation (Figure 4.14). Similar effects were also observed for **azo-bis 10**.

TEM images of the films cast from solution of **azo-bis 8** in 90% water/DMSO indicated the presence of vesicles (Figure 4.17b, 4.26a). The same solution was initially exposed to 355 nm laser pulses to induce *trans* to *cis* photoisomerization of the azobenzene moiety (Figure 4.23).

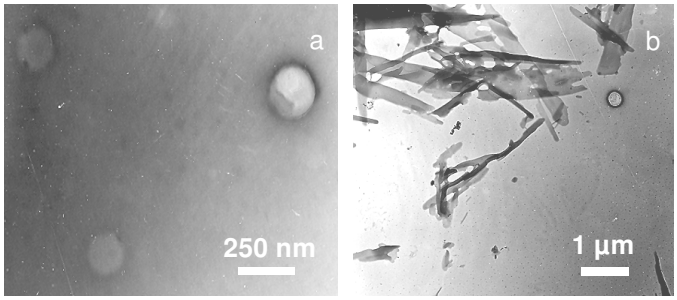

Figure 4.26. TEM images for **azo-bis 8** aggregates (2.7×10^{-5} м) in 90% water/DMSO showing photoinduced changes in aggregation: a) before irradiation; b) following irradiation at 355 nm and keeping in the dark for 24 h.

The solution was kept in the dark for 24 h to allow the thermal recovery of the *trans* isomers. For these solutions, recovery of the aggregated form was indicated in both the UV-vis and NMR spectra. TEM images of aggregates obtained from these solutions indicated mainly the existence of a large number of flat sheets and fibers alongside a few vesicles (Figure 4.26b). These flat fibrils could be formed by aggregation of the back isomerized *trans*-isomer during the 24 h period. The *cis*-isomer is not usually known to aggregate. The addition of water to a DMSO solution of azo-bola maintained at the photostationary state did not bring about aggregation (no change in UV-vis wavelength of absorption and CD silent). The resulting solution when monitored by UV-vis spectroscopy showed decrease in intensity in the region of *cis*-isomer absorption with concomitant enhancement of

intensity of the *trans*-isomer absorption. Aggregation was also indicated by appearance of CD couplet and increase in scattering nature of the solution. In the solutions containing flat sheets and fibers, which were heated to 97 °C and cooled to room temperature under ambient conditions, formation of vesicles were observed by TEM, similar to that observed in the freshly made un-photolyzed solutions.

4.3. Aggregation of CnGB Bolaamphiphiles

The aggregation behavior of diphenylbutadiene cored bolaamphiphiles (Chart 4.3) whose thermotropic properties were discussed in Chapter 3 was also investigated in solution.

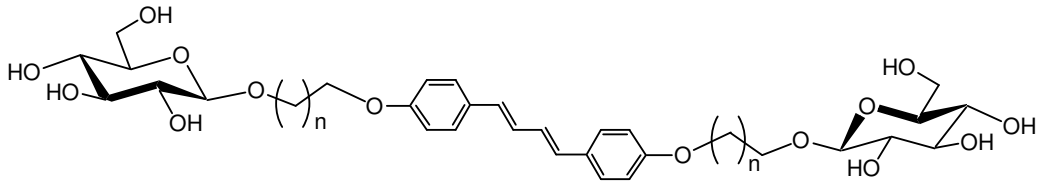

n = 9: **C10GB**, 11: **C12GB**

Chart 4.3

4.3.1. Aggregation behavior in acetonitrile

The bolaamphiphile **C10GB** was insoluble in acetonitrile, but dilute solutions could be obtained by ultrasonication. The UV-vis spectrum of this solution showed an absorption band with a λ_{max} at 344 nm. The absorption maximum was 5 nm blue-shifted with respect to its molecularly dissolved solution

in THF (for spectrum in THF, see Chapter 3). A small hump was observed in this spectrum at 386 nm which could be due to absorption by the aggregated form (Figure 4.27a). The fluorescence spectrum in acetonitrile was structured with a red-shifted main peak (417 nm; Figure 4.27b) compared to the monomer emission peak (at 398 nm) in THF. The excitation spectra (Figure 4.27c) were similar in nature with the absorption spectrum.

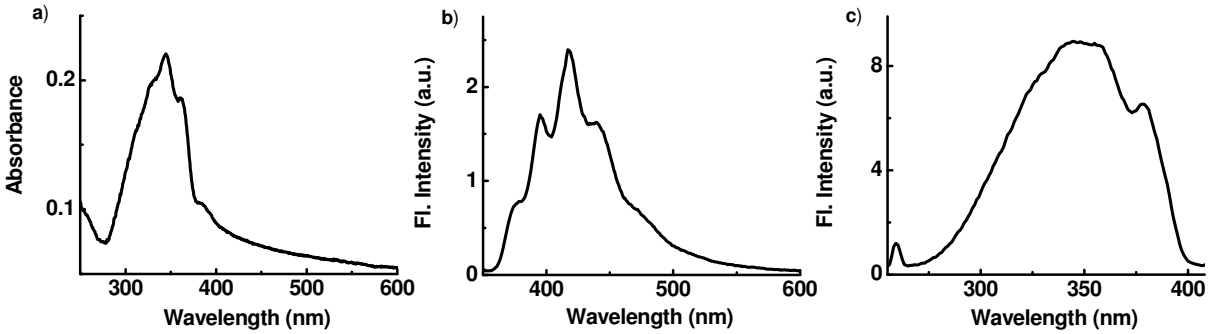

Figure 4.27. Optical spectra of **C10GB** in acetonitrile solutions: (a) UV-vis absorption spectra, (b) fluorescence emission spectra (λ_{ex} = 340 nm) and (c) fluorescence excitation spectra (λ_{em} = 420 nm). All spectra were recorded at room temperature.

With increasing temperature, reduction in intensity of the aggregate hump (at 386 nm) was observed with increase in absorbance of the main absorption band at 344 nm. Also significant reduction in scattering nature of the solution indicated dissociation of the aggregate into the molecularly dissolved **C10GB** (Figure 4.28a). On cooling from this state a hypochromicity of the main band was observed indicating re-aggregation (Figure 4.28b).

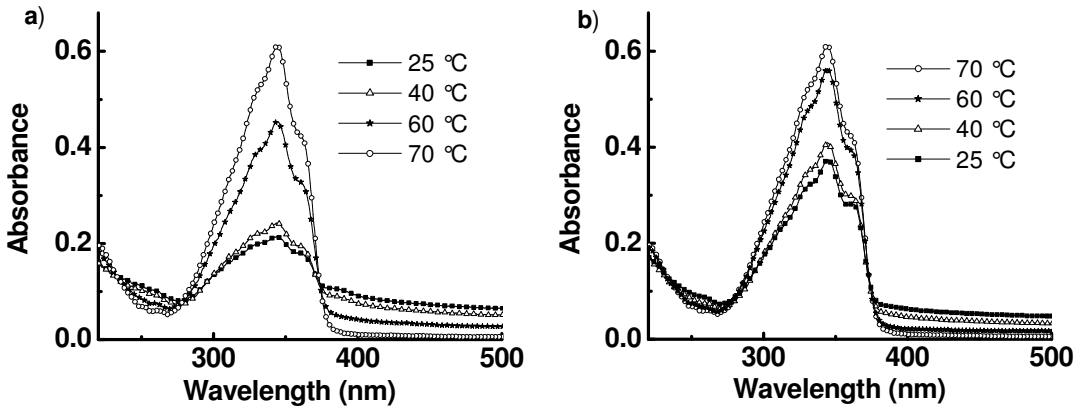

Figure 4.28. Effect of temperature on the UV-vis absorption spectra of **C10GB** in acetonitrile on a) heating and b) cooling.

Interestingly this solution was found to be CD active, which confirmed that **C10GB** existed as an aggregate in MeCN (Figure 4.29).

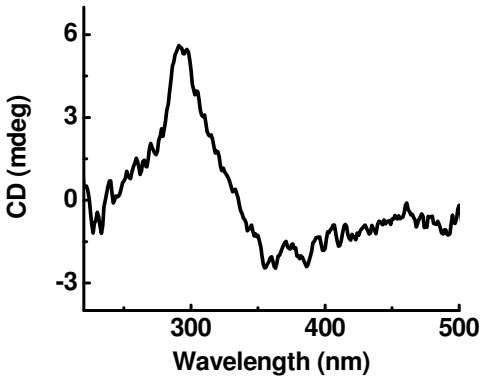

Figure 4.29. Circular dichroism spectra of **C10GB** in acetonitrile solution. Spectra were recorded at room temperature.

The effect of temperature on the CD spectrum was studied. Above 60 °C, the aggregate became CD silent, indicating dissociation of the aggregate to the monomer. On cooling this solution, the CD signal reappeared in the 45–50 °C range indicating reformation of the aggregate.

4.3.2. Aggregation in DMSO/Water mixed solvents

The diphenylbutadiene-sugar bolaamphiphile, **C12GB** was highly soluble in DMSO and practically insoluble in water. Its solution in pure DMSO (10^{-6} M) showed a structured absorption spectrum with a strong $\pi \rightarrow \pi^*$ band at 353 nm (ε = 58380 $M^{-1}cm^{-1}$) and shoulders at 339 and 371 nm. This spectrum corresponds to the molecularly dissolved species. Increase of water content in these solutions (30% water/DMSO) resulted initially in a steady decrease in intensity of the main band at 353 nm with the concomitant appearance of a blue-shifted band at 294 nm ($\Delta\lambda_{max}$ = 58 nm). With subsequent increase in water content, the monomer band almost disappeared with increase in intensity of the blue-shifted band at 294 nm. These changes were marked by the presence of an isosbestic point at 310 nm (Figure 4.30a). Formation of a blue-shifted band by aromatic derivatives in aqueous or water rich media is attributed to the formation of H-type aggregates, which essentially consist of a "card pack" array of transition moments of the individual molecules.[23-29,44]

The absorption band attributable to the aggregates was CD active indicating a chiral arrangement of the transition moments of the diphenylbutadiene segment within the aggregates. Figure 4.30b shows the CD spectra of **C12GB** aggregates in the water/DMSO solvent mixtures. Whereas **C12GB** in pure DMSO solution was CD silent, a Cotton effect was observed for solutions containing water, indicating a chiral arrangement of the transition moments of the diphenylbutadiene units

within the aggregates. The zero-crossing point was close to the absorption maximum of the aggregated chromophore, indicating the CD spectra to be due to the exciton coupling bands of the aggregate.

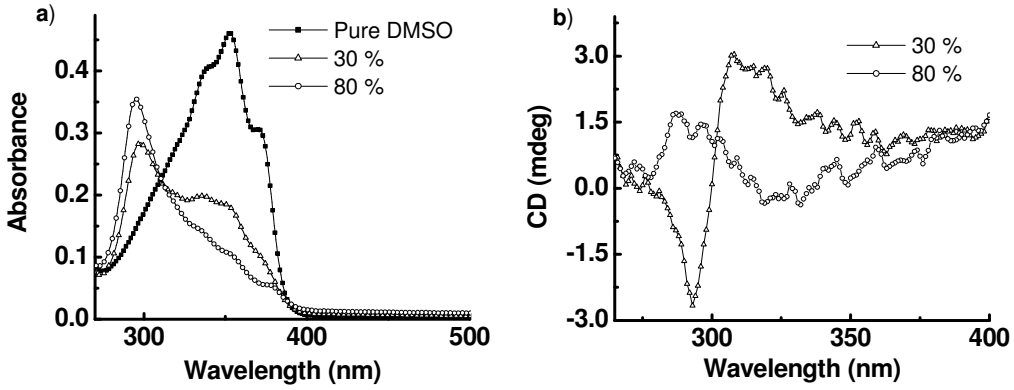

Figure 4.30. (a) UV-vis absorption and (b) CD spectra of **C12GB** in water/DMSO solvent mixtures.

4.3.2.1. Effect of temperature on the UV-vis spectra

The UV-vis spectrum of **C12GB** in 30% water/DMSO at room temperature, indicated the presence of monomer and aggregated species. On heating a decrease in absorbance at the aggregate peak and concomitant increase in absorbance of the monomer peak was observed. An isosbestic point was observed at 317 nm (Figure 4.31a). At ~60 °C, the spectrum appeared very similar to that of molecularly dissolved **C12GB**. This indicated that all the aggregates present were dissociated and molecularly dissolved at this temperature. When cooled from 60 °C to room temperature this solution underwent aggregation to the initial aggregated state through the same isosbestic point at 317 nm (Figure 4.31b).

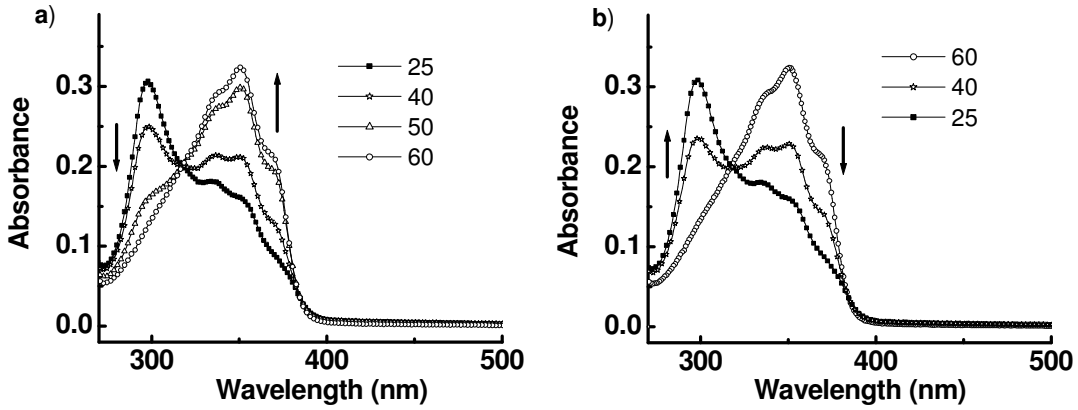

Figure 4.31. Effect of temperature on the UV-vis absorption spectra of **C12GB** in 30 % water/DMSO on (a) heating and (b) cooling.

In 80% water/DMSO, **C12GB** existed predominantly in aggregated form. The aggregate formed in this solution exhibited enhanced thermal stability compared to those formed in solutions containing less amount of water. On heating this solution, only a decrease in absorbance at the aggregate peak wavelength could be observed which indicated that there was a slight weakening in the tightly packed H-aggregate (Figure 4.32a). Formation of the monomer band was not observed. On cooling to room temperature, the absorbance of this solution increased to the original value (Figure 4.32b).

The thermo-reversibility of aggregates was found to be much better for the butadiene based bolas compared to that of the azo-bolas.

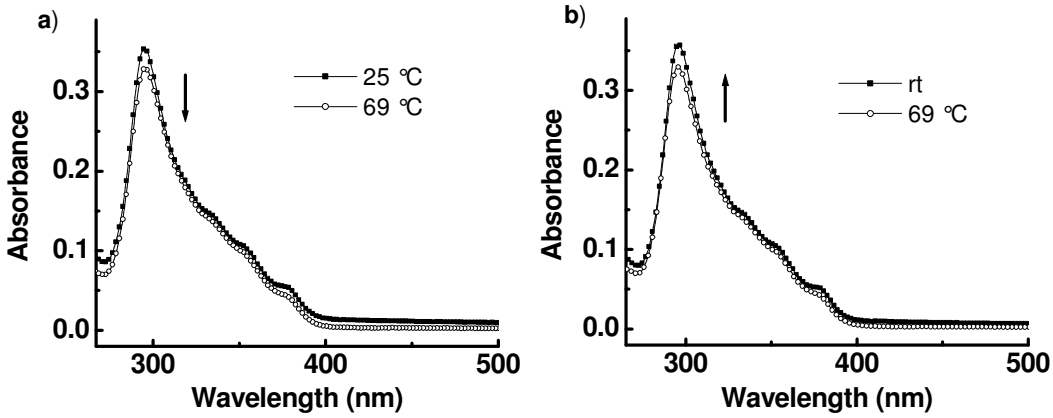

Figure 4.32. Effect of temperature on the UV-vis absorption spectra of **C12GB** in 80 % water/DMSO on (a) heating and (b) cooling.

4.3.2.2. Fluorescence properties of the C12GB aggregates

The solutions containing aggregates were studied for their fluorescence properties. From the UV-vis absorption studies it could be understood that at lower water concentrations (30% water/DMSO), **C12GB** existed as a mixture of monomer and aggregate. As a result, excitation dependent emission was observed in these solutions. Excitation of the aggregate band centered at 294 nm resulted in a weak red-shifted structured emission (peaks at 419, 442 and 474 nm) characteristic of the aggregate. The H-aggregate is generally known to be non-fluorescent.[45] However in some cases excitation of the H-aggregate is known to be followed by relaxation to a lower state from which emission becomes an allowed process.[15,45,46] This is schematically shown in Figure 4.33.

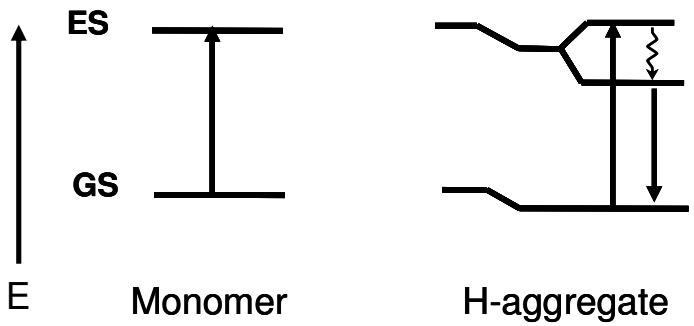

Figure 4.33. Schematic representation illustrating electronic transitions occurring in the monomer and H-aggregate.

When the residual monomer species absorbing at 353 nm was excited, it resulted in a strong molecular emission spectrum centered at 405 nm (blue-shifted with respect to aggregate emission) (Figure 4.34a).

When the excitation spectra were monitored at the aggregate emission peaks, the spectrum corresponded to the combined UV-vis absorption spectrum of monomer and aggregate. When the monitoring wavelength was moved towards the monomer emission (towards blue region), the excitation spectrum became increasingly similar to the UV-vis spectrum of molecularly dissolved **C12GB** (Figure 4.34b).

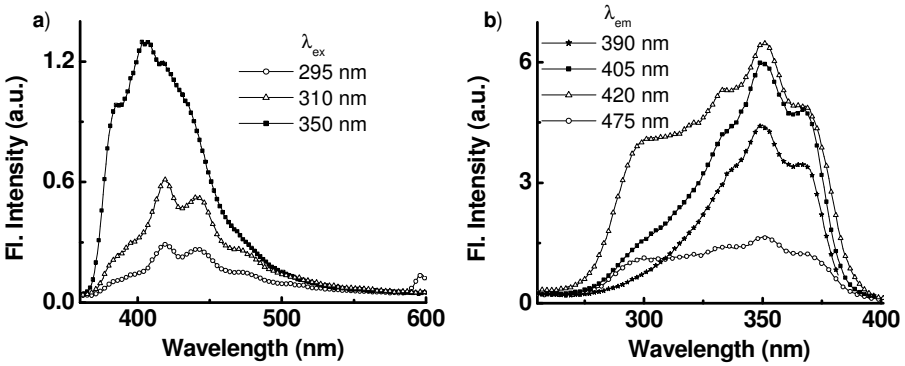

Figure 4.34. (a) Fluorescence emission and (b) excitation spectra of **C12GB** in 30% water/DMSO.

In solutions with higher water concentration, **C12GB** existed predominantly in the aggregated state. Thus there was only one emitting species and that was the aggregate. The emission intensity was considerably reduced (Figure 4.35).

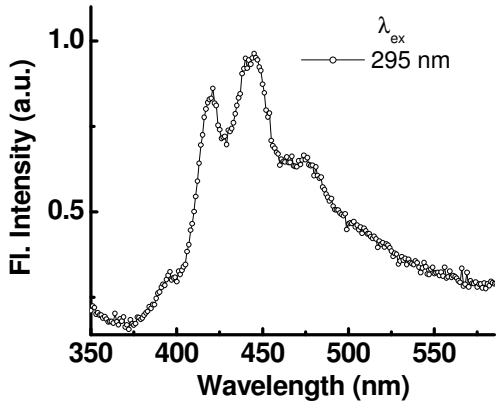

Figure 4.35. Fluorescence emission spectrum of **C12GB** in 80% water/DMSO.

4.4. Discussion

Sugar-based amphiphiles and bolaamphiphiles have been shown to be very useful for generating a wide range of self-assembled structures. Recently Shimizu, Masuda and co-workers have shown that the morphology of the self-assembled

structures of some amphiphilic sugars could be controlled by controlling the structure of the seed materials used.[47] Thus crystalline materials precipitated from methanol gave rise to tapes, whereas solid films of the same materials obtained by evaporating a DMF solution gave rise to nanotubes. In both cases the self-assembled materials were obtained by preparing hot aqueous dispersions (100 °C) of the two solids. These studies indicate that the supramolecular structural information stored in the seed materials are retained, at least partially at the high temperatures allowing the materials to self-assemble into different structures on cooling. In the azo-bolas investigated in the present study, the presence of the azo chromophore made it possible to monitor the stability of the aggregates formed as a function of the length of the intervening oligomethylene spacer and temperature. The ease of formation of the highly ordered H* aggregates, which was indicated by the formation of an intense, narrow, blue-shifted band compared to that of the azobenzene monomer, increased with increase in the length of the oligomethylene spacers. The stability of the aggregates as a function of temperature was also dependent on the length of the spacers. Whereas the absorption spectra of **azo-bis 5** indicated complete break-up of the aggregate to the monomer form on heating, in the absorption, CD and NMR spectra, the presence of substantial amounts of residual aggregates was indicated for **azo-bis 8**, **azo-bis 10** and **azo-bis 12** at temperatures >90 °C.

Microscopic studies of films deposited from aggregated solutions of **azo-bis 5** and **azo-bis 8** indicated the presence of vesicles. Films deposited from solutions of the **azo-bis 10** aggregates however, indicated the formation of fibers. Solutions of **azo-bis 10** heated above 95 °C and cooled to room temperature however, resulted in the formation of vesicles. A possible explanation for this effect may be that in **azo-bis 10**, the strong interaction between the individual molecules, due to the longer oligomethylene spacers, could initially lead to the formation of the kinetically trapped aggregates,[48-50] resulting in the formation of fibers. In solutions that are cooled from above 95 °C to room temperature under ambient conditions, the self-assembly process can be slowed down sufficiently, resulting in the formation of the thermodynamically more stable vesicles. It is interesting to note that in the case of the photolyzed solutions of **azo-bis 8**, the reverse *cis* to *trans* isomerization of the azobenzene unit resulted in a preferential formation of flat sheets and fibers. Under such conditions the *trans*-isomer, which is the only species capable of aggregating, becomes available at a very slow rate (controlled by the rate of the thermal *cis* to *trans* isomerization), which may not be conducive for the formation of vesicles. Formation of vesicles capable of trapping solvent within them can be expected to be a more spontaneous process. In contrast, when these solutions in which the thermal *cis* to *trans* isomerization had been completed, are heated and cooled to room temperature, formation of vesicles was observed.

Preliminary studies on the aggregation of diphenylbutadiene cored bolaamphiphiles in acetonitrile and water/DMSO showed that they were also capable of self-aggregating as observed in azo-bolas. Changes in absorption spectra and onset of CD activity indicated the formation of H-type aggregates. The water rich solutions of the aggregates were found to exhibit enhanced thermal stability. The change in fluorescence spectra on aggregation of these donor–donor substituted diphenylbutadienes was also studied. The aggregates were observed to be fluorescent unlike most reported H-type aggregates.[45] Under certain conditions however, H-type aggregates are known to fluoresce.[15,45,51] At certain water/DMSO concentrations when both monomer and aggregated species were present in the same solution, the emission spectra depended on excitation wavelength.

4.5. Experimental

4.5.1. Materials and methods

Ultraviolet-visible (UV-vis) and Circular Dichroism (CD) spectra were recorded in quartz cuvettes. UV-vis spectra were recorded on a Shimadzu UV-2401 PC UV-vis scanning double-beam spectrophotometer. CD spectra were recorded in the Jasco J-810 spectropolarimeter equipped with Jasco PTC-423S Peltier type temperature control system. (1S)-(+)-10-Camphorsulfonicacid, ammonium salt (0.06% aqueous solution, 1 cm light path) was used for calibration of the spectropolarimeter sensitivity and wavelength (CD = +190.4 mdeg at 291.0 nm). The CD exciton couplet amplitude was calculated as $A_{CD} = CD_{\text{first Cotton}}$ (at the

long-wavelength maximum of the couplet) – $CD_{second\ Cotton}$ (at the short-wavelength maximum).[33] The CD spectra obtained were similar in stirred and un-stirred sample solutions. Contribution from linear dichroism (LD) was negligible since the aggregate solutions placed at different angles had no effect on the type of Cotton effect and the solutions were clear at the temperatures studied. Fluorescence excitation and emission spectra in solution were recorded on a SPEX Fluorolog-2 spectrofluorometer. ^{1}H NMR experiments were carried out in a 300 MHz Bruker Avance DPX or a Bruker Avance DRX 500 spectrometer equipped with a Bruker BVT 3000 digital temperature controller. TMS was the internal standard and spectra were recorded without sample spinning. At higher D_2O volumes, the residual proton resonance in DMSO was used for calibration since the TMS peak was difficult to locate. The *trans* to *cis* photoisomerization in DMSO solution was investigated by irradiating with 364 nm monochromatic light isolated from a 450 W ozone free Xe lamp using the excitation monochromator of SPEX Fluorolog–2. Laser irradiation was carried out with 355 nm laser pulses (10 Hz, 6 ns pulse width) from a Spectra-Physics Quanta-Ray GCR-12S Nd:YAG laser.

Size distribution measurements of aggregates in solution were performed in a Malvern Instruments Nano-ZS by dynamic light scattering (DLS) employing a 633 nm He-Ne laser. Each experiment was repeated three times and the data was averaged.

Atomic force microscopy (AFM) was performed under normal atmosphere using tapping and contact mode probes on a Digital Instruments NanoScope IV MultiMode scanning probe microscope (Tapping Mode – Model: Veeco RTESP/Material: Phosphorus (n) doped Silicon, resonance frequency of 299 kHz and a spring constant of 20-80 Nm^{-1}; Contact mode – Model: Veeco NP-20/Material: Silicon Nitride). The samples for AFM studies were obtained by drop-casting and air-drying aggregate containing solutions on freshly cleaved mica. Blank experiments were conducted with only solvent mixtures on freshly cleaved mica to rule out any artifacts. Transmission electron microscope, TEM bright-field images were obtained using a Hitachi H-600 instrument operating at an accelerating voltage of 75 kV with sample solutions drop-cast and air-dried on copper grids (mesh 200) having a formvar carbon support film. Scanning electron microscope, SEM (signal: SEI) images were obtained using the JEOL JSM-5600 LV at 10 kV with the samples drop-cast and air-dried on a flat surface of cylindrical brass stubs and coated with gold in a JEOL JFC-1100 ion sputter, prior to viewing.

Solvents were of spectroscopy grade. Water was doubly distilled and deionized (resistivity of 18.2 MΩcm) using a Millipore Milli-Q-Plus water purifier. The solutions containing aggregates were prepared from stock solutions of compounds in DMSO or THF. To a constant volume pipetted out from the stock solution, various volume fractions of DMSO/water or THF/*n*-hexane were added.

Aggregates were spontaneously formed upon adding non-solvent to the stock solution of azo-bola, without the need for ultrasonication or any other special treatment. The solutions containing aggregates exhibited a slight blue hue due to the scattering of white light. The percentages of water/DMSO mentioned refer to volume percentage of water. On adding water to DMSO solutions of the compounds, exothermicity ($\Delta H = -715$ calmol^{-1} for 0.36 mole fraction DMSO in water at 22–25 °C),[52] caused the solutions to warm up. The solutions were left to equilibrate to room temperature for 1 h after preparation before carrying out further studies.

4.6. Conclusion

In conclusion, this work provides an understanding of the controlled thermal and photochemical transformation of organized assemblies in a series of azobenzene and diphenylbutadiene cored bolaamphiphiles. Further studies along these lines are expected to lead to more versatile photoresponsive vesicles which will be of interest from the point of view of developing controlled release systems.[39,50,53]

References

(1) Fuhrhop, J.-H.; Wang, T. *Chem. Rev. (Washington, DC, U. S.)* **2004**, *104*, 2901–2937.

(2) Shimizu, T.; Masuda, M.; Minamikawa, H. *Chem. Rev. (Washington, DC, U. S.)* **2005**, *105*, 1401–1443.

(3) See in the web page of American Society for Microbiology at the link below http://www.microbeworld.org/microbes/archaea/

(4) Menger, F. M.; Chen, X. Y.; Brocchini, S.; Hopkins, H. P.; Hamilton, D. *J. Am. Chem. Soc.* **1993**, *115*, 6600–6608.

(5) Snyder, F., Ed., *Ether Lipids: Chemistry and Biology*; Academic Press: New York, 1972.

(6) Auzély-Velty, R.; Benvegnu, T.; Plusquellec, D.; Mackenzie, G.; Haley, J. A.; Goodby, J. W. *Angew. Chem., Int. Ed.* **1998**, *37*, 2511–2515.

(7) Fraser-Reid, B. O.; Tatsuta, K.; Thiem, J. Eds., *Glycoscience: Chemistry and Chemical Biology*, Springer-Verlag: Berlin, 2001; Vol. I–III.

(8) Masuda, M.; Vill, V.; Shimizu, T. *J. Am. Chem. Soc.* **2000**, *122*, 12327–12333.

(9) Soussan, E.; Pasc-Banu, A.; Consola, S.; Labrot, T.; Perez, E.; Blanzat, M.; Oda, R.; Vidal, C.; Rico-Lattes, I. *ChemPhysChem* **2005**, *6*, 2492–2494.

(10) Menger, F. M.; Bian, J.; Sizova, E.; Martinson, D. E.; Seredyuk, V. A. *Org. Lett.* **2004**, *6*, 261–264.

(11) Ringsdorf, H.; Schlarb, B.; Venzmer, J. *Angew. Chem., Int. Ed.* **1988**, *27*, 113–158.

(12) John, G.; Masuda, M.; Okada, Y.; Yase, K.; Shimizu, T. *Adv. Mater. (Weinheim, Ger.)* **2001**, *13*, 715–718.

(13) van Doren, H. A.; Smits, E.; Pestman, J. M.; Engberts, J. B. F. N.; Kellogg, R. M. *Chem. Soc. Rev.* **2000**, *29*, 183–199.

(14) Kobayashi, H.; Koumoto, K.; Jung, J. H.; Shinkai, S. *J. Chem. Soc., Perkin Trans. 2* **2002**, 1930–1936.

(15) Kumar, N. S. S.; Varghese, S.; Narayan, G.; Das, S. *Angew. Chem., Int. Ed.* **2006**, *45*, 6317–6321.

(16) Narayan, G.; Kumar, N. S. S.; Paul, S.; Srinivas, O.; Jayaraman, N.; Das, S. *J. Photochem. Photobiol., A* **2007**, *189*, 405–413.

(17) Abraham, S.; Paul, S.; Narayan, G.; Prasad, S. K.; Rao, D. S. S.; Jayaraman, N.; Das, S. *Adv. Funct. Mater.* **2005**, *15*, 1579–1584.

(18) Coldren, B. A.; Warriner, H.; van Zanten, R.; Zasadzinski, J. A.; Sirota, E. B. *Langmuir* **2006**, *22*, 2465–2473 and references cited therein.

(19) Fendler, J. H. *Acc. Chem. Res.* **1980**, *13*, 7–13.

(20) Stone, M. T.; Heemstra, J. M.; Moore, J. S. *Acc. Chem. Res.* **2006**, *39*, 11–20.

(21) Kawasaki, T.; Tokuhiro, M.; Kimizuka, N.; Kunitake, T. *J. Am. Chem. Soc.* **2001**, *123*, 6792–6800.

(22) Asanuma, H.; Shirasuka, K.; Takarada, T.; Kashida, H.; Komiyama, M. *J. Am. Chem. Soc.* **2003**, *125*, 2217–2223.

(23) Kasha, M.; Rawls, H. R.; El-Bayoumi, M. A. *Pure Appl. Chem.* **1965**, *11*, 371–392.

(24) Kuiper, J. M.; Engberts, J. B. F. N. *Langmuir* **2004**, *20*, 1152–1160.

(25) Song, X.; Perlstein, J.; Whitten, D. G. *J. Am. Chem. Soc.* **1997**, *119*, 9144–9159.

(26) Yagai, S.; Karatsu, T.; Kitamura, A. *Langmuir* **2005**, *21*, 11048–11052.

(27) Xie, H.; Liu, L.; W. Wang, L. Xu, *Chem. Phys. Lett.* **2005**, *403*, 175–179.

(28) Kim, I.; Rabolt, J. F.; Stroeve, P. *Colloids Surf., A* **2000**, *171*, 167–174.

(29) Würthner, F.; Yao, S.; Beginn, U. *Angew. Chem., Int. Ed.* **2003**, *42*, 3247–3250.

(30) Herz, A. H. *Photogr. Sci. Eng.* **1974**, *18*, 323–335.

(31) Iwaura, R.; Hoeben, F. J. M.; Masuda, M.; Schenning, A. P. H. J.; Meijer, E. W.; Shimizu, T. *J. Am. Chem. Soc.* **2006**, *128*, 13298–13304.

(32) Lewis, F. D.; Zhang, L.; Liu, X.; Zuo, X.; Tiede, D. M.; Long, H.; Schatz, G. C. *J. Am. Chem. Soc.* **2005**, *127*, 14445–14453.

(33) Berova, N.; Nakanishi, K. In *Circular Dichroism: Principles and Applications,* 2nd ed., Berova, N., Nakanishi, K., Woody, R. W. Ed., Wiley-VCH: New York, 2000; pp. 337–382.

(34) Sanders, J. K. M.; Hunter, B. K. *Modern NMR Spectrosopy,* 2nd ed., Oxford University Press: New York, 1993, p. 161.

(35) Escuder, B.; LLusar, M.; Miravet, J. F. *J. Org. Chem.* **2006**, *71*, 7747–7752.

(36) Tait, K. M.; Parkinson, J. A.; Bates, S. P.; Ebenezer, W. J.; Jones, A. C. *J. Photochem. Photobiol., A* **2003**, *154*, 179–188.

(37) Menger, F. M.; Seredyuk, V. A.; Apkarian, R. P.; Wright, E. R. *J. Am. Chem. Soc.* **2002**, *124*, 12408–12409.

(38) Yang, M.; Wang, W.; Yuan, F.; Zhang, X.; Li, J.; Liang, F.; He, B.; Minch, B.; Wegner, G. *J. Am. Chem. Soc.* **2005**, *127*, 15107–15111.

(39) Vriezema, D. M.; Aragonès, M. C.; Elemans, J. A. A. W.; Cornelissen, J. J. L. M.; Rowan, A. E.; Nolte, R. J. M. *Chem. Rev. (Washington, DC, U. S.)* **2005**, *105*, 1445–1489.

(40) Elliott, S. R. In *Physics of Amorphous Materials*; Longman: London, 1984.

(41) Harris, J. K.; Rose, G. D.; Bruening, M. L. *Langmuir* **2002**, *18*, 5337–5342.

(42) Gunn, E.; Sours, R.; Benedict, J. B.; Kaminsky, W.; Kahr, B. *J. Am. Chem. Soc.* **2006**, *128*, 14234–14235.

(43) John, G.; Jung, J. H.; Minamikawa, H.; Yoshida, K.; Shimizu, T. *Chem. –Eur. J.* **2002**, *8*, 5494–5500.

(44) Whitten, D. G.; Chen, L.; Geiger, H. C.; Perlstein, J.; Song, X. *J. Phys. Chem. B* **1998**, *102*, 10098–10111 and references cited therein.

(45) Rösch, U.; Yao, S.; Wortmann, R.; Würthner, F. *Angew. Chem., Int. Ed.* **2006**, *45*, 7026–7030 and references therein.

(46) Whitten, D. G. *Acc. Chem. Res.* **1993**, *26*, 502–509.

(47) Kameta, N.; Masuda, M.; Minamikawa, H.; Goutev, N. V.; Rim, J. A.; Jung, J. H.; Shimizu, T. *Adv. Mater. (Weinheim, Ger.)* **2005**, *17*, 2732–2736.

(48) Boettcher, C.; Schade, B.; Fuhrhop, J.-H. *Langmuir* **2001**, *17*, 873–877.

(49) Paraschiv, V.; Crego-Calama, M.; Ishi-i, T.; Padberg, C. J.; Timmerman, P.; Reinhoudt, D. N. *J. Am. Chem. Soc.* **2002**, *124*, 7638–7639.

(50) Zhang, L.; Eisenberg, A. *Polym. Adv. Technol.* **1998**, *9*, 677–699.

(51) Spano, F. C. *Chem. Phys. Lett.* **2000**, *331*, 7–13.

(52) Szmant, H. H. In *Dimethyl Sulfoxide: Basic concepts of DMSO*, Jacob, S. W., Rosenbaum, E. E., Wood, D. C. Eds., Marcel Dekker: New York, 1971; Vol. 1, p. 30.

(53) Gerasimov, O. V.; Boomer, J. A.; Qualls, M. M.; Thompson, D. H. *Adv. Drug Delivery Rev.* **1999**, *38*, 317–338.

Annexure

X-ray crystallography data for DBC1

Projection view of the **DBC1** molecule with 50% thermal ellipsoids:

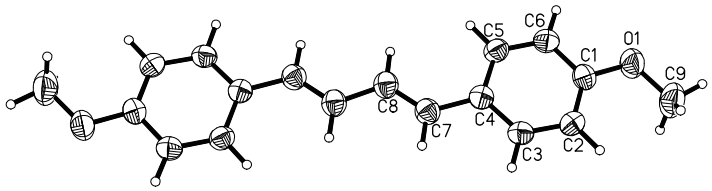

Table 1. Crystal data and structure refinement for sd4306.

Identification code	d4306/rt/DBC1	
Empirical formula	$C_{18}H_{18}O_2$	
Formula weight	266.32	
Temperature	293(2) K	
Wavelength	0.71073 Å	
Crystal system	Orthorhombic	
Space group	Pbca	
Crystal Habit	pyramidal	
Unit cell dimensions	a = 7.3543(3) Å	α= 90°.
	b = 6.2617(3) Å	β= 90°.
	c = 31.3872(13) Å	γ = 90°.
Volume	1445.39(11) $Å^3$	
Z	4	
Density (calculated)	1.224 Mg/m^3	
Absorption coefficient	0.078 mm^{-1}	
F(000)	568	
Crystal size	0.25 x 0.22 x 0.22 mm^3	
Theta range for data collection	1.30 to 27.47°.	
Index ranges	$-8\leq h\leq 9$, $-8\leq k\leq 8$, $-40\leq l\leq 37$	
Reflections collected	40427	
Independent reflections	1658 [R(int) = 0.036]	

Completeness to theta = 27.47°	100.0 %
Absorption correction	Numerical
Max. and min. transmission	0.9880 and 0.9847
Refinement method	Full-matrix least-squares on F^2
Data / restraints / parameters	1658 / 0 / 127
Goodness-of-fit on F^2	1.057
Final R indices [I>2sigma(I)]	R1 = 0.0433, wR2 = 0.1098
R indices (all data)	R1 = 0.0593, wR2 = 0.1185
Largest diff. peak and hole	0.116 and -0.146 e.Å^{-3}

Table 2. Atomic coordinates (× 10^4) and equivalent isotropic displacement parameters (Å^2 × 10^3) for sd4306. U(eq) is defined as one third of the trace of the orthogonalized U^{ij} tensor.

	x	y	z	U(eq)
O(1)	-187(2)	4251(2)	1996(1)	59(1)
C(1)	-67(2)	4944(2)	1582(1)	43(1)
C(2)	792(2)	3852(2)	1258(1)	46(1)
C(3)	822(2)	4737(2)	854(1)	45(1)
C(4)	42(2)	6709(2)	762(1)	40(1)
C(5)	-848(2)	7754(2)	1096(1)	44(1)
C(6)	-902(2)	6886(2)	1498(1)	46(1)
C(7)	259(2)	7618(2)	338(1)	46(1)
C(8)	-188(2)	9586(2)	209(1)	47(1)
C(9)	743(4)	2337(4)	2103(1)	79(1)

Table 3. Bond lengths [Å] and angles [°] for sd4306

O(1)-C(1)	1.3714(15)
O(1)-C(9)	1.420(2)
C(1)-C(2)	1.3777(19)
C(1)-C(6)	1.3880(18)
C(2)-C(3)	1.3839(19)
C(3)-C(4)	1.3920(18)
C(4)-C(5)	1.3986(18)
C(4)-C(7)	1.4581(19)
C(5)-C(6)	1.3734(19)
C(7)-C(8)	1.338(2)
C(8)-C(8)#1	1.438(3)
C(1)-O(1)-C(9)	117.43(13)
O(1)-C(1)-C(2)	124.80(12)
O(1)-C(1)-C(6)	115.37(12)
C(2)-C(1)-C(6)	119.83(12)
C(1)-C(2)-C(3)	118.99(12)
C(2)-C(3)-C(4)	122.56(12)
C(3)-C(4)-C(5)	116.93(12)
C(3)-C(4)-C(7)	119.38(12)
C(5)-C(4)-C(7)	123.63(12)
C(6)-C(5)-C(4)	121.08(13)
C(5)-C(6)-C(1)	120.56(12)
C(8)-C(7)-C(4)	127.46(13)
C(7)-C(8)-C(8)#1	124.06(18)

Symmetry transformations used to generate equivalent atoms:

#1 -x,-y+2,-z

Table 4. Anisotropic displacement parameters ($Å^2 \times 10^3$) for sd4306. The anisotropic displacement factor exponent takes the form: $-2\pi^2[h^2 a^{*2}U^{11} + ... + 2 h k a^* b^* U^{12}]$

	U^{11}	U^{22}	U^{33}	U^{23}	U^{13}	U^{12}
O(1)	78(1)	57(1)	41(1)	6(1)	2(1)	6(1)
C(1)	45(1)	45(1)	38(1)	1(1)	-1(1)	-5(1)
C(2)	49(1)	40(1)	50(1)	1(1)	1(1)	6(1)
C(3)	46(1)	44(1)	45(1)	-3(1)	5(1)	4(1)
C(4)	37(1)	41(1)	42(1)	-1(1)	-2(1)	-3(1)
C(5)	45(1)	40(1)	48(1)	-1(1)	0(1)	5(1)
C(6)	49(1)	44(1)	45(1)	-5(1)	3(1)	4(1)
C(7)	46(1)	49(1)	42(1)	0(1)	-1(1)	-1(1)
C(8)	47(1)	49(1)	44(1)	2(1)	-4(1)	-4(1)
C(9)	112(2)	69(1)	57(1)	20(1)	-1(1)	15(1)

Table 5. Hydrogen coordinates (× 10^4) and isotropic displacement parameters (Å^2 × 10^3) for sd4306.

	x	y	z	U(eq)
H(2)	1354(19)	2450(20)	1310(4)	56(4)
H(3)	1450(20)	3960(20)	628(4)	53(4)
H(5)	-1424(19)	9130(20)	1042(4)	54(4)
H(6)	-1510(20)	7590(20)	1729(4)	55(4)
H(7)	870(20)	6690(20)	134(5)	63(5)
H(8)	-790(20)	10580(20)	408(5)	59(4)
H(9A)	240(30)	1170(40)	1942(8)	120(9)
H(9B)	510(30)	2110(30)	2406(8)	101(7)
H(9C)	2100(40)	2540(40)	2043(7)	133(10)

Table 6. Torsion angles [°] for sd4306.

C(9)-O(1)-C(1)-C(2)	4.3(2)
C(9)-O(1)-C(1)-C(6)	-176.17(16)
O(1)-C(1)-C(2)-C(3)	-179.73(12)
C(6)-C(1)-C(2)-C(3)	0.80(19)
C(1)-C(2)-C(3)-C(4)	1.1(2)
C(2)-C(3)-C(4)-C(5)	-2.22(19)
C(2)-C(3)-C(4)-C(7)	174.93(13)
C(3)-C(4)-C(5)-C(6)	1.60(18)
C(7)-C(4)-C(5)-C(6)	-175.42(12)
C(4)-C(5)-C(6)-C(1)	0.1(2)
O(1)-C(1)-C(6)-C(5)	179.09(12)
C(2)-C(1)-C(6)-C(5)	-1.39(19)
C(3)-C(4)-C(7)-C(8)	-170.79(14)
C(5)-C(4)-C(7)-C(8)	6.2(2)
C(4)-C(7)-C(8)-C(8)#1	175.41(15)

Symmetry transformations used to generate equivalent atoms:

#1 -x,-y+2,-z

Publications of Mr. Narayan Gopinathan

1. Aggregation and Photoresponsive Behavior of Azobenzene–Oligomethylene–Glucopyranoside Bolaamphiphiles
   Narayan, G.; Kumar, N.S. S.; Paul, S.; Srinivas, O.; Jayaraman, N.; Das, S.
   J. Photochem. Photobiol., A **2007**, *189*(2-3), 405–413.
2. Hierarchical Self-assembly of Donor-Acceptor-substituted Butadiene Amphiphiles into Photoresponsive Vesicles and Gels
   Kumar, N. S. S.; Varghese, S.; **Narayan, G.**; Das, S.
   Angew. Chem., Int. Ed. **2006**, *45*(38), 6317–6321.
3. Observation of a Chiral smectic Phase in Azobenzene-Linked Bolaamphiphiles containing Free Sugars
   Abraham, S.; Paul, S.; **Narayan, G.**; Prasad, S. K.; Rao, D. S. S.; Jayaraman, N.; Das, S.
   Adv. Funct. Mater. **2005**, *15*(10), 1579–1584 (Highlighted as Inside Cover Page).
4. Manifestation of Chiral smectic C phase in Diphenylbutadiene cored Bolaamphiphilic Sugars
   Das, S.; **Narayan, G.**; Abraham, S.; Jayaraman, N.; Singh, M. K.; Prasad, S. K.; Rao, D. S. S. *Adv. Funct. Mater.* (Communicated).

Posters presented:

1. Thermotropic liquid crystals and supramolecular aggregates of sugar based photoresponsive bolaamphiphiles, **Narayan, G.**; Abraham, S.; Kumar, N. S. S.; Paul, S.; Jayaraman, N.; Das, S. at the 9th CRSI National Symposium in Chemistry (NSC–9) held at University of Delhi, Delhi, 1–4 February **2007**.

2. Thermotropic liquid crystals and supramolecular aggregates of sugar containing photoresponsive bolaamphiphiles, **Narayan, G.**; Abraham, S.; Kumar, N. S. S.; Varghese, S.; Jayaraman, N.; Das, S. during the 2nd JNC Research Conference on Chemistry of Materials held at Aquaserene, Quilon, Kerala, 29–31 October **2006**.

3. Study of phase transition behavior and fluorescence properties of some photoresponsive liquid crystals, **Narayan, G.**; Abraham, S.; Kumar, N. S. S.; Das, S. during the three-day seminar on "Recent Trends in Liquid Crystal Research" conducted by India-UK Science Networks (DST, New Delhi and The Royal Society, London) at Raman Research Institute, Bangalore, 14–16 November **2005**.

4. Photoresponsive carbohydrate amphiphiles, **Narayan, G.**; Antharjanam, P. K. S.; Mallia, V. A.; Das, S.; Paul, S.; Srinivas, O.; Jayaraman, N. at the 3rd Trivandrum International Symposium on Recent Trends in Photochemical Sciences, organized by Photosciences and Photonics, NIST, Trivandrum, 5–7 January **2004**.

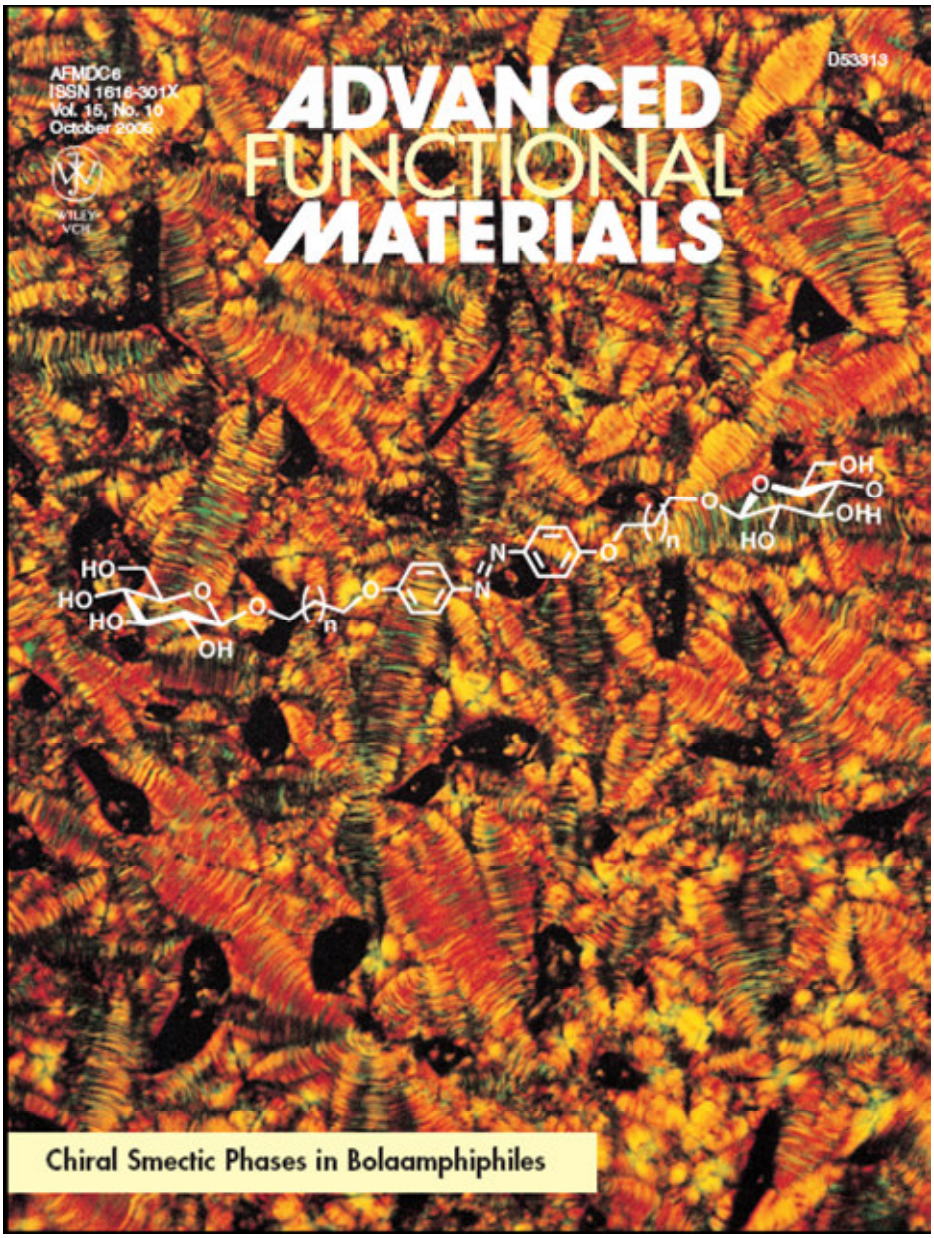
AFMDC6
ISSN 1616-301X
Vol. 15, No. 10
October 2005
WILEY-VCH
ADVANCED FUNCTIONAL MATERIALS
D53313
Chiral Smectic Phases in Bolaamphiphiles